EVALUATION OF PHYSICO-MECHANICAL PROPERTIES OF CLAYEY SOILS USING ELECTRICAL RESISTIVITY IMAGING TECHNIQUE

by

GOLAM KIBRIA

Presented to the Faculty of the Graduate School of

The University of Texas at Arlington in Partial Fulfillment

of the Requirements

for the Degree of

DOCTOR OF PHILOSOPHY

THE UNIVERSITY OF TEXAS AT ARLINGTON

May 2014

ACKNOWLEDGEMENTS

I would like express my sincere gratitude to my supervising professor Dr. Sahadat Hossain for the accomplishment of this work. It was always motivating for me to work under his sincere guidance and advice. The completion of this work would not have been possible without his constant inspiration and feedback.

I also like to convey my appreciation to Dr. Laureano R. Hoyos, Dr. Stefan A. Romanoschi, Dr. Xinbao Yu, and Dr. Chien-Pai Han for accepting to serve in my committee. I wish to acknowledge Dr. Laureano R. Hoyos and Dr. Hyeok Choi for giving me the opportunity to work in their laboratories. The statistical model chapter would not have been possible without direction and generous help of Dr. Han. I express my sincere gratitude to Texas Department of Transportation and City of Denton Landfill authority for the provision of sites. Special thank goes to Jose Andrez Cruz, Mohtasim Bellah and Noor E Alam Siddique for helping me in consolidation, SEM, and EDS analysis.

I wish to acknowledge the cooperation and assistance of my colleagues and friends throughout my graduate study, and accomplishment of this work. Finally, I want to dedicate this work to my family. Without constant inspiration of my parents, wife, and sisters, it would not be possible to complete the work. I would like to thank almighty ALLAH for giving me the strength and patience to overcome every difficulty throughout my life.

March 5, 2014

ABSTRACT

EVALUATION OF PHYSICO-MECHANICAL PROPERTIES OF CLAYEY SOILS USING ELECTRICAL RESISTIVITY IMAGING TECHNIQUE

Golam Kibria, Ph.D.

The University of Texas at Arlington, 2014

Supervising Professor: MD. Sahadat Hossain

Resistivity imaging (RI) is a promising approach to obtaining continuous profile of soil subsurface. This method offers simple technique to identify moisture variation and heterogeneity of the investigated area. However, at present, only qualitative information of subsurface can be obtained using RI. A study on the quantification of geotechnical properties has become important for rigorous use of this method in the evaluation of geohazard potential and construction quality control of landfill liner system. Several studies have been performed to describe electrical resistivity of soil as a function of pore fluid conductivity and surface conductance. However, characterization tests on pore water and surface charge are not typically performed in a conventional geotechnical investigation. The overall objective of this study is to develop correlations between geotechnical parameters and electrical resistivity of soil, which would provide a mean to estimate geotechnical properties from RI. As a part of the study, multiple regression

analyses were conducted to develop practically applicable models correlating resistivity with influential geotechnical parameters.

The soil samples considered in this study were classified as highly plastic clay (CH) and low plasticity clay (CL) according to Unified Soil Classification System (USCS). Based on the physical tests, scanning electron microscope (SEM), and energy dispersive X-ray spectroscopy (EDS) analysis, kaolinite was identified as the dominant mineral with some traces of magnesium, calcium, potassium, and iron. Electrical resistivity tests were conducted on compacted clays and undisturbed samples under varied geotechnical conditions. The experimental results indicated that the degree of saturation substantially influenced electrical resistivity. Electrical resistivity decreased as much as 11 times from initial value for the increase of degree of saturation from 23 to 100% in the laboratory tests on compacted clays. In case of undisturbed soil samples, resistivity decreased as much as sixteen fold (49.4 to 3.2 Ohm-m) for an increase of saturation from 31 to 100%. Furthermore, the resistivity results were different for the specimens at a specific degree of saturation because of varied surface activity and isomorphous substitution of clayey soils. In addition to physical properties, compressibility of clays was correlated with electrical conductivity. Based on the investigation, it was determined that the electrical conductivity vs. pressure curves followed similar trends as e vs. logp curves.

Multiple linear regression (MLR) models were developed for compacted and undisturbed samples using statistical analysis software SAS (2009). During model development, degree of saturation and CEC were selected as independent variables. The

proposed models were validated using experimental results on a different set of samples. Moreover, the applicability of the models in the determination of degrees of saturation was evaluated using field RI tests.

TABLE OF CONTENTS

LIST OF ILLUSTRATIONS

LIST OF TABLES

CHAPTER 1

INTRODUCTION

1.1 Introduction

Geohazards and corresponding failures of slopes present an important threat to transportation systems. Each year, geohazards cause significant damage to the infrastructure and environment, which often imposes significant maintenance cost for the transportation agencies. Therefore, it is important and necessary to improve the knowledge of geohazard potential at a given site, and use this knowledge to mitigate the failure of such geo-structures.

During rainfall events, infiltrated water causes a decrease in negative pore water pressure and results in reduction of shear strength. Therefore, the stability of the slope is affected by the increase in degree of saturation at shallow depths. Moreover, slopes constructed using highly plastic clays are characterized by the presence of cracks and fissures due to wetting and drying cycles. The effect of wet-dry cycle can extend as much as 1.5 to 3.6 m (Zornberg, 2007; Hossain, 2012). An increase in the degree of saturation in this zone immediately after rainfall can further exacerbate the stability of slopes. Therefore, it is important to know the degree of saturation at shallow depths in slopes to determine the geohazard potential.

Degree of saturation is also an important parameter in the construction of bottom liners and final covers of landfills. Compacted clay soils are widely used to line waste impoundments, and successful design involves stringent quality control to avoid water infiltration. Benson et al. (1999) performed a study to evaluate the importance of

compaction parameters in the construction of clay liners. According to the study, compaction condition has been identified as an important parameter to reduce hydraulic conductivity. It was observed that an increase in degree of saturation caused a reduction in hydraulic conductivity of clay liner.

Additionally, evaluation of change in degree of saturation in vertical and horizontal direction is important for the effective performance of evapotranspiration (ET) cover. An increase in saturation indicates that the cover system is approaching its storage capacity. Specifically, when the ET cover consisted of capillary barrier, percolation may not occur at low degrees of saturation (Hakonson, 1997). Moreover, the study conducted by Hamamoto et al. (2011) showed that the total methane oxidation is also associated with the saturation properties of cover soils. Therefore, degree of saturation is regarded as an important parameter in the liner systems of landfill.

The use of geophysical methods to evaluate geohazard potential and saturation profile of cover soil is gaining notable recognition from the engineering community. During site investigations and failure analyses, geologists and geotechnical engineers investigate several parameters using drilling, instrumentation, and soils testing. However, they can obtain information at certain key locations, and are generally left to infer and interpolate soil conditions area wide. Geophysical methods, in this case, Resistivity Imaging (RI) has the possibility to give an “image” or “view” of the subsurface. RI is a non-destructive method of site investigation and soil characterization. The method is less expensive, and subsurface investigation of a large area can be conducted in a short time period. Advantages of RI over conventional methods include: (1) a continuous image of

subsurface conditions, (2) coverage of a large area within a short time period, (3) low cost, (4) observations of site heterogeneity and zones of high moisture content, and (5) data can be processed in a very short time. Because of these benefits, the use of RI has increased significantly in recent years. It is one the most convenient available technique for preliminary subsurface investigation and geohazard studies.

1.2 Problem Statement

At present, engineering properties of geomaterials are investigated using laboratory experiments, in-situ tests, and geophysical surveys. Laboratory tests are well-established approaches to determine soil properties in a controlled environment. However, during geohazard analysis and construction quality control of liner system in landfill, laboratory investigation is not often possible due to time and cost constraint. Several in-situ tests are used for subsurface investigation; nonetheless, these methods provide information at some site-specific points. Therefore, a subsurface investigation method is required which can evaluate geotechnical parameters and provide continuous image of subsoil. A continuous profile with the quantification of degree of saturation can help to alleviate the existing problem in geotechnical investigation.

Resistivity imaging (RI) is a promising approach to obtain continuous profile of the subsurface. This method offers simple technique to identify moisture variation and heterogeneity of the investigated area (Hossain et al. 2010). Although significant improvements in equipment and techniques for soil resistivity test have occurred over the last decade, the application of RI in geotechnical engineering is limited because electrical resistivity responses under different soil conditions are not well understood. Moreover,

quantification of geotechnical properties has become important to bridge the gap that currently exists between geophysical tests and geotechnical engineering.

Several studies have been conducted to describe resistivity as a function of pore fluid conductivity and surface conductance (Archie, 1942; Sauer et al. 1955; Waxman and Smits, 1968; Shah and Singh, 2005). However, a general model to explain the variation of electrical conduction with soil properties is not available due to the inherent complexity of soil-water matrix and interconnectivity among the influential parameters. Furthermore, the experimental methods to determine pore water properties and surface conductance are often time and cost intensive. Therefore, correlations are required to understand the effects of geotechnical parameters on resistivity. In addition, these correlations may be helpful to quantify degree of saturation of subsoil from RI.

1.3 Objective of the Study

The overall objective of this study is to develop correlations between geotechnical properties and electrical resistivity of clayey soils. The correlations would provide a mean to evaluate geotechnical parameters from RI. As a part of the study, multiple regression analyses were conducted on the experimental results and practically applicable models were developed. The specific objectives of the current work can be mentioned below:

- Characterize the soil samples using conventional and advanced methods.
- Determine the effects of water content, void ratio and degree of saturation on resistivity of soil specimens.

- Investigate the effects of clay properties i.e. CEC, LL, PI, SSA on electrical resistivity using clay minerals and artificial soils.
- Identify the variation of electrical conductivity with compressibility and pressure.
- Develop correlations between geotechnical properties and geotechnical parameters i.e. moisture content, unit weight, void ratio, degree of saturation, CEC, pore water properties, one-dimensional consolidation etc.
- Determine influential physical properties to develop a simple multiple linear regression model.
- Develop practically applicable models to correlate resistivity with geotechnical properties.
- Compare the model predicted degree of saturation with laboratory and field tests.

The flow diagram of the current research can be presented in Figure 1.1

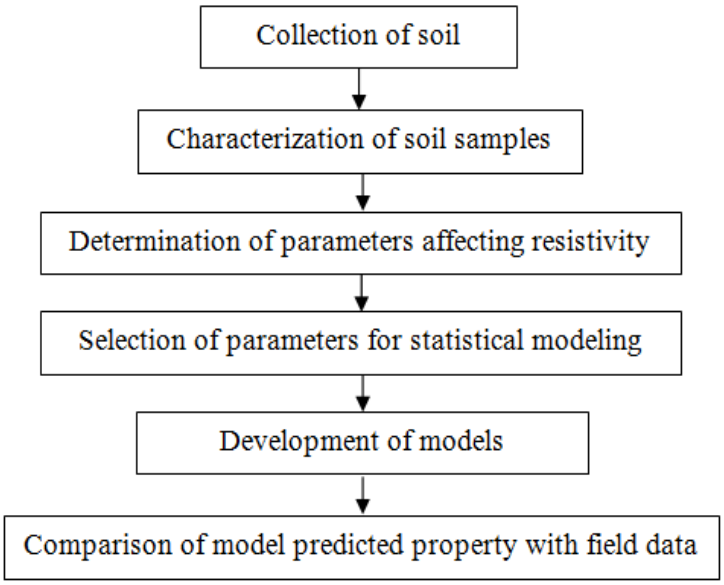

Figure 1.1 Flow chart of research activities undertaken in the current study

1.4 Organization of Dissertation

Chapter 1 presented problem statement and objective of the current study.

Chapter 2 described literature review on the clay properties, characterization method, and effects of geotechnical properties on electrical resistivity of soils.

Chapter 3 emphasized on the research methodologies of the current study. This section includes collection of test specimens, characterization of soil samples, and electrical resistivity tests on compacted and undisturbed soil specimens. In addition, the design of modified oedometer, calibration, and repeatability of the test results were also presented in this chapter.

Chapter 4 suggested soil characterization results, which included grain size distribution, Atterberg limits, cation exchange capacity, compositional element, fabric morphology, and pore water properties of the soil specimen.

Chapter 5 presented a detail investigation of the influential parameters affecting electrical resistivity of clayey soils. The properties were divided into three categories i.e. parameters related to phase relationship, physicochemical properties, and compressibility of clay soils.

Chapter 6 described development of multiple linear regression (MLR) models using statistical analysis software (SAS, 2009). MLR models were developed for compacted and undisturbed soils. The proposed models were validated using separate experimental results.

Chapter 7 presented field assessment of developed models in compacted clay liner and slopes. Resistivity imaging (RI) tests were conducted to evaluate the applicability of the models in field condition.

Chapter 8 summarized the conclusions of the study and proposed recommendations for future works.

CHAPTER 2

ELECTRICAL RESISTIVITY OF CLAYS: A REVIEW

2.1 Clay as a Geomaterial

Clays are generally composed of micro-crystalline particles of a group of minerals. Since clay science has been the interest of people from different backgrounds, a specific definition of this material is not available. According to Joint Nomenclature Committees (JNCs), "Clays are naturally occurring material primarily composed of fine-grained minerals, show plasticity when mixed with appropriate amount of moisture and become hard when dried or fired" (Bargaya and Lagayli, 2006). Mitchell and Soga (2005) indicated the characteristics of clay, which included a) small particle size (usually smaller than 0.002 mm) b) net negative charge c) plasticity when mixed with moisture, and d) weathering resistance. However, two specific properties of clayey soils, i.e. plasticity and cohesion are of particular interest in geotechnical engineering.

The presence of electrochemically active particles and their affinity to the moisture cause significant variation in the engineering and physico-chemical behavior of clays. The net negative charge in clay particles are developed due to the isomorphous substitution of ions, broken edges, and imperfection at the crystal lattice. Since, the crystals want to neutralize the charge; they are attracted by the water dipoles in the presence of moisture and adsorbed. In addition to that, the effects of surface activity are different depending on the present minerals in clayey soils. Therefore, it is important to have a clear understanding on the crystalline structure of the minerals to understand the clay behavior.

2.2 Clay Mineralogy

Clay minerals are crystalline sheet like structure, which consist of hydrous aluminosilicates and metallic ions. There are two fundamental crystal units of clay minerals, i.e. tetrahedral and octahedral. A tetrahedral unit belongs to four oxygen enclosing silicon, where as an octahedral unit composes of six oxygen or hydroxyls at corners surrounding aluminum, magnesium, iron or other ions. The schematic of basic tetrahedral and octahedral unit are presented in Figure 2.1 and 2.2, respectively.

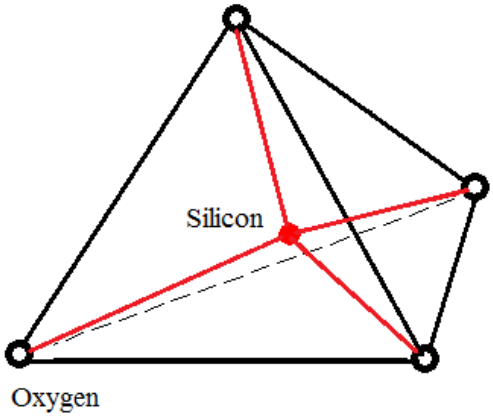

Figure 2.1 Single unit of tetrahedral mineral (redrawn from Holtz and Kovacs, 1981)

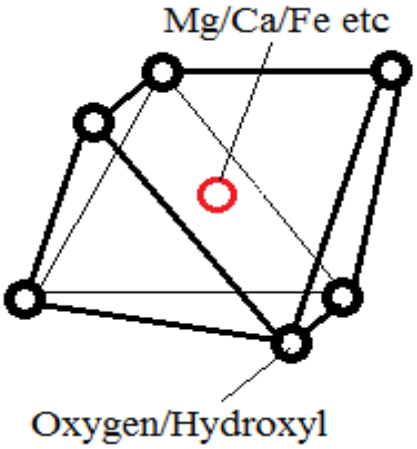

Figure 2.2 Single unit of octahedral mineral (redrawn from Holtz and Kovacs, 1981)

Based on the arrangement of stacks, bonding, isomorphous substitution, and presence of metallic ions, different clay minerals can be constituted. Some of the common clay minerals are kaolinite, montmorillonite, illite, nontronite, muscovite, etc (Mitchell and Soga, 2005). However, for engineering purpose kaolinite, montmorillonite and illite have particular importance in geotechnical engineering (Holtz and Kovacs, 1981).

2.2.1 Kaolinite

Kaolinite is known as 1:1 mineral because the inherent crystal structure consists of one tetrahedral and one octahedral sheet. Successive basic layers are bonded together by hydrogen bond between hydroxyls of the octahedral sheet and oxygen of the tetrahedral sheet. Due to this hydrogen bond, a large crystal of kaolinite is developed. The thickness of the basic crystal layer is 0.72 nm. A schematic of the crystal structure of kaolinite is presented in Figure 2.3.

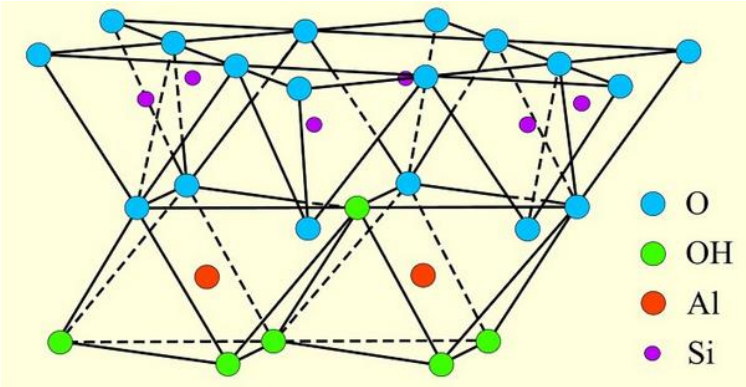

Figure 2.3 Structure of kaolinite crystal (http://pubs.usgs.gov)

Since the hydrogen bond is very strong, hydration cannot occur in the crystal of kaolinite. However, net negative charge can be developed in the structure due to broken

bonds and ion substitution. Typically, exposed hydroxyl can be replaced by exchangeable ions, and Al^{3+} can be substituted for Si^{4+}. Moreover, the presence of a divalent ion can cause a substitution of divalent ion for Al^{3+}. The ranges of cation exchange capacity in kaolinite are in between 3 to 15 meq/100gm.

The surface morphology of kaolinite mineral is characterized by six-sided hexagonal plates. The lateral dimension and thickness of the plates are ranged from 0.1 to 0.4 μm and 0.05 to 2 μm, respectively Because of the crystal structure and morphology, the typical specific surface area of kaolinite ranges between 10 and 20 m^2/gm.

2.2.2 Montmorillonite

The basic unit of montmorillonite consisted of two silica sheets and one alumina sheet. This mineral is known as 2:1 mineral where the distance between the unit cells is approximately 0.96 nm. The top of the silica sheets are bonded by Van der Waals force, and there is a net negative charge deficiency in octahedral sheet. Therefore, water and exchangeable ions can enter and break the layer. The structural unit of montmorillonite is presented in Figure 2.4.

Because of the layer separation and hydration, montmorillonite mineral is characterized by swelling behavior. In addition to that, montmorillonite minerals show extensive isomorphous substitution for Si^{4+} and Al^{3+} by available cations. According to the literature, Al^{3+} can replace as much as 15% of Si^{4+} in the tetrahedral sheet (Mitchell and Soga, 2005). The overall charge deficiency resulting from the ion substitution ranges from 0.5 to 1.2 per unit cell. The typical ranges of cation exchange capacity of montmorillonite are between 80 and 150 meq/100 gm.

The surface morphology of montmorillonite mineral is characterized by equidimensional flakes, and may appear as thin films. Furthermore, a directional strain may cause by large amount of substitution of Fe^{3+} and/or Mg^{2+} for Al^{4+}, which may result needle shaped fabric structure in montmorillonite. Due to the inherent configuration and high surface activity, the specific surface area (exclusive of interlayer zone) of montmorillonite can vary from 50 to 120 m^2/gm.

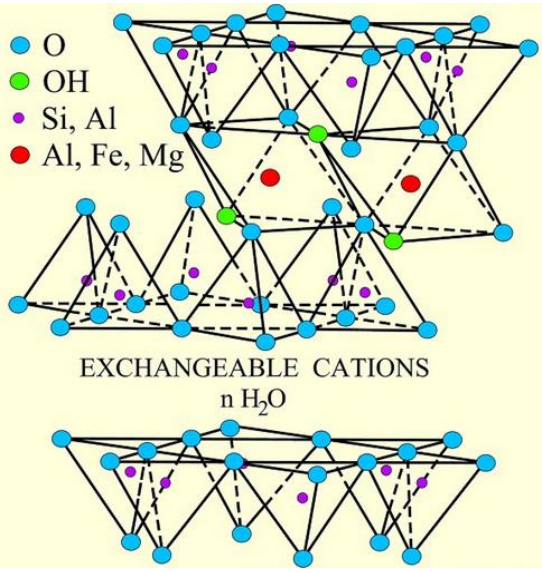

Figure 2.4 Structure of montmorillonite crystal (http://pubs.usgs.gov)

2.2.3 Illite

Illite mineral is composed of two silica sheets and one alumina sheet, and known as 2:1 mineral. The basic unit configuration is similar to montmorillonite; however, the basic layers are bonded by potassium. The diameters of hexagonal aperture in silica sheet are exactly similar to the ionic radius of potassium (K^+). Therefore, the presence of potassium (K^+) makes the bond between the layers very strong. The schematic of the structure of illite is presented in Figure 2.5.

The overall charge deficiency is mostly in the silica sheets, and ranged between 1.3 to 1.5 unit per cell. The additional charge is balanced by non-exchangeable potassium (K^+) ions. The typical cation exchange capacity of montmorillonite ranges from 10 to 40 meq/100 gm.

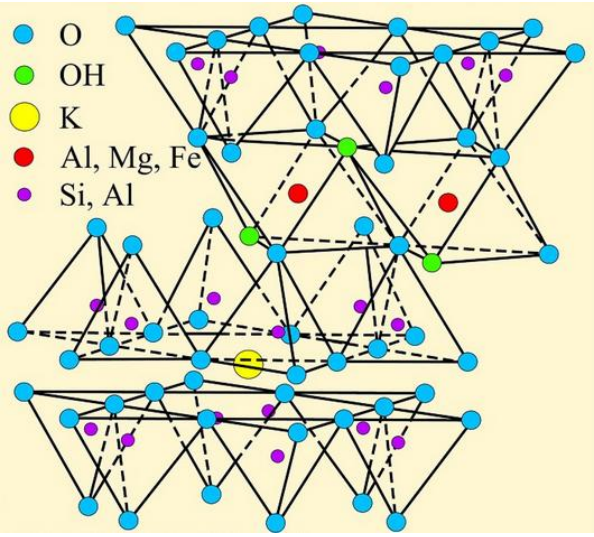

Figure 2.5 Structure of illite crystal (http://pubs.usgs.gov)

The fabric morphology of illite is characterized by hexagonal small flaky particles when well crystallized. According to Mitchell and Soga (2005), the surface area of this mineral ranges from 65 to 100 m^2/gm.

The typical chemical formula of the clay minerals are presented in Table 2.1.

Table 2.1 Chemical formulas of clay minerals (Yang, 2002)

Clay Mineral	**Layer type**	**Typical Chemical Formula**
Kaolinite	1:1	$[Si_4]Al_4O_{10}(OH)_8.nH_2O$ (n= 0 or 4)
Montromorillonite	2:1	$M_x[Si_8]Al_{3.2}Fe_{0.2}Mg_{0.6}O_{20}(OH)_4$
Illite	2:1	$M_x[Si_{6.8}Al_{1.2}]Al_3Fe_{0.25}Mg_{0.75}O_{20}(OH)_4$

2.3. Clay Water Interaction

It is evident that the engineering and physico-chemical behavior of clay are largely influenced by the moisture. Therefore, it is important to know the mechanism of clay water interaction. A brief discussion on the mechanism of water adsorption is presented herein.

The clay particles contain adsorbed counterions and excess ions in the form of precipitated salts at dry condition. The addition of water hydrates the counterions adsorbed in the particle surface. During the hydration process, some of the counterions lose their primary hydration shell (all or partly) and develop inner sphere complex. The ions with primary hydration shells also exist in the form of outer sphere complex. The hydrated counterions are attached to the particles due to the presence of surface charge. The rest of the counterions are separated from the surface of the particles by water.

Mitchell and Soga (2005) summarized the possible causes of clay water interaction, which included hydrogen bonding, attraction by osmosis, hydration of exchangeable cations, charged surface dipole attraction, and presence of London dispersion force as illustrated in Figure 2.6.

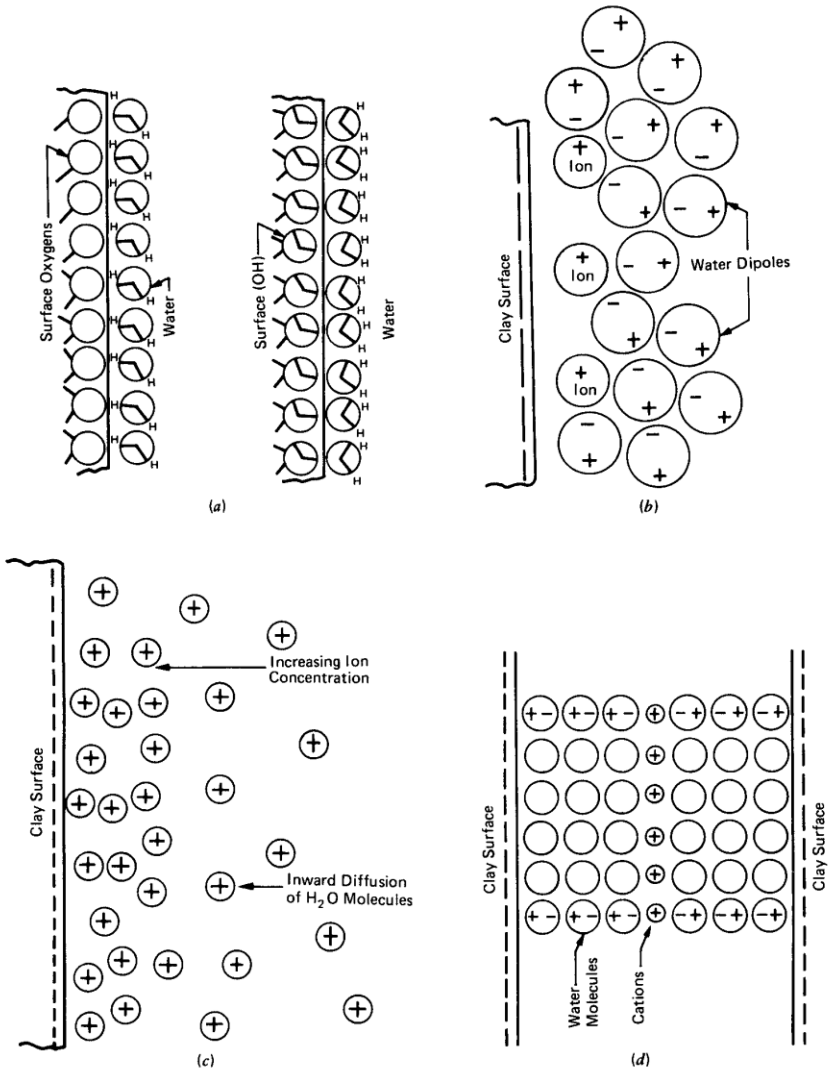

Figure 2.6 Different causes of clay water interaction (a) hydrogen bonding (b) ion hydration (c) attraction by osmosis (d) dipole attraction (Mitchell and Soga, 2005)

2.4. Characterization of Clay Minerals

2.4.1 Index Properties of Soil

The characterization of clay mineral is necessary for the identification of engineering and physico-chemical behavior of fine-grained soils. In addition, design of stabilizers also requires a specific determination of clay mineral (Chittoori and Puppala,

2011). Casagrande utilized Atterberg limits to determine the qualitative mineralogical content of soils. Mitchell and Soga (2005) indicated that ranges of activities in clays minerals were different, and provided an indication about the dominant mineral in a soil sample. Based on the experimental results, a chart was developed for the identification of dominant mineral. Although the chart provides a mean for preliminary assessment of mineral, the information can be useful from engineering point of view. The typical ranges of LL, PI and activity of different minerals are presented in Table 2.2

Table 2.2 Typical ranges of LL, PI and activity of minerals (Mitchell and Soga, 2005)

Mineral	**Liquid limits**	**Plastic limits**	**Activity**
Montmorillonite	100-900	50-100	1-7
Illite	60-120	35-60	0.5-1
Kaolinite	30-110	25-400	0.5

Note: Activity= PI/%<2μm

Chittoori and Puppala (2011) presented a study on the quantification of clay minerals in fine fraction of soil. The CEC, SSA and total potassium tests were performed on the natural and artificial soils. Based on the experimental results, artificial neural networks were developed to quantify the minerals. It was reported that the performance of the neural network incorporating three parameters were in good agreement with mineralogical distribution of the tested soils.

Prakash and Shridharan (2004) correlated free swell ratio of soils with the mineral contents. An extensive experimental program consisting of seventy soil specimens was developed to determine the free swell ratio. Thereafter, a chart was developed (Table 2.3) to determine mineralogy of the specimen using free swell ratio.

Table 2.3 Mineralogy based classification of soil using free swell ratio (Prakash and Shridharan, 2004)

Free swell ratio	**Soil expansivity**	**Clay type**	**Dominant clay mineral type**
≤ 1	Negligible	Non-swelling	Kaolinitic
1.0-1.5	Low	Mixture of swelling and non-swelling	Kaolinitic and Montmorillonitic
1.5-2.0	Moderate	Swelling	Montmorillonitic
2.0-4.0	High	Swelling	Montmorillonitic
>4.0	Very high	Swelling	Montmorillonitic

2.4.2 X-Ray Diffraction (XRD)

X-ray diffraction (XRD) method is widely used to determine the atomic structure and minerals of fine-grained soil. The electromagnetic spectrum with wavelengths ranging from 10^{-3} to 10 nm is known as X-rays. In the laboratory setup, X-rays are generated by decelerating the fast moving electrons. An X-ray tube consisting of a filament electron source and metal target is utilized to produce electromagnetic waves during XRD tests. The X-ray tube is evacuated to avoid absorption of electrons. A specified current (10-30 mA) is allowed to flow through the filament under high voltage (30-50 kV). The current between filament and target is kept constant during the tests. The emerged electrons from filament decelerate rapidly after impinging on the target; as a result, X-ray radiates (Harris and White, 2007).

The mechanism of X-ray radiation has been discussed by Mitchell and Soga (2005). According to them, one of the two following phenomena can occur when high-energy electrons hit the target:

- The electrons from the inner shell of the target electron can be displaced and the electrons located in the outer shell fill the vacancy. During the process, X-ray photons with the wavelengths and intensity characteristics of the target atoms are emitted. However, electronic transfer at different shells may result different characteristic wavelength and intensity.
- The high-speed electrons can slow down the electrical field of the target material. This deceleration converts the energy to heat and X-ray photons. The X-ray photons produced in this way are independent and appeared as a band of wavelengths.

The spacing between the crystals of atomic planes is in the order of X-ray radiation. Therefore, X-ray can be utilized to analyze the crystal structure of a particular material. The coherently scattered radiations (without loss of energy) develop an interference pattern when the distance between the scattering centers are comparable with wavelengths and the radiated lights are arranged in a regular array. This phenomenon is known as diffraction. The phases of radiations depend on the spacing of the planes and wavelength.

The conceptual framework of mineral identification can be stated as "the two minerals have different atomic distances in three dimensional spaces and therefore, produce different radiation wavelengths."

An illustration of X-ray radiations and their dependency on the crystal spacing is presented in Figure 2.7. The present minerals can be identified using Bragg's law during XRD tests. According to the law:

$$n.\lambda = 2dSin\theta \quad (2.1)$$

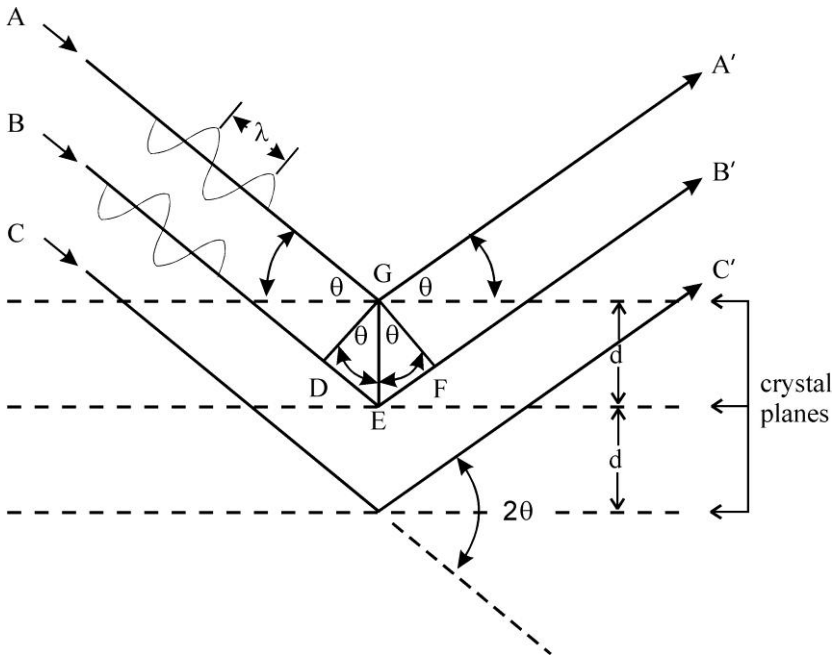

Figure 2.7 Bragg's law (Harris and White, 2007)

Figure 2.7 indicates a parallel X-ray beam impinges the target material at an angle of ɵ. The crystal planes are separated at a distance of d. If the wave reflected from plane E is to reinforce the wave reflected from plane G, then Bragg's law can represent length difference between the two waves. Bragg's law correlates crystal spacing and angle with the integer of wavelength.

Harris and White (2007) emphasized the importance of sample preparation for XRD tests. According to him, the soil sample should be fine enough to ensure adequate statistical representation of the constituents crystal planes and to minimize diffraction-related artifacts. It is important to homogenize the sample to obtain representative patterns before XRD tests. Therefore, randomly-oriented powders can be used in the

XRD analysis of soils to minimize the orientation preference of the wave length (Deng et al. 2009).

2.4.3 Scanning Electron Microscope (SEM)

Scanning electron microscope (SEM) uses high-energy electron beams to analyze the objects on a very fine scale. SEM has the ability to provide information about the topography (surface features of an object), morphology (size and shape of the constituent particles), composition (the elements and compounds) and crystallographic information (the arrangement). Voutou and Stefanaki (2008) described the mechanism of SEM in a review. A brief description of the mechanism can be presented herein.

A series of monochromatic electrons are produced from a point source, typically known as electron gun. There are two types of guns, i.e. conventional and field emission electron guns. The basic differences between two electron guns are the mechanism of electron production and potential in the vacuum tube. However, the overall objective of the guns is to generate high-energy electron beams.

When an electron beam strikes the atoms of the target material, both elastic and inelastic scattering of electrons can occur. As a result, back scattered, secondary and auger electrons are emitted from the surface. Secondary electrons are important to identify fabric structure of soil using SEM. The incident electron excites an electron in the specimen and it loses a substantial portion of its energy during this process. The excited electrons try to move towards the surface of the specimen, and are subjected to elastic and inelastic collisions until it reaches the surface. The electrons can escape from the surface if it has sufficient energy.

The development of secondary electrons is closely related with the topography of the specimen. These electrons (located close to surface, <10 nm) can escape from the sample surface due to their low energy (5eV). The number of the secondary electrons is generally higher for targets consisted of high atomic number and angle of incidence. Moreover, it indicates the strongest region of the electron energy spectrum. Therefore, secondary electrons provide information about the surface topography.

The constituent of the specimens can be differentiated using the back scattered electrons. The number of backscattered electrons varies with the atomic number of the specimen. The electrons emitted from the elements consisted of higher atomic number appear brighter than the elements with lower atomic number. A schematic of the type of radiation during SEM tests is presented in Figure 2.8.

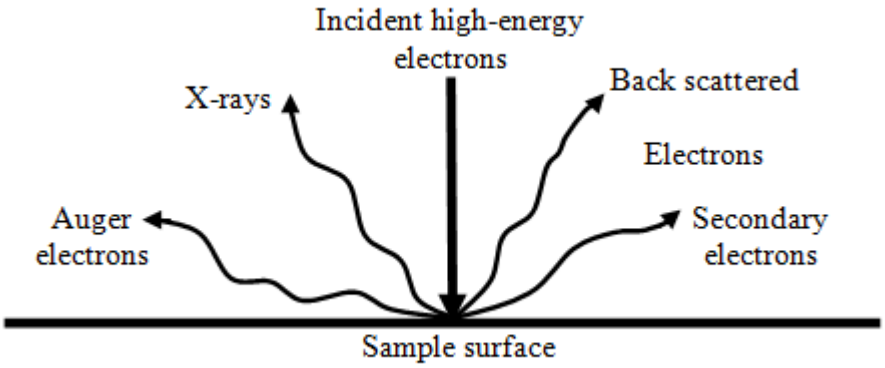

Figure 2.8 Effects produced by electron bombardment of a material

2.4.4 Elemental Analysis using Energy Dispersive Spectroscopy (EDS)

Energy-dispersive X-ray spectroscopy (EDS) is an analytical method for the identification of constituent elements of a specimen. The basic physics of this technique is to analyze the unique interaction of a specific atomic structure under X-ray excitation. At rest, the electrons remain in discrete energy levels and bound to the nucleus. Due to the strike of incident high-energy beam, excitation may occur in an inner shell, which allows the electron to escape from the existing shell. The excited electrons jump into the next energy level while creating a void in the parent shell. An electron from higher-energy shell fills the void space and release energy in the form of X-rays. The number and energy of the X-rays emitted from a specimen can be evaluated by an energy-dispersive spectrometer, which can also provide information about the constituent elements.

According to Voutou and Stefanaki (2008), the excitation in electrons occurs due to inelastic scattering. All the unstable or excited electrons have an affinity to return to the ground state. Therefore, atomic relaxation occurs which allows the electrons to radiate additional energy. The relaxation energy is the constitutive characteristics of each element. Based on the relaxation energy, elemental composition can be determined using EDS X-ray detector.

2.4.5 Soil Pore Water Characterization

The ion composition analysis of soil pore water is typically performed using Ion Chromatography (IC) test. During IC tests, the extracted pore water is injected into the carrier fluid. The compound mixture is then allowed to pass through a column, which

contained adsorbent. The composed ions are separated due to the interaction of dissolved ions in the pore water, carrier fluid and adsorbent. It is recommended to reduce the movement of carrier fluid and enhance the conductance of separated ions during IC tests. The schematic of IC test method is presented in Figure 2.9.

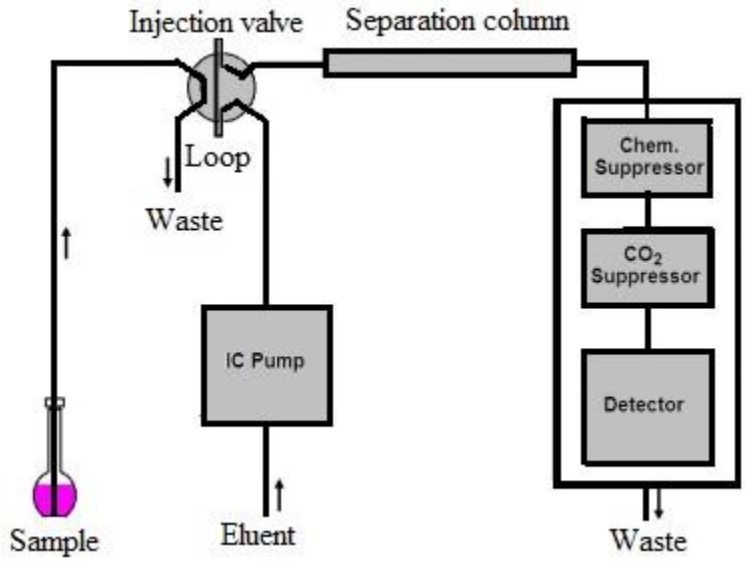

Figure 2.9 Ion chromatography (IC) test procedures (http://www.metrohm.co.uk)

2.5 Electrical Conduction in Geomaterials

2.5.1 Electrical Conduction Phenomena

The fundamental physics utilized in the measurement of electrical resistivity of soil is related to the Ohm's law where voltage is the product of current and resistance of the material. A schematic of current flow through a cylindrical section is presented in Figure 2.10.

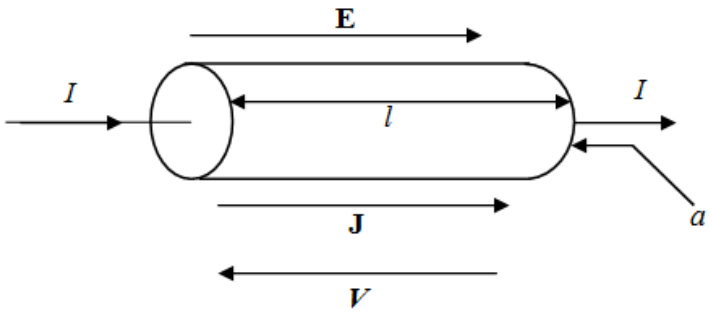

Figure 2.10 Flow of current through a cylindrical cross section

The current density (J) is a microscopic vector quantity and can be defined as the electric current per unit cross sectional area. The current is represented by the dot product of current and cross sectional area as follows:

$$\boldsymbol{I} = \int \boldsymbol{J}.d\boldsymbol{A} \tag{2.2}$$

If the electric field vector is E, then the potential difference ΔU can be written as

$$\Delta\, U = -\int \boldsymbol{E}.d\boldsymbol{l} \tag{2.3}$$

dl is the element along the integration path of electric field vector E.

In a uniform electric field, the above two equations can be substituted in Ohm's law:

$$U = IR \text{ (Ohm's law)} \tag{2.4}$$

$$E.l = J.A.\frac{\rho.l}{A} \tag{2.5}$$

$$E = J.\rho, Or\ E = \frac{J}{\sigma} \tag{2.6}$$

where, ρ is the resistivity of the material, which is a function of resistance, length of conduction path and cross sectional area of the conductive material. σ is the conductivity of the material that is reciprocal of resistivity.

The DC resistivity can also be regarded as the retardation of low frequency alternative current (AC) signals. Therefore, magnetic properties of the material can be ignored at low frequency condition and Maxwell's equation can be written as :

$$\nabla . \boldsymbol{E} = \frac{1}{\varepsilon_0} q \tag{2.7}$$

$$\nabla \times \boldsymbol{E} = 0 \tag{2.8}$$

where E is the electric field in the vector form, ε_0 is the dielectric permittivity of the free space (8.854×10^{-12} F/m) and q is the charge density. The electric field (E) can be presented as the gradient of electric poetical (U) as follows:

$$\boldsymbol{E} = -\nabla U \tag{2.9}$$

In a three dimensional space (x, y, z)

$$\nabla . \boldsymbol{E} = \frac{1}{\varepsilon_0} q\,(x, y, z) \tag{2.10}$$

$$\boldsymbol{E} = -\nabla U\,(x, y, z) \tag{2.11}$$

substituting the vector **E**, the expression can be presented as

$$\nabla^2 U\,(x, y, z) = -\frac{1}{\varepsilon_0} q(x, y, z) \tag{2.12}$$

The Dirac delta function can be employed to describe the continuity equation of a point in 3D space (Loke, 2001).

$$\nabla . \boldsymbol{J}\,(x, y, z, t) = -\frac{\partial q\,(x,y,z,t)}{\partial t} \partial(x)\partial(y)\partial(z) \tag{2.13}$$

Based on the vector form of Ohm's law, the above equation can be rearranged to

$$-\nabla . [\sigma(x, y, z)\nabla U(x, y, z)] = \frac{\partial q(x,y,z,t)}{\partial t} \partial(x - x_s)\partial(y - y_s)\partial(z - z_s) \tag{2.14}$$

where x_s, y_s and z_s are the coordinates of the injected current source. The source of current can be represent considering an elemental volume ΔV:

$$\frac{\partial q(x,y,z,t)}{\partial t}\partial(x-x_s)\partial(y-y_s)\partial(z-z_s)=\frac{I}{\Delta V}\partial(x-x_s)\partial(y-y_s)\partial(z-z_s) \quad (2.15)$$

The current *I* can be injected through a point source i.e. electrodes in the field condition. At an isotropic non-uniform 3D medium, a partial differential equation of electric potential can be developed by replacing the equation 2.14 into 2.15.

$$-\nabla.[\sigma(x,y,z)\nabla U(x,y,z)]=\frac{I}{\Delta V}\partial(x-x_s)\partial(y-y_s)\partial(z-z_s) \quad (2.16)$$

This is the basic equation for the determination of potential distribution in the subsurface under the application of current from a point source.

2.5.2 Electrical Conduction in Clayey Soil

Electrical conduction in a particulate media generally occurs by the movement of ions through electrolytic pore water in the void and surface charge (Bryson, 2005). In coarse-grained soil, conduction is largely electrolytic and depends on the interconnected pore space, granular skeleton, electrolyte conductivity and degree of saturation (Santamarina et al. 2001). However, surface charge is an important parameter in the electrical conduction of clayey soils. Clay particles possess charge deficits due to substitution of ions at crystal structure and acid-base reaction of silanol-aluminol (Si-O-H and Al-O-H) groups with water. Adjacent cations are attracted to the clay particles to counter balance the net negative charge. The density of cations is high around the solid surface; however, concentrated cations try to diffuse to equalize concentration throughout the structure. The diffusion phenomena are restricted by the negative electrical field of clay particles and anions are also moved away because of the negative force of the particles. As a result, relatively mobile ions consisting both positive and negative charges

exist contiguous to the adsorbed layer. The charged surface and distributed charge surface together is known as electrical double layer. The plane along which the counter ions are strongly adsorbed with negative charge of particles is designated as Stern layer. An application of external electrical field results charge separation in the diffuse double layer along Z-potential plane (Revil et al. 1998; Rinaldi and Cuestas, 2002). Therefore, electrical conduction in clayey soil depends on bulk fluid and surface conductivity. A schematic of the location of diffuse double layer (DDL), Stren layer and precipitated ions in clays is presented in Figure 2.11.

The interaction of water with clayey soil also plays a pivotal role in the electrical conduction. In dry condition, adsorbed cations are tightly held together by the negative charge of clay particles. After neutralizing the net negative charges of clay particles, excess cations exist as salt precipitates. Precipitated salts go into the soil-water solution in the presence of moisture. Previous study indicated that the electrical and thermodynamic properties of adsorbed water are different from free water (Holtz and Kovacs, 1981). In addition, Revil et al. (1996) emphasized the role of chemical reaction in clay surface in the presence of water. According to the study, a particle surface with silanol group can be dissociated to positive or negative charges ($SiOH \leftrightarrow SiO^{-}+H^{+}$/ $SiOH+ H^{+}\leftrightarrow SiOH_2^{+}$) based on the chemical reaction in the presence of water.

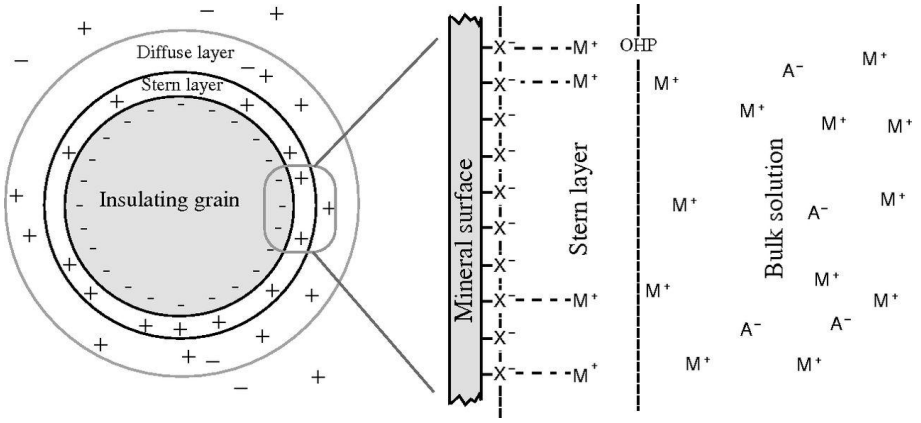

Figure 2.11 Location of diffuse double layer (DDL), stren layer and precipitated ions in clays (http://geophysics.geoscienceworld.org)

2.6 Electrical Mixing Models of Soil

Archie (1942) developed an empirical formula to correlate bulk resistivity of saturated soil with the pore fluid resistivity and porosity. If the resistivity of soil is ρ, resistivity of pore fluid is ρ_w and porosity is n, then Archie's formula can be stated as:

$$\rho = a.\rho_w.n^{-m} \tag{2.17}$$

where, a and m are the fitting and cementation parameters, respectively. According to the study, the value of m depends on the interconnectivity of pore network and tortuosity. In an unsaturated media, Archie's law can be presented as:

$$\rho = a.\rho_w.n^{-m}.S^{-B} \tag{2.18}$$

where, S is the degree of saturation.

Archie's law was developed based on the sandy soil; therefore, the role of surface charge in electrical conduction of clayey soil was not described in the model. However, surface charge has been reported as an important parameter in the electrical conduction of

fine-grained soil. Therefore, several theoretical and experimental investigations have been performed to explain the electrical conduction in clayey soil.

Sauer et al. (1955) suggested flow of current through soils using three-element network model. According to the authors, current flows through surface charge and pore fluid along a combined series and parallel paths in clayey soils. The conductivity of a clayey particulate media (σ) can be described by the following equation:

$$\sigma = \frac{a.\sigma_s.\sigma_W}{(1-e).\sigma_W + e.\sigma_s} + b.\sigma_s + c.\sigma_W \quad (2.19)$$

where σ_s is the surface conductance, σ_w is the pore water conductivity, constants a, b, c, d, and e are functions of porosity and degree of saturation. The current flow paths and equivalent circuit diagram of three element network model is illustrated in Figure 2.12.

Waxman and Smits (1968) developed a simplified model, where the series effects of surface conductance and pore fluid conductivity were not considered. The contribution of series path was substituted by a constant surface conductance. The system was equivalent to a circuit composed of two resistors connected in parallel direction. Therefore, the proposed expression is known as two parallel resistor model. According to the model, the electric conductivity of a soil (σ) can be expressed as:

$$\sigma = X.(\sigma_s + \sigma_W) \quad (2.20)$$

where, X is a constant that is reciprocal to formation factor.

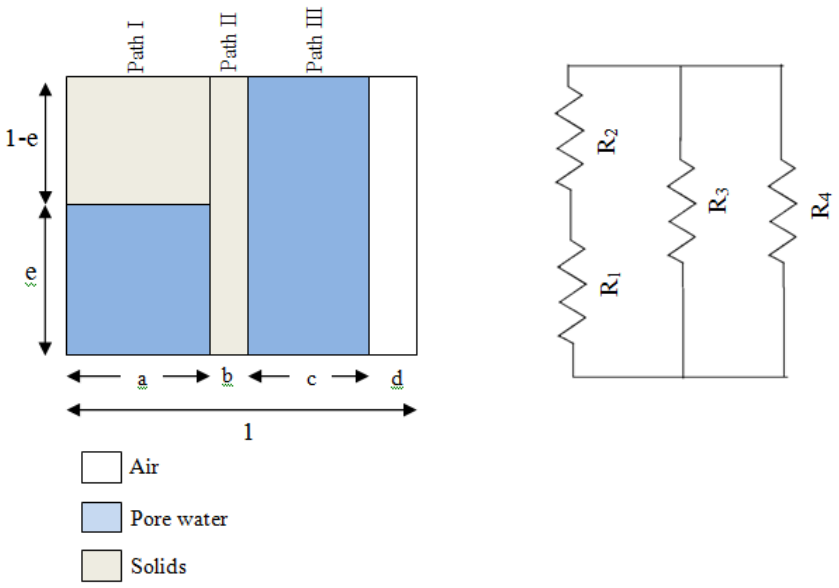

(a) (b)

Figure 2.12 Three element network model a) possible current flow paths (b) equivalent resistance

Shah and Singh (2005) suggested a generalized form of Archie's law for fine-grained soil. According to the authors, the effect of surface conductivity can be included in the cementation factor of Archie's law. Hence, the proposed relationship in terms of conductivity can be presented as:

$$\sigma = c.\ \sigma_w.\ \theta^m \tag{2.21}$$

c= 1.45 when CL<5% and c=0.6 $CL^{0.55}$ when CL≥5%

m= 1.25 when CL<5% and m=0.92 $CL^{0.2}$ when CL≥5%

where, σ is bulk conductivity of soil, σ_w is pore water conductivity, θ is volumetric moisture content and CL is percentage of clay fraction in soil.

In most of the geophysical application, relation between bulk soil resistivity and pore water resistivity is measured with the aid of formation factor (F). Formation factor can be given by the ratio of bulk resistivity (ρ) and pore water resistivity (ρ_w) such as

$$F = \frac{\rho}{\rho_w} \tag{2.22}$$

It is evident from the electrical mixing models that clay soil is more conductive than sandy soil. However, saturated sandy soil may demonstrate low resistivity than dry compacted clay. Because of these factors, overlapping of resistivity values is observed for different type of soils. Typical ranges of electrical resistivity value of water, soil and rock are presented in Table 2.4.

Table 2.4 Typical ranges of resistivity for different materials (Delleur, 2007)

Material	**Resistivity (Ohm-m)**
Sand (dry)	10^3-10^7
Sand (saturated)	10^2-10^4
Silts	10^2-10^3
Shale	10-10^3
Clays	1-10^3
Humid Soil	50-100
Cultivated Soil	200
Rocky Soil	1000
Sandy Soil (dry)	7100
Sandy Soil (saturated)	150
Loamy Soil (dry)	9100
Loamy Soil (saturated)	500
Clayey Soil (dry)	3700
Clayey Soil (saturated)	20
Sandstone (saturated)	25
Limestone (dry)	10^9
Limestone (saturated)	40
Basalt	100
Granite	10^3-10^5
Coal	10^4
Fresh Water	30-10^4
Permafrost	10^2-10^5
Dry Snow	10^5-10^6
Ice	10^3-10^5

2.7 Geotechnical Parameters Affecting Electrical Resistivity

There are several factors that may affect the electrical resistivity of soil. Moisture content is identified as one of the major factors that cause change in soil resistivity

(McCarter 1984). The effect of degree of saturation (Abu-Hassanein et al. 1996), organic content (Ekwue and Bartholomew 2011), pore water composition (Kalinski and Kelly 1993), and geologic formation (Giao et al. 2003) are also significant. Because of the interaction of moisture with the surface charge of clay particles, the ion content has a significant effect on the electrical conductivity of clayey soil (Fukue et al. 1999; Yang 2002). A detail discussion on the influential factors affecting electrical resistivity are presented in the following subsections

2.7.1 Moisture Content

The engineering behavior of clayey soils is highly influenced by the presence of moisture. Due to high surface activity, clay particles are easily hydrated by water, and surrounded by several layers of moisture films. The water adjacent to the crystal structure of the clayey soil is known as adsorbed water. The physico-chemical phenomena of clayey soils largely depend on this water. Therefore, the amount of moisture present in the soil is one of the basic parameters a geotechnical engineer needs to know. Typically moisture content of soils are determined either weight (gravimetric) or volume (volumetric) basis. Gravimetric moisture content can be defined as the ratio of water present in the void to the soil solids. On the other hand, volumetric water content measures moisture content in terms of volume of water. It is calculated from the ratio of water volume present in soil and total volume.

Electrical conductivity occurs due to the displacement of ions in the pore water. When moisture content increases from air dry to full saturation, adsorbed ions in the solid particles are precipitated in the pore water. Free electrical charges cause a reduction in

electrical resistivity under the application of electric field. Therefore, electrical resistivity decreases with the increase in moisture. It is reported that the rate of reduction in resistivity with moisture is significant below 15% moisture content (Samouelian et al., 2007).

Mojid and Cho (2006) described the variation of electrical conductivity (EC) with moisture based on the formation stages of diffuse double layer (DDL). Tests were conducted on marine clays, bentonites and bentonite-sand mixtures. The study results indicated that the EC of the test specimens was low at their dry state and increased to a maximum value at high moisture contents. After that, the EC of the soil remained constant over a small range of moisture content; however, decrease in EC occurred for further increase in moisture. According to the authors, the variation of EC with water content was associated with the developmental stages of DDL in the samples. At low water content, the present cations in the clay surface are exposed to the moisture and adsorbed to develop DDL. However, the thickness of DDL is very thin at this moisture condition and clay particles are not in electrical contact through their DDLs. With the increase of moisture, the cations and adsorbed water surround the clay particles. At this condition, electrical conductivity increases because of the presence of continuous pathway. However, the DDLs start dissociating from each other at very high moisture contents.

Pozdnyakov (2006) divided electrical resistivity vs. natural logarithm of moisture content curve into various segments as presented in Figure 2.13. The segments of the curve were designated as adsorbed water, film water, film capillary water, capillary

water, and gravitational water. According to the author, electrical resistivity decreased rapidly with the increase of moisture content in the adsorption water zone. Although the ions of water molecules are immobile in the adsorbed water zone, the dipolar water creates a conductive path for electrical current. Therefore, electrical resistivity decreased substantially with the increase of moisture in the adsorption zone. However, the rate of reduction decreased in the film water zone because of the increase in Van der Waals' force. When maximum possible thickness of water film was developed, pore water goes from film to fissure. The molecular attraction force is higher than the capillary force in the film capillary water zone. Therefore, electrical resistivity decreased less dramatically in the film capillary and capillary water zone. In the gravitational water zone, mobility of electrical charges become independent of movement of water molecule ions, and electrical resistivity is almost independent of water content.

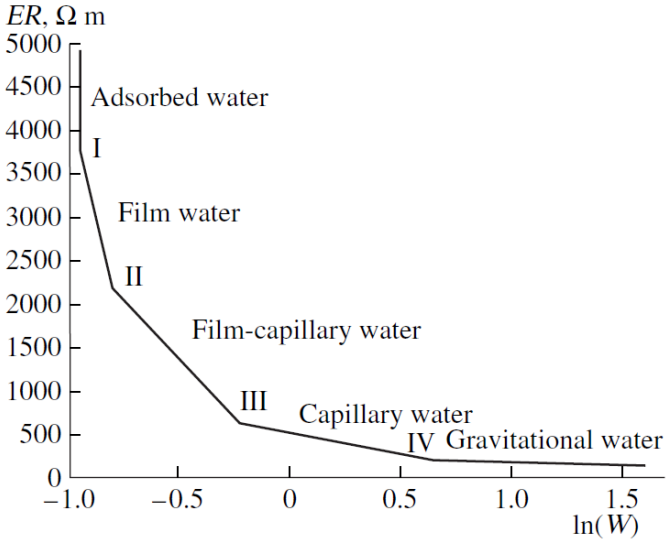

Figure 2.13 Soil moisture and electrical resistivity relationship (Pozdnyakov, 2006)

2.7.2 Degree of Saturation

According to the literature, an increase of degree of saturation causes reduction in soil resistivity; however, the relationship is highly influenced by critical degree of saturation. Critical degree of saturation is corresponded to minimum amount of water required for the development of continuous water film around soil particle. Typically, an abrupt increase of soil resistivity occurs below critical degree of saturation (Bryson, 2005).

According to the study of Rinaldi and Cuestas (2002), relationship curve of conductivity and degree of saturation is concave upward. The observed variations might occur due to the reduction in pore space and enhanced contacts between the particles at high degree of saturation. The effect of degree of saturation on conductivity at different electrolyte concentration is presented in Figure 2.14.

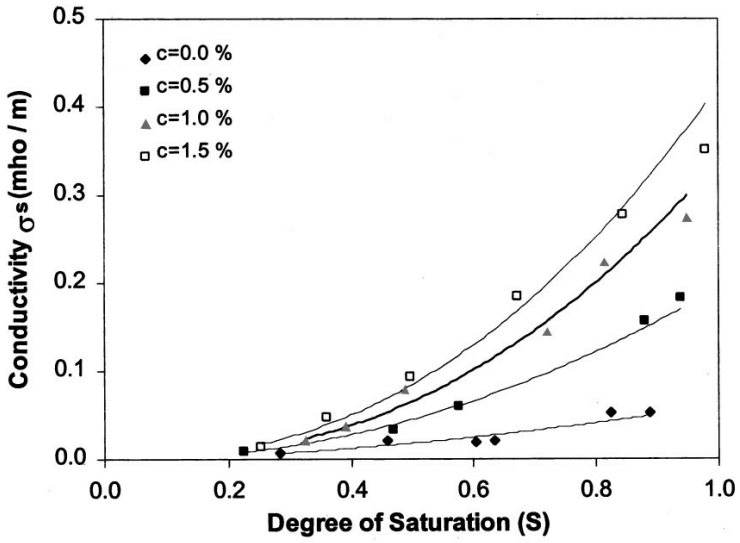

Figure 2.14 Influence of degree of saturation in soil conductivity (Rinaldi and Cuestas, 2002)

Matsui et al. (2000) performed a study on the correlation between electrical resistivity and physical properties of rock. Various types of granites and sedimentary rocks of Japan were utilized for the study. The rock specimens were saturated with tap water, and resistivity of the samples were measured at different stages of natural drying and artificial desiccation. The study results indicated that the resistivity decreased with the increase of degree of saturation up to a certain level; however, the variation was insignificant beyond that point.

Abu Hassanein et al. (1996) conducted resistivity measurements of four different soils at different initial degree of saturations. It was observed that the electrical resistivity was inversely correlated with initial degree of saturation. It was also mentioned that the initial degree of saturation and electrical resistivity was independent of compactive effort.

2.7.3 Pore Water Characteristics

Electrical conductivity in a porous media depends on the mobility of ions present in the pore fluid. The hydration of precipated salts leads to the formation of electrolytes in the pore water of clayey soil. Hydrated cations and anions move towards cathode and anode under the applied electric field. The movement of ions reaches a terminal velocity when applied electric field and charge interactions (viscous drag force) are in equilibrium (Santamarina et al. 2001). Ion mobility is defined as the terminal velocity of an ion subjected to a unit electric field and be presented by Einsten-Nernst equation as presented below:

$$u = \frac{V(ion)}{E} = \frac{ze}{6\Pi\eta R_h} \quad (2.23)$$

here, V(ion) is the velocity of ion (m/s), E is the electric field (V/m), z is the valence of ion, η is the viscosity of the solution (Pa.s), e is the charge of electron (1.602×10^{-19} C) and R_h is the Stokes' radius of the hydrated ions. A summary of ionic mobility of different ions is presented in Table 2.5.

Table 2.5 Ionic mobility of ions at 25°C (Santamarina et al. 2002)

Cation	**Ionic mobility ($m^2V^{-1}s^{-1}$)**	**Anion**	**Ionic mobility ($m^2V^{-1}s^{-1}$)**
H^+	36.2×10^{-8}	OH^-	20.5×10^{-8}
K^+	7.6×10^{-8}	SO_4^{2-}	8.3×10^{-8}
Ba^{2+}	6.6×10^{-8}	I^-	8.2×10^{-8}
Al^{3+}	6.5×10^{-8}	Br^-	8.1×10^{-8}
Ca^{2+}	6.2×10^{-8}	Cl^-	7.9×10^{-8}
Mg^{2+}	5.5×10^{-8}	NO_3^-	7.4×10^{-8}
Na^+	5.2×10^{-8}	F^-	5.7×10^{-8}
Li^+	4.0×10^{-8}	HCO_3^-	4.6×10^{-8}

The electrical conductivity is affected by present ions in the soil because of the varied ionic mobility. Different ions such as H^+, OH^-, SO_4^{2-}, Na^+, Cl^- present in the soil. They do not affect the conductivity in the same way because of their difference in ion mobility. A study conducted by Kalinski and Kelly (1993) indicated that electrical resistivity of soil decreases with the increase of pore water conductivity. Based on the experimental results, the following equation was developed to estimate pore water conductivity:

$$ECw = ECo - \frac{ECs}{\theta(a\theta+b)} \quad (2.24)$$

where, EC_w = pore water electrical conductivity, EC_s= apparent Soil particle surface electrical conductivity, EC_o= bulk Soil electrical conductivity, Θ = volumetric water content, a and b= constant.

Rinaldi and Cuestas (2002) emphasized the influence of sodium chloride and other electrolytes on loess soil of Argentina. The soil samples were compacted at a constant density and electrolytes were added. Electrical conductivity was measured at different concentrations of various electrolytes. The study results suggested a linear relationship between conductivity of soil and electrolyte as presented in Figure 2.15. According to the study, samples contain sodium showed highest conductivity, followed by magnesium and potassium. The difference in conductivity was due to the ion mobility of different electrolytes, adsorption and soil structure.

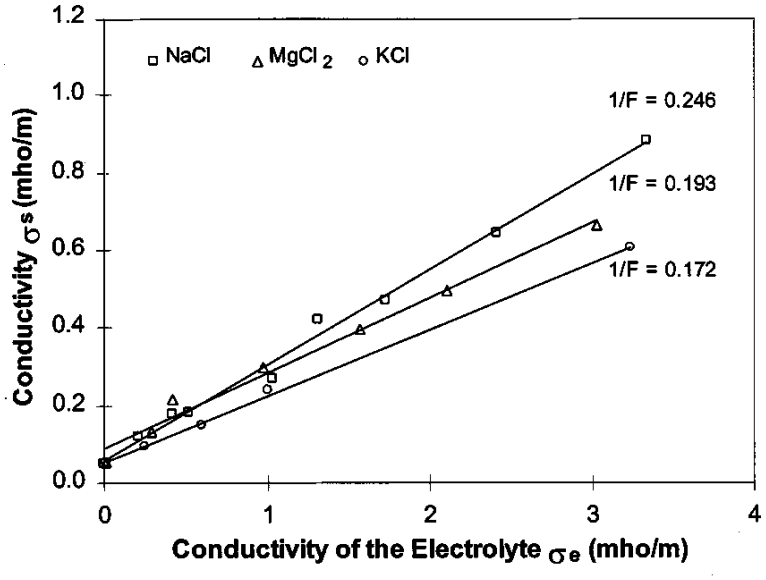

Figure 2.15 Relationship between conductivity of saturated sample at different electrolytes (Rinaldi and Cuestas, 2002)

Although electrical conductivity increases with the presence of ions in pore water, the mobility of charge may be restricted due to the availability of ions at a high concentration. A reduction in conductivity may occur at that condition (Santamarina et al. 2001).

2.7.4 Clay Fraction and Atterberg Limits

Abu Hassanein et al. (1996) evaluated the variation of electrical resistivity with Atterberg limits of the soil specimens. The specimens were compacted at optimum moisture contents and dry unit weights using Standard Proctor method. It was observed that soil with higher LL and PI had lower resistivity as presented in Figure 2.16. However, the soil sample with 47% coarse fraction showed high resistivity.

The variation of resistivity with the increase of LL and PI was explained using the mineralogy of the samples. The clay samples with smectite content (high LL and PI) are more active and exhibit higher surface conductivity.

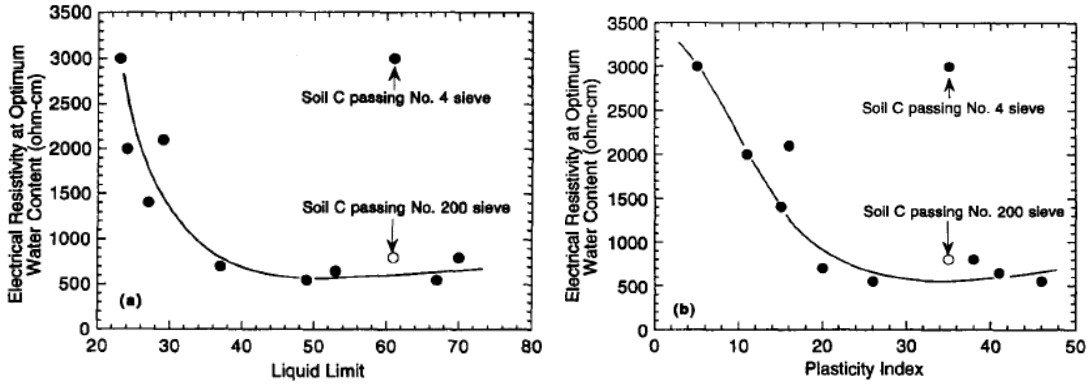

Figure 2.16 Relationship between electrical resistivity and atterberg limits at optimum water content (Abu Hassanein et al., 1996)

Clay fraction is also indicative of the presence of surface charge of a soil specimen. The surface activity and affinity to water increases with the increase of clay fraction. Therefore, electrical resistivity varies with the clay fraction. According to study of Shah and Singh (2011), the cementation (c) and fitting parameters (m) of Archie's law are functions of clay fraction (equation 2.20).

2.7.5 Cation Exchange Capacity and Specific Surface Area

The contribution of adsorbed cations is significant in electrical resistivity of medium and fine-grained soil. It is evident from the literature that the physico-chemical properties such as adsorbed ions, pore water conductivity and surface charge are correlated with cation exchange capacity (CEC) of the soils (Friedman, 2005; Tabbagh and Cozenza, 2007; Schwartz et al. 2008)

Kibria and Hossain (2012) presented a study on the electrical resistivity responses of high plastic clays at varied moisture contents and unit weights. Authors indicated that the effect of specific surface area in electrical conductivity was substantial in fine-grained soil. According to the study, soils with high specific surface area required large amount of moisture for the formation of water film. Thus, electrical resistivity was high for the soils with high SSA when tests were conducted at low moisture contents (below saturation).

2.7.6 Temperature

Electrical resistivity decreases with the increase of temperature because of the agitation of ions. It was observed that an increase in temperature per degree celsius

decreases electrical resistivity by 2.02% (Campbell, 1948). According to the study of Abu Hassanein et al. (1996), an exponential relationship exists between electrical resistivity and soil above zero deg. C. As the electrical resistivity of soils depends on the temperature, experimental measurements should be corrected with respect to a reference temperature to explain the variation of moisture content, unit weight, soil structure and soil type with resistivity.

Several conversion models were developed to express electrical resistivity at a reference temperature. Besson et al. (2008) performed a study on the analysis soil resistivity of two soils at varied temperature conditions. Two types of soils were utilized for the evaluation of performance of the existing models. The study results suggested that the models were mostly empirical and the parameters of the available model depended on the soil solution properties. The available models indicated good accuracy at high volumetric moisture contents. However, a known relationship between resistivity and temperature was required to identify the best conversion model. Based on the investigation results the following model was developed:

$$f(T_m, T_{ref}) = (\frac{T_{ref}}{T_m})^s \; or \; \rho_{ref} = \rho_m \, (\frac{T_{ref}}{T_m})^{-s} \tag{2.25}$$

Here, T_m = medium temperature, T_{ref} = reference temperature, ρ_{ref} = corrected resistivity at reference temperature, ρ_m = resistivity of the medium at T_m, and s= empirical parameter.

2.7.7 Structure and Packing of Soil

Zha et al. (2007) presented a study on the evaluation of expansive soil structure using electrical resistivity measurement. The average formation factor, shape factor and electrical anisotropy index were investigated at different stages of swelling. It was identified that the formation factor and shape factor linearly varied with the increase of swell percentages. In addition, the initial, primary and secondary swellings were determined using the relationship among log-time, formation factor, and shape factor. According to the authors, the decrease in average formation factor was related to microstructure changes, formation destruction, increase in water content and porosity; and decrease in strength, cementation and stability of soils.

2.8 Evaluation of Geotechnical Properties using Electrical Resistivity

2.8.1 Moisture Content

Determination of a representative subsurface moisture profile is difficult because of the heterogeneity and complex hydro-geologic system of soil. Time domain reflectrometry (TDR), neutron probes, gypsum blocks, tensiometers and gravimetric scaling are commonly used to measure moisture distribution in subsoil. However, some of these methods have certain operational limitations. For an example, determination of moisture using TDR is possible within a region of only tens of centimeters around the probe (Goyal et al. 1996). In contrast, electrical resistivity can be utilized to determine moisture condition of subsurface. Previous study indicated that resistivity decreases with the increase of soil moisture. This phenomenon led to several studies to quantify moisture content of soil from resistivity in the laboratory and field scale.

Crony et al. (1951) described a methodology to determine soil moisture using electrical resistance method. The measurement was based on three relationships: the suction of the water in the absorbent and moisture content of the absorbent, moisture content of the absorbent and the resistance of the gauge, the suction of water in the soil and moisture content of the soil. Plaster of Paris and high alumina cement were used as absorbent materials. It was observed that the electrical resistance gauges could be used to determine the soil suction and soil moisture. However, their reliability as a soil moisture meter was doubtful because of the disturbance of the soil. According to the study, calibration of electrical gauges was important to obtain precise results. The measurement of suction and moisture content of the absorbent were identified as major problems in this method because very small differences in mixing and curing of absorbent influenced the results significantly.

Kalinski and Kelly (1993) conducted a laboratory investigation to determine volumetric moisture content from electrical conductivity of soil. The electrical resistivity of soil was measured using four-probe circular cell. Porous plates were utilized to extract water from the soil, and electrical conductivity (EC_w) was determined. The experimental results indicated that the EC_o/EC_w (ratio of soil conductivity and pore water conductivity) increased with the increase of volumetric water content as presented in Figure 2.27. In addition, the following regression equation was developed to determine volumetric water content assuming surface conductivity of 0.24 mho/cm (ECs= 0.24 mho/ cm). It was observed that predicted and measured volumetric moisture contents were in good agreement.

$$EC_0 = EC_s + EC_w\theta(1.04\theta - 0.09) \quad (2.26)$$

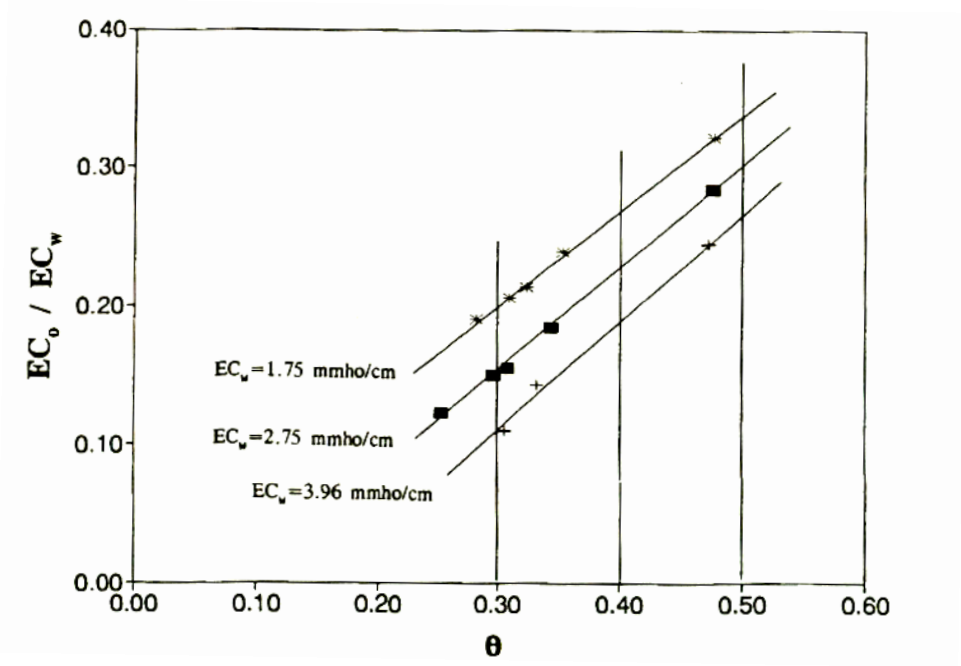

Figure 2.17 Relationship between ratio of bulk soil and pore water conductivity with volumetric moisture content (Kalinski and Kelly, 1993)

Ozcep et al. (2009) presented a study to determine relationship of soil resistivity and water content in Istanbul and Golcuk, Turkey. Electrical resistivity was measured using Vertical Electrical Sounding (VES) in 210 points of two sites. In addition, soil test boring was conducted for the collection of samples. The soil resistivity and moisture content ranged from 1 to 50 Ohm-and 20% to 60%, respectively. Two exponential equations, correlating moisture content with resistivity, were developed for Istanbul and Golcuk area as presented below:

$$W = 51.074\, e^{-0.0199R}, R^2 = 0.76\ (for\ Istanbul) \quad (2.27)$$

$$W = 47.579\, e^{-0.0158\,R}, R^2 = 0.75\ (for\ Golcuk) \quad (2.28)$$

Schwartz et al. (2008) conducted a study to quantify field-scale moisture content using 2D electrical resistivity imaging (ERI) method at Virginia Tech Kentland experimental farm, Mongomery County, Virginia. The ERI and time domain reflectometry (TDR) were used simultaneously to obtain resistivity and moisture content. The 1D resistivity profile was determined from 2D ERI using EarthImager software. The coefficients of Archie's law were numerically optimized for the quantification of moisture content from 1D resistivity. The proposed model utilized extractable cations to represent the role of pore water conductivity in developing Archie's law. The use of extractable cations eliminated difficulties in measuring extracted pore water resistivity. It was observed that the model provided useful results to determine meter-scale moisture heterogeneities compared to small-scale variation.

Brunet et al. (2010) conducted a research to obtain water deficit from electrical resistivity tomography (ERT) in Southern Cevennes, France. During, February 2006 and December 2007, more than 10 ERT were performed on the study area, and volumetric water contents were measured using TDR. Archie's law was calibrated in the laboratory to quantify moisture content and water deficit from ERT. A constant porosity and soil solution resistivity were (porosity of 0.42 and soil solution with resistivity of 22 Ohm-m) considered in the calibration. Based on the laboratory test results, the cementation (m) and saturation coefficient (n) were determined as 1.25 and 1.65, respectively. In-situ soil moisture content and water deficit were calculated from the calibrated Archie's law at 25^0C temperature. Authors indicated that interpretation of water content or water deficit from resistivity was sensitive to temperature, water solution resistivity, porosity, and

inversion algorithm of resistivity tests. The ERT profiles and comparison of predicted and observed water content at different depths are presented in Figure 2.18 and 2.19. It can be mentioned that the solid lines in Figure 2.19 indicates ERT predicted moisture contents.

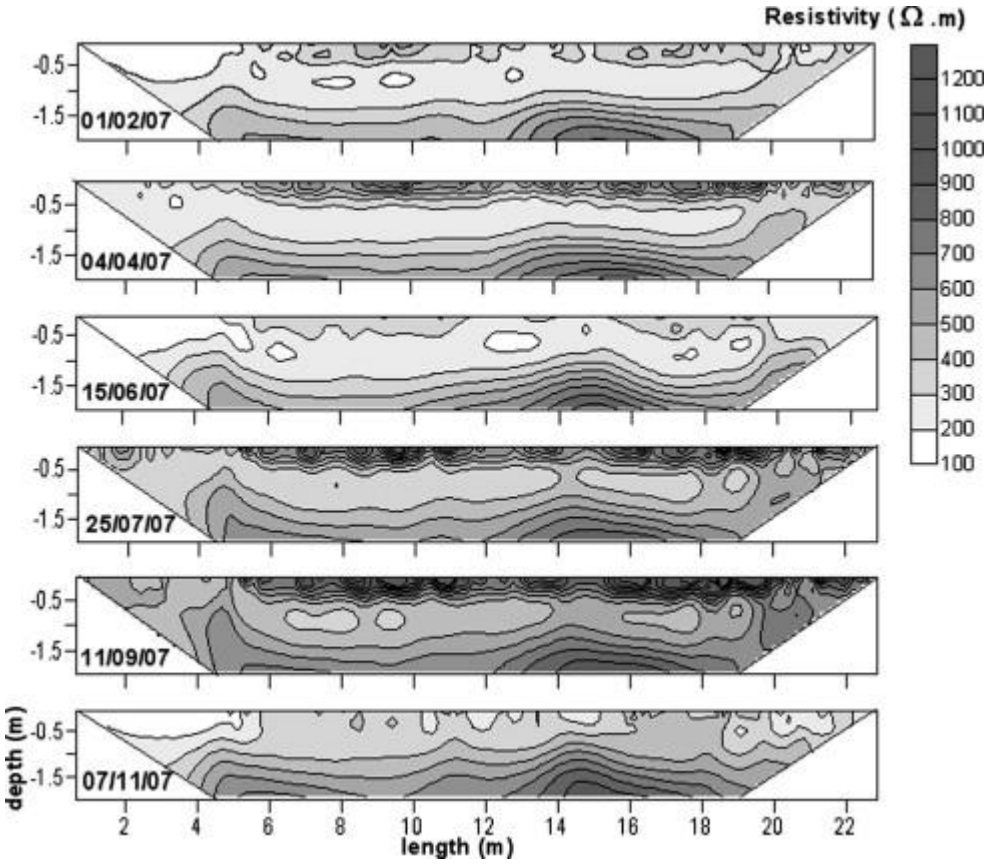

Figure 2.18 ERT (resistivity corrected at 25 deg C) during the year of 2007 (Brunet et al. 2010)

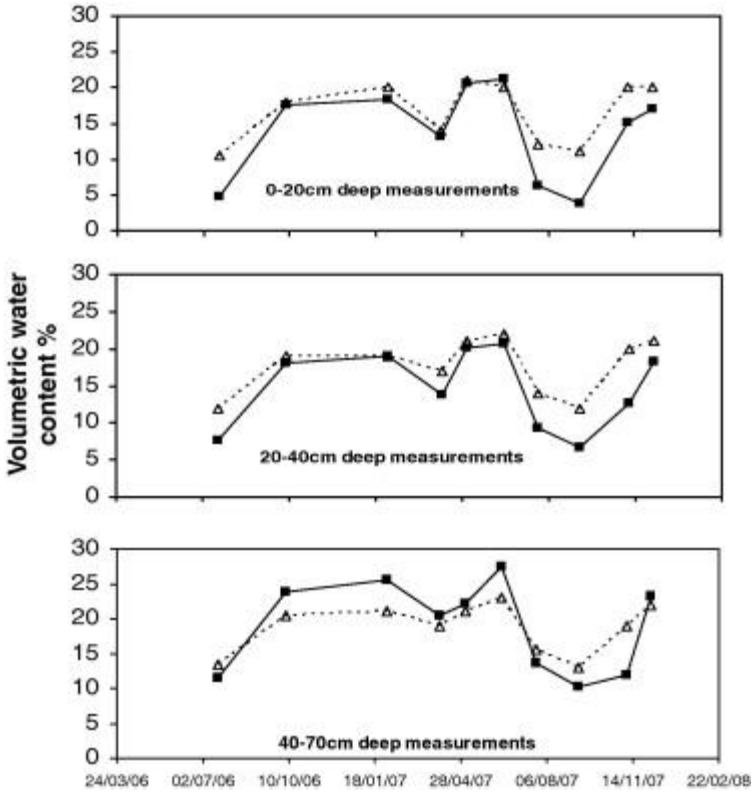

Figure 2.19 Comparison of ERT and TDR predicted water content at depths (a) 0-20 cm (b) 20-40 cm (c) 40-70 cm (Brunet et al. 2010)

2.8.2 Compaction Condition

Rinaldi and Cuestas (2002) performed a laboratory investigation to evaluate the relationship between electrical conductivity and compaction. The soil samples were sieved through No. 40 sieve, and compacted at 18% moisture content. Compaction was conducted using Standard Proctor method in a rectangular mixing pan. After compaction, conductivity was measured using four probe electrode device. Based on the experimental results, iso-conductivity contour was obtained from the test as illustrated in Figure 2.20.

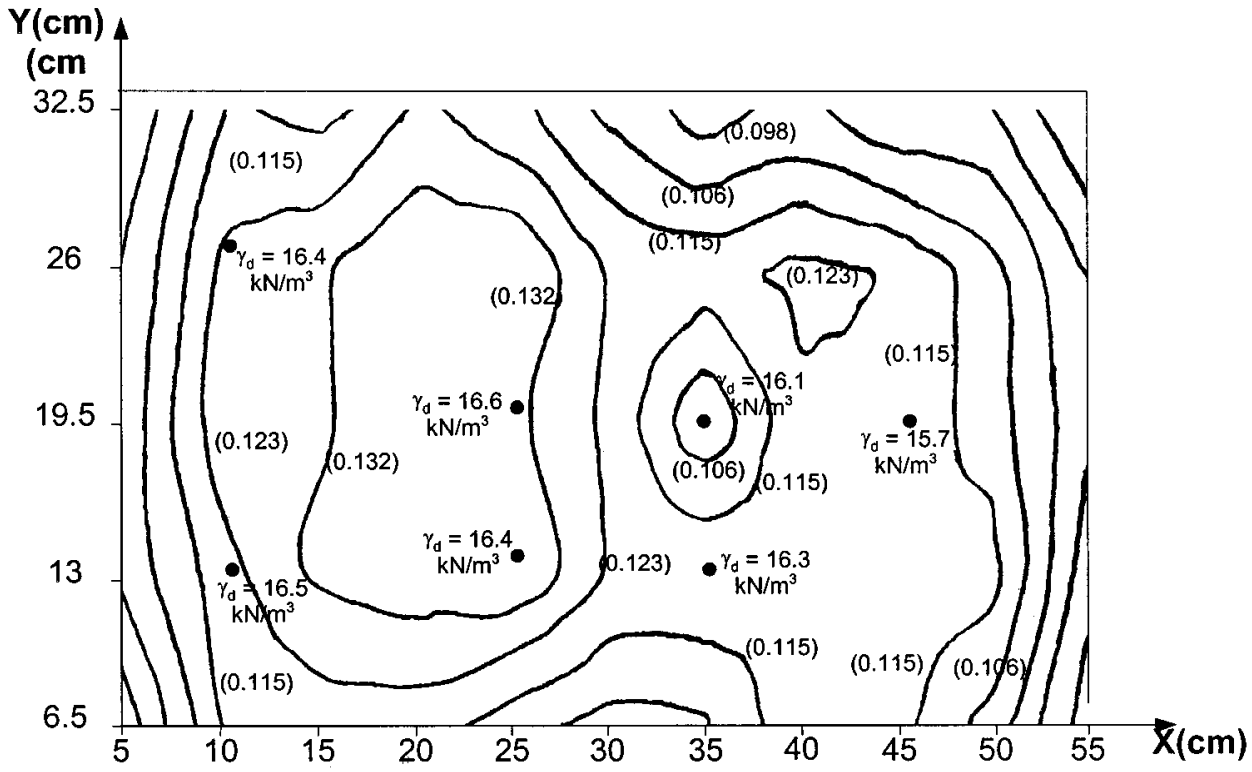

Figure 2.20 Iso conductivity contour of compacted sample, parentheses showed electrical conductivity in mho/m (Rinaldi and Cuestas, 2002)

According to Figure 2.20, the conductivity at central portion was higher than right hand side and border. Authors indicated that the variation of conductivity was attributed due to the variation of soil unit weight. The unit weight was higher at left hand side and decreased at right hand side and border due to the low stiffness of the wall of the mixing pan.

McCarter (1984) conducted a study to evaluate the effect of air void ratio in soil resistivity on Cheshire and London clay. A substantial decrease in soil resistivity was observed for the increase of degree of compaction or degree of saturation. The study

results emphasized compaction condition as an important factor in addition to moisture content for resistivity variation.

Abu Hassanein et al. (1996) performed a comprehensive study on the effect of molding water content and compactive effort in soil resistivity. The soil specimens were compacted at three different compaction methods: a) Standard, b) Modified and c) Reduced Proctor. It was observed that the resistivity was high when soil was compacted at dry optimum, and low when compacted at wet optimum. Moreover, resistivity was sensitive of molding water content below optimum condition. At wet of optimum, resistivity was almost independent of molding water content. Authors indicated that this relation might be useful to evaluate compaction condition of soil. The observed test results on the study are presented in Figure 2.21.

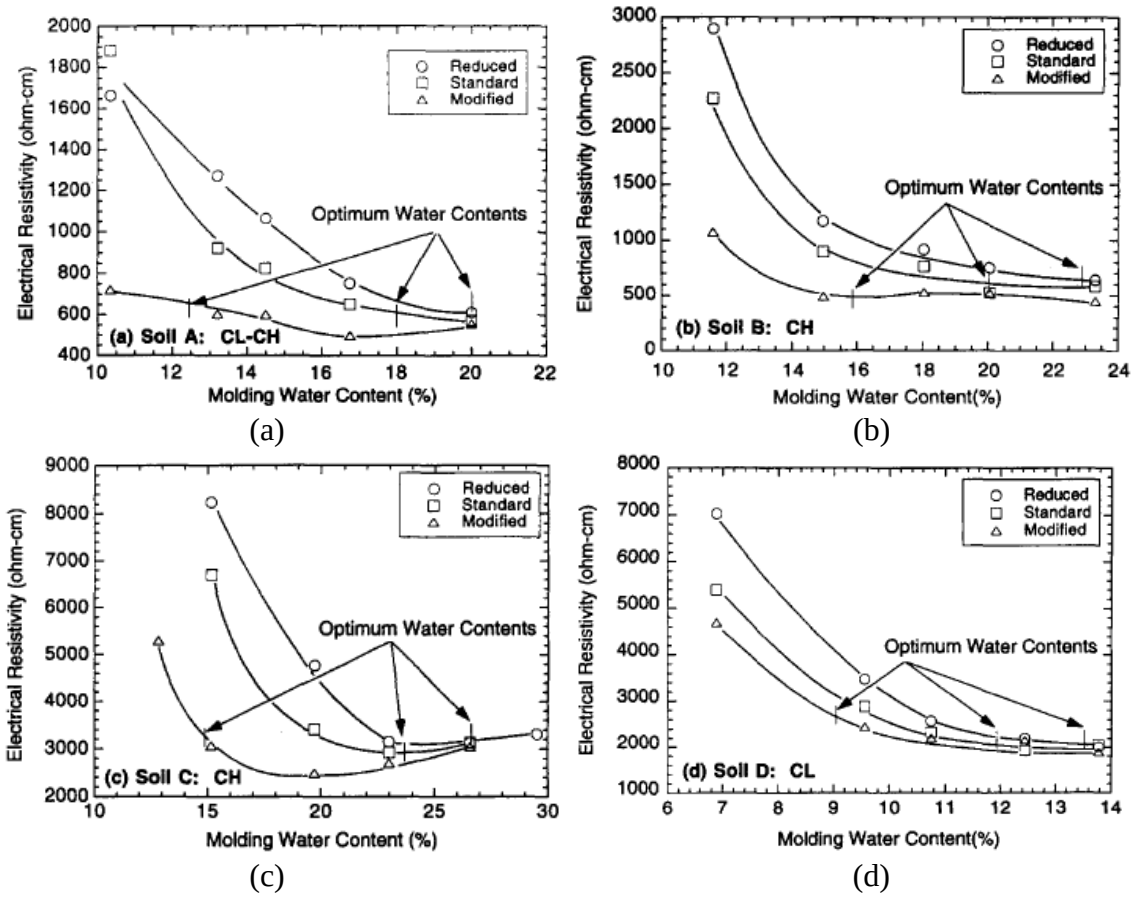

Figure 2.21 Relationship among electrical resistivity, molding water content and compactive effort for different soils (a) Soil A (b) Soil B (c) Soil C (d) Soil D (Abu Hassanein et al. 1996)

The variation of resistivity with molding water content can occur due to structural change of soil during compaction. At low compactive effort and dry of optimum water content, clay clods are difficult to remold. The interclod pores are also relatively large, pores are filled with dielectric air, diffuse double layers are not fully developed, and inter particle contacts are poor at this condition. In contrast, clods of clay can be easily remolded at wet of optimum and high compactive effort, which results in increase in

saturation. An enhanced particle-to-particle contact and formation of bridge between particles improve electrical conductivity of soil (Abu Hassanein et al. 1996).

2.8.3 Hydraulic Conductivity

Hydraulic conductivity depends on the porosity, structure, saturation and tortuosity of soil. As the electrical resistivity also depends on these parameters, several researches have been undertaken to correlate hydraulic conductivity with electrical resistivity (Bryson, 2005).

Sadek (1993) performed a study to explore the possibility of using electrical conductivity as an alternative of hydraulic conductivity in compacted clay liner. An extensive research program was developed which included a) comprehensive review of the influential parameters affecting electrical and hydraulic conductivity b) development of theoretical model to incorporate pore water conductivity and surface conductance, and c) design of a new equipment to study the electro-kinetic properties. The study results indicated that the electrical conductivity of soils were not sensitive enough for the use as an alternative of hydraulic conductivity. The electrical conductivity of a sample with dispersed structure and low hydraulic conductivity was similar to the sample with flocculated structure and high hydraulic conductivity. Author indicated that incorporating surface conductance and internal pore geometry using "Cluster model" might provide a better correlation; however, this required quantification of internal geometry. Although, the electrical conductivity was not proved as a reliable indicator of hydraulic conductivity, the study provided useful insight of electrical properties of soils.

Abu Hassainein et al. (1996) considered four soil specimens to correlate hydraulic conductivity increased with resistivity. However, the study results did not indicate a specific correlation between these parameters.

Arulanandan (1968) discussed the electrical conductivity of saturated kaolinite, illite, and montmorillonite clay in the 50-10^8 cycle/sec frequency range. It was observed that the electrical conductivity increased with the increase of frequency and the required frequency for the first dispersion was independent of particle size. Based on the electrical properties, the microscopic permeability coefficients were evaluated. The study results indicated that the coefficients of Darcy's law were correlated with several electrical properties i.e. conductivity of AC and DC range and ratio of phenomena logic transport coefficient. An schematic of the study results is presented in Figure 2.22.

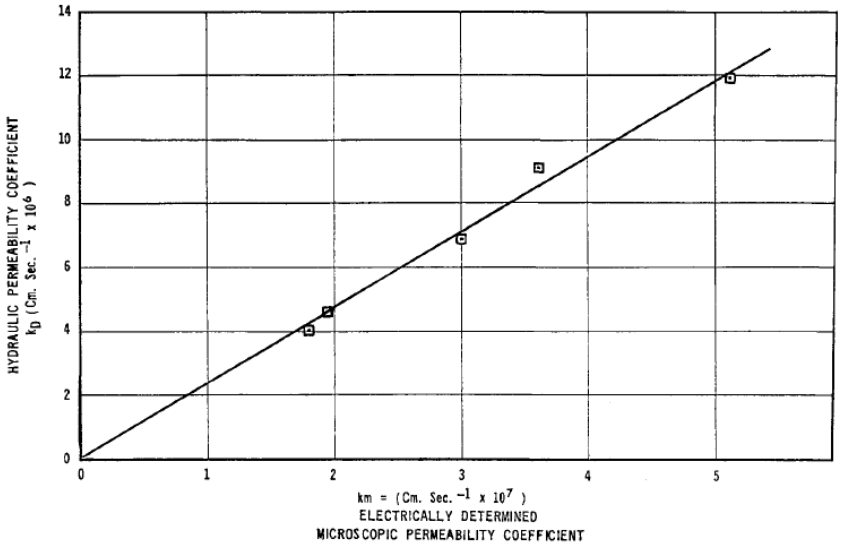

Figure 2.22 Correlation between microscopic and hydraulic permeability coefficients during consolidation of a kaolinite-hydrite MP made homo-ionic to 0.001N NaCl (Arulanandan, 1968)

2.8.4 Consolidation Properties

Consolidation in soil is associated with the dissipation of pore water, reduction in void ratio and change in fabric morphology. Therefore, consolidation properties of soil can be evaluated using electrical properties. McCarter and Desmazes (1997) investigated the changes in electrical conductivity of clayey soil in response to consolidation stages. A modified consolidation cell was utilized to measure the variation in electrical properties with void ratio at saturated condition. The electrical conductivity was determined in the vertical and horizontal direction. It was identified that the changes in void ratio and conductivity with effective stress were very similar. According to the authors, conduction in saturated soil occurred through continuous interstitial water. Therefore, the fractional volume of water and composition of pore fluid influenced electrical properties significantly. Nonetheless, electrical conductivity of soil decreased with the progression of consolidation process due to the dissipation of pore water.

Bryson (2005) correlated void ratio with conductivity from the curve obtained by McCarter and Desmazes (1997). The developed correlation provided a mean to determine consolidation properties from electrical conductivity of soils. One dimensional settlement equation and compression index for normally consolidated clay are presented below (Bryson, 2005):

$$S = \frac{\Delta e}{(1+e)} H = \frac{\Delta \sigma}{1+\sigma v} (\xi)\, H \tag{2.29}$$

$$C_c = \varepsilon\, (\Delta\sigma) \log \left(\frac{P}{P_o}\right) \tag{2.30}$$

where, Δe= change in void ratio, e= initial void ratio, $\Delta\sigma$ = change in vertical conductivity, σ_v= Initial vertical conductivity, ξ= factor relating vertical conductivity and void ratio, H= sample height, P= consolidating pressure and Po= initial pressure.

McCarter et al. (2005) presented a study on the evaluation of structural change during consolidation using electrical resistivity measurements. A typical oedometer was modified to measure the load-deformation and electrical conductivity of a specimen simultaneously. The modified oedometer can accommodate a sample with 250 mm diameter and 185 mm of height. The horizontal and vertical resistivity were determined during loading and unloading conditions. Based on the experimental results, changes in soil structural, formation factor and anisotropy were investigated.

Comina et al. (2008) developed an advanced EIT oedometer for the evaluation of 3D electrical tomography and measurement of seismic wave velocity of soil specimen. The inner walls of the test cell was covered by stiff polyamide to ensure insulation during current flow and reduce wall friction. The concentric rings, having a permeability of 6× 10-6 m/sec, were utilized for the drainage. The electrical resistivity was measured using 42 electrodes hosted on the internal boundary of the cell. In addition, P- and S-wave velocity were determined using the sensors at the top and bottom caps of the cell. A vertical load was applied on the specimen under one-dimensional condition. The diameter of the specimen was 130 mm and the height was ranged between 20 and 60 mm. The newly designed EIT oedometer, wave sensors and measurement setup are illustrated in Figure 2.23.

(a)

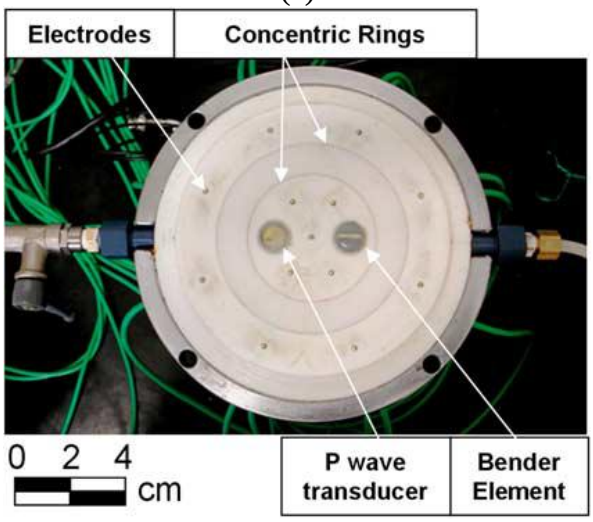

(b)

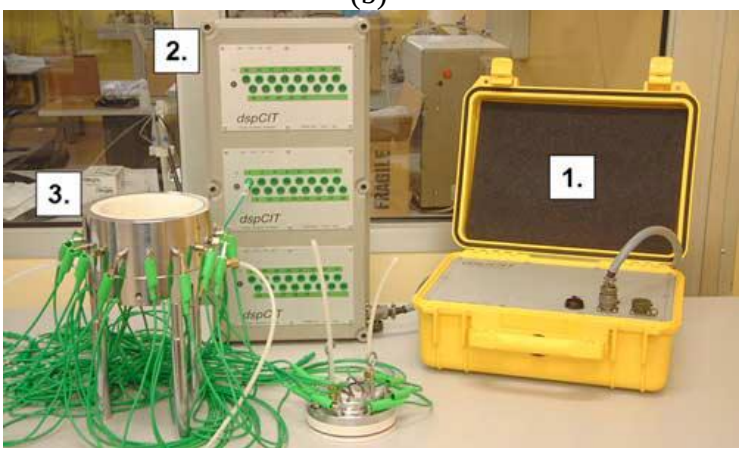

(c)

Figure 2.23 Newly designed EIT oedometer (a) EIT oedometer, (b) wave sensors and (c) measurement setup (Comina et al., 2008)

A number of trial experiments were performed to identify the 3D imaging performance of the cell using homogenous sample, and sample with resistive and conductive inclusion. In addition to that, Ticino sand was utilized to for the simultaneous measurement of deformation, shear wave, compression wave and topographic imaging. It was observed that P-wave velocity of the saturated sample was not varied significantly, while S-wave velocity increased from 120 to 180 m/sec in the 100 to 400 kPa pressure range. The experimental results of electrical conductivity, void and pressure are presented in Figure 2.24. Based on the preliminary results, authors indicated that the newly designed cell was able to evaluate transient process of chemical diffusion, preferential flow path during conduction and changed in mechanical properties.

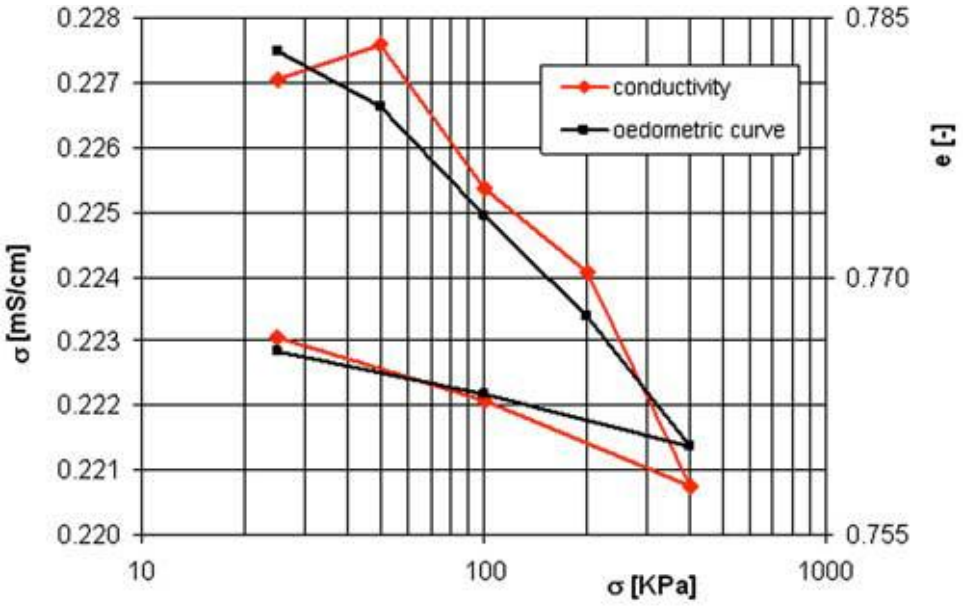

Figure 2.24 The experimental results of electrical conductivity, void and pressure (Comina et al., 2008)

2.8.5 Atterberg Limits

The surface activity is also an influential factor in the liquid limits (LL) and plastic limits (PL) of the soils. Therefore, it is expected that the electrical resistivity and index properties of the soils can be correlated. Bryson (2005) indicated that the LL and PI were related with electrical conductivity according to power function as presented below:

$$LL = (BQ)^{\beta 1}\alpha_1 \tag{2.31}$$

$$PI = (BQ)^{\beta 2}\alpha_2 \tag{2.32}$$

where, BQ= conductivity in siemens/m, LL and PI are in decimals. The coefficient α and β are the function of clay mineralogy.

It can be mentioned that the study of Abu Hassanein et al. (1996) indicated the effect of clay mineralogy on electrical resistivity and index properties of soil. The soil with high smectite content showed increased LL, PI, and electrical conductivity.

2.8.6 Clay Content

Shevinin et al. (2007) conducted a study on the estimation of clay content in soils using electrical resistivity model. The resistivity model considered electrochemical process of soil micropores in the prediction of clay contents. The experimental tests were performed on brine saturated soil samples where the concentration of NaCl ranged from 0.6 to 100 gm/L. Authors suggested that the soil properties i.e. clay content, CEC and porosity can be obtained from resistivity measurements at salinity concentration 0.6 to100 gm/L. The proposed method was compared with the sand-clay mixtures, and indicated an overall error of 20% in the prediction. The method was applied in the several sites of Mexico to determine the clay content, CEC and porosity. It was identified that the

clean and oil contaminated soils were differentiated by a boundary resistivity value; therefore, the model was able to identify the oil contaminated zone.

2.8.7 Mineral Content

Abu Hassanein et al. (1996) described an innovative method to determine bentonite content of soils using electrical conductivity. A detail sedimentation analysis was performed on the test specimens and a calibration curve was developed to correlate electrical conductivity with bentonite concentration at a given temperature. The proposed methods were simple, and required less time to measure the bentonite contenets; however, the performance of the method was not evaluated in the field condition. Moreover, the calibration curve should be verified for the in-situ soil conditions.

2.9 Measurement of Electrical Resistivity

2.9.1 Laboratory Scale

The electrical properties can be studied in the laboratory using direct current (DC) or alternative current (AC). During material characterization using AC, frequency ranging from low Hz to microwave can be used. On the other hand, the working principle in DC method is associated with Ohm's law where voltage drop across the electrodes are measured under the application of electric current. Based on the electrode configuration, resistivity tests can be performed with two- and four-electrode configurations. A brief description of both methods is presented herein.

2.9.1.1 Two-Electrode System

Two-electrode measurements of electrical resistivity are described in ASTM G187-05 standard test method. A two-electrode soil box, current source, resistance measuring equipment, and electrical connections are utilized in the tests as presented in Figure 2.25. In this method, same electrodes are used for the current application and voltage measurements. The two-electrode soil box should be made of insulated and durable material to avoid short circuit during experiments. Two end plates constructed with polished and corrosion resistant metal, can be used for current flow and voltage measurements. It is recommended to correct the measured resistivity at 15.5 deg. C temperature in ASTM G187-05 standard according to the following equation:

$$\rho_{15.5} = \frac{(24.5+T)}{40}\ \rho_T \tag{2.33}$$

here, $\rho_{15.5}$ = resistivity corrected at 15.5 deg. C, ρ_T= measured resistivity at medium temperature, T = temperature during experiment.

Santamarina et al. (2001) indicated the possible errors in two-electrode resistivity measurements. The electrical conduction in the electrode and cable generally involves electron flow; however, the flow of current is mostly ionic in the soil. Therefore, charge accumulation may occur in the soil-metal interface. This phenomenon is called polarization, and is the main source of error in a two-electrode measurement. In addition to polarization, presence of air gap at the interface, presence of non-uniform electric field and possibility of chemical reaction may cause additional error in this method. The test setup of a two-electrode system is presented in Figure 2.25.

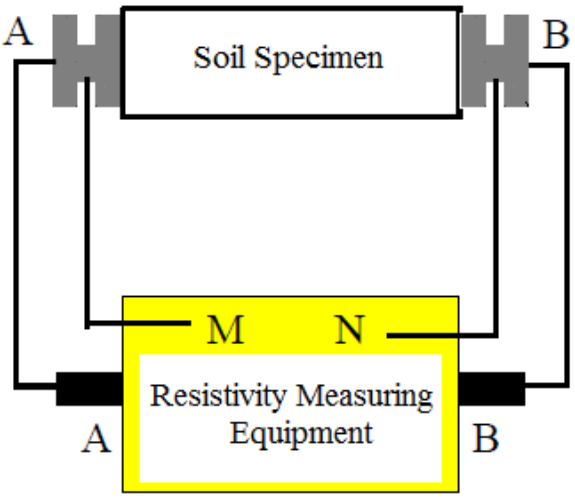

Figure 2.25 Two-electrode electrical resistivity measurement system

2.9.1.2 Four-Electrode System

A current is applied using two electrodes located at the end of soil resistivity box and potential drop is measured between two points at the specimen in a four-electrode system. This method has advantages over the two-electrode measurements because potential is determined within the sample which is away from the charge transfer process of current electrodes. Therefore, polarization can be largely avoided using a four-electrode measurement method. In addition, this method measures the voltage within the sample; thus, the actual electric field of the sample can be encountered during the tests. As the voltage and current electrodes are different, the possible effect of chemical reaction on electrical resistivity measurement may not be significant in this case. The experimental setup of four-electrode measurements is presented in Figure 2.26.

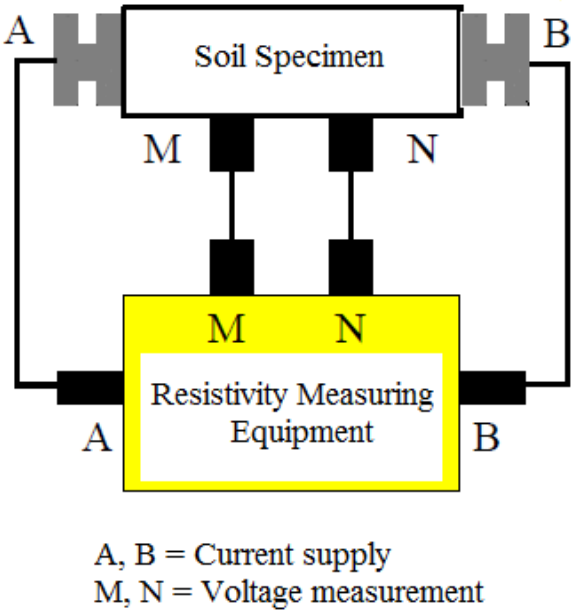

Figure 2.26 Four-electrode electrical resistivity measurement system

2.9.2 Field Measurement

Electrical resistivity measurement has been utilized in the investigation of near surface geology since early 20th century. However, this method has become very popular in recent years with the improvement of test methods and data processing. At present, geo-electrical measurements have become a useful tool in geophysics, soil science, hydro-geological studies, environmental, and geotechnical engineering (Aizebeokhai, 2010; Hossain et al. 2010).

A current (I) is injected through the current electrode C1 in isotropic homogenous half space of earth (Figure 2.27). The electric potential decreases inversely with the increase of distance from the current source. The current distribution follows an outward radial direction through shell area of $2\pi r^2$, perpendicular to equipotential lines. The potential for one electrode can be mentioned as:

$$\emptyset = \frac{\rho I}{2\pi r} \tag{2.34}$$

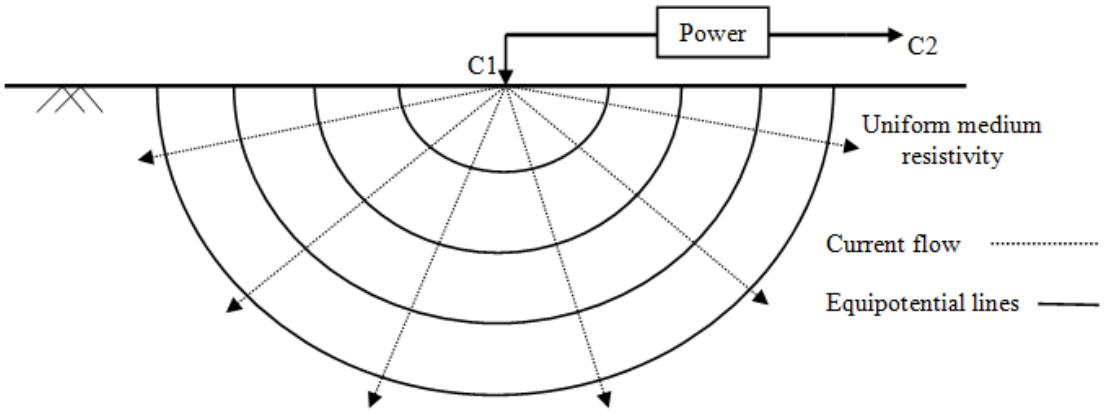

Figure 2.27 Current flow and equipotential lines due to a point source

Typically, two current electrodes are used in a conventional resistivity survey as positive and negative end. In this case, the potential distribution has a symmetric pattern around vertical plane centered at the midpoint of the electrodes. The potential for two-electrode configuration can be defined as:

$$\emptyset = \frac{\rho I}{2\pi}\left(\frac{1}{r_1} - \frac{1}{r_2}\right) \tag{2.35}$$

r_{c1} and r_{c2} are the distances of the measured point from the first and second current electrodes.

According to Figure 2.28, the equation can be extended for four-electrode system as:

$$\emptyset = \frac{\rho I}{2\pi}\left(\frac{1}{r_1} - \frac{1}{r_2} - \frac{1}{r_3} + \frac{1}{r_4}\right) \tag{2.36}$$

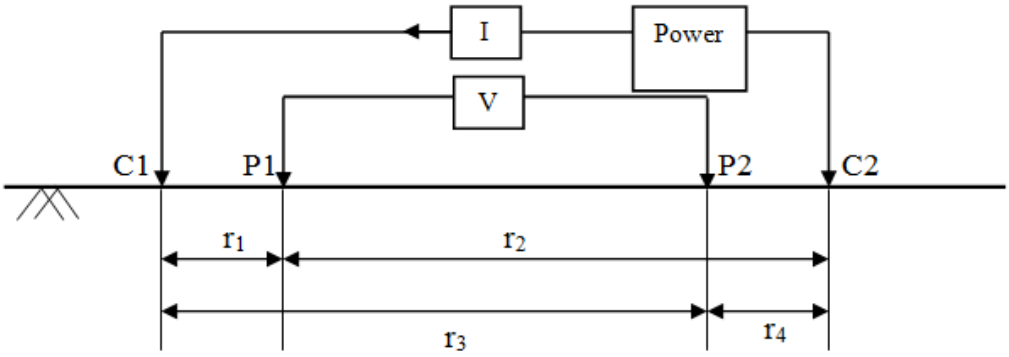

Figure 2.28 Four electrode measurement of resistivity in the field

Although the equations presented here are applicable for homogenous isotropic medium, actual field surveys are associated with the anisotropic and inhomogeneous subsurface. Therefore, an apparent resistivity is calculated from measured current and potential according to the following equation:

$$\rho_a = \frac{k\,\Delta\emptyset}{I} \tag{2.37}$$

where, k is a geometric factor that depends on the arrangement of the four electrodes and can be expressed as:

$$k = \frac{2\pi}{\left(\frac{1}{r_{c1p1}} - \frac{1}{r_{c2p1}} - \frac{1}{r_{c1p2}} + \frac{1}{r_{c2p2}}\right)} \tag{2.38}$$

The apparent resistivity can be defined as the electrical resistivity of a homogenous subsurface medium that will provide same resistance in the same electrode configuration. It can be considered as a weighted average of the resistivity of the subsurface volume under the four electrodes. The apparent resistivity depends on the electrode arrays, and inversion modeling is required to determine the true resistivity from apparent measurements (Loke, 2001; Aizebeokhai, 2010).

Typically, Wenner, Dipole-dipole, Schlumberger, pole-pole and pole-dipole arrays are utilized in the one, two and three dimensional resistivity survey. A brief description of the arrays is presented in the following subsections.

2.9.2.1 Wenner Array

The use of Wenner array has become popular by the extensive research of University of Birmingham. The array is sensitive to vertical changes compared to horizontal variation in resistivity. Typically, Wenner array can evaluate horizontal structures; however, the performance is poor in mapping of narrow vertical structures. Moreover, Wenner array is preferred for the survey where substantial noise is anticipated in the field condition (Dahlin and Loke, 1997). The electrode configuration of Wenner alpha array is presented in Figure 2.29.

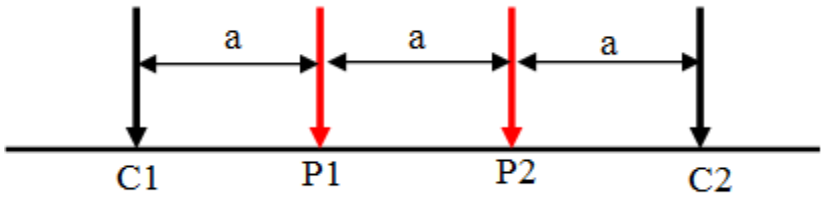

Figure 2.29 Wenner array

2.9.2.2 Dipole-dipole Array

Dipole-dipole array is characterized by low electromagnetic coupling; therefore, is regarded as an efficient method in field survey (Loke, 2001). The spacing between current and potential electrodes is same in this array as illustrated in Figure 2.30. This array is sensitive to variation in horizontal direction compared to the vertical changes in resistivity. Dipole-diople array is a popular method in the imaging of vertical structures.

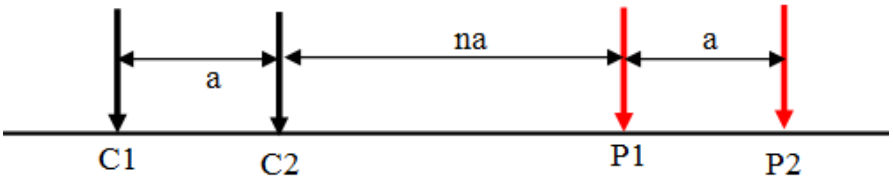

$K = \pi n (n+1) (n+2) a$

Figure 2.30 Dipole-dipole array

2.9.2.3 Schlumberger Array

The schematic of Schlumberger array is presented in Figure 2.31. This array is sensitive to vertical resistivity compared to horizontal variation. The horizontal coverage can be decreased with the increase of electrode spacing (Aizebiokhai, 2005). In recent years, a relatively new method i.e. Wenner-Schlumberger method are being utilized for the resistivity sounding.

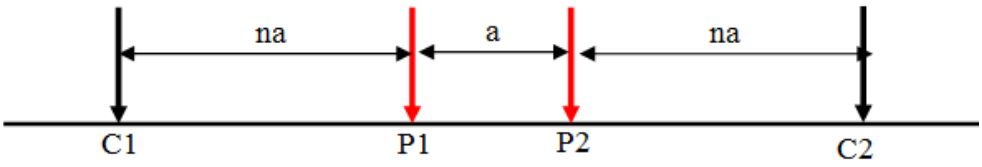

$K = \pi n (n+1) a$

Figure 2.31 Dipole-dipole array

2.9.2.4 Pole-Pole Array

The conventional Pole-pole array consists of one current and one potential electrode (C1 and P1). The second current and potential electrodes are located at a distance more than 20 times of the spacing between C1 and P1. This method is not typically used in resistivity sounding compared to Wenner, Schlumberger and Dipole-dipole array. This method has the highest coverage area in horizontal and vertical

direction. However, the resolution of the obtained image is not satisfactory because of the large spacing between the electrodes. The electrode configuration in pole-pole array is presented in Figure 2.32.

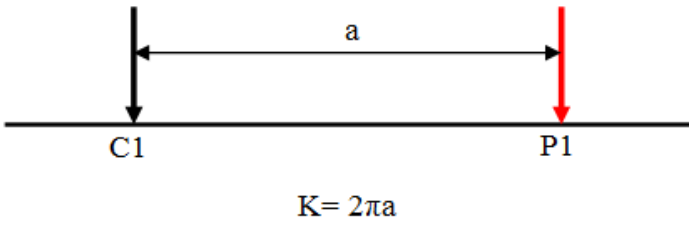

Figure 2.32 Pole-pole array

2.9.2.5 Pole-Dipole Array

The Pole-dipole method is characterized by high signal strength and less sensitivity in response to telluric current. This is an asymmetric method and has a relatively high horizontal coverage. Due to asymmetric electrode configuration, Pole-dipole method is divided into two groups such as forward and reverse pole-dipole array. The schematic of the electrode configuration in a Pole-Dipole array is presented in Figure 2.33.

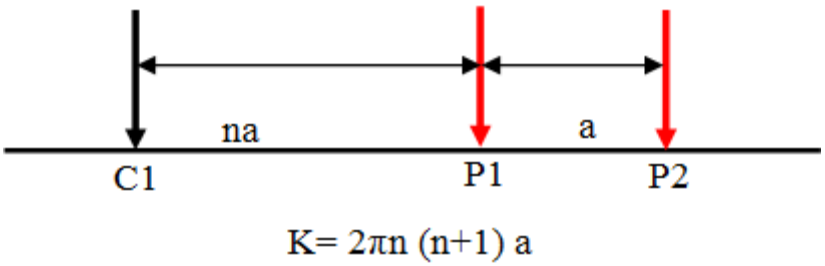

Figure 2.33 Pole-dipole array

A summary of characteristics of different surveys is presented in Table 2.6.

Table 2.6 Summary of characteristics of different arrays (Arjwech, 2011)

	Wenner	**Wenner Schlumberger**	**Dipole-Dipole**	**Pole-Pole**	**Pole-Dipole**
Sensitive to horizontal	4	2	1	2	2
Sensitive to vertical	1	2	4	2	1
Depth of investigation	1	2	3	4	3
Horizontal Data Coverage	1	2	3	4	3
Signal Strength	4	3	1	1	2

Poor sensitivity = 1 and high sensitivity = 4

2.9.3 One-Dimensional Resistivity Survey

One dimensional resistivity measurement at the field condition is generally known as vertical electrical sounding (VES). The center of the electrodes remains constant; however, the spacing is successively increased to obtain resistivity at deeper section in this method. This method provides resistivity variation along vertical direction and does not consider the changes in horizontal resistivity (Loke, 2001).

2.9.4 Two-Dimensional Resistivity Survey

Two-dimensional multi-electrode arrays can provide a 2D continuous image of the subsurface. The current and potential electrodes are placed at a fixed spacing, and measurements progressively moved from one end to another as illustrated in Figure 2.34. Based on the measurement of apparent resistivity, a 2D pseudo-section can be developed. Thereafter, inversion modeling is performed on the measured apparent resistivity to obtain a 2D continuous image of the subsurface (Samouelian at al. 2005).

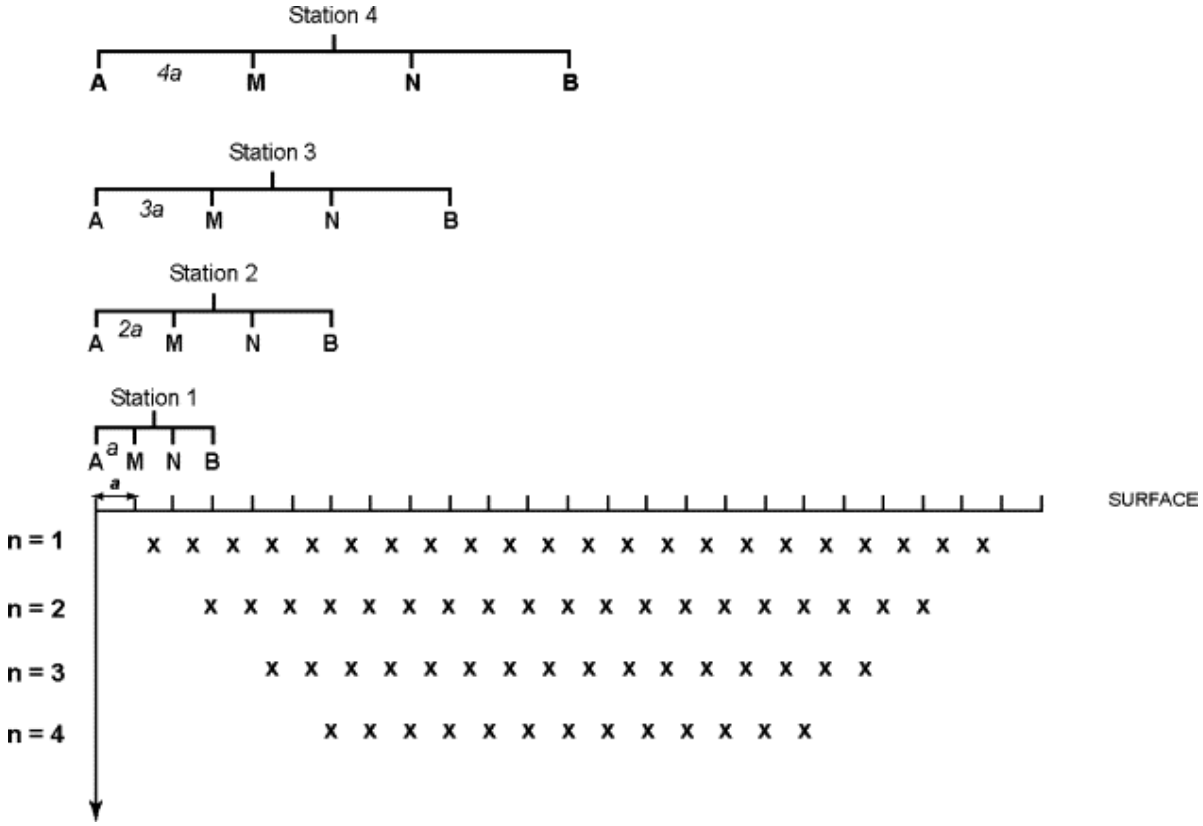

Figure 2.34 2D resistivity measurement (Samoulien et al. 2005)

2.9.5Thee Dimensional Resistivity Survey

Three dimensional resistivity survey can provide robust information of the subsurface in the three dimensional area. There are two methods for determining 3D resistivity profile of subsurface: a) quasi 3D and b) actual 3D resistivity survey. In a quasi-3D resistivity survey, different 2D parallel pseudo-sections can be combined to evaluate 3D profile of the investigated area. On the other hand, the measurements should be performed in X and Y directions to obtain an actual 3D resistivity profile (Arjwech, 2011).

2.9.6 Electrical Resistivity Inversion Modeling

When a current is injected through a point source, the basic equation for the determination of potential distribution in the earth can be expressed as:

$$-\nabla.[\sigma(x,y,z)\nabla U(x,y,z)] = \frac{I}{\Delta V}\partial(x-x_s)\partial(y-y_s)\partial(z-z_s) \quad (2.39)$$

A forward modeling method can be employed to solve the equation. Typically, the finite difference and finite element modeling are utilized to solve the equation for 2D and 3D resistivity measurements, where as analytical method can be used for the cases of 1D resistivity survey.

During inversion of resistivity measurements, a model is determined that can provide a similar response to the actual values. The model consisted of a set of parameters which are the physical quantities estimated from the observed data (Loke, 2001). In a subsurface resistivity distribution, forward modeling can be utilized to provide theoretical values of apparent resistivity. Typically, finite difference and finite element modeling are used to calculate the theoretical apparent resistivity. Eventually inversion methods determine a subsurface model whose responses matches with the measured quantities under certain conditions. A detail of mathematical procedures for the inversion modeling is presented in study of Loke (2001) and review of Arjwech (2011). A typical flow diagram in an inversion modeling is presented in Figure 2.35.

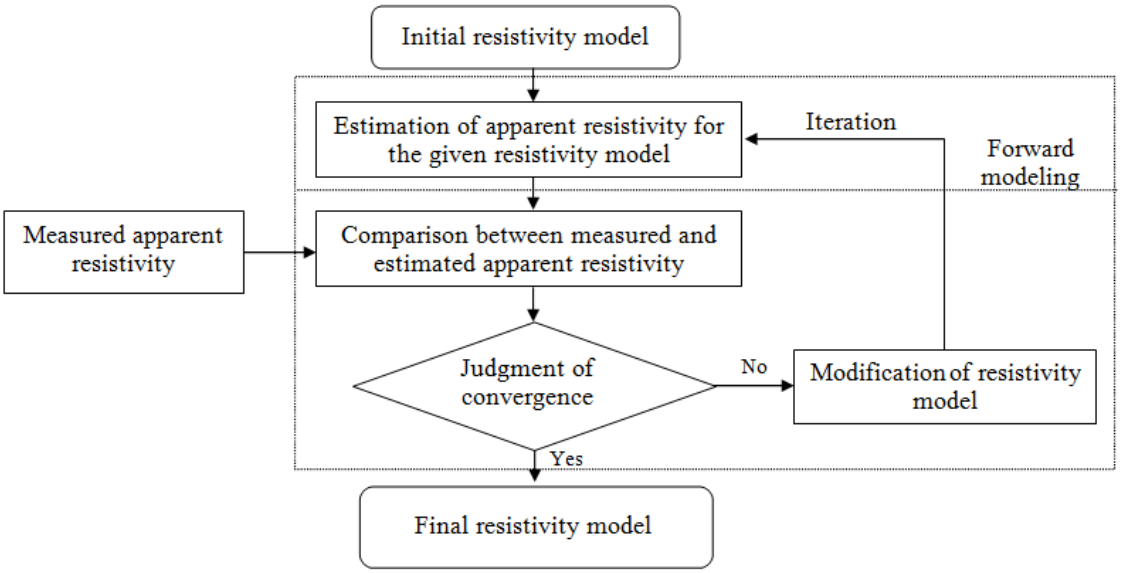

Figure 2.35 Algorithm of inversion modeling (Arjwech, 2011)

2.10 Summary

This chapter presented a review on clay soil structure from engineering point of view, available methods of characterization, and electrical conduction phenomena in clayey soils. The major points of the review can be summarized as follows:

1. According to Joint Nomenclature Committees (JNCs), "Clays are naturally occurring material primarily composed of fine-grained minerals, show plasticity when mixed with appropriate amount of moisture, and become hard when dried or fired" (Bargaya and Lagayli, 2006). Mitchell and Soga (2005) indicated the characteristics of clay, which included a) small particle size (usually smaller than 0.002 mm) b) net negative charge c) plasticity when mixed with moisture, and d) weathering resistance. However, two specific properties of clayey soils, i.e. plasticity and cohesion are of particular interest in geotechnical engineering.

2. There are two fundamental crystal units of clay minerals, i.e. tetrahedral and octahedral. A tetrahedral unit belongs to four oxygen enclosing silicon, where as an octahedral unit composes of six oxygen or hydroxyls at corner surrounding aluminum, magnesium, iron or other ions. Based on the arrangement of stacks, bonding, isomorphous substitution, and presence of metallic ions different clay minerals can be constituted. However, for engineering purpose kaolinite, montmorillonite, and illite have particular importance in geotechnical engineering (Holtz and Kovacs, 1981).
3. The qualitative mineralogical content of soils can be determined using Atterberg limits, activity, and free swell ratio. For the accurate assessment, X-ray diffraction (XRD), scanning electron microscope (SEM), energy dispersive X-ray spectroscopy (EDS), etc can be utilized.
4. Electrical conduction in a particulate media generally occurs by the movement of ions through electrolytic pore water in the void and surface charge (Bryson, 2005). In coarse-grained soil, conduction is largely electrolytic and depends on the interconnected pore space, granular skeleton, electrolyte conductivity, and degree of saturation (Santamarina et al. 2001). However, surface charge is an important parameter in the electrical conduction of clayey soils.
5. Several factors may affect the electrical resistivity of soil. Moisture content is identified as one of the major factors that cause change in soil resistivity. The effect of degree of saturation, pore water composition, geologic formation, ion

content, and fabric structure were substantial in the electrical conductivity of clayey soil.

6. According to the literature, moisture content, compaction condition, clay mineralogy, hydraulic conductivity and consolidation properties can be evaluated using electrical resistivity.
7. The electrical properties (DC resistivity) can be studied in the laboratory with two- and four-electrode configurations. In two- electrode method, same electrodes are used for the current application and voltage measurements. However, a current is applied using two electrodes located at the end of soil resistivity box and potential drop is measured between two points at the specimen in a four-electrode system.
8. Typically, Wenner, Dipole-dipole, Schlumberger, pole-pole, and pole-dipole arrays are utilized in the one, two, and three dimensional resistivity survey in the field condition. However, the sensitivity of the array should be evaluated based on the intended purpose of the test.
9. Once apparent resistivity of different locations is measured in the field, forward and inversion modeling are performed to obtain continuous image of surface.

CHAPTER 3

MATERIALS AND METHODS

3.1 Introduction

An experimental program was developed to investigate the relationship between electrical resistivity and soil properties. The test specimens included a) undisturbed soil b) disturbed soil c) two clay minerals, and d) four artificial soils. The engineering properties of the soil specimens were determined using conventional geotechnical tests and advanced methods. After the soil characterization, the electrical resistivity tests were conducted at varying geotechnical conditions. The test methodologies considered in the current study can be summarized as follows:

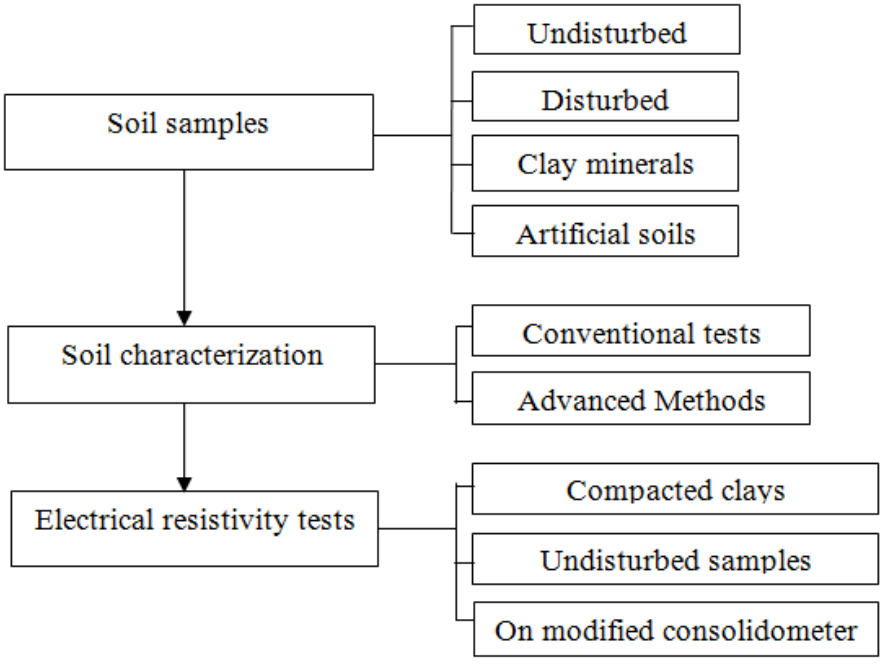

Figure 3.1 Flow diagram of test methodology

3.2 Collection of Soil Samples

The soil specimens were collected from a slope along highway Loop 12 near Union Pacific Rail Road (UPRR), Dallas, TX. Two soil test borings were conducted using a truck-mounted rig, and samples were collected from every 1.5 m. Both disturbed and undisturbed samples were utilized in the current study. In addition to natural soils, Ca-bentonite and kaolinite minerals were used to determine the resistivity responses at two specific mineralogical conditions. Bentonites are highly plastic clay, and referred as montmorillonite because of the existence of expanding lattice. On the other hand, the ion substitution and surface charges are relatively low in kaolinite, and known as less active mineral.

A total of four types of soil samples were utilized for the investigation of geotechnical properties affecting electrical resistivity and development of statistical model for compacted clays. The soil specimens included a) highly plastic clay (CH) b) low plastic clay (CL) c) Ca-bentonite, and d) kaolinite.

The undisturbed soil samples were stored in the humid chamber to avoid moisture loss from specimens. Six undisturbed samples were utilized in this study for the determination of geotechnical and electrical properties. For the ease of representation of test results, undisturbed samples are designated according to the boring locations and depths as presented in Table 3.1.

Table 3.1 Designation of soil specimens

Sample ID	Designation
BH-1 @ 15 ft	B1-15
BH-1 @ 25 ft	B1-25
BH-2 @ 20 ft	B2-20
BH-1 @ 10 ft	B1-10
BH-2 @ 25 ft	B2-25
BH-2 @ 10 ft	B2-10
BH-2 @ 5 ft	B2-5
BH-1 @ 30 ft	B1-30

Although artificial soil samples were not utilized in the development of statistical model, the effects of clay properties were investigated using these specimens. Moreover, artificial samples were used to evaluate the performance of the statistical model. The artificial soil samples were prepared using Ca-bentonite and fine sands at different weight percentages. A summary of artificial soils are presented in Table 3.2.

Table 3.2 Artificial soil specimens utilized in the study

Mineral by weight (%)	Sand by weight (%)
80	20
60	40
40	60
20	80

3.3 Determination of Geotechnical Properties

An experimental program was developed to determine the geotechnical properties of the test specimens which included a) grain size distribution b) Atterberg limits c) specific gravity d) cation exchange capacity (CEC) e) moisture content (undisturbed soil samples), and f) unit weight (undisturbed soil samples). The specific surface areas (SSA) of the samples were determined using the correlation proposed by Farrar and Coleman (1967). In addition, dominant minerals of the soil samples collected from boreholes were determined using free swell ratio and index properties. A summary of geotechnical tests performed on the soil samples is presented in Table 3.3.

Table 3.3 Summary of geotechnical tests performed on the soil samples

Name of Test	**Test Method**
Grain size distribution	ASTM D422-63
Atterberg limits	ASTM D431
Specific gravity	ASTM D854-00
Cation exchange capacity	ASTM D7503-10
Moisture content	ASTM D2216-90
Unit weight	ASTM D2937-00

3.3.1 Grain Size Distribution

Grain size distributions of the specimens were determined according to ASTM D422-63 standard test method. The soil samples were dried in the oven at 100-110 deg. C temperature for 24 hours. The aggregation of the oven-dried sample was broken by mortar and rubber covered pestle, and approximately 300 gm sample was considered for the sieve analysis. The soil sample was washed using #200 sieve with flowing water until

the leached water was completely clean. The retained and leached samples were dried in the oven at 100-110 deg. C temperature for 24 hours. After that, the retained soils were sieved using #4, #10, #30, #40, #60, #100, and #200 US standard sieve. The mass of retained sample in each sieve was determined after completion of the test. Soil passed through No. 200 sieve during wash sieving was utilized in the hydrometer test.

3.3.2 Atterberg Limits

Atterberg limits tests were performed on the soil specimens according to ASTM D4318 standard method. The soil specimens passing through No. 40 sieve were considered in the test. After addition of water, the soil sample was chopped, stirred, and kneaded repeatedly. A portion of the soil was placed in the Cassagrande liquid limit device, and a groove was cut at the center of the cup. The cup of the device was lifted and dropped at a rate of 2 drops/second until the groove was closed around 13 mm. The test was repeated for three times, and the number of blows was plotted against moisture content. The moisture content corresponding to 25 blows was considered as the liquid limit of the specimen.

For the determination of plastic limit, water was added in the soil and kneaded repeatedly. The soil masses were rolled in the glass plate until threads of about 3 mm were formed. When the threads were broken at 3 mm diameter, they were taken in the moisture cans. Samples were dried in the oven at 100-110 deg. C temperature for 24 hours. The moisture content at this condition was considered as plastic limit of the specimen.

The observed Atterberg limits were utilized to identify the plasticity index and activity of the specimens. It should be mentioned that activity was calculated according to the Skempton (1953) method, where the particles smaller than 2μm was considered as clay fraction. In addition, the liquid limits of the soil samples were employed for the determination of the specific surface area (SSA) according to the following correlations (Farrar and Coleman, 1967):

$$LL = 19 + 0.56\,SSA \left(SSA = \frac{m^2}{gm}\right) \tag{3.1}$$

3.3.3 Specific Gravity

Specific gravity of the soil samples were determined using water pycnometer according to ASTM D854-00 standard test method. A total of 50 gm soil mass passing through No. 10 sieve was considered in the test. The weights of the empty pycnometer, and pycnometer with specimen were measured. The soil specimen was soaked with distilled water under the application of partial vacuum for at least 16 hours. Then water was added up to the mark of the pycnometer, and weighed. After that, distilled water was added in the clean pycnometer, and the combined weight was determined.

3.3.4 Cation Exchange Capacity (CEC)

Cation exchange capacities (CEC) of the soil samples were determined according to ASTM D7503-10 standard test method. The CEC is a measure of the total negative surface charge of the clay particles, which can be balanced by bound cations. A total of 25 gm oven dried soil sample passing No. 10 sieve was taken in a flask. The ammonium acetate solution (125 ml 1M) was added in the soil sample, and mixed thoroughly. Then

the soil sample with the solution was kept in the laboratory for 24 hours. After that, the mixer was transferred into a filtering flask, and low suction (<10 kPa) was applied using Buchner funnel. The soil sample was further washed four times using 25 ml ammonium acetate in each instance. In addition, the soil was rinsed with eight separate addition of ethanol (95%), and leachate was discarded. Then the soil was rinsed again using eight separate 25 ml addition of 1M potassium chloride. The extract solution was diluted to a volume of 250 ml by adding distilled water. The diluted solution was mixed with the reagent TNT plus™ 832 (following Salicylate method), and shook thoroughly. After 15 minutes, the amount of ammonia in the solution was determined using bench-top spectrophotometer.

During the addition of ammonium acetate and ethanol, soil was not allowed to dry and crack. The followed procedures in CEC tests of the specimens are illustrated in Figure 3.2.

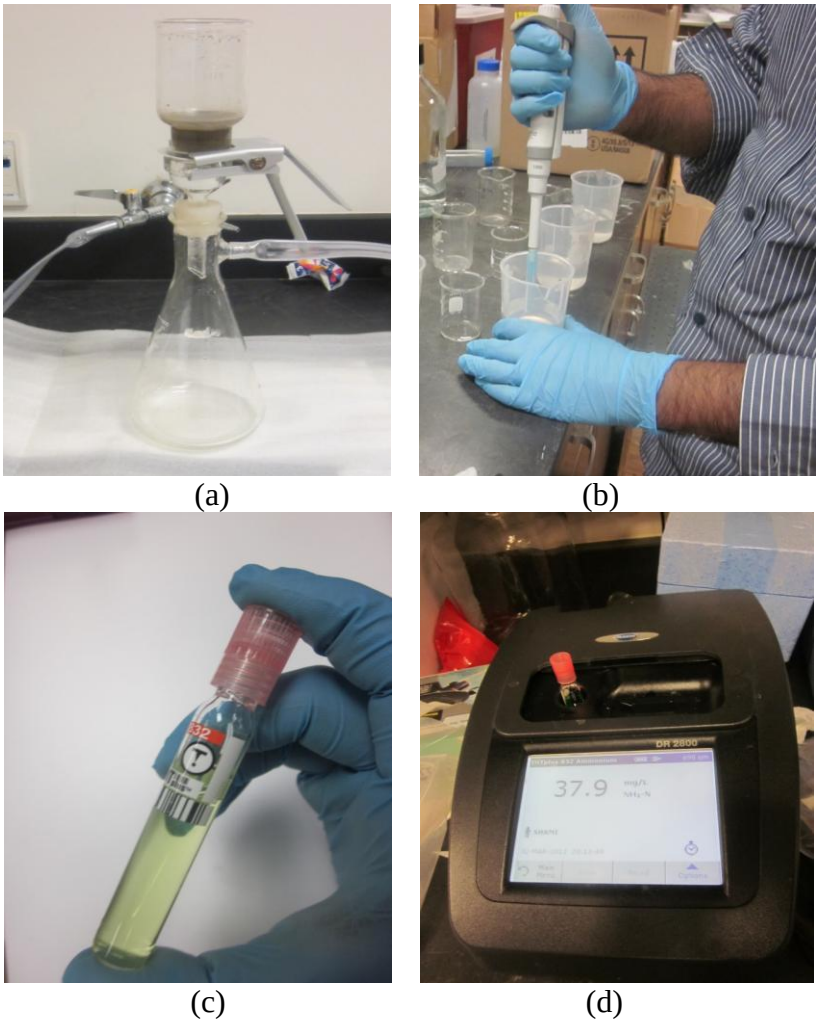

Figure 3.2 CEC tests of the soil samples (a) application of vacuum using Buchner funnel (b) Mixing of the leachate with distilled water (c) diluted leachate in the chemical (d) measurement ammonia

The observed CEC of the soil specimens were compared with the proposed correlations of Farrar and Coleman (1967), Smith et al. (1985), and Yukselen and Kaya (2006). The correlations of CEC with index properties are presented in Table 3.4.

Table 3.4 Correlation of CEC with index properties

Correlations	Name of Investigator
CEC=0.55LL-12.2	Farrar and Coleman (1967)
CEC=1.74LL-38.15	Smith et al. (1985)
CEC=3.57PL-61.3	Smith et al. (1985)
CEC = 0.2027 LL + 16.231	Yukselen and Kaya (2006)

3.3.5 Moisture Content and Unit Weight of Undisturbed Soil Samples

The moisture contents of the soil samples collected from boreholes were determined according to ASTM D2216-90. The soil sample was taken in a non-erodible container, and weighed. Then the soil sample was dried in the oven for 16-24 hours at 105 to 110 deg. C. temperature. The weight of the oven-dried sample was determined to calculate moisture content of soil.

The unit weight of the soil sample was determined according to ASTM D2937-00 method. The soil sample was extracted from Shelby tube, and the height, diameter and weight of a representative portion was measured. The sample was oven dried at 105-110 deg. C, and moisture content was determined. The moist and dry unit weights of the sample were calculated using the weight-volume relationship.

3.3.6 Mineral Content from Physical Properties

The dominant mineral content of the soil samples collected from boreholes were determined using Atterberg limits (Holtz and Kovac, 1981), activity (Mitchell and Soga, 2005), and free swell ratio (Prakash and Sridharan, 2001). Skempton (1953) defined the

activity of the clayey soil as the ratio of plasticity index with the percentages of particles finer than 2 μm.

The experimental method described by Prakash and Sridharan (2001) was followed in the current research for the determination of dominant clay mineral. A total of 10 gm oven-dried sample passing through #40 sieve was mixed with 100 ml distilled water. The soil slurry was transferred into a 250 ml cylinder. The same amount of soil was added with 100 ml kerosene, mixed thoroughly, and transferred to a 250 ml cylinder. After 24 hours, the variations in the volume in distilled water and kerosene cylinders were measured, and free swell ratio (FSR) was calculated using the following relationship:

$$FSR = \frac{V_d}{Vk} \tag{3.2}$$

where, FSR=free swell ratio, V_d = the equilibrium sediment volume of the suspension in distilled water, V_k = the equilibrium sediment volume of the suspension in kerosene.

Based on the correlation of FSR and mineralogy (Prakash and Sridharan, 2001), the dominant clay minerals were identified.

3.4 Advanced Characterization of Clays

3.4.1 Scanning Electron Microscope (SEM)

The powdered samples were utilized for the study of fabric morphology in scanning electron microscope (SEM). The images were produced by scanning the sample using high-energy beam of electrons. The induced electrons interacted with the inherent electrons of the atoms, and secondary electrons were reflected. These electrons contained

information about the surface topography of the soil specimen. In the current study, the accelerated energy of the induced electrons was less than 25 keV. It was observed that the induced electrons interacted with the clay particles, and accumulated at the surface. The tendency of charge accumulation increased with the increase of voltage of electrons. Although charge accumulation can be reduced by applying a silver coating on the specimen, the elemental composition of the sample changes in the presence of silver layer. Therefore, tests were conducted without putting silver coating, and employing low voltage electrons. The working distance (distance between electron discharge and object) was varied during the tests to obtain clear images of fabrics. The SEM used for fabric study is presented in Figure 3.3.

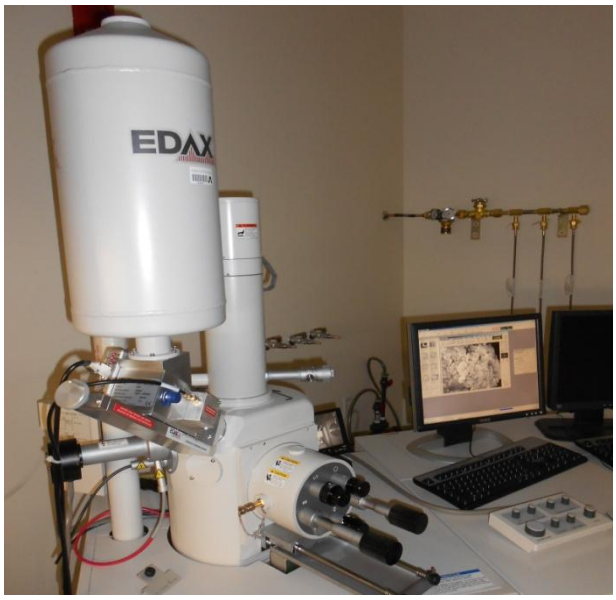

Figure 3.3 Scanning electron microscope

It should be mentioned that SEM analyses were conducted on the soil samples before and after consolidations. The objectives of SEM tests on undisturbed and

consolidated samples were to evaluate the changes in fabric morphology under the application of stresses.

Sedimentation method was utilized for the preparation of SEM test specimens. In this technique, the soil samples were kept under water for at least 72 hours. Thereafter, the soil slurry was filtered and dried to obtain powdered sample.

3.4.2 Energy Dispersive X-Ray Spectroscopy (EDS)

Energy dispersive X-ray spectrometry (EDS) is a popular method for the determination of compositional elements. In the current study, EDS was utilized for the elemental analyses of the soil samples. The inherent electrons of specimens were excited using induced X-ray beam during the tests. Based on the unique characteristics of emitted X-ray spectrum, elements of specimens were determined. Tests were performed in conjunction with SEM analysis at a fixed magnification and working distance configuration of the equipment. However, the energy of the accelerated electrons was increased during EDS tests to enhance the measurement efficiency, and reduce the information collection time.

3.4.3 Pore Water Analysis using Ion Chromatography (IC)

In addition to SEM and EDS, the ion content of pore water was investigated using ion chromatography (IC) method. A total of four types of specimens i.e. Ca-bentonite, kaolinite, CH, and CL were utilized in the pore water extraction. The soil specimens and clay minerals were thoroughly mixed with deionized water at their liquid limits using a rotary mixer, and the slurry was transferred to a modified consolidometer. The

consolidometer was equipped with a connection pipe beneath the porous stone, and pore water was extracted from soil specimens under applied loads at different stages of consolidations. The collected pore water was transferred to the test tube and stored at 4.0 deg. C temperature. The electrical conductivity and pH of the pore water was measured using bench-top conductivity/pH meter (Oakton Instruments). The methods of pore water extraction are presented in Figure 3.4.

(a)

(b)

Figure 3.4 Extraction of pore water from soil (a) mixing of soil with distilled water at liquid limits (b) extraction of water under the applied load

Ion chromatography (IC) method was employed to determine ion composition of the extracted pore water from soil samples. It is a well-known technique to measure concentration of cations and anions in liquids. Extracted pore water was injected into the methane sulphonic acid and sodium carbonate (for cation), and sodium bicarbonate solution (for anion). The compound mixture was then allowed to pass through separation columns. Based on the interaction of dissolved ions in the pore water with carrier fluid and adsorbent, composed ions were separated. Conductivity detector was used to detect the concentration of cations and anions. In addition, cationic and anionic suppressors were utilized to reduce the movement of carrier fluid, and enhance the conductance of separated ions. The equipment used for IC tests is illustrated in Figure 3.5.

Figure 3.5 Ion chromatography (IC) test equipment

3.5 Laboratory Investigation of Electrical Resistivity of Soils

Electrical resistivity tests were conducted on disturbed and undisturbed soil samples. Super Sting IP resistivity equipment was utilized for the application of direct current (DC) and measurement of resistance of the soils. Soil resistivity box (similar to Miller resistivity box), made of high strength plexi-glass, was used for the testing of compacted soils. On the other hand, two circular stainless steel electrodes were fabricated in the machine shop of UT Arlington for the resistivity measurement of undisturbed soil samples. Moreover, an oedometer was designed to determine the electrical conductivity in conjunction with consolidation. A summary of electrical resistivity tests are presented in Table 3.5.

Table 3.5 Summary of resistivity tests

Soil Specimen	**Sets of specimens**	**Test condition**	**Comments**
Undisturbed	6	At subsequent drying stages	Use for model development
Compacted clays	4	At varied moisture content, dry unit weight, and temperature	Use for model development
Undisturbed	4	Consolidation stages	Use to develop correlation between compressibility and resistivity
Artificially prepared samples	4	At varied moisture content, dry unit weight and mineral percentages	Use to identify the relationship between clay properties and resistivity

3.5.1 Electrical Resistivity Tests on Compacted Clays

Soil resistivity tests were performed at varied gravimetric moisture contents and dry unit weights. It should be mentioned that the resistivity tests were conducted using distilled water (conductivity 12.94 micro-siemens). The soil samples were compacted in the resistivity box at a predetermined moisture content and dry unit weight, and electrical resistivity of soils were measured with four electrode configuration using Super Sting IP equipment. A current was employed to the soil through two current electrodes, and voltage drop was determined between two points within the specimen. Santamarina et al. (2001) indicated that the electrode polarization can be reduced significantly using a four terminal electrode configuration. The laboratory set up of electrical resistivity test of compacted soil is presented in Figure 3.6.

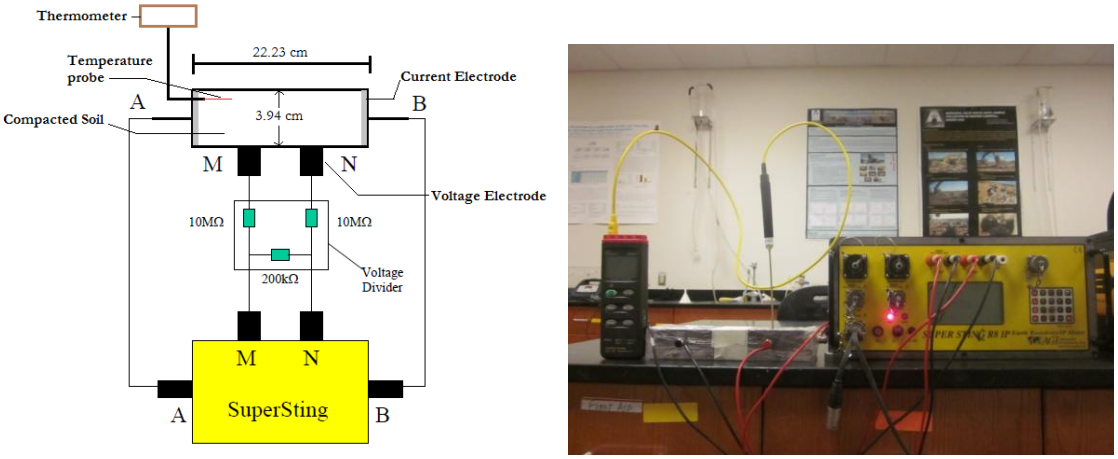

(a) (b)

Figure 3.6 Laboratory set up for soil resistivity tests of compacted soils (a) circuit diagram (b) resistivity tests in laboratory

A summary of soil resistivity test conditions for compacted clays is presented in Table 3.6.

Table 3.6 Summary of soil resistivity tests condition for compacted clays

Fixed Parameters	Variable Parameters	Comments
Dry unit weight	Moisture content, Temperature	Moisture content range 10-40%, temperature range 3-35 deg. C
Moisture content	Dry unit weight, Temperature	Dry unit weight range 11.8-14.9 kN/m^3, temperature range 3-35 deg. C

Before the tests, calibrations were conducted to evaluate the effects of temperature and current variations on electrical resistivity of soils. Literature indicated that resistivity decreased 2.02% for per degree increase of temperature from 15 to 35 deg. C (Campbell, 1948). Therefore, the measured resistivity should be corrected, and presented at a specific temperature. According to ASTM G187-05 test method, the measured resistivity of soil sample should be corrected for 15.5 deg. C. In the current study, temperatures were varied from 3-35 deg. C during resistivity tests. The objective of temperature variations were to evaluate the applicability of ASTM recommended correction factor in the current study.

In addition to temperature, calibrations were performed to identify the effects of electric current variations on resistivity of soils. The calibration of electric current was conducted to evaluate the sensitivity of the equipment on the resistivity measurement. A brief description of the calibration procedure is presented herein.

3.5.1.1 Calibration for Temperature

Soil resistivity tests were performed at temperatures ranged from 3 to 35 ^{o} C. Temperature controlled environmental growth chambers were utilized to vary soil

temperature during tests. The resistivity box containing soil samples was sealed to avoid moisture loss during temperature variations. After the measurement at each temperature, the observed resistivity was corrected for 15.5 deg. C according to the ASTM G187-05 recommendation. The temperature corrected resistivity (at 15.5 deg. C) was then compared with the actual measurement at 15.5 deg. C to evaluate the applicability of the ASTM correction factor. The comparison of observed and corrected resistivity is presented in Figure 3.7. It was identified that observed resistivity were in agreement with the ASTM corrected resistivity in the soil samples. Therefore, ASTM recommended coefficient was utilized to correct resistivity at 15.5 deg. C for all the measurements.

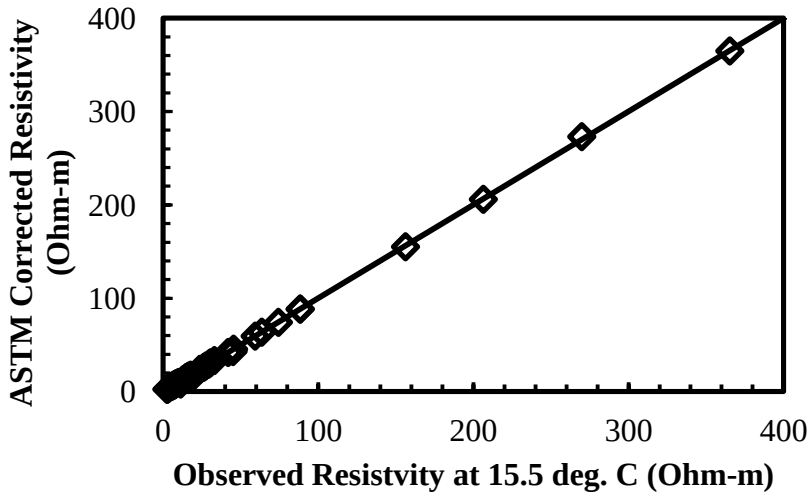

Figure 3.7 Comparison of ASTM corrected and observed resistivity measurements

3.5.1.2 Calibration for Electrical Current

According to the recommendation of Super Sting IP 8 manufacturer (Advaced Geoscience), the applied current should be equal or below 250 mA in the laboratory resistivity tests. Therefore, tests were conducted on a highly plastic (CH) specimen to

identify the effect of current variations between 1-250 mA ranges. The samples were compacted at 13.4 kN/m^3 dry unit weight and four different moisture contents. The magnitude of applied current was varied from 1.0 to 250 mA in each case. It should be mentioned that the liquid limit, plasticity index, and specific gravity of the specimen were 53, 30, and 2.68, respectively. The observed resistances for different currents and moisture contents are presented in Figure 3.8. From graphical point of view, the variation in resistance with current (1-250 mA) for specific moisture content was not substantial.

A summary of the statistical properties of the different test conditions are presented in Table 3.7. It was observed that the standard deviation, variance, and coefficient of variance (COV) of the observed results in the sample compacted at 10% moisture content were 0.188, 0.035, and 1.65, respectively. However, statistical variations were low at high moisture contents compared to the experimental results at 10% moisture content.

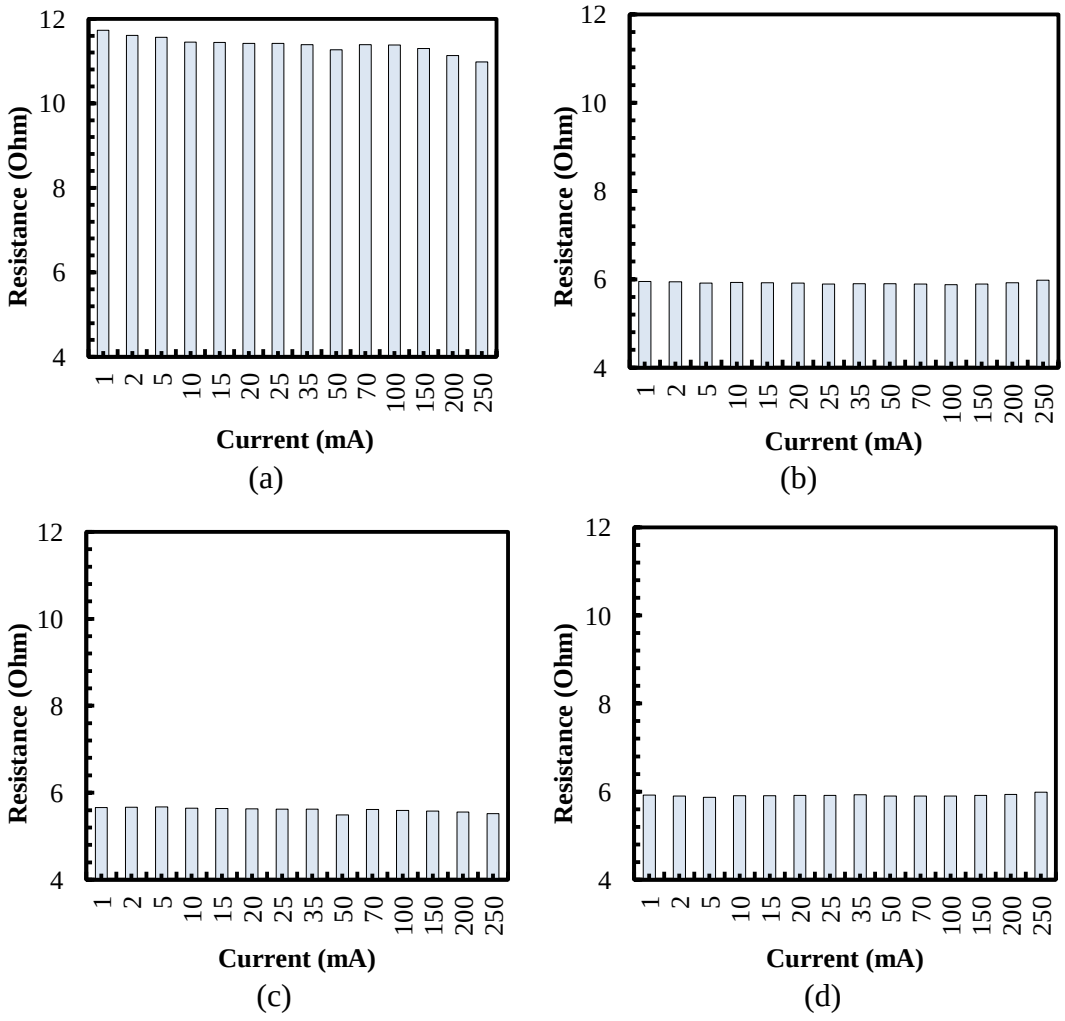

Figure 3.8 Calibration of current for resistivity measurement (a) moisture content 10% (b) moisture content 20% (c) moisture content 30% (d) moisture content 40%

Table 3.7 Statistical properties of the variation

Moisture content	Mean Current (mA)	Std. Dev. (mA)	Variance	COV (%)
10%	11.39	0.188	0.035	1.65
20%	5.92	0.027	0.001	0.46
30%	5.61	0.054	0.003	0.96
40%	5.91	0.027	0.001	0.46

3.5.2 Electrical Resistivity Tests on Undisturbed Specimens

At present, standard methods are not available to determine electrical resistivity of undisturbed soil samples. Therefore, an experimental procedure was developed to perform resistivity tests on the collected samples at subsequent drying phases. During resistivity tests, weights of the samples were measured at each drying phase. It should be mentioned that shrinkage cracks were developed when the samples were significantly dry. Therefore, electrical resistivity tests were not carried out when substantial shrinkage cracks were observed. After completion of the test, specimens were dried in the oven for 24 hours, and water contents at different drying phases were determined using the final moisture content. The measured resistivity was corrected for 15.5 deg. C temperature according ASTM G187-05 recommendation. The circuit diagram and laboratory setup of resistivity tests are presented in Figure 3.9.

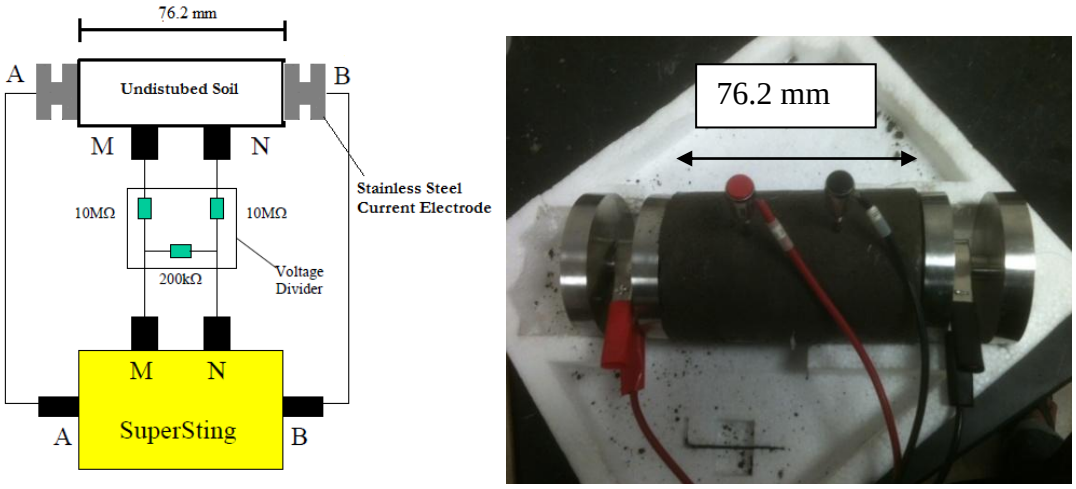

(a) (b)

Figure 3.9 Electrical resistivity rest (a) circuit diagram (b) laboratory setup

3.5.2.1 Effect of Sample Size on Resistivity of Undisturbed Soils

In case of resistivity measurement of undisturbed soil samples, the size of the test specimen was determined before the tests. According to Santamarina et al. (2001), the conductivity of soil samples depends on the size of the specimen. The relationship between conductivity and specimen size can be described by fractal dimension. A fractal system follows self-similar pattern that indicates the properties of a specimen repeat recursively at different dimensions. In the current research, electrical resistivity tests on undisturbed samples were performed on three different specimen sizes, i.e. 76.2, 114.3, and 142.2 mm. However, the diameters of the samples were remained same in each case (73.2 mm). The soil samples were compacted in a mold at 20% and 25% gravimetric moisture contents. It should be mentioned that the compaction of test specimens were performed at their field unit weights. The observed variations in resistivity with specimen sizes are presented in Figure 3.10.

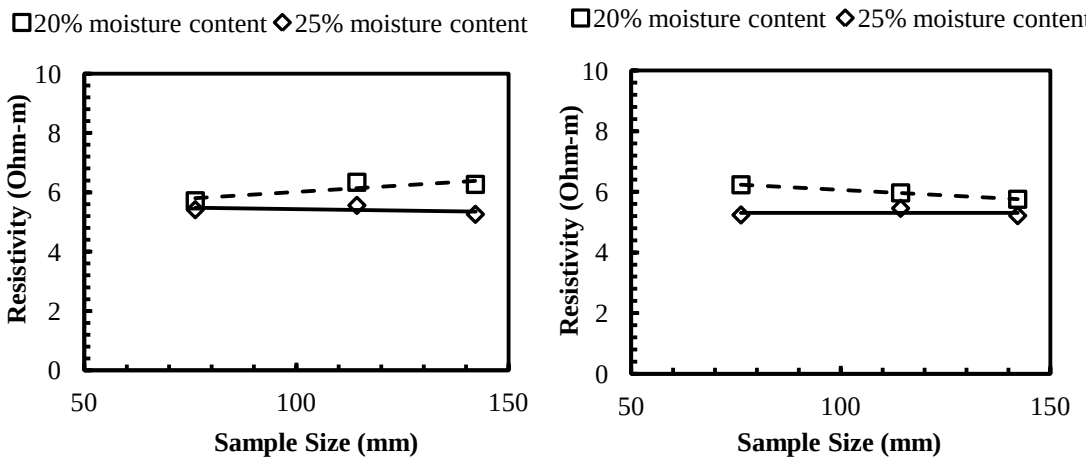

Figure 3.10 Variation of resistivity with specimen sizes (a) B1-15 (b) B 2-20

Test results indicated that resistivity ranged from 5.7 to 6.3 Ohm-m at 20% moisture content in B1-15 samples. The total variations were 0.5 and 0.2 Ohm-m for the increase of sample size from 76.2 to 142.2 mm in B1-15 at 20% and 25% moisture content, respectively. Therefore, the experimental results indicated that the measured resistivity of the specimens were not highly sensitive to the sample sizes. The diameters of samples were not varied during the tests; that might result insignificant variations.

Based on the investigation, a sample size of 76.2 mm was selected for the resistivity tests of undisturbed soil samples. The presence of shrinkage cracks were not substantial in the specimen of 72.6 mm compared to 114.3 and 142.2 mm sample sizes.

3.5.3 Electrical Resistivity Tests on Modified Oedometer

3.5.3.1 Description of the cell

The effect of compressibility on electrical resistivity of soil samples were investigated using a modified oedometer. A new cell was designed to determine the

changes in electrical conductivity at different consolidation stages. The newly designed cell was similar to the fixed-ring consolidation equipment where the sample moved downward relative to the ring. According to Bardet (1997), the fixed-ring type consolidation cell can be used as falling head permeameter. Therefore, the cell was also utilized to observe the variation in electrical and hydraulic conductivity in conjunction with the changes in void ratio.

A schematic of the modified cell is presented in Figure 3.11. The cell was made of high strength plexi-glass to avoid short-circuit during electrical resistivity measurements. The oedometer is consisted of two cylindrical chambers where an outer chamber (A) enclosing an inner one (C). A sample, with a diameter and height of 63.5 and 25.4 mm, was placed in the inner chamber. The porous plexi-glass was utilized for the drainage from top and bottom of the specimen during consolidation. Two perforated stainless steel plate was used as the electrodes, which were in contact with the soil specimens during consolidation (E and G). The diameter of the annular pores of steel plate electrodes and porous plexi-glass (for drainage) were 6 and 23.5 mm, respectively. Electrical conductivity at different consolidation stages were determined using two-electrode configuration. The filter papers were attached with the electrodes on top of the annular pores while keeping solid metallic area open for current flow through soil. The electrode plate was attached in the bottom of the modified oedometer cell, and the undisturbed soil sample was placed. After that, another electrode was put on the top of the specimen. The drainage from the top and bottom of the specimen occurred through two porous plexi-glass on both sides of the electrodes (D and H). The straight rods were

connected with the steel plates (electrodes), and were attached with the cables for the current and voltage measurements (J and K).

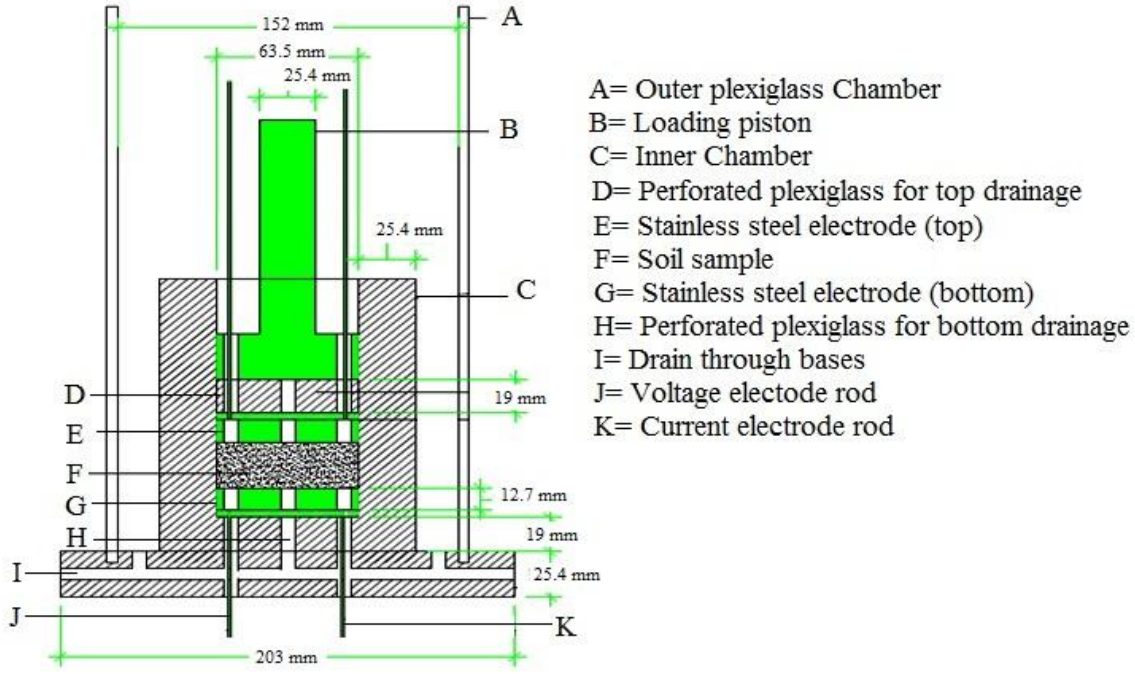

Figure 3.11 A schematic of modified consolidation cell

3.5.3.2 Calibration for Applied Pressure in Modified Oedometer

A pneumatic loading piston was utilized for the application of load during consolidation. The top of the piston was attached with the air pressure valve of Civil Engineering Laboratory Building (CELB) through a regulator. The loading on the specimen was employed through the bottom of the piston, where the pneumatic piston was attached with the load piston of the cell (B). Due to frictional loss in the pneumatic piston, the induced pressure might be different from the applied pressure. Therefore, pressure on the valve and induced pressure on the specimen was verified using a pressure cell. For calibration, the pressure cell was placed under the piston and different loads

were applied. The dial gauge reading on the pressure cell at each loading condition was measured. The pressure calibration method is presented in Figure 3.12.

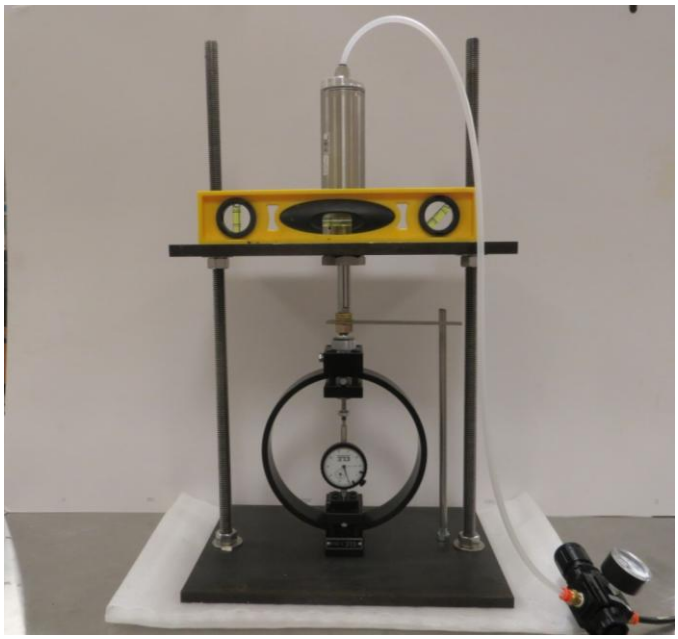

Figure 3.12 Calibration for pressure in the piston

Each division of the pressure cell was corresponded to a specific load as presented below:

$$Y\ (lb - f) = 0.897118\ \times\ \mathrm{X\ (Divisions)} + \ 3.032881\ (\mathrm{lb - f}) \qquad (3.3)$$

The applied pressure in the regulator, observed dial-gauge reading, and calculated pressure is shown in Table 3.8.

A calibration curve was developed correlating applied and induced pressure on the specimen. Based on the calibration equation, stresses on the test specimen were calculated. The developed calibration curve is illustrated in Figure 3.13.

Table 3.8 Calibration of induced pressure in the loading piston

Pressure on Air valve (kPa)	Division	Force in the pressure cell (lb-f)	Force in the pressure cell (Newton)
0.00	0.00	3.03	13.49
25.00	7.50	9.76	43.42
50.00	15.25	16.71	74.35
75.00	27.75	27.93	124.23
175.00	60.20	57.04	253.72
200.00	77.75	72.78	323.76
275.00	102.75	95.21	423.52
325.00	128.50	118.31	526.28
425.00	189.70	173.22	770.50
500.00	222.50	202.64	901.39
600.00	283.25	257.14	1143.82
700.00	329.20	298.36	1327.19
800.00	390.50	353.36	1571.81

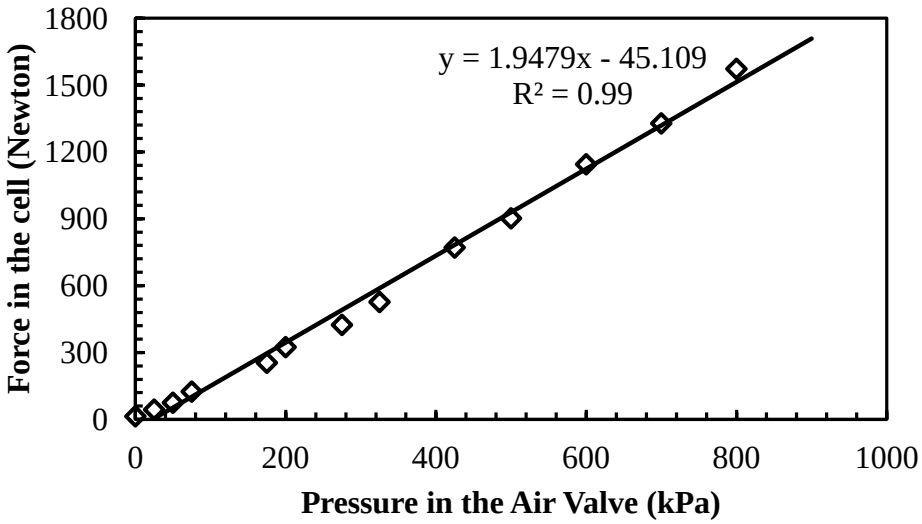

Figure 3.13 Calibration curve for pressure

3.5.3.3 Electrical Conductivity at Different Consolidation Stages

The magnitude of the current ranged from 70-100 mA during tests. The electrodes were placed in the cell and the annular pores were sealed to avoid water leaking. The inside wall of the modified oedometer was lubricated to reduce wall-friction during the consolidation. A dial gauge was attached to monitor the settlement of soil specimen during consolidation tests.

Tests were conducted on four undisturbed soil samples. The soil samples were trimmed at a dimension of 25 mm (height) × 62.5 mm (diameter). The soil specimen was saturated for three days before starting the consolidation tests, and induced pressure on the soil sample during saturation was 20 kPa. The consolidation test was conducted in the pressure range of 200-800 kPa (at air valve) with an increment of 100 kPa. It should be mentioned that the induced load on the soil samples were calculated utilizing the developed equation. For each load case, measurements were carried out for 24 hours i.e. 0.5, 1.0, 2.0, 4.0, 8,0, 15.0, 30, 60, 120, 240 and 1440 min. The water was drained during the conductivity measurements to avoid short circuit of electrical current. To maintain saturation, water was poured into the cell immediately after electrical measurements.

It should be mentioned that the contact between the electrodes and soil sample was important to determine the two-point electrical conductivity. Therefore, the cell was manufactured using transparent plexi-glass to monitor the contact between soil and electrodes. It was assumed that the voltage drop in electrodes were similar to the soil specimen because a) the height of the specimen was 25 mm, and b) the specimen was in

contact with the electrodes. The experimental setup of the test is illustrated in Figure 3.14.

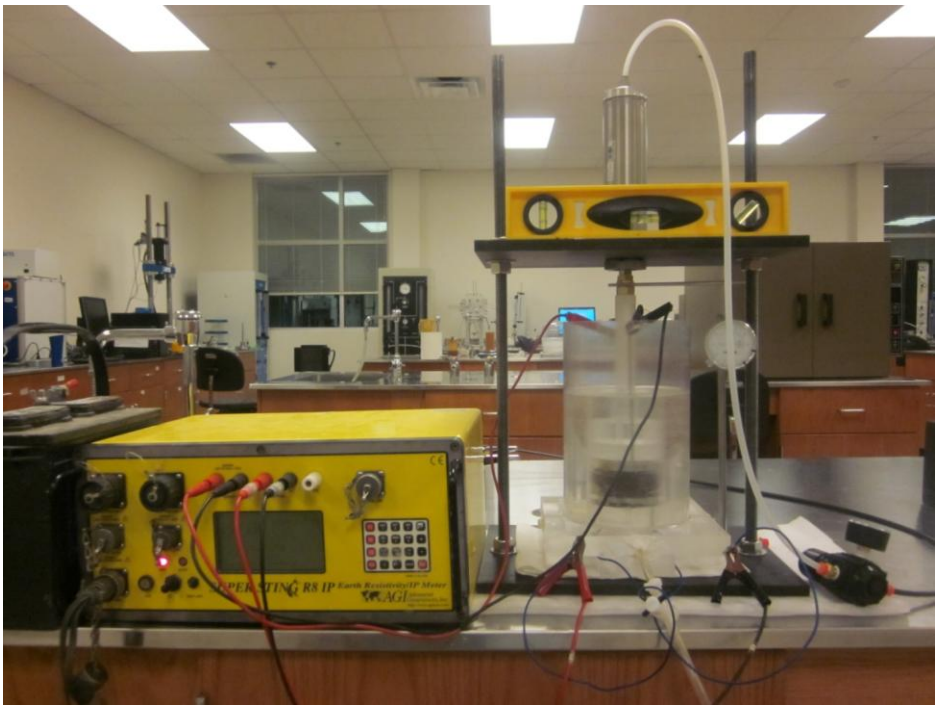

Figure 3.14 Laboratory set-up for electrical conductivity measurements at different consolidation stages

3.6 Repeatability of Electrical Resistivity Measurements

Repeatability indicates the variations in experimental results when tests are conducted on different samples using the same equipment, under the same conditions, and by the same operator. ASTM G187-05 standard test method, which describes the determination of soil resistivity using two-electrode methods, suggested verifying the repeatability of the measurements using coefficient of variation (COV). The COV is the ratio of standard deviation and average of the measurements and expressed in

percentages. In the current study, the repeatability of the soil resistivity was determined using both compacted and undisturbed soil specimen.

3.6.1 Compacted Soil Specimens

Two types of soils i.e. highly plastic clay (B2-20: CH) and low plastic clay (B2-5: CL) were utilized for the tests. Soil resistivity tests were conducted at a fixed dry unit weight and temperature (13.4 kN/m^3 dry unit weight and 72 deg F temperature), whereas the moisture content varied from 10 to 40%. Five different specimens were considered for the repeatability tests on a specific type of soil. The observed resistivity was corrected at 15.5 deg C temperature according to ASTM G187-05 recommendation. The experimental results of the test specimens are presented in Figure 3.15 and 3.16.

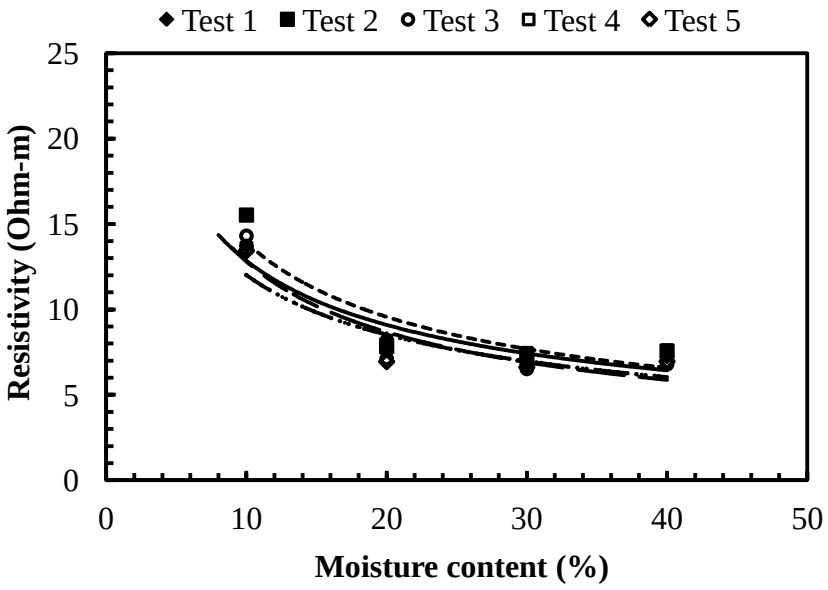

Figure 3.15 Repeatability tests on compacted highly plastic clay (CH)

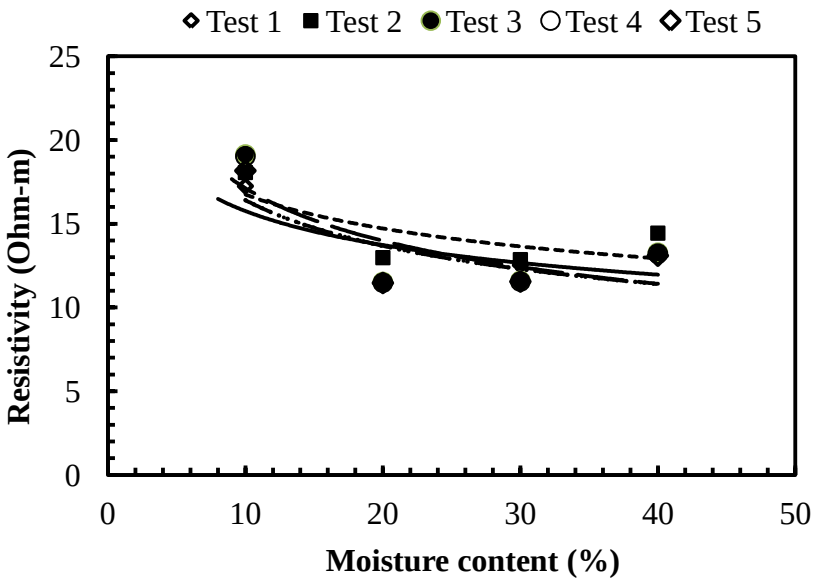

Figure 3.16 Repeatability tests on compacted low plastic clay (CL)

The statistics of the experimental results are presented in Table 3.9 and 3.10. It was observed that the standard deviation and variance of the results of high plastic clay (CH) were 0.85 and 0.72, respectively. However, the maximum values of standard deviation and variance of low plastic clay (CL) were 0.78 and 0.6. The COVs in CH sample ranged from 4.98 to 6.31%. On the other hand, the COVs of CL sample were in between 4.2 and 5.63%. The statistics of Inter-laboratory test results on soil resistivity, determined using two-electrode system, indicated a coefficient of variation of 6.6%. In the current research, the observed COV in the tests were always less than this value (6.6%).

Table 3.9 Statistics of repeatability tests of high plastic clay (CH)

Moisture Content	Test 1	Test 2	Test 3	Test 4	Test 5	Mean	Std. Dev.	Variance	COV (%)
10	13.72	15.53	14.31	13.61	13.44	14.12	0.85	0.72	6.02
20	8.28	7.83	7.11	7.78	7.2	7.64	0.55	0.30	6.31
30	6.79	7.33	6.52	7.46	6.62	6.94	0.42	0.18	6.10
40	7.23	7.55	6.79	7.62	6.96	7.23	0.36	0.13	4.98

Table 3.10 Statistics of repeatability tests of low plastic clay (CL)

Moisture Content	Test 1	Test 2	Test 3	Test 4	Test 5	Mean	Std. Dev.	Variance	COV (%)
10	17.25	18.06	19.14	19.03	18.17	18.33	0.78	0.60	4.23
20	11.51	12.98	11.52	11.48	11.46	11.79	0.66	0.44	5.63
30	12.54	12.86	11.60	11.55	11.55	12.02	0.63	0.40	5.26
40	13.17	14.44	13.27	13.21	13.10	13.44	0.56	0.32	4.20

3.6.2 Undisturbed Soil Specimens

The soil resistivity tests of the undisturbed soil samples were conducted at subsequent drying stages and the observed resistivity results were corrected at 15.5 deg. C temperature. Two soil types i.e. CH (B1-15) and CL (B1-10) were considered for the repeatability tests. Although resistivity was measured at a regular time interval, the variation in moisture was not same for the soil specimens. In addition, the tests were conducted on two specimens for each type of soil. Therefore, test statistics were not determined on the observed results. However, from the graphical point of view, the repeatability of the tests was quite satisfactory. The repeatability of the resistivity results for the undisturbed soil samples are presented in Figure 3.17 and 3.18.

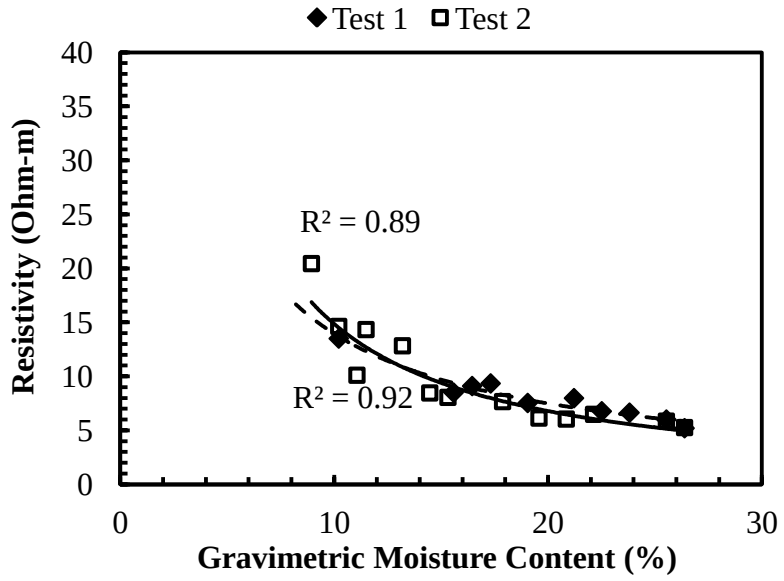

Figure 3.17 Repeatability tests on undisturbed samples (CH)

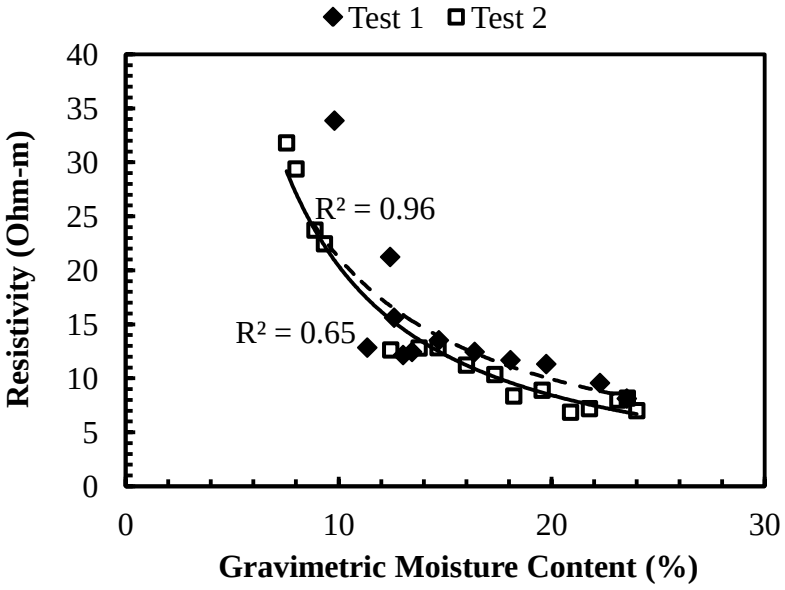

Figure 3.18 Repeatability tests on undisturbed samples (CL)

3.7 Statistical Modeling

Multiple linear regression (MLR) analyses were conducted to correlate electrical resistivity of soils with influential index properties. The statistical analysis software SAS

was utilized for the MLR modeling. Two MLR models were developed for undisturbed and compacted soil specimens. An initial analysis was performed and the following MLR model assumptions were verified:

- applicability of linear regression for the current data set
- constant variance of the error terms
- independent error terms
- normal distribution of the errors
- presence of outlier, and
- multicollinearity among the predictor variables

After the development of the model, the predictive capability of the models was evaluated using experimental results of separate soil specimens.

3.8 Model Validation

The developed statistical models were utilized for the prediction of degree of saturation in the field condition using resistivity imaging (RI) results. RI tests were conducted on compacted clay liner at Cell 4 of City of Denton MSW Landfill, and slopes along highway Loop 12 and US 287 south. Super Sting R8/IP multichannel system, manufactured by Advanced Geosciences Inc. (AGI), was used for the RI tests. EarthImager 2D software was utilized for the analysis of observed apparent resistivity and construction of resistivity image of the subsurface. To obtain RI image, a finite element method with Cholesky decomposition equation solver and Dirichlet boundary condition was employed for forward modeling.

3.9 Summary

The objective of this chapter was to describe the test methodologies of the current study. Tests were conducted on varied types of soil specimens to investigate the potential clay properties affecting electrical resistivity of the specimens. A summary of the soil characterization and electrical resistivity tests procedure can be mentioned below:

1. Both disturbed and undisturbed soil samples were collected from two soil test borings, conducted on a slope at highway Loop12 near Dallas, TX. In addition, two clay minerals i.e. Ca-bentonite and kaolinite, and four artificial soils were utilized to identify the effect of physicochemical properties of clays on electrical resistivity.
2. The grain size distribution, Atterberg limits, cation exchange capacity (CEC), specific gravity, moisture content, and unit weight of the samples were determined according to ASTM standard methods. Moreover, specific surface area (SSA) and dominant mineral were identified using index properties of the soil samples.
3. In addition to conventional geotechnical properties, scanning electron microscope (SEM) and energy dispersive X-ray spectroscopy (EDS) methods were used for the investigation of fabric morphology and elemental composition of the specimens. As the pore water properties substantially affects electrical properties of soils, the ion composition and electrical conductivity of pore water were determined using ion chromatography (IC).

4. After the characterization of specimens, electrical resistivity tests were conducted with four-electrode configuration using Super Sting equipment. For the compacted clays four samples: a) highly plastic clay (CH), b) low plasticity clay (CL), c) Ca-bentonite, and d) kaolinte were utilized. Before the initiation of the tests, calibrations were performed to evaluate the sensitivity of resistivity measurement of the equipment. Moreover, the applicability of the coefficient for temperature correction in ASTM G187-05 standard was evaluated.
5. Two cylindrical stainless steel plates were fabricated to determine the electrical resistivity of the undisturbed soil samples. A series of tests were conducted to determine the effects of sample size on resistivity. It can be mentioned that the electrical resistivity tests were performed on six specimens at subsequent drying stages.
6. To identify the relationship between compressibility and electrical conductivity, a new cell was designed, and fabricated. A pneumatic piston was utilized for the application of load, and a calibration curve was developed using pressure cell. Electrical conductivity was measured in conjunction with consolidation on four undisturbed samples.
7. Multiple linear regression (MLR) analyses were conducted using statistical analysis software SAS (2009) to correlate resistivity with influential geotechnical properties.
8. The MLR model was utilized for the prediction of degree of saturation in the field condition using resistivity imaging (RI) results. RI tests were conducted on

compacted clay liner at Cell 4 of City of Denton MSW Landfill, slopes along highway Loop 12, and US 287 south.

CHAPTER 4

SOIL CHARACTERIZATION

4.1 Introduction

The objective of soil characterization was to evaluate the behavior of test specimens, and to establish quantitative correlations between soil resistivity and geotechnical properties. Therefore, an experimental program was developed to determine the soil properties, elemental composition, and fabric morphology. This chapter presents soil characterization results, which include a) physical properties, b) mineralogical content, and c) pore water characteristics.

4.2 Geotechnical Properties

4.2.1 Grain Size Distribution

Grain size distribution of the soil samples are presented in Figure 4.1. It was observed that the percent passing through No.200 sieve ranged from 64.3 to 94.3% in the soil samples. The soil sample B1-15, B2-20, and B2-25 were characterized as highly fine grained with percentages passing through No. 200 sieve was more than 90%. On the other hand, fine fraction was small compared to the other specimen in B1-10 (64.3% passed through No. 200 sieve).

The grain size distribution of Ca bentonite and kaolinite emphasized that the percent passing No.200 sieve were 94% and 100%, respectively.

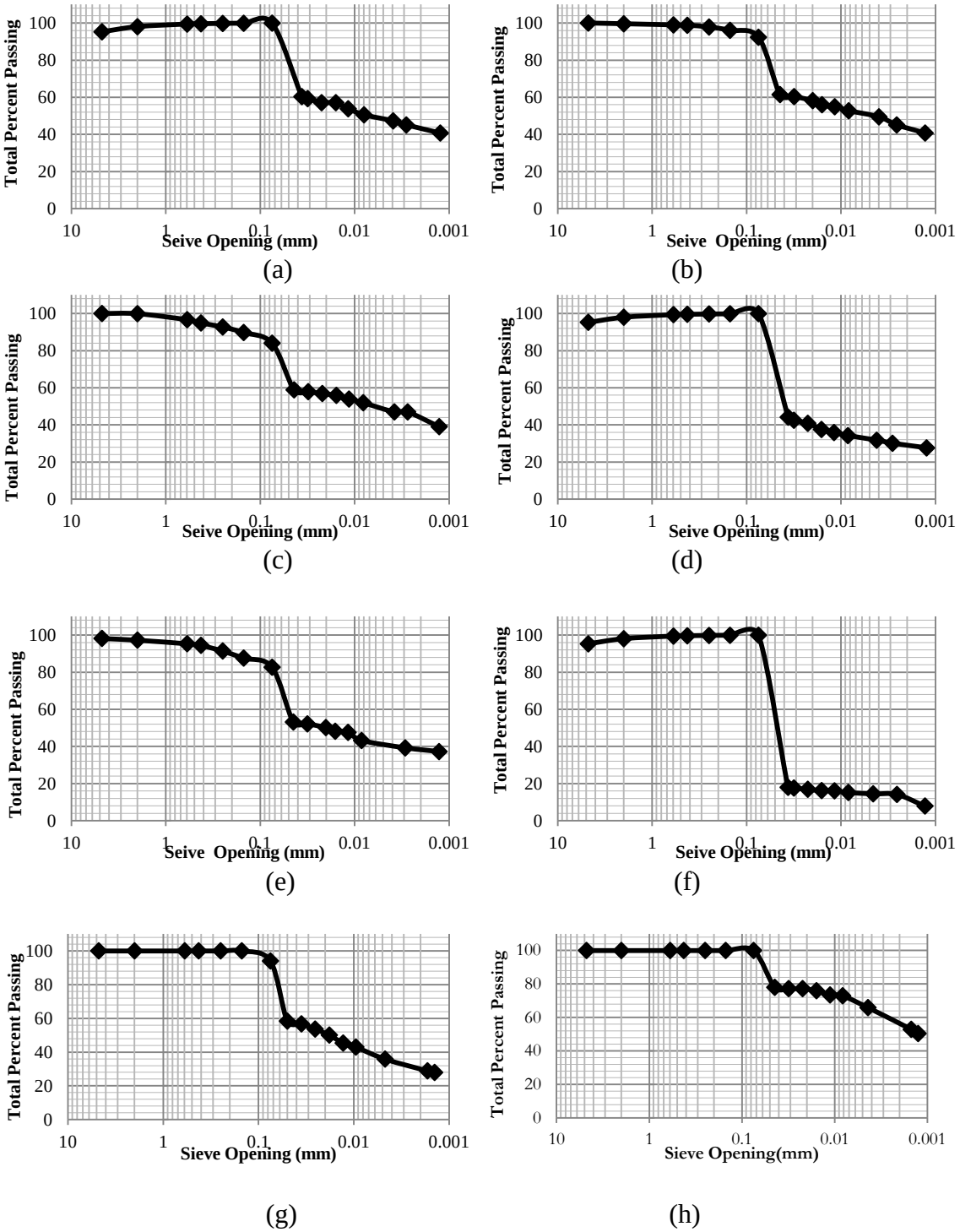

Figure 4.1 Grain size distribution of the test specimen (a) B1-15, (b) B2-20, (c) B1-10 (d) B2-5, (e) B2-10, (f) B2-25, (g) Ca bentonite, and (h) Kaolinite

4.2.2 Atterberg limits

Typically, liquid limits of bentonite, illite, and kaolinite range from 100-900, 60-120, and 30-110, respectively (Mitchell and Soga, 2005). However, according to White (1949), liquid limit of illite can be as low as 29.

The observed liquid limits and plasticity indices of the soil samples collected from soil test boring were in between 36 to 53 and 15 to 33, respectively. However, the liquid limit of Ca bentonite was as much as 107. Although kaolinite sample was characterized with liquid limit and plasticity index of 61 and 24, the activity of the mineral was 0.43. A summary of Atterberg limits of the test specimens are presented in Table 4.1.

Table 4.1 Atterberg limits of the natural soils and minerals

Sample ID	**LL**	**PI**	**Activity (Skempton, 1953)**	**USCS Classification**
B1-15	52	33	0.65	CH
B2-20	53	30	0.57	CH
B1-10	36	21	0.40	CL
B2-25	53	30	1.97	CH
B2-5	41	21	0.61	CL
B2-10	50	22	0.51	CL
B1-30	32	15	0.52	CL
Ca-bentonite	107	55	1.83	-
Kaolinite	61	24	0.43	-

Based on the grain size distribution and Atterberg limits test results, soil samples were classified as high plasticity clay (CH) and lean clay (CL) according to Unified Soil Classification System (USCS).

In addition to minerals and natural soil specimens, Atterberg limits tests were performed on artificial soil samples as presented in Table 4.2. It was observed that the soils with high percentages of Ca bentonite fractions were characterized by high LL and PIs. Moreover, LL and PIs of the artificial specimens are linear functions of the mineral percentages as presented in Figure 4.2.

Table 4.2 Atterberg limits of artificial soils

% Wt of Ca-bentonite	LL	PL	PI
80	80	37	43
60	55	29	26
40	40	22	18
20	22	15	7

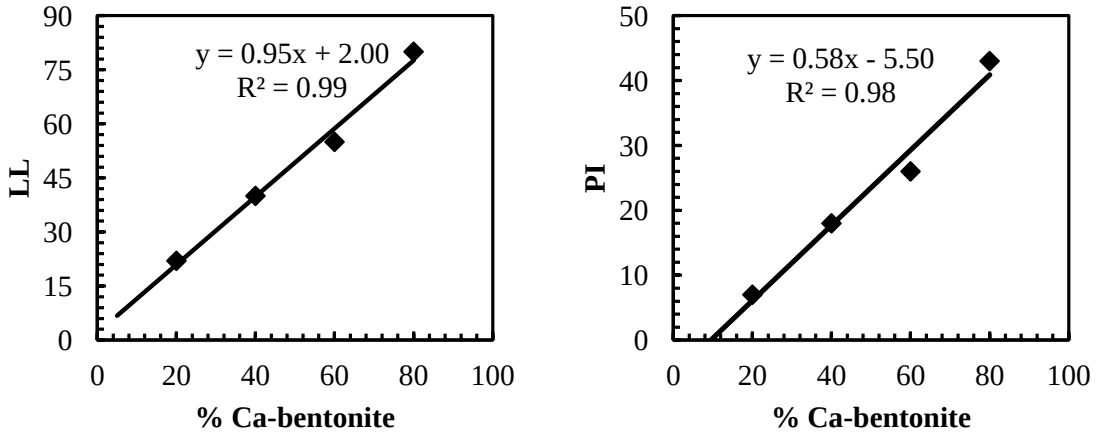

(a) (b)

Figure 4.2 (a) LL vs. Ca bentontie (b) PI vs. Ca bentonite

4.2.3 Moisture content and Unit weight of the Samples

The moisture contents and unit weights of the samples collected from the soil test boring were investigated. According to the test results, moisture contents of the samples varied from 20.8 to 32.4%, and the dry units of the specimens were over 13 kN/m^3. The moisture contents and dry unit weights of the specimens are presented in Table 4.3.

Table 4.3 Moisture content and dry unit weight of the specimen

Sample ID	**Moisture content (%)**	**Dry unit weight (kN/m^3)**
B1-15	32.4	13.1
B2-20	27.6	14.8
B1-10	29.7	13.8
B2-25	20.8	16.2
B2-5	22.2	16.1
B2-10	22.2	16.1

4.2.4 Specific Gravity

Specific gravity of collected soil samples, minerals, and artificial soil samples were determined. The specific gravity of the test specimens are summarized in Table 4.4 and 4.5. It can be mentioned that the specific gravity of artificial soil samples are linear function of bentonite percentages as presented in Figure 4.3.

Table 4.4 Specific gravity of the soil specimens

Sample ID	Specific Gravity
B1-15	2.67
B2-20	2.65
B1-10	2.73
B2-25	2.56
B2-5	2.73
B2-10	2.66
B1-30	2.67
Ca bentonite	2.42
Kaolinite	2.68

Table 4.5 Specific gravity of the artificial soils

% Wt of Ca-bentonite	Specific Gravity
80	2.44
60	2.63
40	2.56
20	2.69

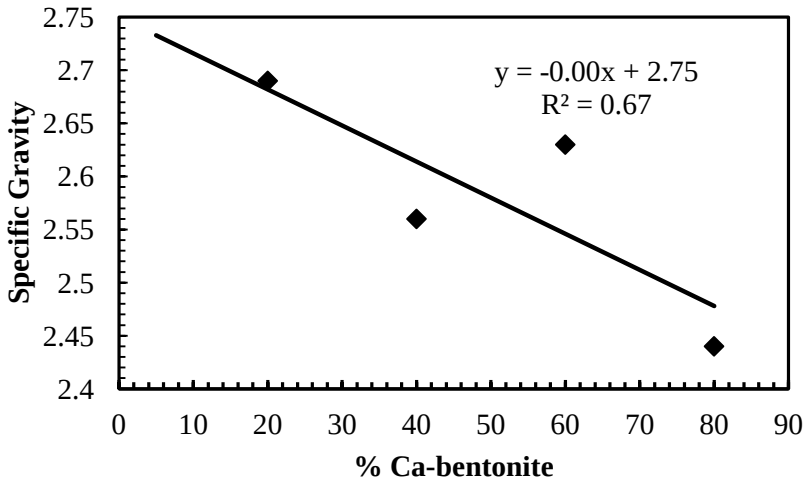

Figure 4.3 Specific gravity vs. percentages Ca bentonite

4.2.5 Cation Exchange Capacity (CEC) and Specific Surface Area

The CEC and SSA of the soil specimens are summarized in Table 4.6. The CEC of the soil specimens ranged from 13.3 to 79.9 cmol+/kg. It is evident that electrical conductivity enhances with the presence of ions in the pore water. The exchangeable ions in kaolinite mineral are located at the edges of the crystal where as bentonite composed of exchangeable ions both at the edges and within lattice structure. Therefore, the contribution of precipitated ions is significant in bentonite compared to kaolinite.

SSA of the soil samples were calculated using the correlation indicated by Farrar and Coleman (1967). The observed liquid limits of the samples were utilized to determine SSAs. The SSA of Ca bentonite was high compared to the natural soils and kaolinite.

Table 4.6 CEC and SSA of the test specimens

Sample ID	CEC (cmol+/kg)	SSA (m^2/gm)
B1-15	29.9	58.93
B2-20	40.9	60.71
B1-10	27.7	30.36
B2-25	30.2	60.71
B2-5	23.9	39.29
B2-10	30.2	55.36
B1-30	19	23.2
Ca bentonite	79.9	157.14
Kaolinite	13.3	75

The CEC and SSA of artificial soils indicated that the clay properties linearly increased with the increase of bentonite percentages. For the increase of bentonite percentages 20 to 80%, CEC and SSA increased 27.86 to 63.5 cmol+/kg and 5.36 to 108.9 m^2/gm, respectively. The CEC and SSA of the artificial specimens are illustrated in Table 4.7.

Table 4.7 CEC and SSA of the artificial soils

% Wt Ca bentonite	CEC (cmol+/kg)	SSA (m^2/gm)
80	63.5	108.93
60	45.52	64.29
40	38.11	37.50
20	27.86	5.36

The linear correlations of CEC and SSA with bentonite percentages are presented in Figure 4.4.

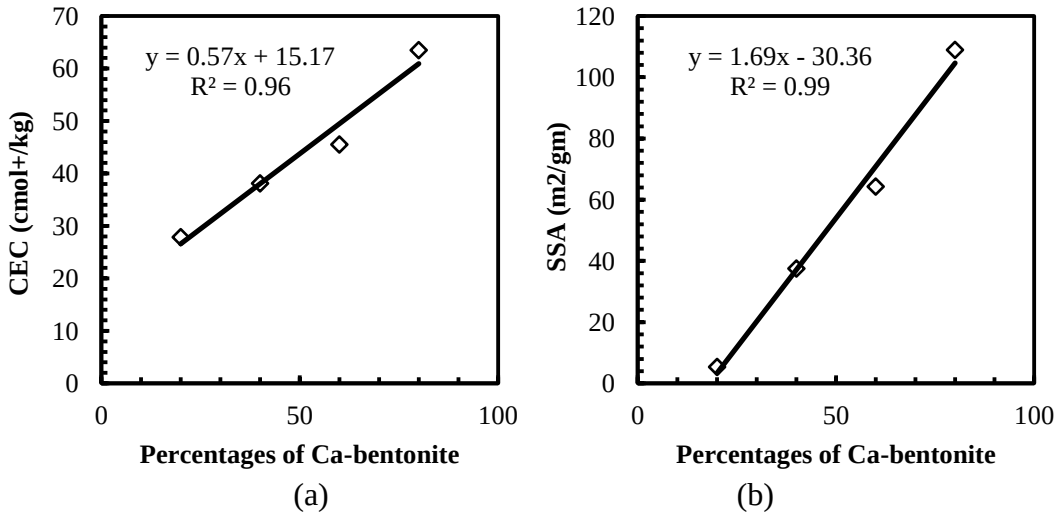

Figure 4.4 (a) CEC vs. bentonite percentages (b) SSA vs. bentonite percentages

It should be mentioned that the CEC of the soil samples were also determined using the correlations of Farrar and Coleman (1967), Smith et al. (1985), and Yukselen and Kaya (2006). The available correlations can be used to determine CEC using the index properties. The obtained CEC values are presented in Table 4.8. It was observed that the proposed correlation by Yukselen and Kaya (2006) were close to the measured CEC results.

Table 4.8 Determination of CEC using correlations

Sample ID	Measured CEC	Yukselen and Kaya (2006)	Farrar and Coleman (1967)	Smith et al. (1985)	Smith et al. (1985)
	cmol+/kg	0.2027 LL + 16.231	0.55LL-12.2	1.74LL-38.15	3.57PL-61.3
B1-15	29.9	26.7714	16.4	52.33	6.53
B2-20	40.9	26.9741	16.95	54.07	20.81
B1-10	27.7	23.5282	7.6	24.49	-7.75
B2-25	30.2	26.9741	16.95	54.07	20.81
B2-5	23.9	24.5417	10.35	33.19	10.1
B2-10	30.2	26.366	15.3	48.85	38.66

4.2.6 Mineral Characterization from Physical Properties

The dominant mineral content of the soil samples collected from boreholes were determined using Atterberg limits (Holtz and Kovac, 1981), activity (Mitchell and Soga, 2005), and free swell ratio (Prakash and Sridharan, 2001). The study results are summarized in Table 4.9.

Table 4.9 indicated that the dominant clay mineral of the soil samples was illite according to Holtz and kovacs (1981) correlation. It can be mentioned that Holtz and kovacs (1981) used LL and PI for the prediction. However, the soil samples were characterized as kaolinite according to Prakash and Sridharan (2001) and Mitchell and Soga (2005). Prakash and Sridharan (2001) utilized free swell ratio to determine the dominant clay mineral in a soil sample. On the other hand, Mitchell and Soga (2005) used LL and PI for the prediction of dominant clay mineral.

Based on the physical properties, soil samples were classified as illite or kaolinite. Although exact information about the clay mineral was not determined, the correlations provided an indication about the swell properties of the soil. To identify the clay mineralogy, advanced characterization was conducted on the soil samples, which included a) scanning electron microscope (SEM) and b) Energy dispersive x-ray spectroscopy (EDS).

Table 4.9 Determination of dominant clay mineral from physical properties

Sample ID	**Clay Mineral from LL and PI Mitchell and Soga (2005)**	**Clay Mineral from LL and PI Holtz and kovacs (1981)**	**Clay Mineral from FSR Prakash and Sridharan (2001)**
B1-15	Kaolinite/Dehydrated Hallosite	Illite	Kaolinite
B1-25	Kaolinite/Dehydrated Hallosite	Illite	Kaolinite
B2-20	Kaolinite/Dehydrated Hallosite	Illite	Kaolinite
B2-15	Kaolinite/Dehydrated Hallosite	Illite	Kaolinite
B1-10	Nontronite/close to Kaolinite	Illite	Kaolinite
B2-25	Kaolinite/Dehydrated Hallosite	Illite	Kaolinite
B2-5	Nontronite/close to Kaolinite	Illite	Kaolinite and Montmorillonite
B2-10	Nontronite/close to Kaolinite	Illite	Kaolinite and Montmorillonite

4.3 Elemental Composition and Fabric Study

4.3.1 Scanning Electron Microscope (SEM)

An assessment of microstructure is important from geotechnical engineering viewpoint because soil behavior largely depends on the fabric structure. In the current study, fabric structure was analyzed using scanning electron microscope (SEM) at different magnifications. SEM images of the minerals are presented in Figure 4.5. According to Mitchell and Soga (2005) the main difficulties of SEM study is the preparation of surface replicas. Therefore, special attention is required to obtain undisturbed sample for SEM analysis. In the current study, sedimentation method was employed to prepare sample for SEM study.

The SEM image of well crystallized kaolinite looks like six sided plate. Lateral dimensions of the plate are in the order of 0.1 to 0.4 micrometer and their thickness ranged from 0.05 to 2 micrometer (Mitchell and Soga, 2005). However, the hexagonal shape of poorly crystallized kaolinite is not distinct. On the other hand, surface morphology of montmorillonite mineral is characterized by equidimensional flakes, and may appear as thin films. Furthermore, a directional strain caused by large amount of substitution of iron and/or magnesium with aluminum may result needle shaped fabric structure in montmorillionite.

Illite is generally flaky particles, and a well crystallized illite may consist hexagonal outline (Mitchell and Soga, 2005). However, illite typically consists of other clay and non-clay material.

The surface topography of Ca bentonite appeared as flaky structure (Figure 4.5 f). The presences of few thin strips were identified in Ca-bentonite structure. Therefore, the fabric of Ca-bentonite indicated a probable isomorphous substitution of aluminum ions with iron and magnesium. According to EDS analyses, a total of 8.83% of iron and magnesium ions were present in this specimen. The directional strain caused by isomorphous substitution might result needle like fabric shape in Ca-bentonite mineral.

The analysis on the SEM images of the sample showed that the fabrics were not consisted of flaky structure. Although very distinct hexagonal shape were not observed in the soil samples, there was an indication of hexagonal fabric structure. Therefore, there is a good possibility of occurrence of poorly crystallized kaolinite in the samples. However, specific conclusions about the clay mineral was not possible only from SEM images.

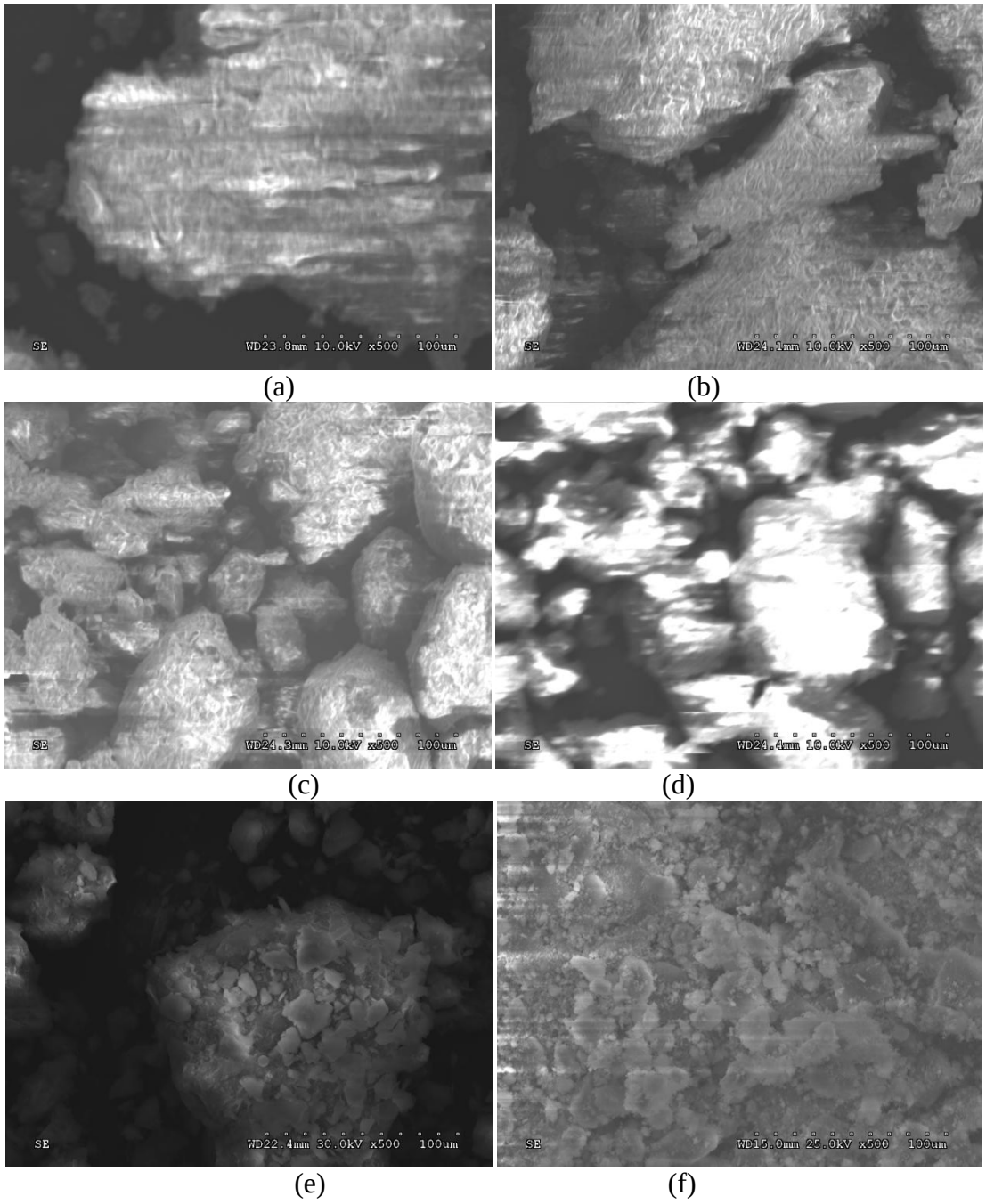

(a) (b)

(c) (d)

(e) (f)

Figure 4.5 SEM images of the soil samples (a) B1-10 (b) B1-15(C) B2-15 (d) B2-25 (e) Ca-bentonite (f) Kaolinite

4.3.2 Energy Dispersive Spectroscopy

EDS analyses results are presented in Figure 4.6, and summarized in Table 4.10. It was observed that Ca-bentonite consisted of high percentages of oxygen (28.1%), aluminum (6%), and silicon (21.8%). In addition, substantial amount of iron (7%), calcium (2.7%), and carbon (31.3%) were identified in Ca-bentonite mineral. In case of kaolinite mineral, oxygen, aluminum, and silicon consisted of 89.9% of the total proportion. Moreover, the presence of iron and potassium were also identified in this mineral.

The EDS analyses of the soil samples collected from boreholes indicated that the presence of oxygen, aluminum, and silicon are significant in the specimens. In addition, calcium content ranged from 2.34% to 3.43%. Nonetheless, the percentages of potassium contents were not significant in the soil samples.

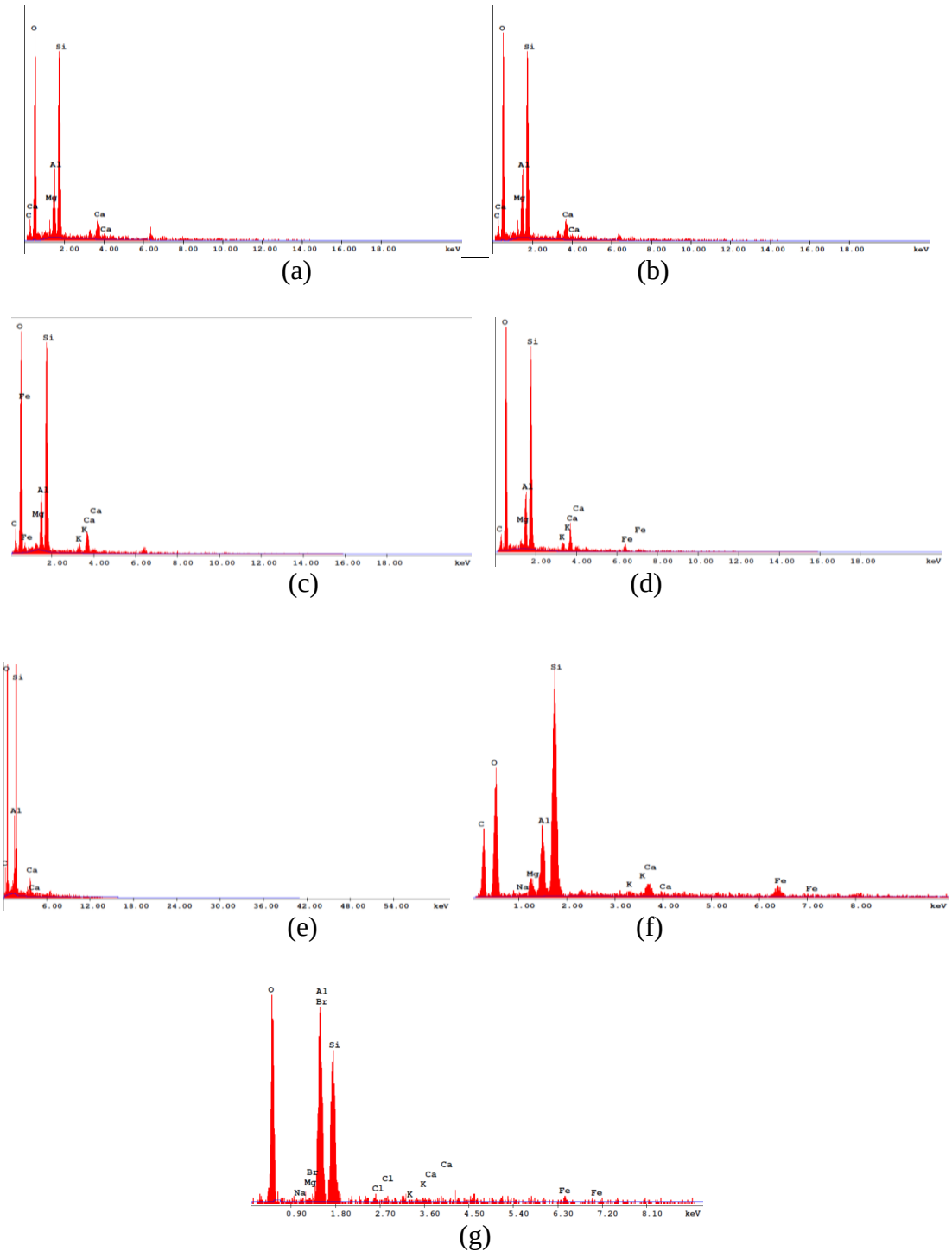

Figure 4.6 EDS analysis results (a) B1-10, (b) B1-15, (c) B2-15, (d) B2-10, (e) B2-25, (f) Ca-bentonite, and (g) Kaolinite

Table 4.10 Summary of EDS results

Sample ID	C	O	Mg	Al	Si	Ca	K	Fe	Na	Br
B1-10	13.99	55.16	0.94	6.8	19.93	3.18				
B1-15	22.66	52.06	0.65	6.38	14.8	2.41	1.03			
B2-15	15.64	47.74	0.62	5.18	18.48	2.96	0.79	8.58		
B2-20	12.85	53.68	0.82	5.94	19.63	3.43	1.06	2.6		
B2-25	14.75	55.63	-	4.75	22.52	2.34				
Ca bentonite	31.32	28.05	1.82	6	21.81	2.75	1.01	7.01	0.23	
kaolinite		43.9		19.8	26.23		0.32	2.44		7.3

Typical empirical formulas of three clay minerals are presented in Table 4.11. It can be observed that kaolinite mineral consists of oxygen, aluminum, hydroxyl, and silicon ion. In contrast, magnesium and iron ions are present in illite. However, percentages of potassium were not substantial in the soil samples collected from boreholes. It can be mentioned that potassium is the binder element in illite mineral.

Based on the physical properties, SEM, and EDS analysis, it was identified that the dominant mineral in the specimen was kaolinite with some traces of magnesium, calcium, potassium, and iron.

Table 4.11 Chemical formulas of clay minerals (webmineral.com)

Clay Mineral	Layer type	Empirical Formula
Kaolinite	1:1	$Al_2Si_2O_5(OH)_4$
Montromorillonite	2:1	(Na,Ca) 0.3 (Al, Mg)$_2$Si$_4$O$_{10}$(OH)$_2$. n H_2O
Illite	2:1	(K,H_3O)(Al,Mg,Fe)$_2$(Si,Al)$_4$O$_{10}$[(OH)$_2$,(H_2O)]

4.4 Ion Chromatography test of Pore water

Pore water properties plays an important role in the electrical conductivity of soil. Therefore, pore water was characterized using ion chromatography (IC) method. The study results are presented in Table 4.12 and 4.13. It can be mentioned that the electrical conductivity and pH of pore water of Ca bentontie, kaolinite, CL, and CH are 1805,414, 1028, and 1436 microsiemens/cm, and 7.46, 5.6, 7.64, and 7.58, respectively. The electrical conductivity of the pore water extracted from Ca-bentonite was high compared to other samples indicating the presence of large amount of surface charge in this mineral. The conductivity and pH of kaolinite were 414 micro- siemens/cm and 5.6, respectively. The pH of 5.6 might emphasize the existence of Lewis acid sites in the surface of kaolinite mineral. Lewis acid sites may develop in kaolinte because of the protonation of surface hydroxyl group (Sposito, 2008).

IC results showed that the concentration of sulphate ion varied significantly among the pore water of the soil samples. The concentration of sulphate ions of Ca-bentonite and kaolinite were 824.3 and 88.5 mg/L, respectively. In addition, the concentrations of nitrate and chloride were high in the pore water of CH and CL. However, significant variations were not observed for the fluoride, formate, and nitrite ions in the extracted pore water of specimens. Cation analyses indicated that magnesium and potassium contents were high in the extracted pore water (Table 4.13). Moreover, sodium and calcium ions were not detected in the kaolinite sample.

Table 4.12 The observed anion from extracted pore water

Sample	Fluoride (mg/L)	Formate (mg/L)	Chloride (mg/L)	Nitrite (mg/L)	Bromide (mg/L)	Nitrate (mg/L)	Phosphate (mg/L)	Sulfate (mg/L)
Ca-bentonite	0.49	0.48	1.85	0.04	0.00	18.30	0.00	824.31
Kaolinite	0.16	0.00	3.93	0.00	0.00	3.09	0.00	88.45
CH	0.72	0.00	19.90	1.79	2.26	10.32	0.00	382.52
CL	0.89	0.62	21.42	0.75	2.59	0.00	0.29	197.77

Table 4.13 The observed cation from extracted pore water

Sample	Lithium (mg/L)	Sodium (mg/L)	Ammonium (mg/L)	Potassium (mg/L)	Calcium (mg/L)	Magnesium (mg/L)
Ca-bentonite	0.19	43.61	0.47	29.44	25.11	249.82
Kaolinite	0.29	-	3.70	10.89	-	28.51
CL	0.19	76.23	6.18	12.52	6.03	144.73
CH	0.26	141.61	11.40	15.50	7.92	185.36

4.5 Summary

The objective of the chapter was to describe the characterization test results of the soil samples. A detail investigation was conducted to determine physical properties, constituent element, fabric morphology, and pore water composition. A summary of the results are presented herein:

1. The soil samples were classified as highly plastic clay (CH) and low plasticity clay (CL) according to Unified Soil Classification Method (USCS). The observed liquid limits and plasticity indices of the soil samples collected from soil test

boring were in between 36 to 53 and 21 to 33, respectively. However, the liquid limit of Ca bentonite was as much as 107.

2. The CEC of the soil specimens ranged from 13.3 to 79.9 cmol+/kg. It can be mentioned that the LL, PI, CEC, specific gravity, and SSA of artificial soils increased with the increase of mineral percentages. Moreover, the trend of variation was linear in each case.
3. The analysis on the SEM images of the samples showed that the fabrics were not consisted of flaky structure. Although very distinct hexagonal shape were not observed in the soil samples, there was an indication of hexagonal outline. Therefore, there is a good possibility of occurrence of poorly crystallized kaolinite in the samples. However, specific conclusion about the clay mineral was not drawn only from SEM images.
4. The EDS analyses of the soil samples collected from boreholes indicated that the presence of oxygen, aluminum, and silicon in all the specimens. In addition, calcium content ranged from 2.34 to 3.43%. Nonetheless, the percentages of potassium content were not significant in the soil samples.
5. Based on the physical properties, SEM, and EDS analysis, it was identified that the dominant mineral in the specimen was kaolinite with some traces of magnesium, calcium, potassium, and iron.
6. IC results showed that the concentration of sulphate ion varied significantly among the pore water of the soil samples. The concentration of sulphate ions of Ca-bentonite and kaolinite were 824.3 and 88.5 mg/L, respectively. Cation

analyses indicated that magnesium and potassium contents were high in the extracted pore water.

CHAPTER 5

ELECTRICAL RESISTIVITY TEST RESULTS

5.1 Introduction

The influences of gravimetric moisture content, degree of saturation, and volumetric moisture content were investigated using compacted clays and undisturbed soil specimens. However, the effects of dry unit weight and void ratio of the samples were analyzed using compacted clays. The electrical resistivity of undisturbed soil samples were measured at varied drying stages. Therefore, the variations of resistivity in undisturbed soil samples were related to the changes in gravimetric water contents, degrees of saturation, and volumetric moisture contents. As the electrical resistivity of clayey soil is influenced by the surface charge and isomorphous substitution, the effects of physicochemical properties on electrical resistivity were also identified. The investigated parameters in the current study are summarized in Table 5.1.

Table 5.1 Investigation of influential parameters affecting resistivity

Influential Properties affecting Resistivity	**Investigated Parameters**
Related to Phase Relationship	Moisture content, void ratio, unit weight, volumetric water content, and degree of saturation
Related to Clay Properties	CEC, PI, LL, SSA, Pore water conductivity, and sulphate content, and mineral percentages
Related to Compressibility	Consolidation properties and hydraulic conductivity

5.2 Influential Parameters Related to Phase Relationship

According to the literature, electrical resistivity of soils substantially influenced by moisture content, void ratio, and dry unit weight. The properties mentioned herein can be described as the parameters related to phase relationship in soils. In addition, degree of saturation and volumetric water content are related to the gravimetric moisture content, dry unit weight, void ratio, and specific gravity. In the following subsections, the electrical resistivity responses under gravimetric moisture content, dry unit weight, void ratio, volumetric water content, and degree of saturation are investigated for compacted clays and undisturbed soil samples.

5.2.1 Effects of Gravimetric moisture contents

The variations of soil resistivity with gravimetric moisture contents at varied dry unit weights are presented in Figure 5.1. It was observed that an increase in moisture content caused significant reduction in resistivity. However, the resistivity responses were different for different soil specimens. According to Figure 5.1, soil resistivity decreased as much as 6.8, 4.8, and 3.5 times of their initial values for the increase of moisture content from 10 to 30% at 13.4 kN/m^3 dry unit weight in Ca-bentonite, CL, and CH specimen, respectively. However, substantial variation in resistivity was not observed in the moisture range 30 to 40% in these samples.

The resistivity decreased from 501 to 46 Ohm-m for the increase of moisture 10 to 30% in kaolinite sample. Moreover, resistivity reduced from 46 to 33 Ohm-m in the moisture range 30 to 40% in this specimen.

The variations of resistivity in response to gravimetric moisture contents for undisturbed soil samples are presented in Figure 5.2. Although initial moisture contents were not similar in the undisturbed soil specimens, reduction in resistivity followed similar trend in each case. In undisturbed soil specimens, resistivity values ranged from 3.2 to 49.4 Ohm-m for the increase in moisture content from 7 to 31.3%.

In the current study, electrical conductivity decreased substantially in between 10 to 30% moisture content; however, the rate of reduction stepped down after 30% water content. The observed phenomena can be discussed using the explanation of Pozdnyakov (2006).

Pozdnyakov (2006) divided electrical resistivity vs. natural logarithm of moisture content curve into various segments (presented in Figure 2.13). The segments of the curve are designated as adsorbed water, film water, film capillary water, capillary water, and gravitational water. According to the author, electrical resistivity decreases rapidly with the increase of moisture content in the adsorption water zone. Although the ions of water molecules are immobile in the adsorbed water zone, the dipolar water creates a conductive path for electrical current. Therefore, electrical resistivity reduces substantially with the increase of moisture in the adsorption zone. However, the rate of reduction decreases in the film water zone because of the increase in Van der Waals' force. When maximum possible thickness of water film is developed, pore water goes from film to fissure. The molecular attraction force is higher than the capillary force in the film capillary water zone. Therefore, the rate of reduction stepped down in the film capillary and capillary water zone. In the gravitational water zone, mobility of electrical

charges becomes independent of movement of water molecule ions, and therefore electrical resistivity is almost independent of water content.

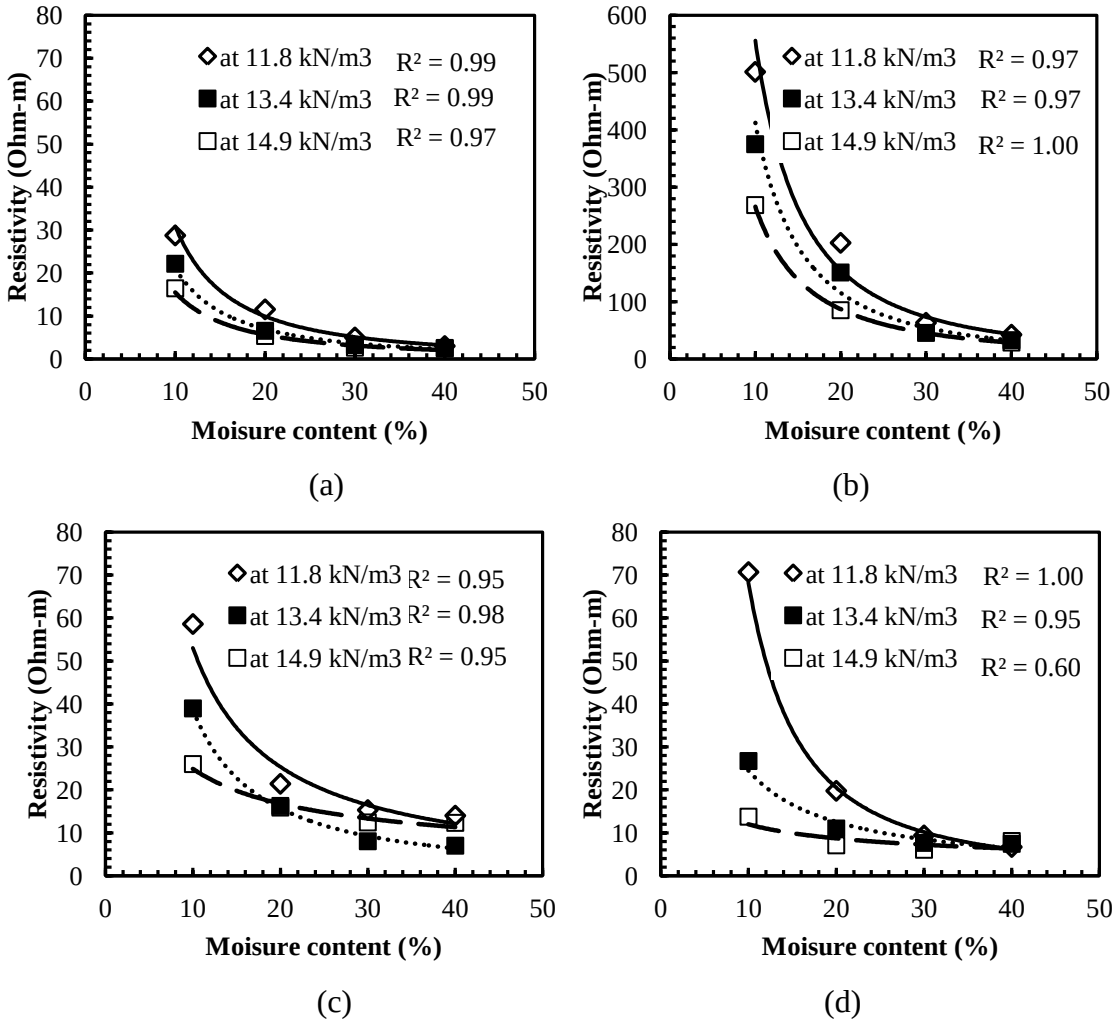

Figure 5.1 Variations in resistivity with gravimetric moisture contents in compacted clays at different dry unit weights (a) Ca-bentonite, (b) Kaolinite, (c) CL (B1-30), and (d) CH (B2-20)

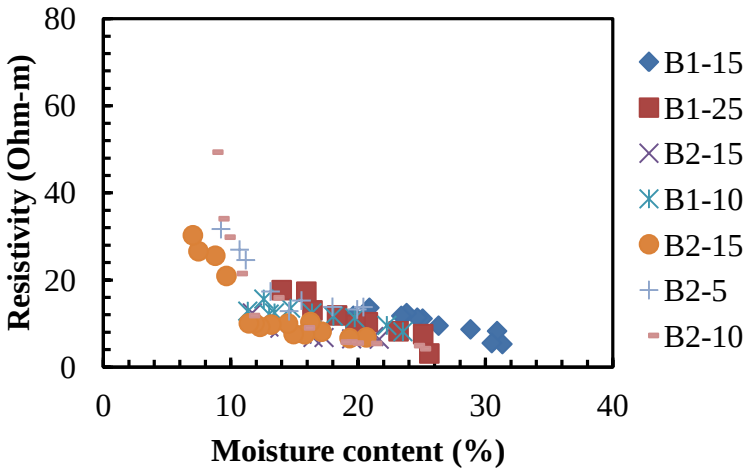

Figure 5.2 Variations in resistivity with gravimetric moisture contents in undisturbed samples

It can be mentioned that the electrical resistivity of Ca-bentonite, CL, and CH were low compared to kaolinite sample. A correlation was developed between resistivity and moisture content for Ca-bentonite, CL, and CH specimens. The statistical significance and regression assumptions of the proposed correlation were investigated. The best-fitted regression line and a comparison with the previous literature are presented in Figure 5.3. It was identified that the study of Abu Hassanein et al. (1996) were in good agreement with the best-fitted regression line. However, a substantial deviation was identified in the comparison of the current results with the study of Ekwue and Bartholomew (2010). The soil specimens were Picaro sand, Maracas clay, and Talparo clay in the study of Ekwue and Bartholomew (2010), and the resistivity was as much as 400 Ohm-m (approximately) at 12% moisture content.

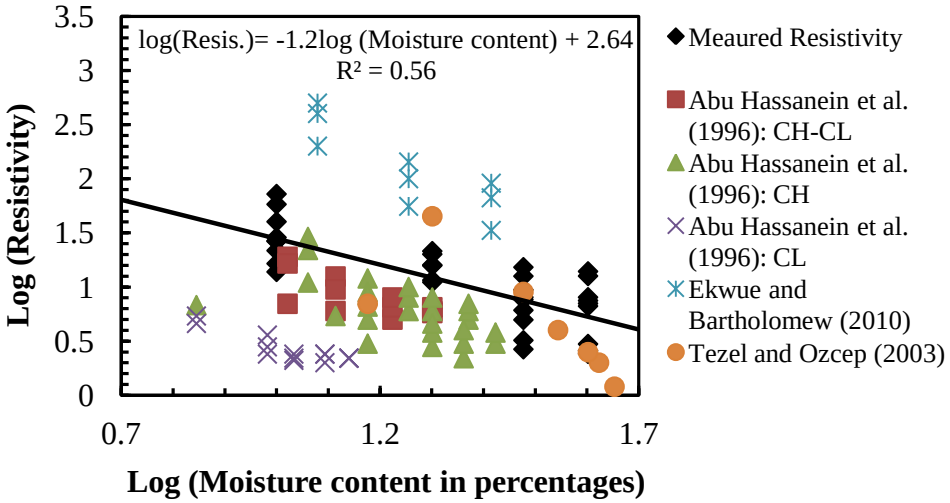

Figure 5.3 Development of correlation between electrical resistivity and moisture content for Ca-bentonite, CH, and CL

Similar correlation was developed for electrical resistivity and moisture content of undisturbed soil specimens. It was observed that the 61% variation in resistivity of undisturbed soil samples was explained by the moisture content. The best-fitted line and proposed correlation is presented in Figure 5.4

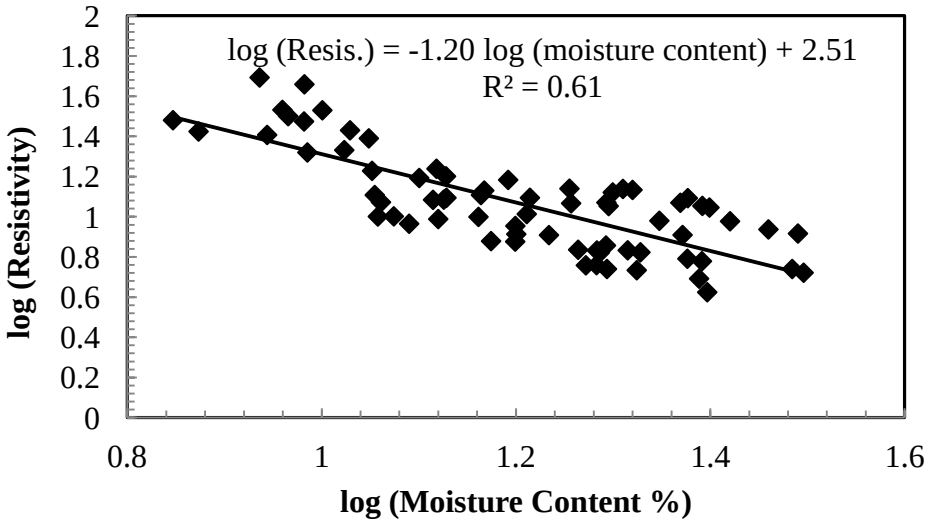

Figure 5.4 Development of correlation between electrical resistivity and moisture content of undisturbed soil samples

5.2.2 Effects of Dry Unit Weight

Figure 5.1 also indicated the variation of resistivity at different dry unit weights. At 20% moisture content and 11.8 kN/m^3 dry unit weight, electrical resistivity values were 11.6, 202.7, 21.4, and 19.8 Ohm-m in Ca-bentonite, kaolinite, CL (B1-30), and CH (B2-20) respectively. Nonetheless, resistivity decreased to 5.4, 85.2, 15.9, and 7.1 Ohm-m in the soil samples at 14.9 kN/m^3 dry unit weight. Therefore, the variations of resistivity values were plotted against dry unit weights at different moisture contents as presented in Figure 5.5. It was identified that resistivity reduction ranged from 5.5 to 12.6 Ohm-m in between 11.8 and 14.9 kN/m^3 dry unit weights at 20% moisture content in Ca-bentonite, CL, and CH samples. However, resistivity reduced as much as 117.5 Ohm-m in kaolinite at this condition.

The observed variation of soil resistivity with unit weight can be explained by the study of Abu Hassanein et al. (1996). At specific moisture content, increase in unit weight is associated with the reduction of pore space, remolding of clay clods, and reorientation of particles. As a result, electrical conduction in the soils increases at high dry unit weights.

As the dry unit weight was not varied during resistivity measurements of undisturbed soil samples, the effects of dry unit weight on electrical resistivity were evaluated in compacted clays only.

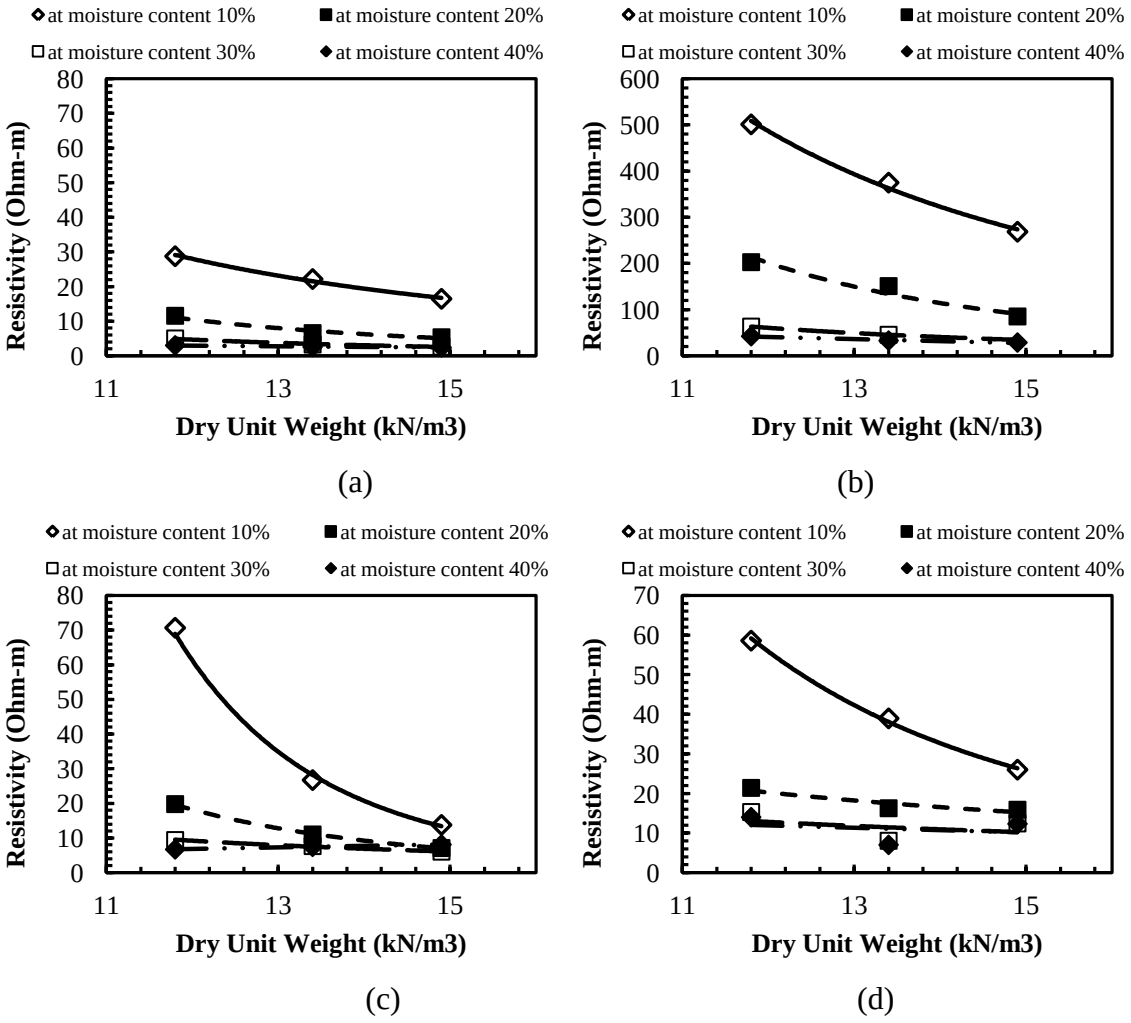

Figure 5.5 Variation of resistivity with dry unit weights for compacted clays at different moisture contents (a) Ca-bentonite, (b) Kaolinite, (c) CL (B1-30), and (d) CH (B2-20)

5.2.3 Effects of Void ratio

Void ratio and associated air void were identified as important factors affecting electrical resistivity of soils. The presence of air voids reduces the interconnectivity of moisture film in the soil grains, which results in a reduction in resistivity.

The void ratio of compacted clay specimens was plotted against resistivity at different moisture contents as presented in Figure 5.6. Electrical resistivity increased from 16.5 to 28.8 Ohm-m for an increase of void ratio 0.59 to 1.01 at 10% moisture content in Ca-bentonite specimen. However, the variation in resistivity was not significant at 40% moisture content in the void ratio range mentioned above. In addition, the observed resistivity results of Ca-bentonite were 11.6 and 5.4 Ohm-m at moisture contents of 10% and 40%, respectively (at 0.78 void ratio). Similar trends of variations were observed in kaolinite, CL, and CH specimens.

According to Figure 5.6, the effect of porosity was significant at low moisture content (i.e. moisture content=10%) because of the presence of air void. However, interconnectivity of moisture with soil particle increased with the increase in moisture content and caused substantial reduction in resistivity.

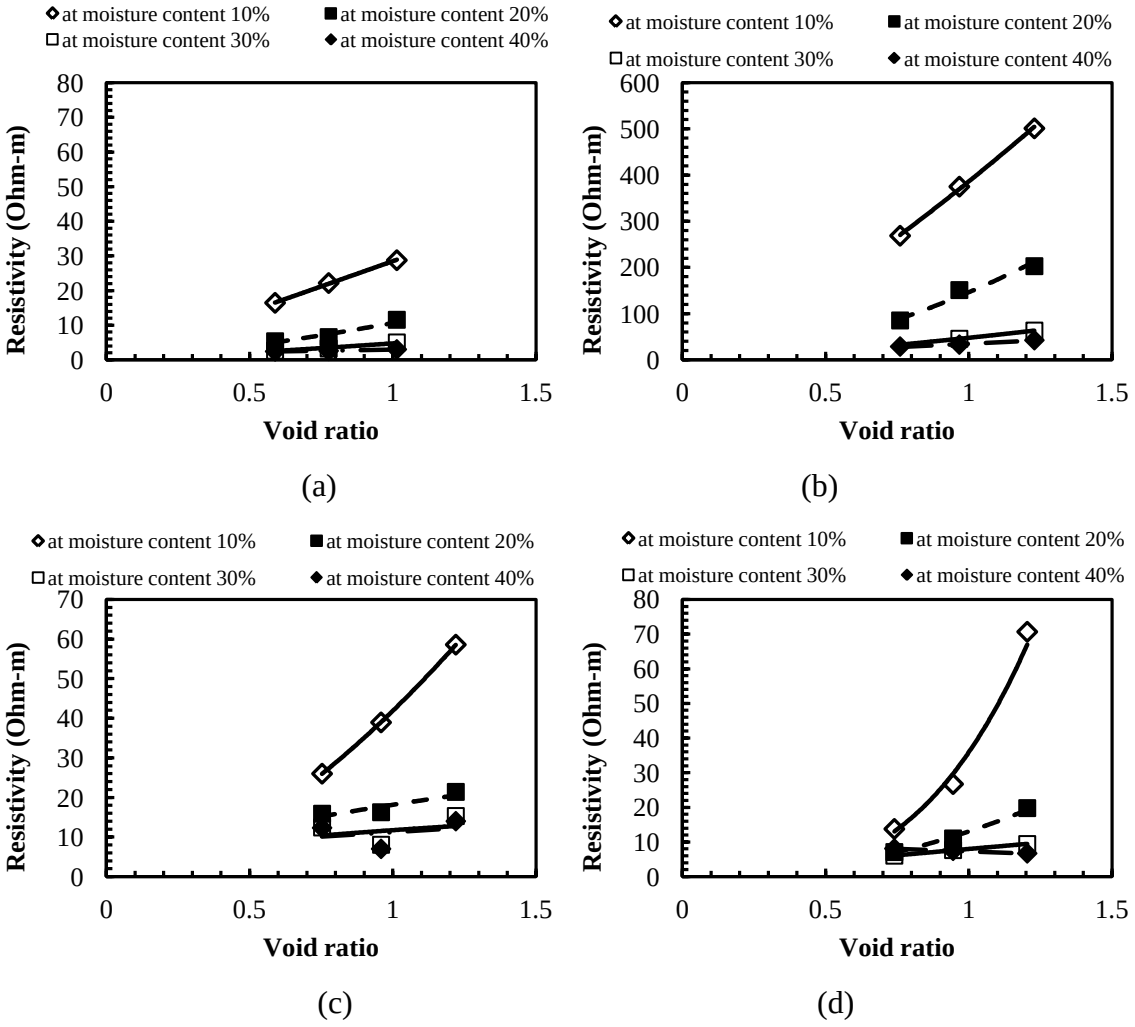

Figure 5.6 Variations in resistivity with void ratio of compacted clays at different moisture contents (a) Ca-bentonite, (b) Kaolinite, (c) CL (B1-30), and (d) CH (B2-20)

5.2.4 Effects of Volumetric Water Content

Volumetric water content is related with the dry unit weight and gravimetric moisture content of soils. In the current study, observed electrical resistivity results were plotted against volumetric water contents of the soil samples. The variation of resistivity with volumetric water content in compacted clay samples is presented in Figure 5.7. An increase in volumetric water content from 12 to 61% caused 11.8 (28.6 to 2.4 Ohm-m),

12.9 (373 to 29 Ohm-m), 4.6 (58.1 to 12.6 Ohm-m), and 9 (72.2 to 8 Ohm-m) times reductions in resistivity of Ca-bentonite, kaolinite, CL, and CH samples, respectively.

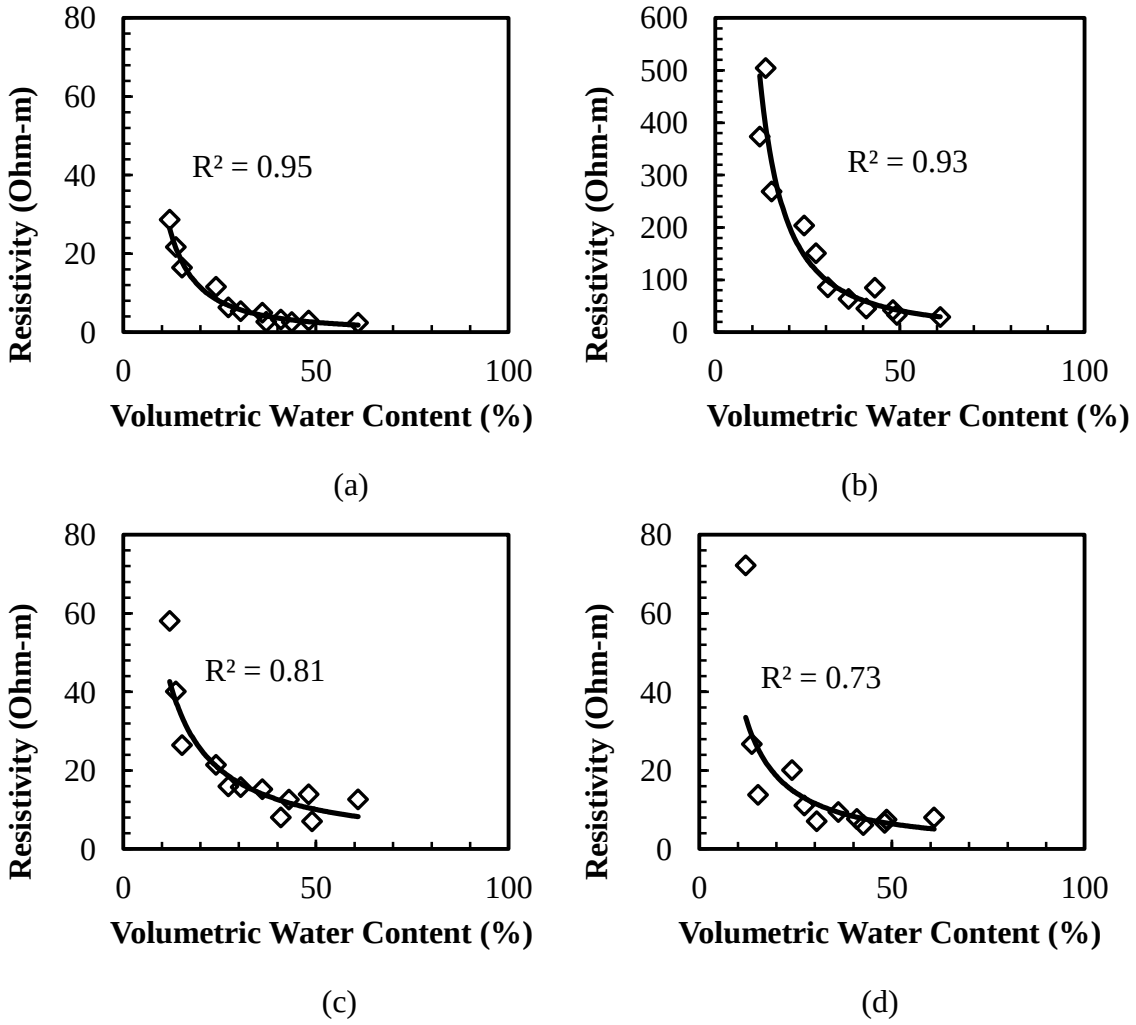

Figure 5.7 Resistivity variations with volumetric water contents in compacted clays (a) Ca-bentonite, (b) Kaolinite, (c) CL (B1-30), and (d) CH (B2-20)

The variation of electrical resistivity with volumetric moisture content of undisturbed soil is presented in Figure 5.8. It was determined that resistivity decreased from 49.4 to 4.2 Ohm-m for the increase of volumetric moisture contents from 14.1 to 40.7% in B2-10 sample. Moreover, significant variations were identified in between

volumetric moisture contents 14 to 31%. The total reduction in resistivity was as much as 44 Ohm-m in these moisture ranges. The observed variation in resistivity with moisture content can be explained by the study of Mojid and Cho (2006). According to the authors, the thickness of diffuse double layer (DDL) in clay surface increases with the increase of moisture, and provides bridging among the particles. In addition, the precipitated ions in clay surfaces expose with the moisture and enhance electrical conductivity.

In addition, the observed resistivity at specific moisture content was different for different soil samples. At 20% volumetric moisture content, the resistivity was 17 Ohm-m in B2-5 sample. However, the resistivity values were 16, 12, and 9 Ohm-m at this moisture content in B2-10, B2-20, and B2-25 specimens, respectively. The variation of resistivity at specific moisture content might occur due to the varied CEC and PI of the samples.

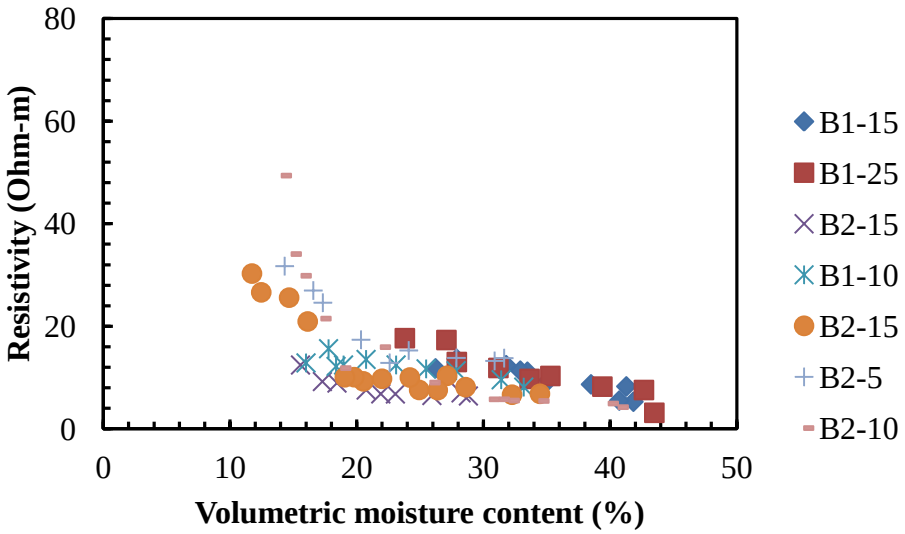

Figure 5.8 Resistivity variations with volumetric water content in undisturbed soils

The correlation between electrical resistivity and volumetric moisture content of disturbed and undisturbed soil samples are presented in 5.9 and 5.10. The developed correlation for compacted soils was also compared with the previous results.

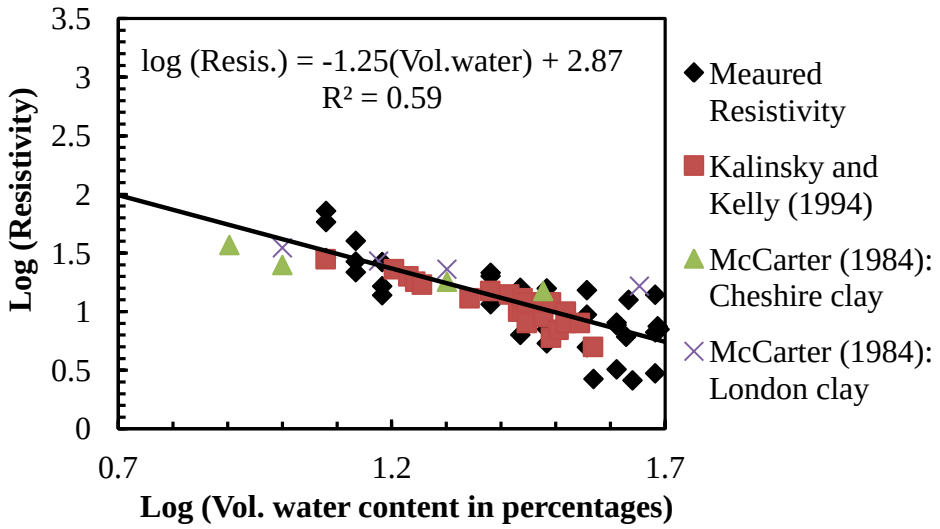

Figure 5.9 Development of correlation between electrical resistivity and volumetric moisture content for compacted Ca-bentonite, CH, and CL

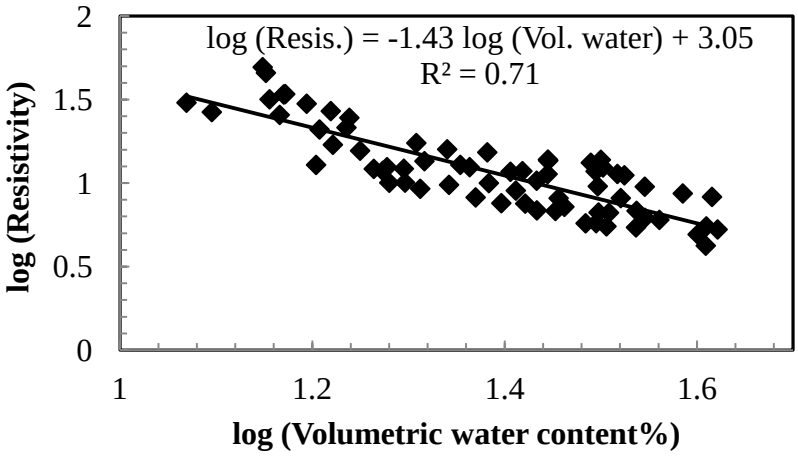

Figure 5.10 Development of correlation between electrical resistivity and volumetric content of undisturbed soil samples

5.2.5 Effects of Degree of Saturation

According to phase relation, degree of saturation is a function of gravimetric water content and void ratio of the soil. Therefore, the combined effect of moisture and unit weight can be evaluated by plotting resistivity against degree of saturation. The variations of resistivity of the compacted samples with degrees of saturation are illustrated in Figure 5.11. Test results showed that the degree of saturation significantly influenced electrical resistivity of soils. Electrical resistivity decreased as much as 11 times of initial value (28.6 to 2.6 Ohm-m) for the increase of degree of saturation 23 to 100% in Ca-bentonite. The observed reductions ranged in between 373 to 33 Ohm-m in kaolinite, 58.1 to 7 Ohm-m in CL, and 72 to 6 Ohm-m in CH at this condition.

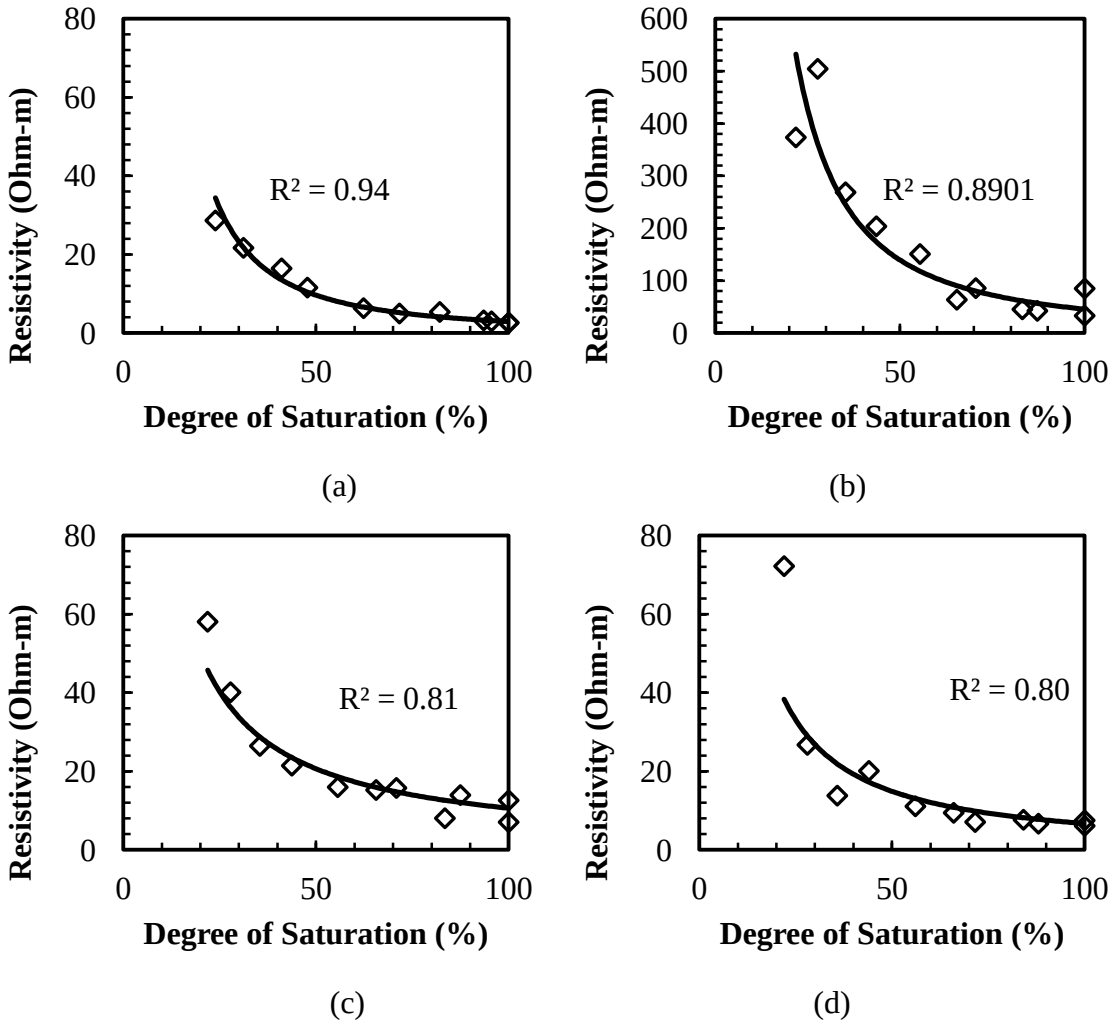

Figure 5.11 Effects of degree of saturation on electrical resistivity (a) Ca-bentonite, (b) Kaolinite, (c) CL (B1-30), and (d) CH (B2-20)

An increase in degree of saturation is associated with the more pronounced bridging between the particles. The connectivity of pore network increases because of the reduction of dielectric air void at higher degrees of saturation. Therefore, moisture bridging enhances the flow of current through a soil mass and results in low resistivity.

Investigation results indicated that resistivity decreased with the increase of degree of saturation. The resistivity of unsaturated soil can be related with saturated soil using Keller and Frischnecht (1966) model as follows:

$$\frac{R}{R_{100}} = S^{-B} \tag{5.1}$$

where, R and R_{100} are resistivity at unsaturated and saturated condition, respectively, S is the degree of saturation, and B is an empirical exponent.

Therefore, the observed results were normalized using resistivity at saturated condition to determine the exponent in the soil samples under consideration. It was observed that the exponents of Ca-bentonite, kaolinite, CL, and CH specimens were 1.72, 1.61, 0.96, and 1.15, respectively. The normalized resistivity vs. saturation curves are illustrated in Figure 5.12.

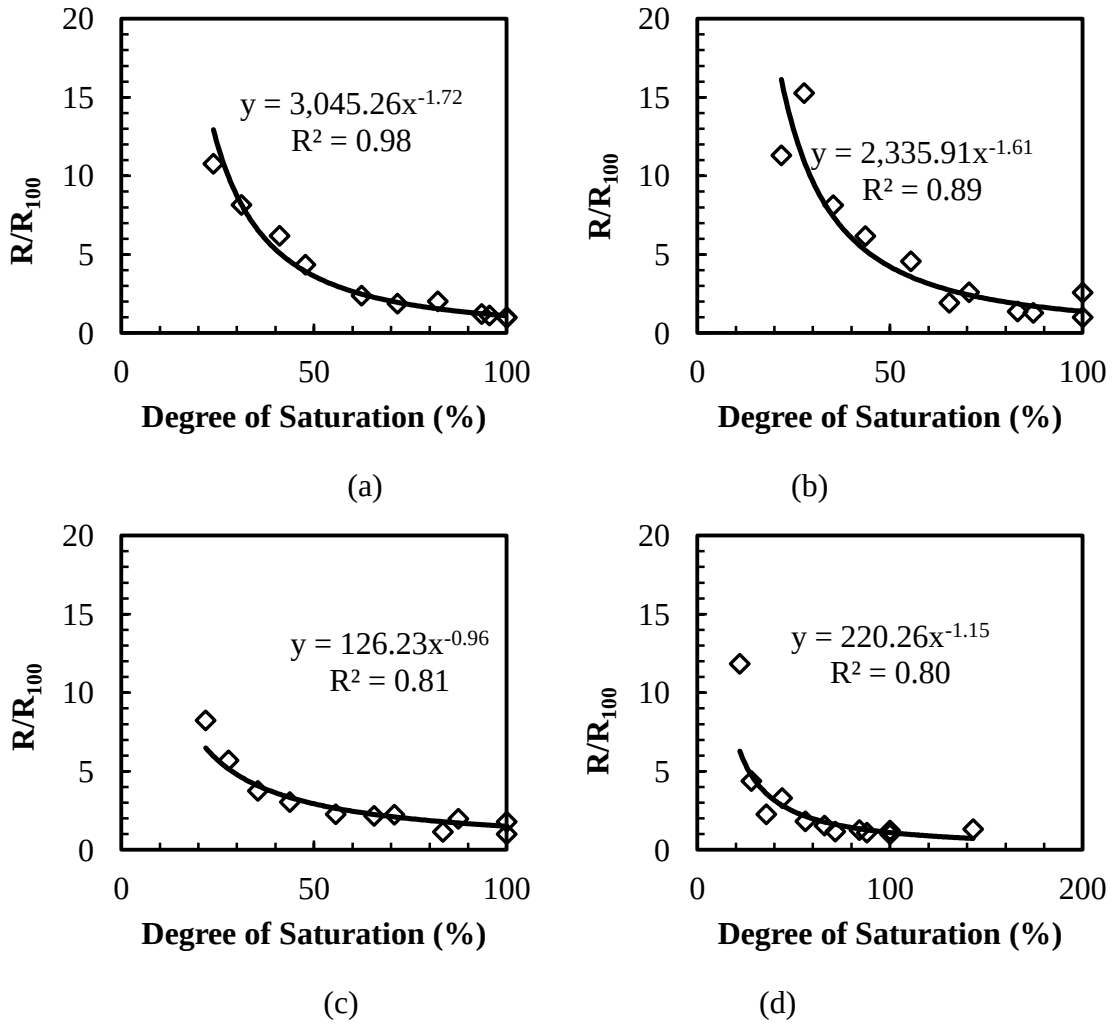

Figure 5.12 Normalized resistivity vs. degree of saturation (a) Ca-bentonite, (b) Kaolinite, (c) CL (B1-30), and (d) CH (B2-20)

Similar to compacted clay samples, electrical resistivity results were also plotted with degrees of saturation of undisturbed soils as presented in Figure 5.13. For an increase of saturation from 31 to 100%, resistivity decreased as much as sixteen fold (49.4 to 3.2) in the test results.

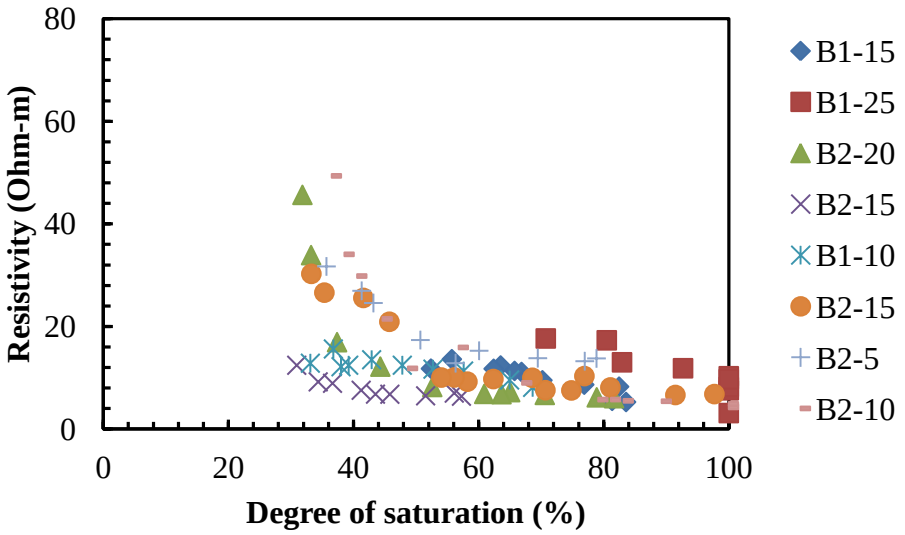

Figure 5.13 Electrical resistivity variations with degree of saturations in undisturbed soils

Based on the statistical analysis of the experimental results, the correlation between degree of saturation and resistivity was determined (Figure 5.14). Previous results were used for the comparison with the best-fitted line. A similar correlation was identified for the undisturbed soil samples as presented in Figure 5.15.

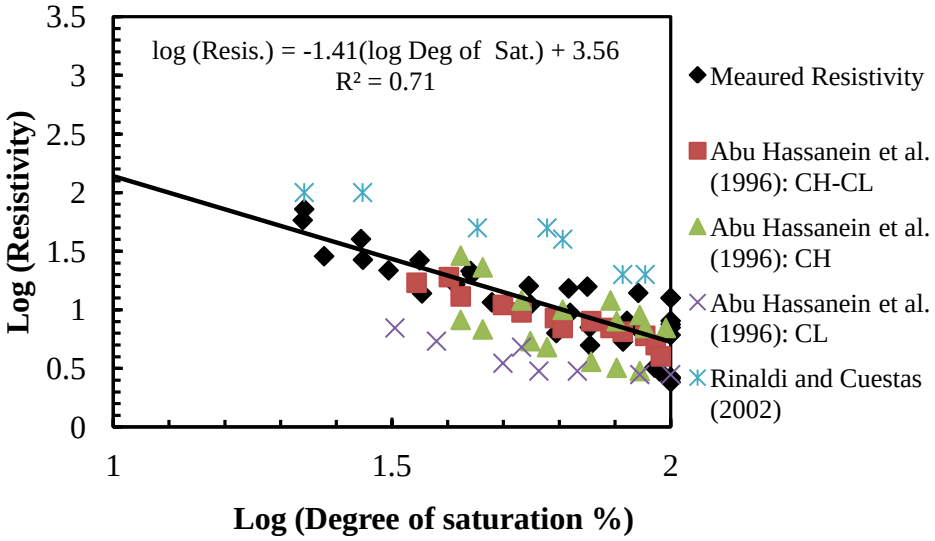

Figure 5.14 Development of correlation between electrical resistivity and degree of saturation for Ca-bentonite, CH, and CL

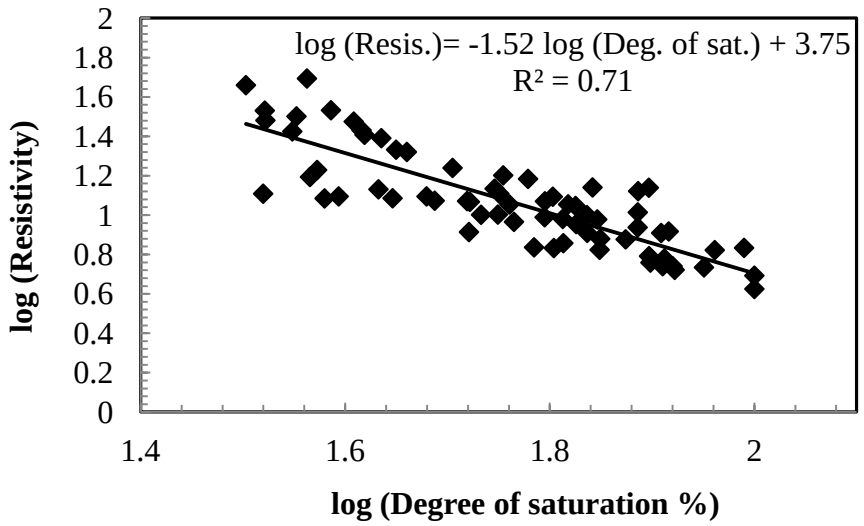

Figure 5.15 Development of correlation between electrical resistivity and degree of saturation of undisturbed soil samples

5.3 Influential Parameters Related to Physicochemical Properties of Clays

The CEC and PI of undisturbed soil samples ranged from 40.1 to 23.2 cmol+/kg and 18 to 33, respectively. On the other hand, CEC and PI of the compacted clay samples were in between 13.3 to 79 cmol+/kg and 15 to 55, respectively. Therefore, compacted clays were utilized to evaluate the effects of physicochemical properties on electrical resistivity. In addition, artificial soil samples were used to determine the influence of clay properties under controlled soil conditions.

5.3.1 Effects of Cation Exchange Capacity (CEC)

The resistivity responses at varied CECs for compacted clay samples were plotted in Figure 5.16. It was observed that the resistivity results were different for the specimens at a specific degree of saturation and temperature. The variation might occur due to varied isomorphous substitution of clay particles. The experimental scatter plots indicated

that the coefficients of regression were the highest in power fitted trend lines. Therefore, power functions were utilized to fit the experimental results.

The resistivity was significantly affected by CEC at relatively low degrees of saturation. A total reduction in resistivity was as much as 385 Ohm-m for the increase of CEC from 13.3 to 79 cmol+/kg at 25% degree of saturation. On the other hand, the total reduction in resistivity was 43.3 Ohm-m at 100% degree of saturation in the above CEC range. In addition, CEC of artificial soil samples were plotted against resistivity as illustrated in Figure 5.17. According to Figure 5.17, an increase in CEC caused significant reduction in resistivity at 25% degree of saturation. For Ca-bentonite-sand specimens, resistivity decreased from 64 to 37 Ohm-m for the increase of CEC from 27.8 and 63.5 cmol+/kg, respectively at this saturation. In contrast, resistivity reduced from 12 to 2.5 Ohm-m in this CEC range at 100% saturation. Therefore, test results emphasized the effect of ion exchange at low degrees of saturation.

The electrical conductivity of soil enhances with the increase of moveable ions in the pore water. Therefore, soil resistivity decreased with the increase of CEC because of the presence of conductive ions. Moreover, kaolinite mineral consisted of exchangeable ions at the edges of the crystal where as bentonite composed of exchangeable ions both at the edges and within lattice structure. Therefore, the contribution of precipitated ions is significant in bentonite compared to kaolinite (Holeman, 1970). According to Mitchell and Soga (2005), cation exchange reactions generally do not induce structural change in clays. However, significant variation in physical and physicochemical properties may occur due to the change in CEC. Test results indicated that the CEC of different artificial

soils significantly influenced resistivity at low degrees of saturation. Nonetheless, resistivity was less sensitive to CEC at high degree of saturation (i.e. S = 100%).

The rate of reduction in electrical resistivity decreased with the increase of CEC. At a specific degree of saturation, the mobility of precipitated ions might decrease with the increase of CEC. Therefore, the response curve was flatter at high CEC compared to low ion exchange condition.

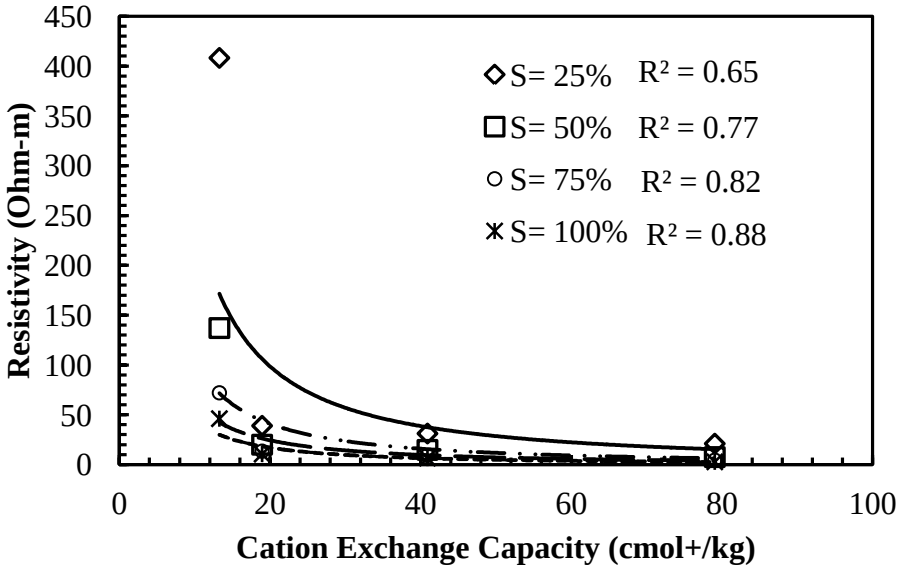

Figure 5.16 Resistivity variations with CEC of compacted clays

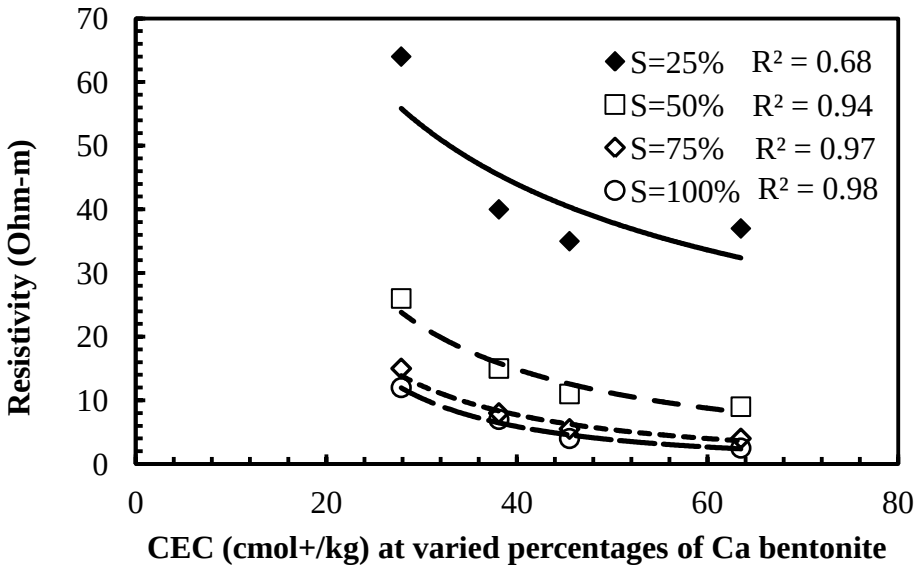

Figure 5.17 Resistivity variations with CEC of artificial samples

Based on the experimental results, a correlation was developed between electrical resistivity and CEC of Ca-bentonite, CL, and CH samples. The correlation was compared with the study of Shah and Singh (2005) as presented in Figure 5.18.

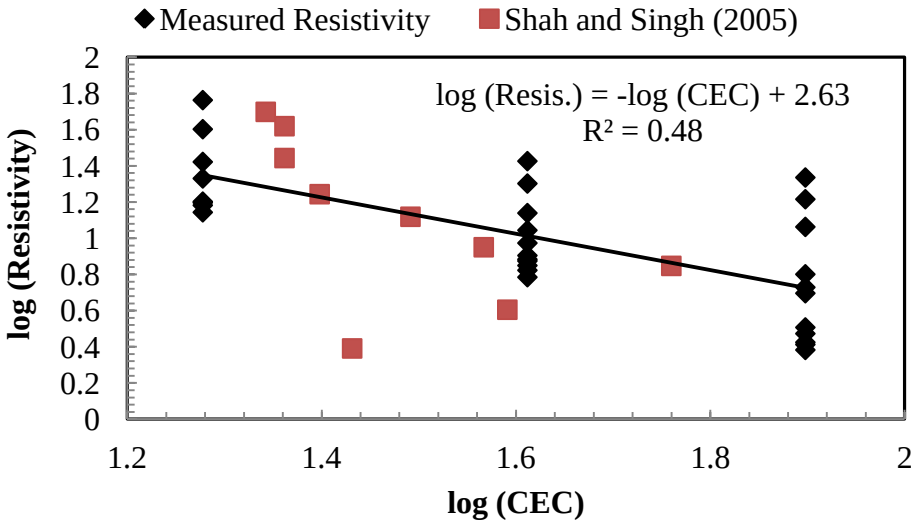

Figure 5.18 Development of correlation between electrical resistivity and CEC for Ca-bentonite, CH, and CL

5.3.2 Effects of Liquid Limits

Surface activity of a soil is related to particle size and amount of fine fraction. In addition, index properties of soils are sensitive to specific surface area, electrolyte concentration, cation valence, and dielectric constant. Therefore, liquid limits and plasticity indices can be designated as two important indicators of physicochemical properties of soils (Mitchell and Soga, 2005).

The variations of resistivity with liquid limits at different degrees of saturation are presented in Figure 5.19. Although overall downward trends were observed in the experimental data points, the coefficients of regressions were not high. Therefore, liquid limits of artificial soil specimens were plotted with the resistivity at varied saturation levels as shown in Figure 5.20. The coefficients of regression ranged from 0.78 to 0.94 in the artificial samples. At 25% degree of saturation, resistivity decreased from 64 to 22 Ohm-m for the increase of liquid limits from 22 to 107. Similar variations were identified at 50, 75, and 100% degrees of saturation; however, the rates of reduction were different.

The observed variation in resistivity among the samples can be explained by the clay-water interaction phenomenon. The net negative charge of clay structure attracts positive area of water ion and adsorbed. The possibility of water adsorption increases with the increase of surface charge. Therefore, moisture bridging among the particles increases with the increase in affinity to water. In addition, minerals consisting 1:1 layers (i.e. kaonite) are composed of siloxane and $(OH)^-$ group surface (Meunier, 2005). Typically, these surfaces are electrically neutral and restrict the adsorption of ions or

molecules in the interlayer surfaces. This might cause an increase in resistivity of kaolinite mineral at low degree of saturation.

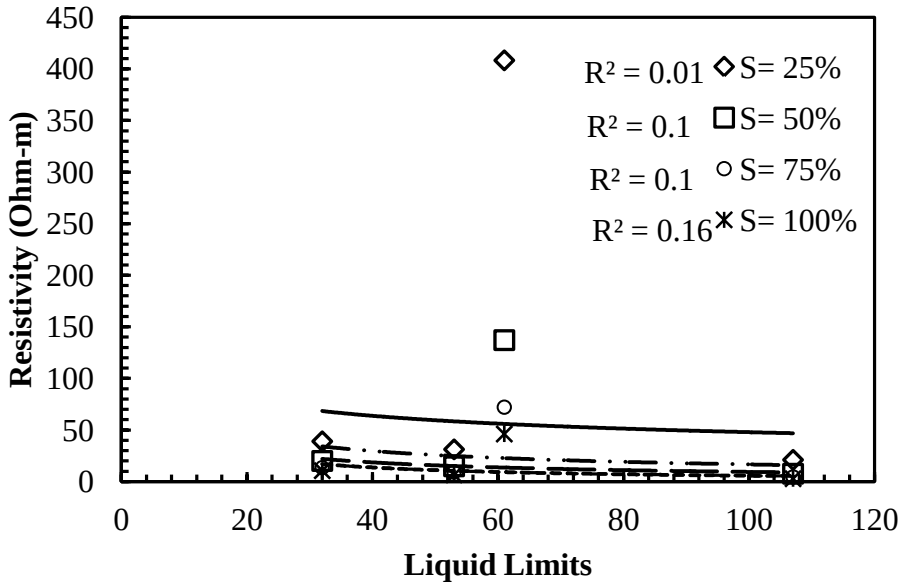

Figure 5.19 Effects of liquid limits on resistivity of compacted clays

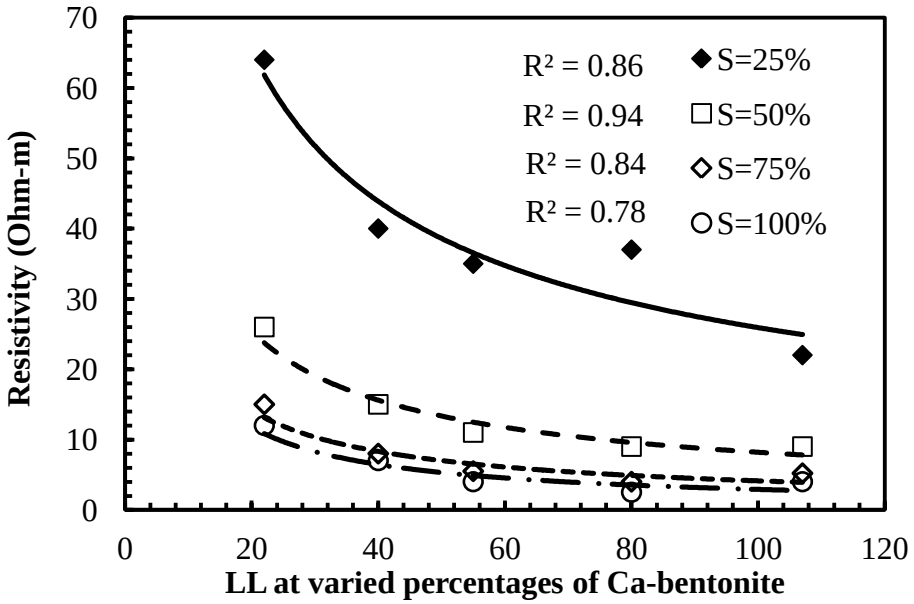

Figure 5.20 Effects of liquid limits on resistivity of artificial soils

The measured electrical resistivity of Ca-bentonite, CL, and CH at varied degrees of saturation were plotted against liquid limits. It was observed that there was linear correlation between logarithm of resistivity and logarithm of liquid limits. The statistical assumptions of the linear correlation were investigated. It was observed that the linear model assumptions i.e. constant error variance, adequacy of the model, and normality were satisfied fairly well in the proposed correlation. The results were also compared with the study results of Abu Hassanein et al. (1996) as presented in Figure 5.21.

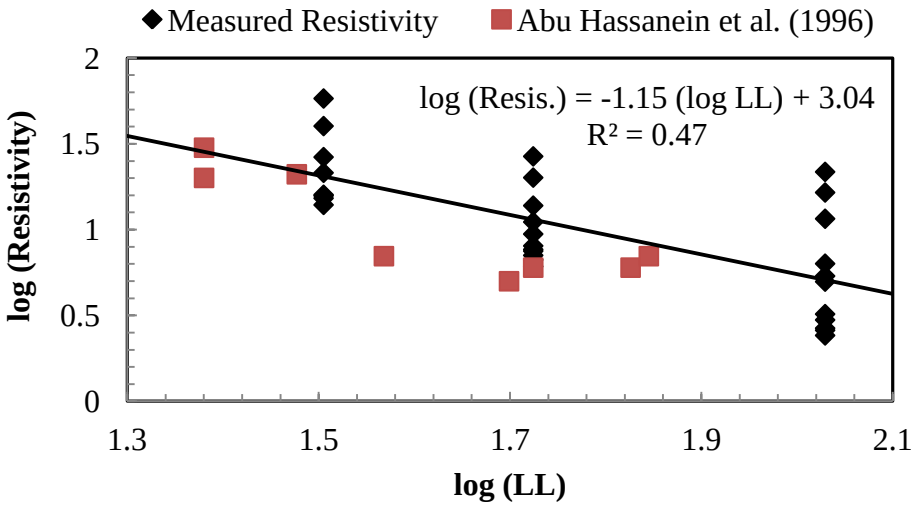

Figure 5.21 Development of correlation between electrical resistivity and LL for Ca-bentonite, CH, and CL

5.3.3 Effects of Plasticity Indices

The variations of resistivity with plasticity indices (PI) of the samples are presented in Figure 5.22. An overall decrease in resistivity was observed for the increase of PI in each soil sample. However, the resistivity responses were different for varied degrees of saturation. Although the PI of kaolinite was 24; the observed resistivity was

always higher compared to other samples. The CEC of kaolinite was 13.3 cmol+/kg, which indicated the isomorphous substitution was not significant in this mineral. Moreover, the presence of electrically neutral surface charge may restrict the adsorption of ions. This might cause an increase in resistivity of kaolinite mineral at low degrees of saturation. Therefore, the effect of clay particle on resistivity can be better explained by the ion exchange properties, i.e. CEC.

Although power functions were used to identify the overall trends of the data, a better fitting method can be utilized to identify the trends of variation in future studies.

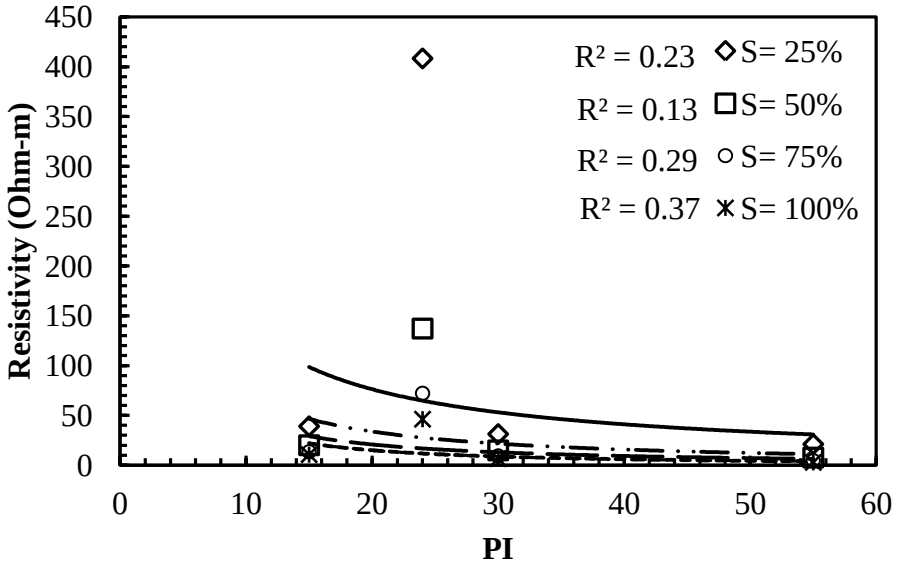

Figure 5.22 Variation of resistivity with plasticity indices of compacted clays

In addition to compacted clay specimens, plasticity indices (PI) at different mineral contents were plotted against resistivity results at different degrees of saturation as presented in Figure 5.23. It was observed that soil resistivity decreased with the increase of plasticity indices. For the increase of plasticity indices from 7 to 43, resistivity

decreased as much as 1.72 times in Ca-bentonite-sand specimens at 25% degree of saturation. However, resistivity reduced from 7 to 2.5 Ohm-m at 100% degree of saturation.

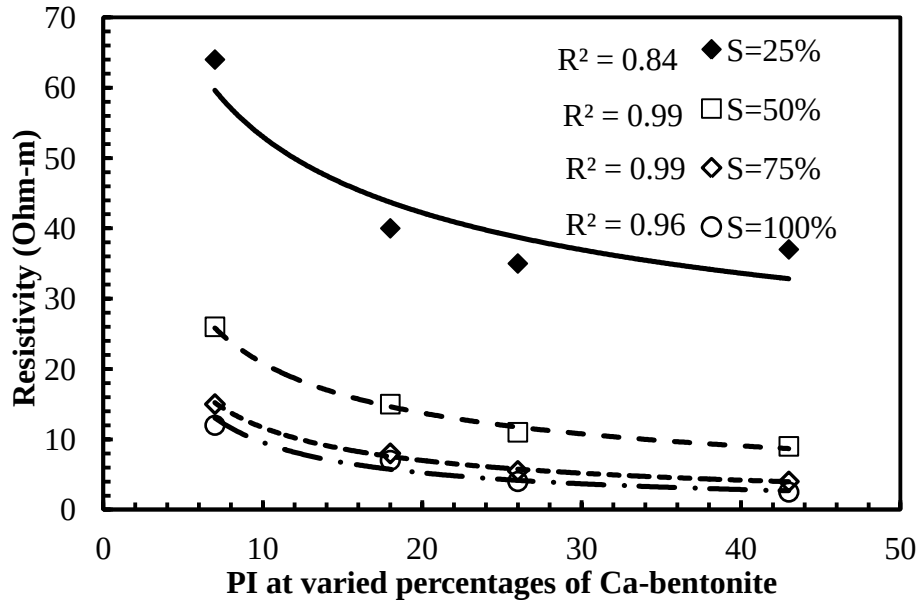

Figure 5.23 Variation of resistivity with plasticity indices of artificial soil samples

A correlation was developed between resistivity and PI for Ca-bentonite, CL, and CH samples as presented in Figure 5.24. The study results were also compared with the experimental results of Abu Hassanein et al. (1996).

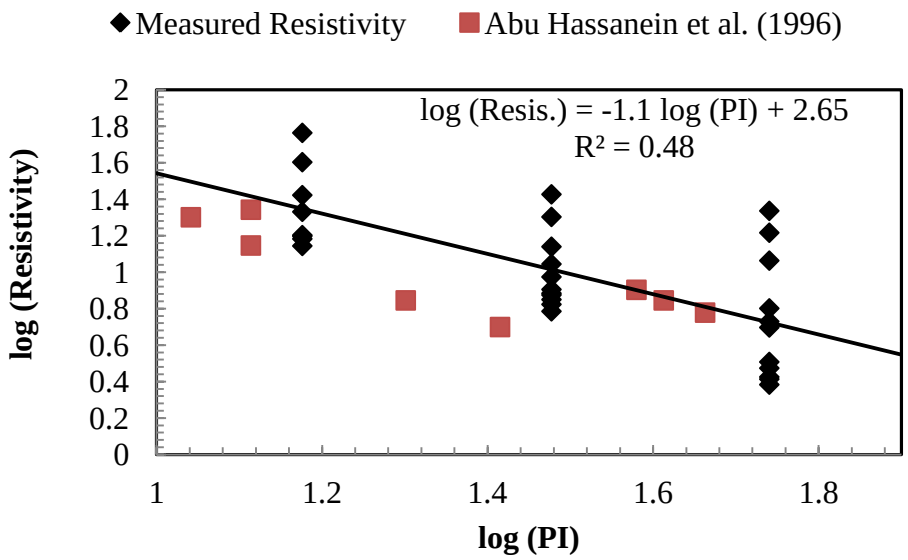

Figure 5.24 Development of correlation between electrical resistivity and PI for Ca-bentonite, CH, and CL

5.3.4 Effects of Specific Surface Area (SSA)

Specific surface area (SSA) of compacted clays and artificial soil specimens were evaluated using the correlation proposed by Farrar and Coleman (1967). The observed SSAs were plotted against electrical resistivity at different degrees of saturation as presented in Figure 5.25. An overall reduction in resistivity was observed with the increase of SSA of the specimens. To evaluate the effects of SSAs in a controlled case, artificial soil samples were utilized. The variation of SSA with resistivity for artificial samples is illustrated in Figure 5.26. Three-fold reduction in resistivity was observed for the increase of SSA from 5.4 to 157 m^2/gm at 25% degree of saturation. Similar variations were observed for 50, 75, and 100% degrees of saturation; however, the rates of reduction were different.

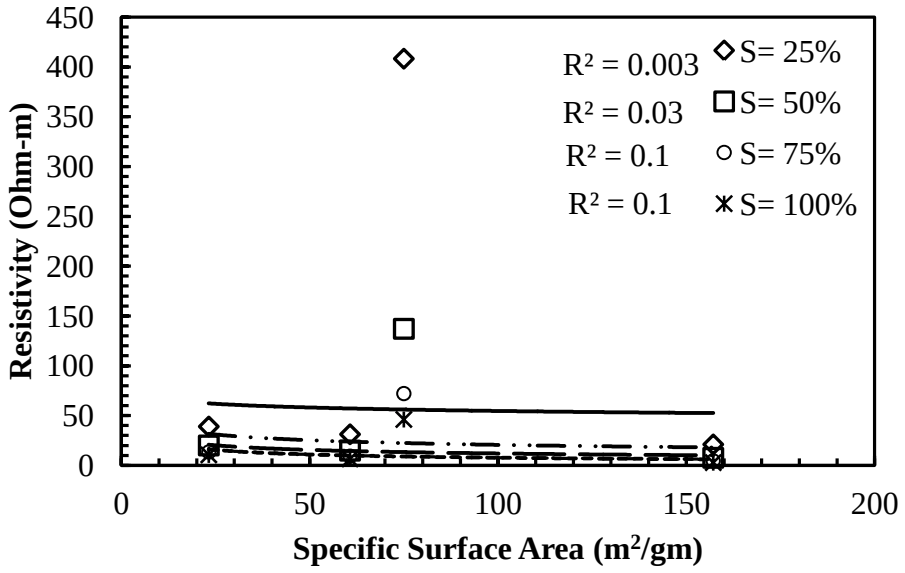

Figure 5.25 Resistivity variation with SSA of compacted clays

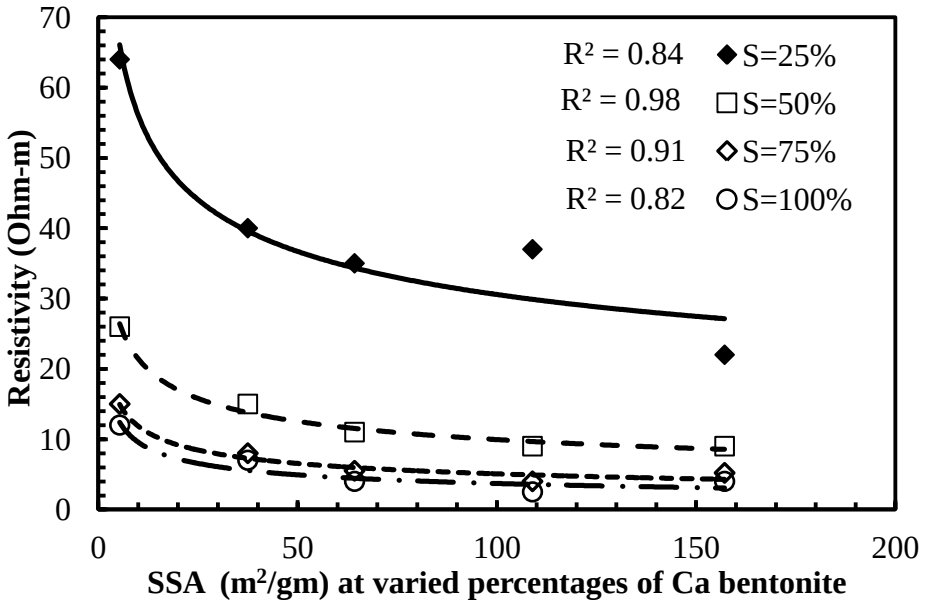

Figure 5.26 Resistivity variation with SSA of artificial soils

5.3.5 Effects of Pore Water Conductivity

The resistivity responses at varied pore water conductivity are illustrated in Figure 5.27. It was identified that the pore water conductivity significantly influenced electrical

resistivity of the soil samples. According to the results, pore-water conductivity of kaolinite mineral was 414 micro-Siemens/cm and associated resistivity values were 435, 140, 75, and 45 Ohm-m at 25, 50, 75, and 100% saturation, respectively. Nonetheless, pore-water conductivity of Ca-bentonite, CL, and CH were 1805, 1028, and 1436 micro-Siemens/cm, and the observed resistivity was below 50 Ohm-m at each saturation level due to the high conductivity of extracted pore water.

Pore water conductivity is an indicator of the presence of precipitated ions from clay structure. It was mentioned that the protonation of kaolinite resulted in a fairly neutral pH (5.6); therefore, the possibility of precipitation was reduced due to the flocculation. However, the pH of pore water extracted from bentonite, CL, and CH were slightly basic (i.e. 7.46, 7.64, and 7.58, respectively) in nature, and induced a favorable condition for the precipitation of surface ions. The pore water with highly precipitated ions might enhance conductivity in bentonite and natural clay specimens under the application of current.

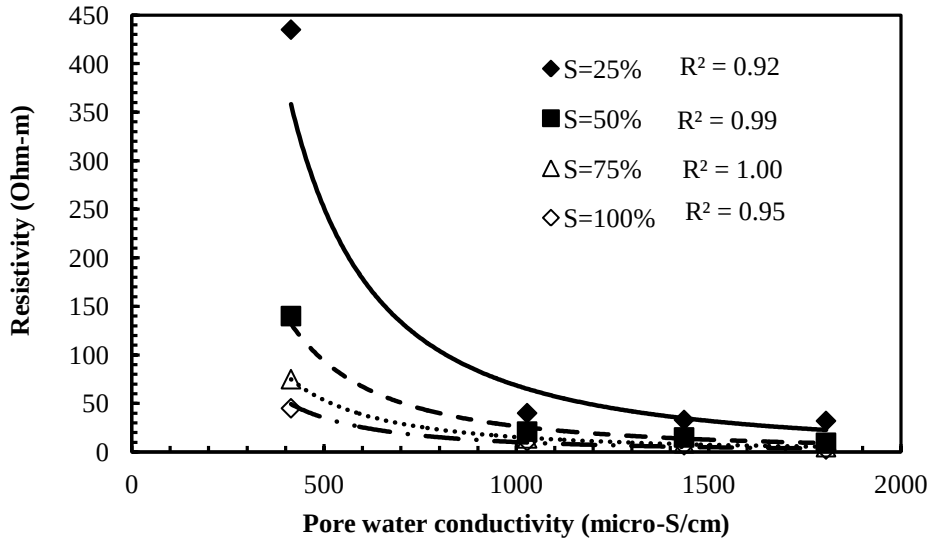

Figure 5.27 Variation of resistivity of samples with pore water conductivity

5.3.6 Effects of Sulphate Content of Pore Water

According to IC of extracted pore water, significant variations of sulphate concentrations were observed among the samples. Therefore, sulphate ions of the pore water was correlated with resistivity at different degrees of saturation. Figure 5.28 indicates that an increase of sulphate ions results in substantial reduction in resistivity. Resistivity reduced from 435 to 32 Ohm-m for the increase of sulphate concentrations from 88.5 to 878.7 mg/L at 25% degree of saturation. The observed variations might occur due to enhanced ionic conduction at high sulphate contents.

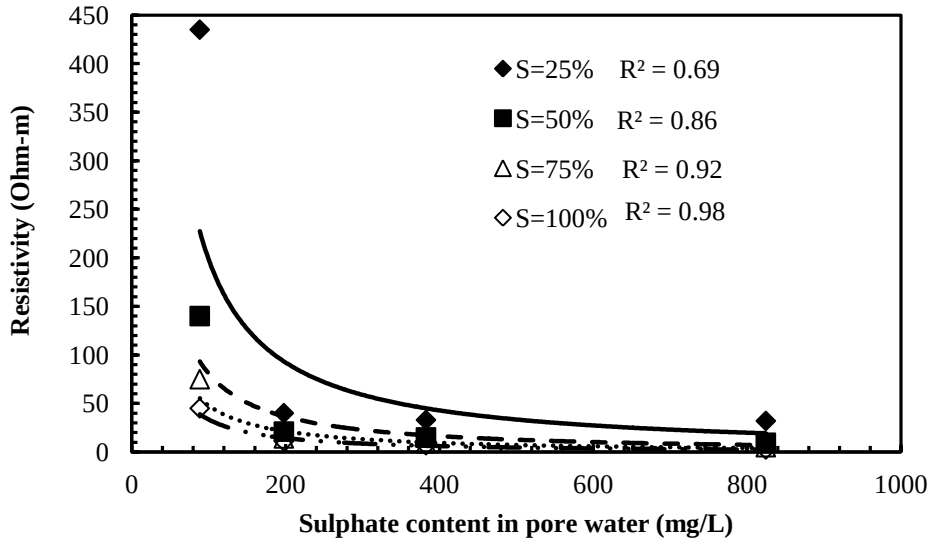

Figure 5.28 Variation of resistivity of samples with sulphate content in pore water

5.3.7 Effects of Mineral Percentages

Figure 5.29 indicates the variation of resistivity with the increase of mineral contents at 25, 50, 75, and 100% degree of saturation.

According to the test results, resistivity decreased from 64 to 37 Ohm-m in the mineral content range of 20 to 80% at 25% degree of saturation. However, the influences of minerals were not significant at 100% degree of saturation. According to the study of Abu-Hassanein et al. (1996), resistivity decreased with the increase of clay fraction. An increase of the interaction of clay particles with water under an applied electric potential might cause the observed reductions at high percentages of clay mineral.

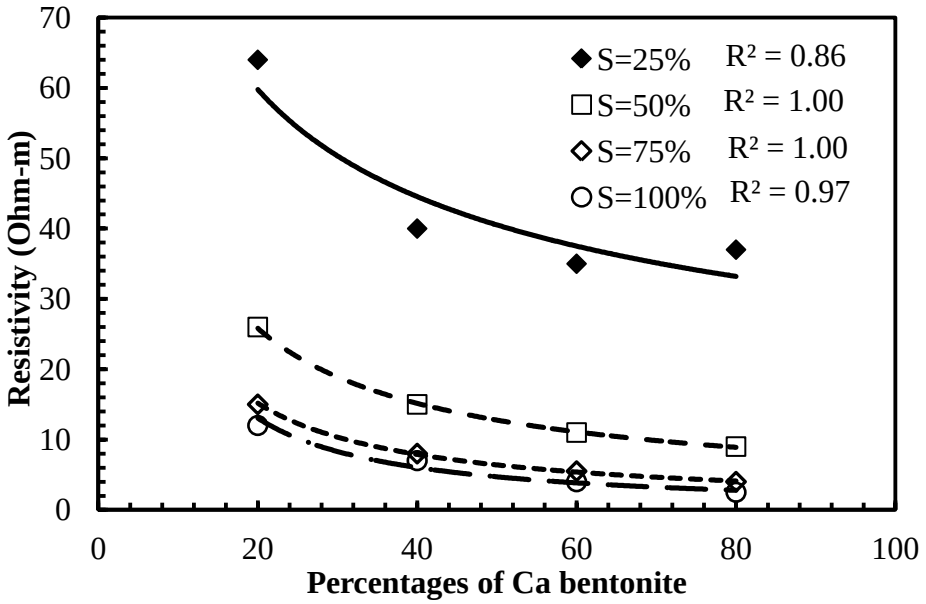

Figure 5.29 Effects of benonite minerals on resistivity

5.4 Effects of Compressibility on Electrical Conductivity of Clays

The interconnected pores have considerable influence on engineering and transport process of soils. Therefore, characterization of pore structure is often required to identify diffusion, packing, and conduction phenomena. Electrical resistivity is an indirect method, which can be utilized to evaluate porous structure and their influence in macro and micro scale behavior of soils. In addition to that, electrical conductivity can provide useful information about consolidation properties of soil samples. In the current study, correlations between consolidation properties and electrical conductivity were developed based on the experimental results. The correlation between load-deformation and electrical properties may provide useful information to utilize electrical conductivity as an alternative of pore network characterization and consolidation analysis. The soil samples considered in the investigation are presented in Table 5.2.

Table 5.2 Properties of soil samples considered in the investigation

Sample ID	Sp. Gravity	LL	PI	%passing # 200	USCS Classification	CEC cmol+/kg
B1-15	2.67	52	33	90.34	CH	29.9
B2-20	2.65	53	30	92.34	CH	40.9
B2-15	2.68	53	30	85.28	CH	29.8
B2-25	2.56	53	30	91.49	CH	30.17
B2-10	2.66	50	22	82.67	CL	30.16

5.4.1 Consolidation Analysis

The changes in void ratio in response to applied pressures are presented in Figure 5.30. The pre-consolidation pressures of the soil samples were determined according to Casagrande method. It was observed that the pre-consolidation pressure of the B1-15, B2-15, B2-10, and B2-20 were 120, 150, 280, and 240 kPa, respectively. Moreover, the compression indices were determined from the e vs. logP curve obtained from laboratory tests. The compression indices of B1-15, B2-15, B2-10, and B2-20 were 0.19, 0.12, 0.19, and 0.22, respectively.

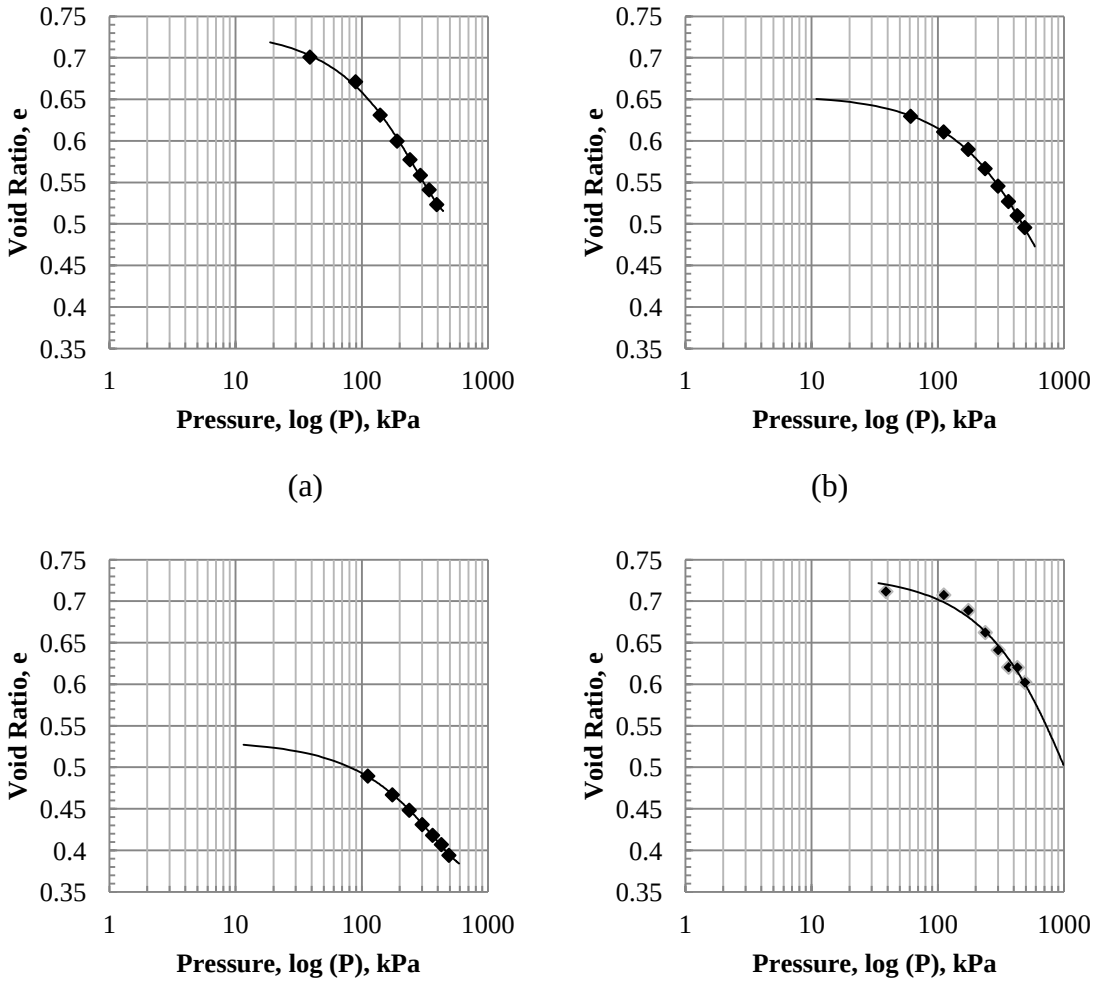

Figure 5.30 Consolidation analyses of the soil samples (a) B1-15, (b) B2-15, (c) B2-20, (d) B2-10

5.4.2 Effects of Pressures on Electrical Conductivity of the Specimens

The compressibility tests were conducted in conjunction with electrical resistivity measurements to identify the correlation between strain and electrical properties. The variations of electrical conductivity of the soil samples with applied stresses at saturated conditions are illustrated in Figure 5.31. The experimental results showed that the trends of variation in electrical conductivities with pressures were similar to e vs. logP curves. A

substantial reduction in conductivity was not observed at low-pressure range; however, the electrical conductivity decreased almost linearly after maximum point of curvature. The study results indicated that the inflection points were associated with pressure 120, 120, 200, and 275 kPa in B1-15, B2-15, B2-10, and B2-20, respectively. Therefore, the inflection points were closely associated with the pre-consolidation pressures of the soil specimens.

As the interstitial water dissipates under the application of loads, the moisture contents of the saturated specimens decrease with the increase of stress. Therefore, reduction in electrical conductivity occurred with the increase of stress. The observed results also indicated that pore water is the dominant mode of electrical conductivity in the specimens under consideration.

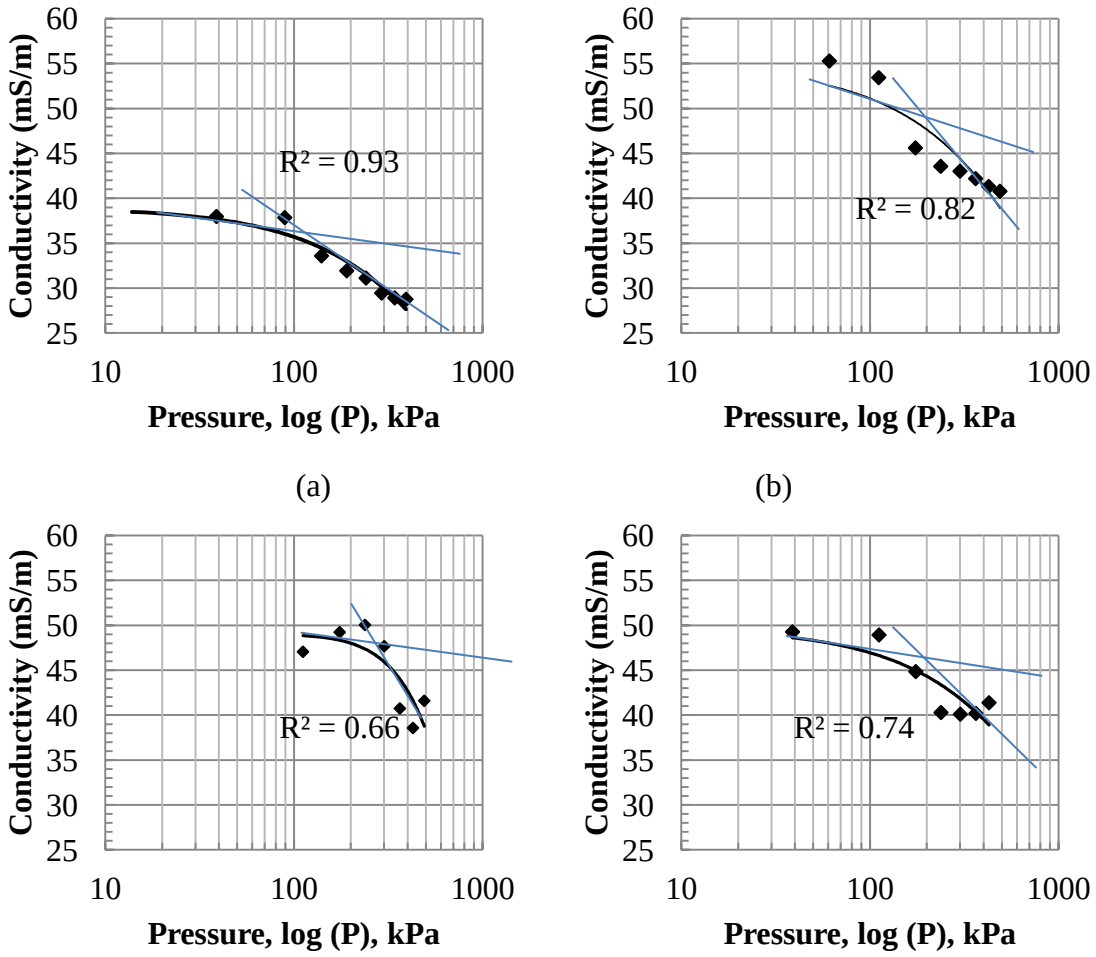

Figure 5.31 Electrical resistivity responses at varied stages of consolidation (a) B1-15, (b) B2-15, (c) B2-20, (d) B2-10

5.4.3 Effects of Void Ratio on Electrical Conductivity at Saturated Condition

As the variations of electrical conductivity and void ratio showed similar trends with the increase of stresses, the relationship between void ratio and electrical conductivity was investigated. The void ratio and electrical conductivity at different consolidation stages are presented in Figure 5.32. It was observed that the void ratio and electrical conductivity was linearly correlated to each other. Although a linear correlation

existed between electrical conductivity and void ratio, the relationship depended on the structural change in clay particles with consolidation stress. Therefore, the gradients of variation were different for the soil samples, and the slopes of the trend lines varied from 61.85 to 106.38.

The variation in void ratio vs. electrical conductivity among different samples indicated that the cementation and packing of the soil samples influenced electrical conductivity variations. The changes in pore distribution depend on the initial packing and fabric structure. Therefore, SEM images were utilized to determine the effect of fabric morphology on electrical conduction.

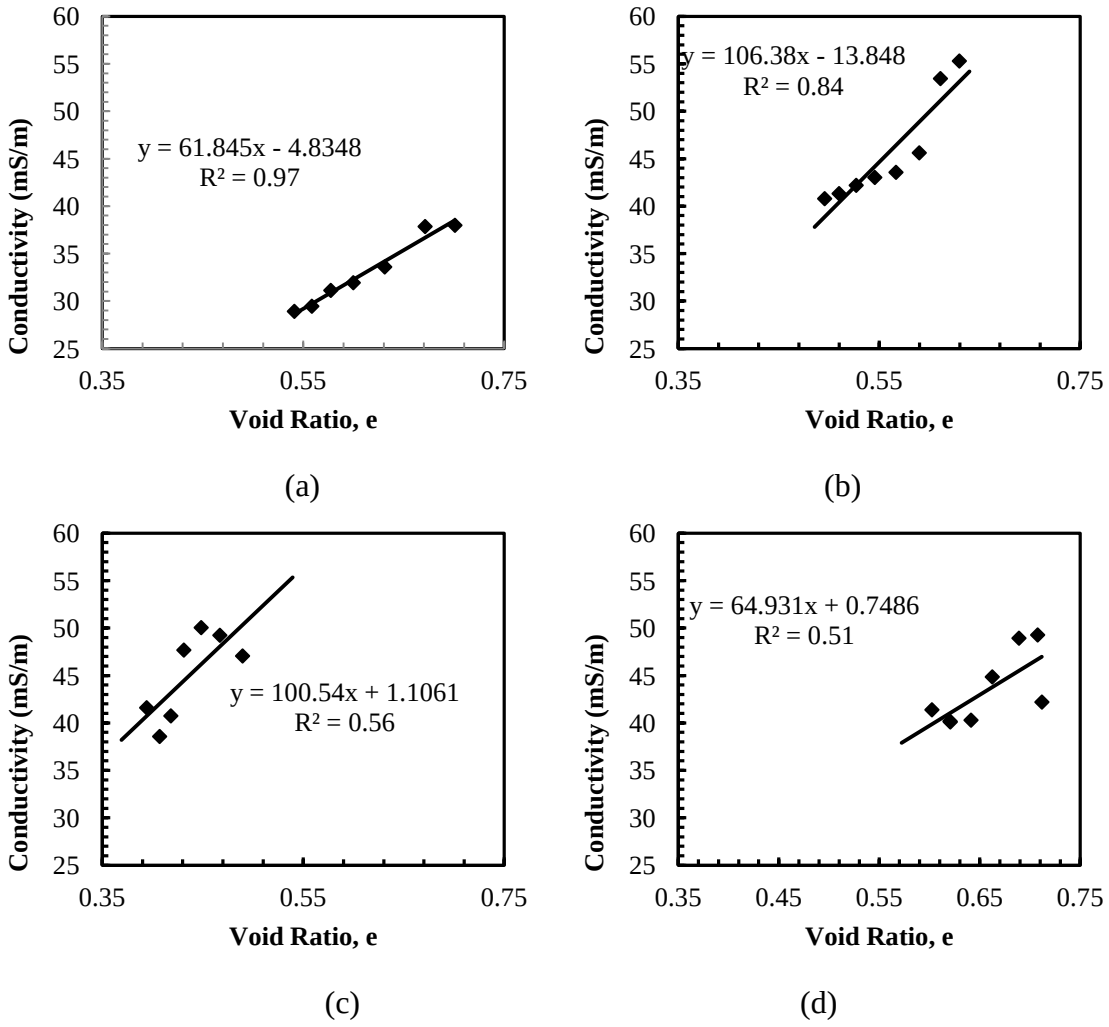

Figure 5.32 Variation of electrical conductivity with void ratio (a) B1-15, (b) B2-15, (c) B2-20, (d) B2-10

5.4.4 Effect of Structural Change on Electrical Conductivity

The study results emphasized that the electrical conductivity was high at initial condition; however, conductivity decreased at high pressures. The causes of variation in conductivity were investigated using SEM images of the clay fabric. The SEM images of B2-10 and B2-15 specimens before and after consolidation are presented in Figure 5.33. It was observed that the slenderness of the soil samples increased after consolidations.

Before consolidation, the slenderness of B1-15, B2-15, B2-10 and B2-20 were 1.61, 1.43, 1.4, and 1.42, respectively. Nonetheless, slenderness increased to 1.84, 1.56, 1.57, and 1.68 in the soils samples after application of pressures.

The changes in the fabric structure might change the tortuous length of the conduction path and influence electrical properties. The change in the tortuous length can be further illustrated in Figure 5.34. SEM image analysis indicated that the conduction path increases with the increase of slenderness of the particles. Therefore, for a given specimen, the current needs to travel circuitous path with the progression of consolidation. This might cause the observed variation in conductivity of the soil samples (Figure 5.31).

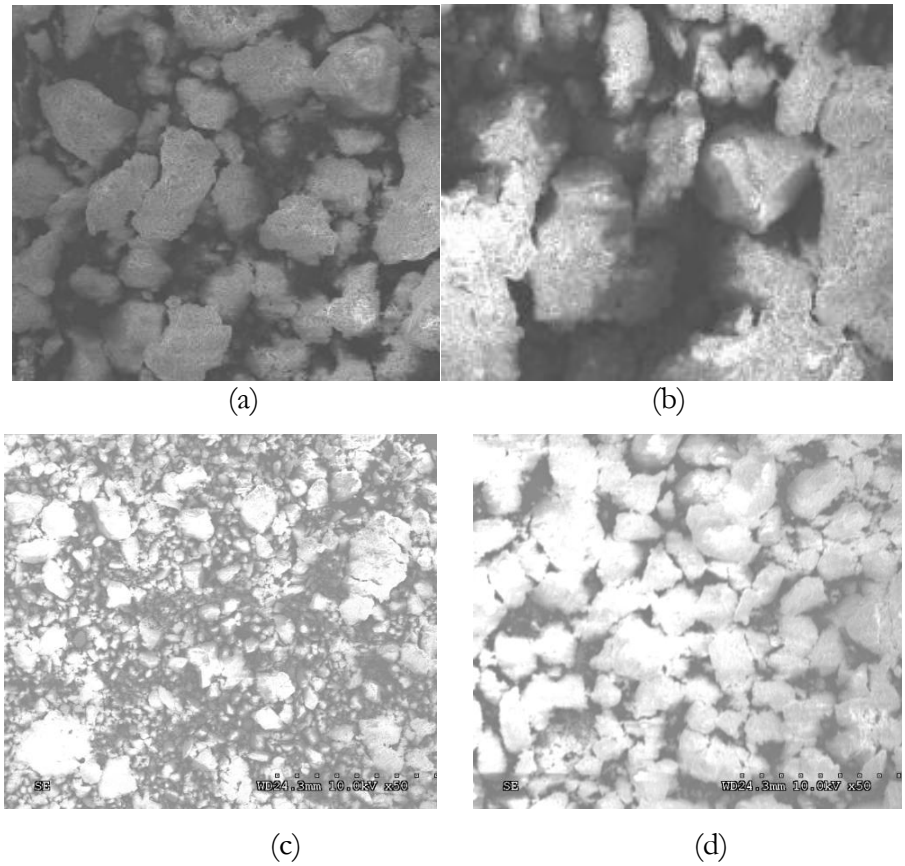

Figure 5.33 SEM images of the soil samples before and after consolidation (a) B2-10-undisturbed (b) B2-10-consolidated (c) B2-15- undisturbed (d) B2-15-consolidated

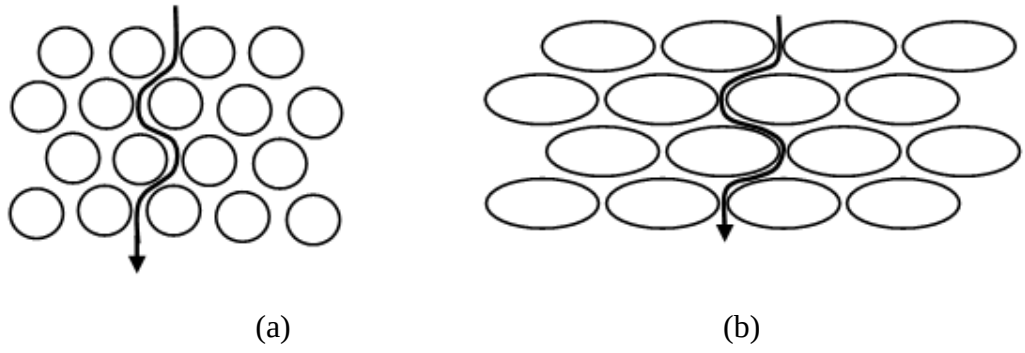

Figure 5.34 Change in conduction path with consolidation (a) before consolidation (b) after consolidation (qualitative diagram)

According to the Capillary model, formation factor can be defined as the ratio of square of tortuosity and porosity (Mithcell and Soga, 2005). Therefore, an increase in tortuosity causes an increase in formation factor and results in a reduction in electrical conductivity. The average change in electrical conductivity was plotted with the average change in slenderness for the soil samples as presented in Figure 5.35. A linear correlation was identified between the average variation in electrical conductivity and shape of particle.

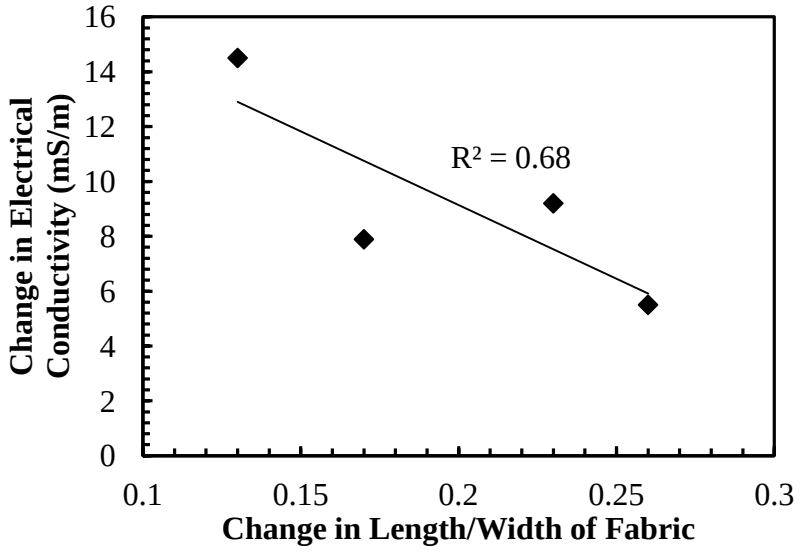

Figure 5.35 Variation in average electrical conductivity with slenderness over the consolidation ranges

5.4.5 Correlation of Electrical Conductivity with Co-ordination number

The relationship of electrical conduction with clay structure and packing were further analyzed using coordination number. The coordination number of a soil sample describes the average number of contacts from surrounding particles. It is an indicator of internal structure and packing arrangement of the soils (Santamarina, 2001). In the

current study, coordination number was determined using the correlation presented in Table 5.3. Thereafter, the average coordination number was calculated from the measured values.

The variations of electrical conductivity with coordination numbers for the soil specimens are presented in Figure 5.36. It was identified that the electrical conductivity decreased with the increase of coordination number. An increase in coordination number is associated with the reduction in pore space, increase in contacts from surrounding particles, and increase in stability of packing. Therefore, reduction in pore space and stability of packing affect electrical conductivity in addition to moisture content.

Table 5.3. Correlation of coordination number with the porosity and void ratio (adapted from Santamarina, 2001)

Coordination number	**Correlations**
CN	$\pi/4$ (0.25<n<0.4)
CN	2exp[2.4(1-n)]
CN	13.28-8e
CN	14-16n
CN	17.2-19.7n
CN	28.486-(10.726/1-n)
CN	(0.5304-n)/0.02539
CN	12/(1+e)
CN	$1/[1-(1-n)^{0.333}]$

Note: CN= coordination number, n=porosity, and e=void ratio

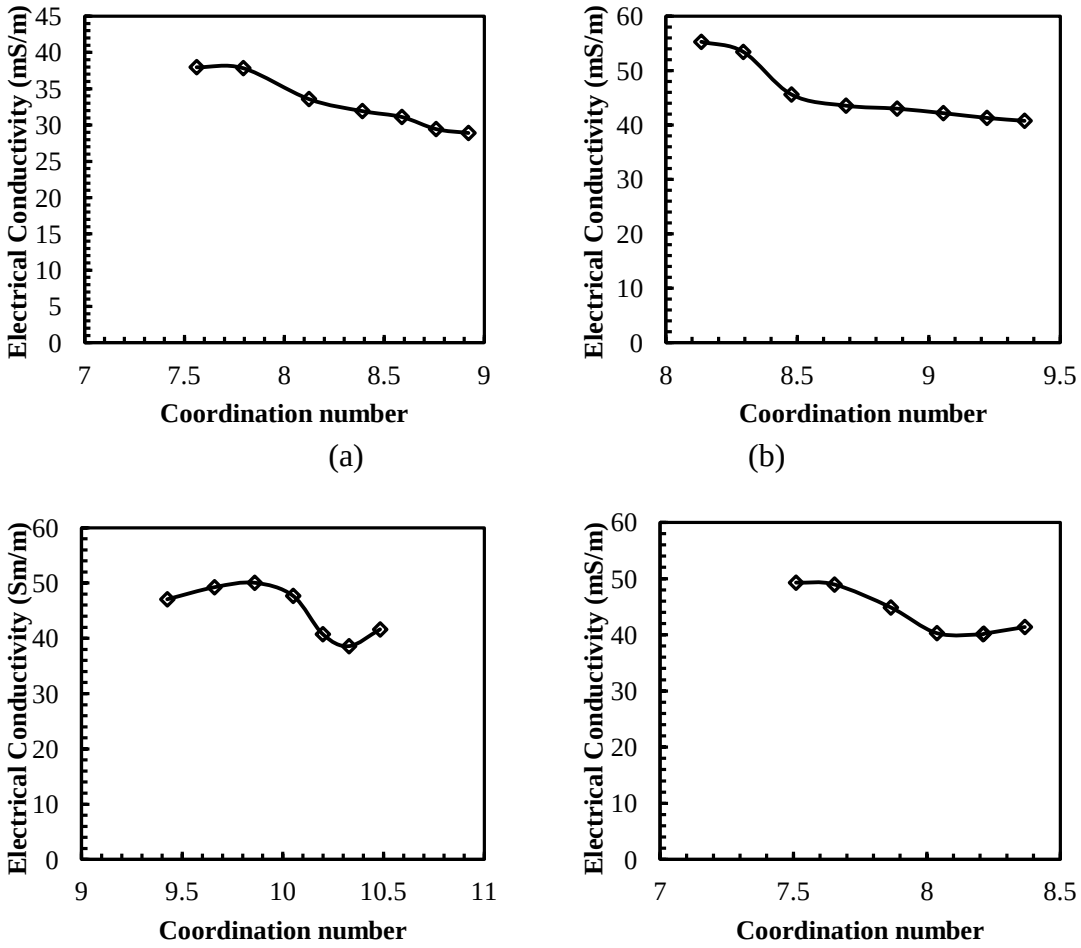

Figure 5.36 Electrical conductivity with the changes of coordination number (a) B1-15, (b) B2-15, (c) B2-20, (d) B2-10

It should be mentioned that the pore water was extracted from the soils during consolidation for high and low plasticity clay samples. The electrical conductivity of extracted pore water for CH and CL specimen were 143 and 103 mS/m, respectively. The measured electrical conductivities of pore water were used for the determination of surface conductivity according to the proposed relationship of Shang et al. (1995). It was

identified that the surface conductivity of the specimen ranged from 0.025 to 0.034 mS/m. Therefore, the effect of surface conductance was not substantial for the soil sample at saturated condition, and electrical conductivity occurred mostly through the interstitial pore water.

As the effect of surface charge was insignificant, the Archie's law was developed for each soil specimen using formation factors. The variations in formation factors with consolidation are illustrated in Figure 5.37.The experimental data points were fitted using power functions to obtain the coefficients of Archie's law.

The cementation factor (m) of Archie's law is a material dependent empirical exponent. According to Friedman (2005), the best-fitted value of cementation factor increases with the decrease of porosity in a consolidated media. Therefore, the specimen with high cementation factor consisted of low inter-particle voids and high coordination number. The best-fitted cementation factors were plotted against the average change in coordination number as presented in Figure 5.38. An overall downward trend was observed between cementation factors and average change in coordination number. Thus, the variation in coordination number under the applied load was low in soil specimens with high cementation factor.

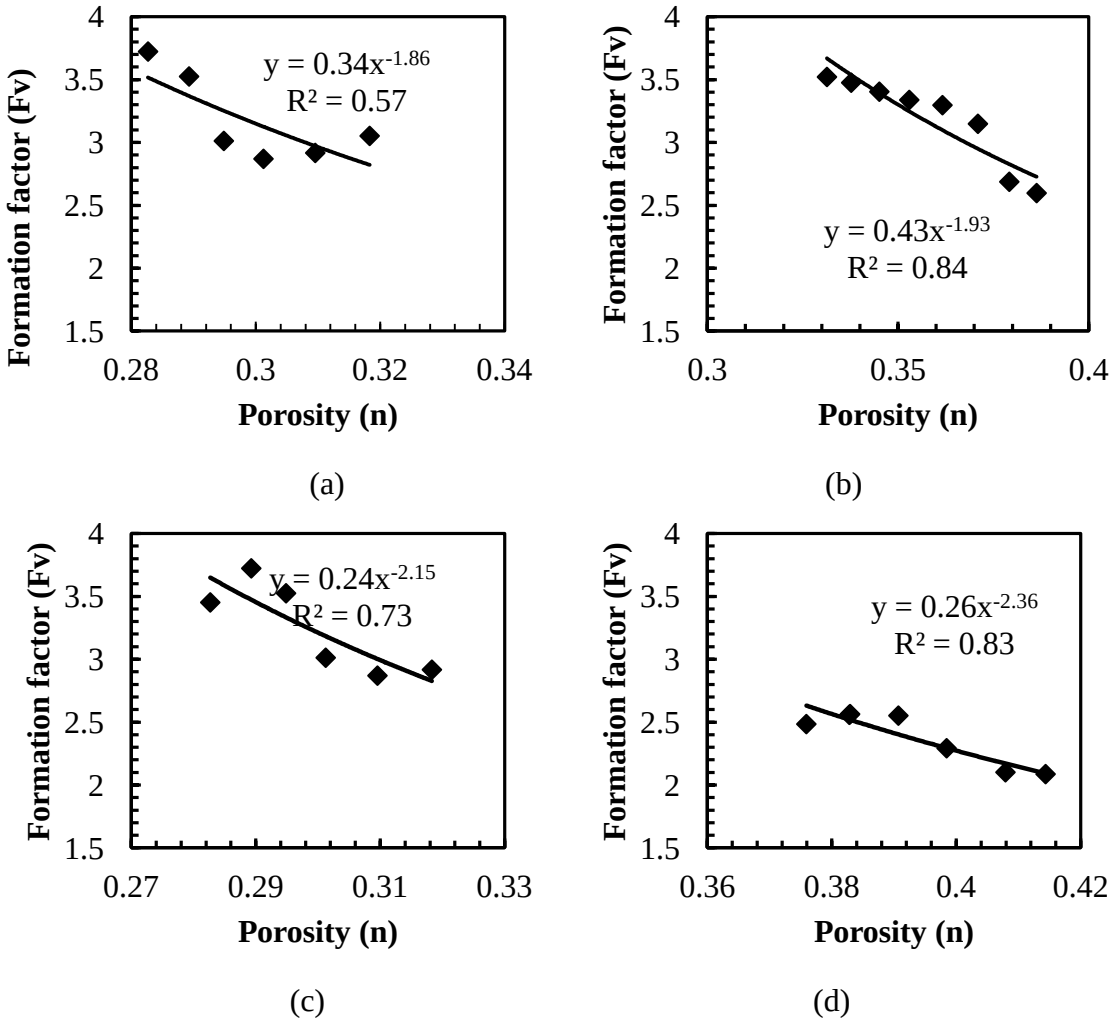

Figure 5.37 Development of Archie's law coefficients for the soil specimens (a) B1-15, (b) B2-15, (c) B2-20, (d) B2-10

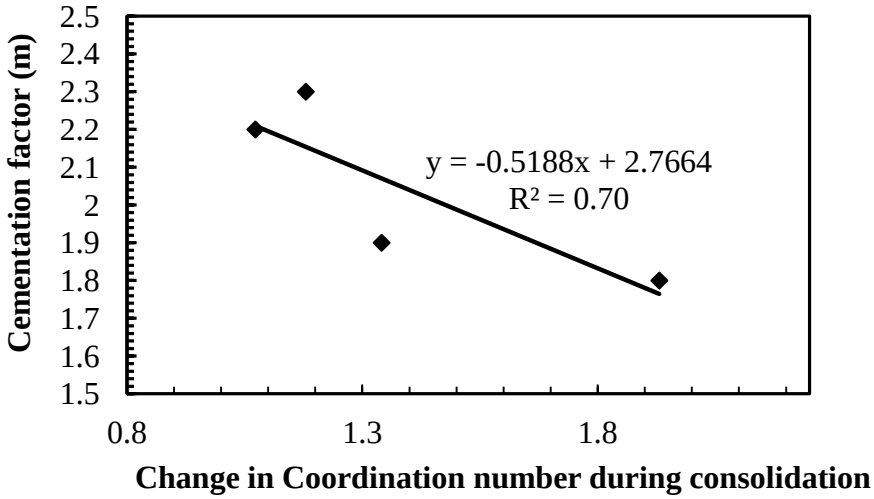

Figure 5.38 The relationship between cementation factors with coordination number

5.4.6 Relationship between compressibility and electrical conductivity

The laboratory investigation indicated that the variations in electrical conductivity under applied stresses were influenced by void ratio, fabric structure, pore configuration, contact between the particles, and cementation. Therefore, the correlations between electrical conductivity with compressibility parameters such as coefficient of consolidation and one dimensional strain equation were investigated. Moreover, permeability of the soil samples were evaluated at varied stages of consolidations, and were correlated with electrical conductivity.

5.4.6.1Coefficient of consolidation

The variations of displacement and resistivity with time in soil sample B2-20 are illustrated in Figure 5.39. It was identified that the resistivity variation was high at initial stages; however, the rate of reduction decreased with time. Therefore, the trends of resistivity changes were similar to the consolidation-time curves. The coefficients of

consolidations were determined using Taylor's method from displacement vs. time and resistivity vs. time curves. The comparisons of coefficients of consolidations obtained from both methods are presented in Figure 5.40. It was identified that observed results were in good agreement, and coefficients of consolidations can be evaluated using electrical resistivity.

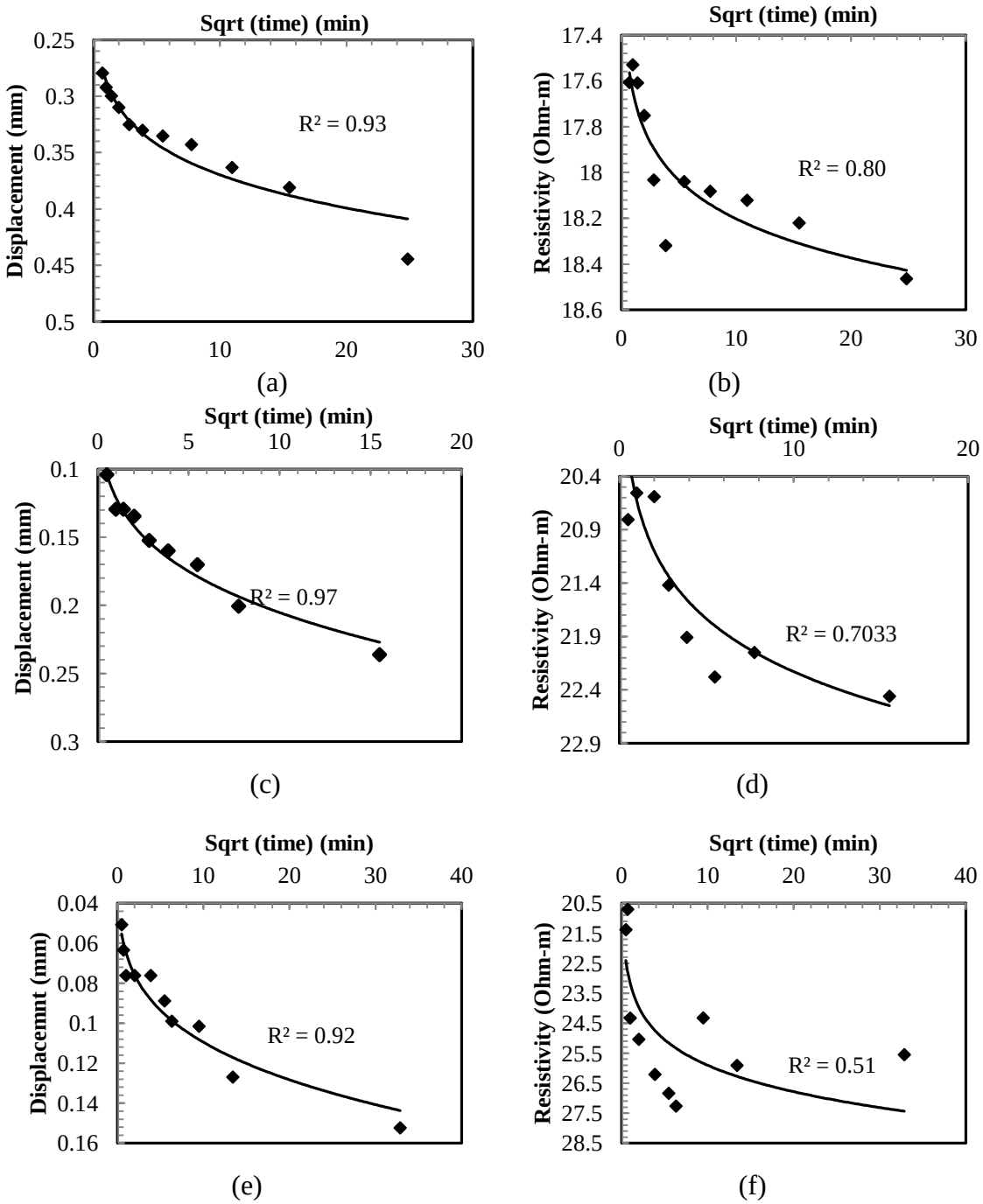

Figure 5.39 The variations of displacement and resistivity with time in soil sample B2-20 (a) pressure 111.6 kPa-displacement vs. sqrt (time) (b) pressure 111.6 kPa-resistivity vs. sqrt (time) (c) pressure 237.2 kPa-displacement vs. sqrt (time) (d) pressure 237.2 kPa-resistivity vs. sqrt (time) (e) pressure 362.8 kPa-displacement vs. sqrt (time) (f) pressure 362.8 kPa-resistivity vs. sqrt (time)

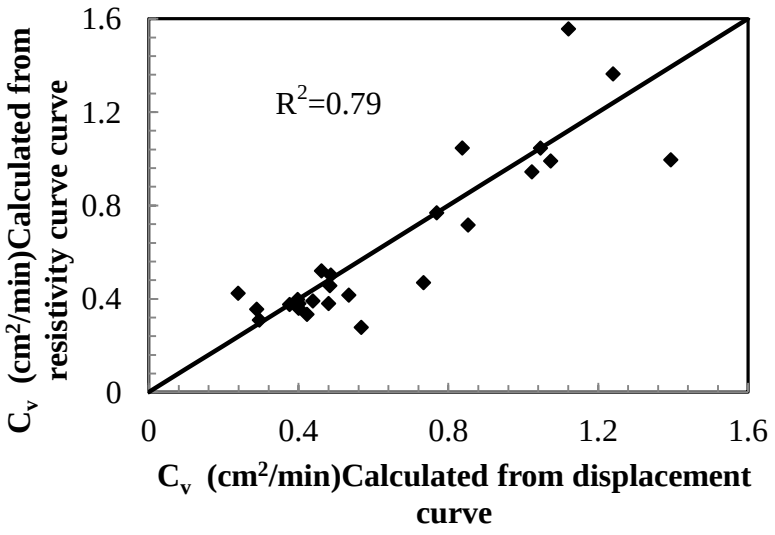

Figure 5.40 Comparisons of measured coefficient of consolidations from displacement and resistivity curves

5.4.6.2 Correlation between 1D Strain with Electrical Conductivity

The relationship between 1D vertical strain with electrical conductivity is illustrated in Figure 5.41. The scatter plot emphasized a linear correlation between the parameters with a correlation coefficient of 63%. Therefore, 63% variation in electrical conductivity can be explained by the strain at saturated soil specimens. Moreover, the linear relationship indicates that the electrical parameters can be used as an alternative of one-dimensional strain in settlement calculation. Bryson (2005) proposed a correlation between void ratio and electrical conductivity as presented below:

$$S = \frac{\Delta e}{(1+e)} H = \frac{\Delta \sigma}{1+\sigma v} (\xi)\, H \qquad (5.3)$$

where, Δe= change in void ratio, e= initial void ratio, $\Delta\sigma$ = change in vertical conductivity, σ_v= Initial vertical conductivity, ξ= factor relating vertical conductivity and void ratio, H= sample height.

Although the proposed equation suggests the relationship between strain and conductivity follows linear trend through origin of the plane, the current experimental results shows an intercept on the vertical axis at 0.02. For the current experimental results, the correlation between void ratio and electrical conductivity can be presented as:

$$\frac{\Delta\sigma}{1+\sigma v} = 3.233\frac{\Delta e}{(1+e)} + 0.023 \quad (5.4)$$

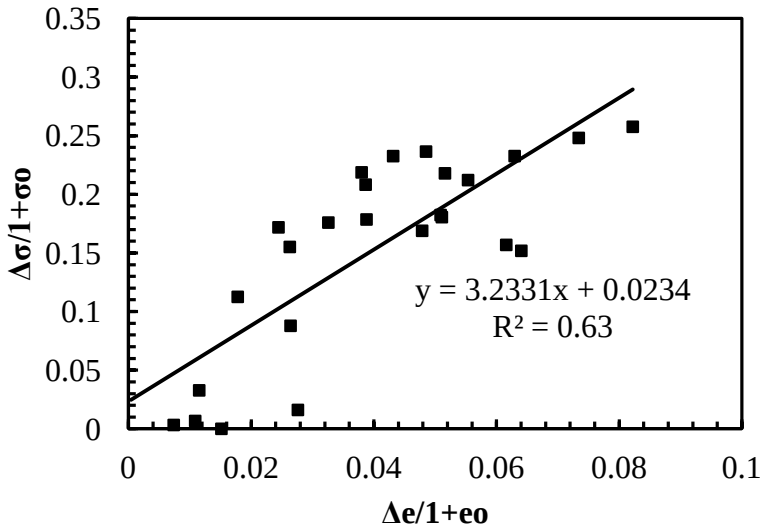

Figure 5.41 The relationship between 1D vertical strain with electrical conductivity

5.4.6.3 Relationship between Electrical and Hydraulic Conductivity

Sadek (1993) and Abu-Hassanein et al. (1996) conducted experimental studies to evaluate the relationship between hydraulic and electrical conductivity for different soils. However, a general correlation between permeability and electrical conductivity was not identified. In the current study, hydraulic conductivity of the soil samples were calculated indirectly from the consolidation tests. According to Lambe (1993), the hydraulic

conductivity of a sample under consolidation test can be determined at each void ratio using the following equation:

$$k = \frac{c_v \, a_v \gamma_w}{1+e} \tag{5.5}$$

where, k= hydraulic conductivity, c_v = coefficient of consolidation, a_v = coefficient of compressibility, γ_w= unit weight of water, and e= void ratio.

The hydraulic conductivity of the soil samples were calculated from the determined coefficient of consolidation, coefficient of compressibility, and void ratio of a corresponding consolidation pressure. The observed experimental results were fitted with power functions as presented Figure 5.42. To obtain, a general correlation which can be applicable for clayey type soils, statistical analysis were performed combining all the test results. Although, permeability was related with the electrical conductivity for individual specimen, a reliable correlation between hydraulic and electrical conductivity was not identified. The variation in cementation factors and packing arrangement of the particles might be responsible for the observed results. Moreover, the changes in soil fabric were not same in the soil samples under the application of pressure.

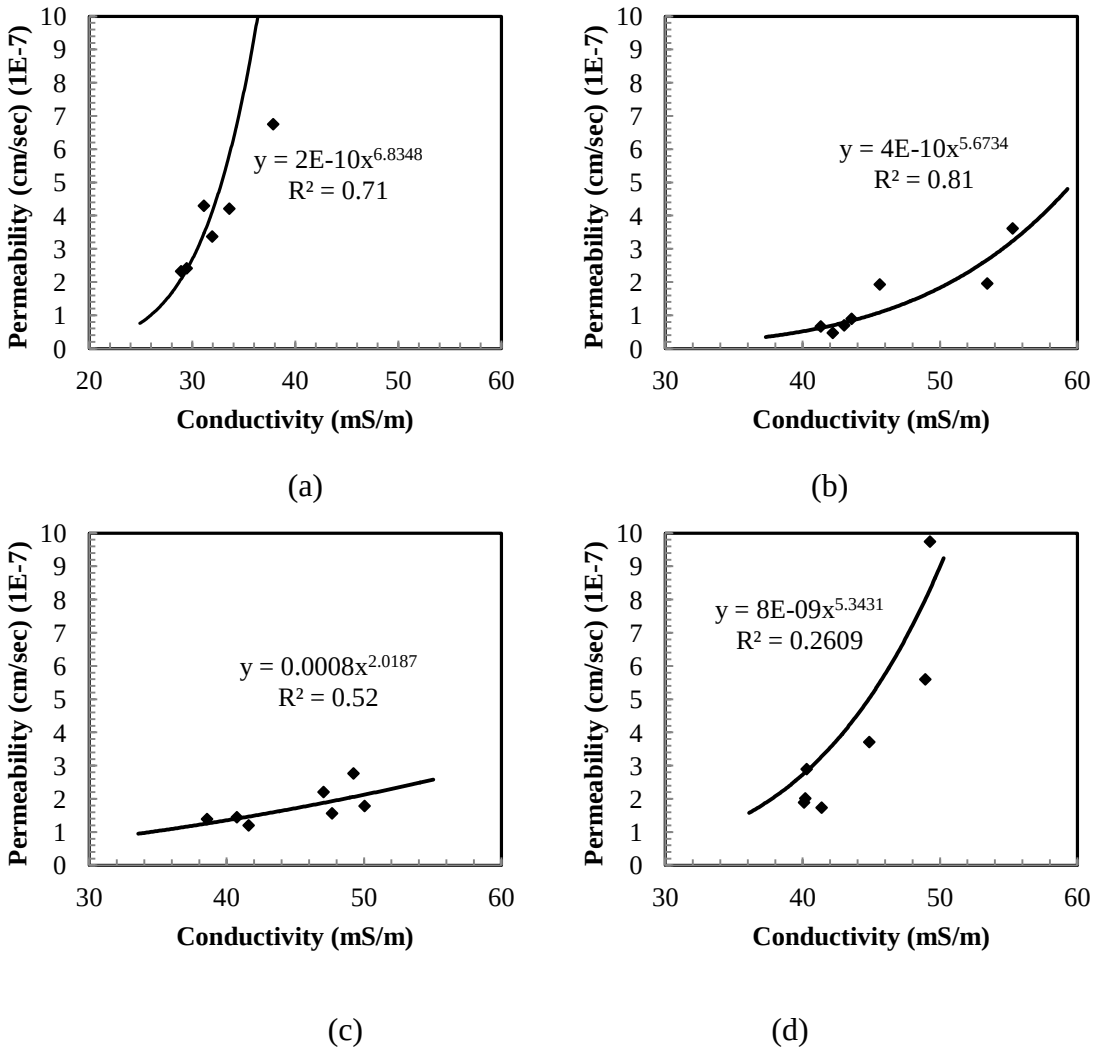

Figure 5.42 Relationship between electrical and hydraulic conductivity (a) B1-15, (b) B2-15, (c) B2-20, (d) B2-10

5.5 Summary

The objective of this chapter was to evaluate the influence of clay properties on electrical resistivity of clayey soils. The properties of the soils were divided into three groups i.e. a) parameters related to phase relationship, b) physicochemical properties, and c) compressibility. The major outcomes of the chapter can be summarized as follows:

1. Electrical resistivity of soils was substantially influenced by moisture content, dry unit weight, and void ratio. These parameters can be represented by a single parameter i.e. degree of saturation. Electrical resistivity decreased as much as 11 times of initial value (28.6 to 2.6 Ohm-m) for the increase of degree of saturation 23 to 100% in Ca-bentonite. The observed reductions ranged in between 6 and 11.3 times in kaolinite (373 to 33 Ohm-m), CL (58.1 to 7 Ohm-m), and CH (72 to 6 Ohm-m), respectively at this condition. In case of undisturbed soil samples, resistivity decreased as much as sixteen fold (49.4 to 3.2) for an increase of saturation from 31 to 100%.
2. It was observed that the resistivity results were different for the specimens at a specific degree of saturation. The variation might occur due to varied isomorpohous substitution of clay particles. Therefore, resistivity variation of the compacted and artificial specimens were plotted against CEC. According to the test results, resistivity was significantly affected by CEC at a relatively low degree of saturation. A total reduction in resistivity was as much as 385 Ohm-m for the increase of CEC from 13.3 to 79 cmol+/kg at 25% degree of saturation. On the other hand, the total reduction in resistivity was 43.3 Ohm-m at 100% degree of saturation in these CEC range. In addition, for Ca-bentonite-sand specimens, resistivity decreased from 64 to 37 Ohm-m, for the increase of CEC from 27.8 to 63.5 cmol+/kg, at 25% saturation. Therefore, test results emphasized the effect of ion exchange at low degree of saturation.

3. An overall downward trend was observed in each case when resistivity was plotted against liquid limits, plasticity indices, specific surface area, and mineralogical contents.
4. It was identified that pore water conductivity and sulphate content of pore water influenced electrical resistivity of the soil samples substantially. According to the results, pore-water conductivity of kaolinite mineral was 414 micro-Siemens/cm and associated resistivity values were 435, 140, 75, and 45 Ohm-m at 25, 50, 75, and 100% saturation, respectively. Nonetheless, pore-water conductivity of Ca-bentonite, CL, and CH were 1805, 1028, and 1436 micro-Siemens/cm, and the observed resistivity was below 50 Ohm-m at each saturation level due to the high conductivity of extracted pore water.
5. In addition to physical properties, compressibility of clays was correlated with electrical conductivity. Based on the investigation, it was determined that the electrical conductivity vs. pressure curves followed similar trends as e vs. logp curves. Moreover, pre-consolidation pressures were closely associated with the point of inflections in electrical conductivity vs. pressure curves.
6. The variation in electrical conductivity was related with the structural change, co-ordination number, and cementation of the soil samples under consideration.
7. The trends of resistivity changes with time were similar to the consolidation vs. time curves. The coefficients of consolidations were determined using Taylor's method from displacement vs. time and resistivity vs. time curves. The comparisons of coefficients of consolidations indicated that observed results were

in good agreement, and coefficients of consolidation can be evaluated using electrical resistivity.

8. The relationship between 1D vertical strain with electrical conductivity was determined. The scatter plot emphasized a linear correlation between the parameters with a correlation coefficient of 68%. Therefore, 68% variation in electrical conductivity can be explained by the void ratio at saturated soil specimens. Moreover, the linear relationship indicates that the electrical parameters can be used as an alternative of one-dimensional strain in settlement calculation. For the current experimental results, the correlation between void ratio and electrical conductivity can be presented as:

$$\frac{\Delta\sigma}{1+\sigma v} = 3.233\frac{\Delta e}{(1+e)} + 0.023$$

9. Although, permeability was related with the electrical conductivity for individual specimen, a reliable correlation between hydraulic and electrical conductivity was not identified. The variation in cementation factors and packing arrangement of the particles might be responsible for the observed results. Moreover, the changes in soil fabric were not same in the soil samples under the application of pressure.

CHAPTER 6

STATISTICAL MODELING

6.1 Introduction

The electrical mixing models of clayey soil describe resistivity as a function of pore fluid conductivity, pore connectivity, and surface conductance. The measurement of pore water conductivity requires extraction of moisture from the soil, and such methods are difficult to conduct in a regular investigation. Furthermore, determination of surface conductance is time intensive. The pore connectivity is defined by tortuosity, which is correlated with the conductive path and length of soil sample (Mitchell and Soga, 2005). An accurate estimation of tortuosity requires fundamental information about the packing of soil samples. Therefore, a practically applicable model is required to estimate soil parameters from electrical resistivity.

The objective of this chapter is to develop statistical models, which can correlate resistivity with influential geotechnical properties of compacted and undisturbed soil samples. Multiple linear regression (MLR) analyses were conducted using statistical analysis software SAS (2009), and model assumptions were investigated. The analysis steps followed in the MLR model development for compacted and undisturbed samples are presented in Figure 6.1.

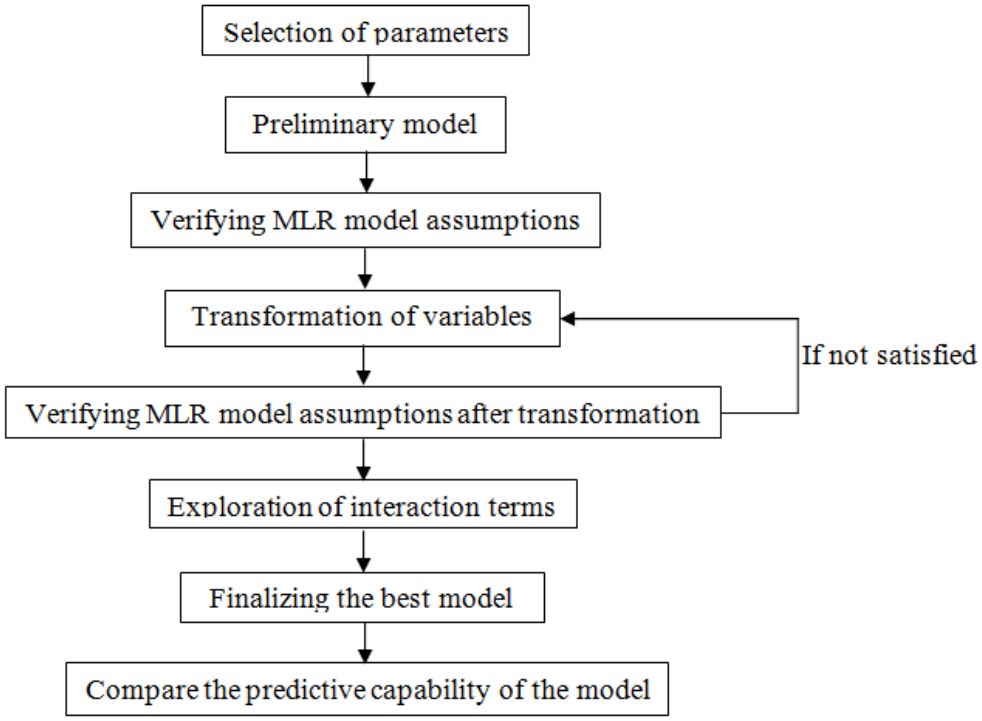

Figure 6.1 Analysis steps for model development using SAS

6.2 Selection of Parameters for Multiple Linear Regression (MLR) Model

According to Kutner et al. (2005), the predictor variables of a MLR model should not be correlated among themselves. However, in practical condition, the predictor variables are often correlated with each other. The problem of interrelation among the independent variables is referred as multicollinearity. The basic interpretation of regression parameters, i.e. change in expected results for unit change in a predictor variable, may not be appropriate in this situation. Multicollinearity may pose three setbacks in a MLR model such as: a) reduce the coefficient of regression b) difficulty in determining the importance of the variables, and c) increase the variance (Stevens, 1995).

The geotechnical parameters such as moisture content, unit weight, and degree of saturation are correlated with each other. Moreover, the CEC was high for a soil with high LL, PI, and fine content. In the current statistical analysis, the independent variables representing substantial properties of clayey soil, and affect resistivity were identified.

The objectives of the intended models were to correlate resistivity with physical properties of soils. Therefore, the compressibility parameters were not included in the model. Moreover, the observed variation in electrical conductivity with compressibility parameters were in the mili-siemens range and mostly fundamental.

6.2.1 Selection of Parameter Related to Phase Relationship

Based on the investigation of influential parameters, it was determined that the gravimetric moisture and dry unit weight simultaneously affect electrical resistivity of soils. The weight-volume relationship of soil indicates a proportional relationship between dry unit weight and void ratio. A soil with high dry unit weight consists of low void ratio and vice versa. The schematic of weight-volume relationship is presented in Figure 6.2.

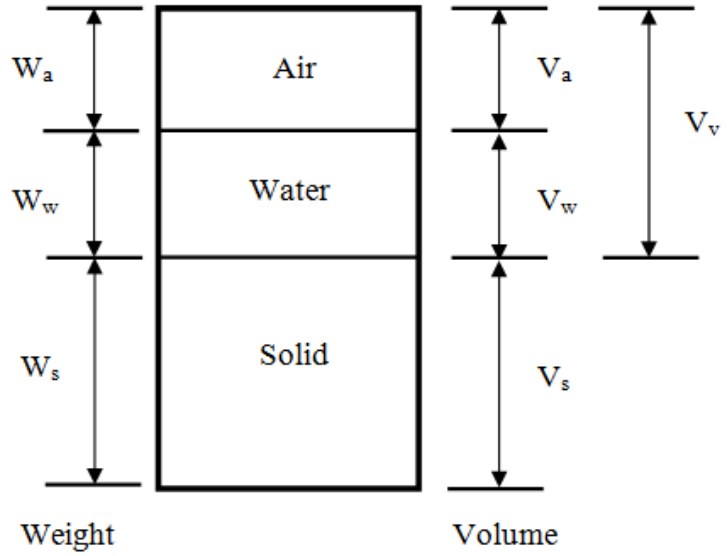

Figure 6.2 Phase relationship of soil

The degree of saturation can be determined from dry unit weight, gravimetric moisture content, and void ratio using the phase diagram as follows:

$$\gamma_d = \frac{\gamma_w G_s}{1+e} \tag{6.1}$$

$$S = \frac{w.G_s}{e} \tag{6.2}$$

here, γ_d = dry unit weight, G_s= specific gravity, w= gravimetric moisture content, e = void ratio and S=degree of saturation.

Therefore, the combined effect of gravimetric moisture content, void ratio, and dry unit weight in resistivity can be represented by a single parameter i.e. degree of saturation. Furthermore, degree of saturation is related to volumetric moisture (Θ_d) content according to the following equation:

$$\theta_d = \frac{S.e}{1+e} \tag{6.3}$$

To avoid potential multicollinearity in the statistical model, degree of saturation was selected as one of the predictor variables in MLR models.

6.2.2 Selection of Parameter Related to Clay properties

The parameter CEC of the artificial soil samples were plotted against clay parameters to observe the relationship among geotechnical properties. The correlations among CEC, Atterbeg limits, and mineral percentages are presented in Figure 6.3. It was observed that the correlation of coefficients were over 70% in each case. Moreover, the percent mineral was a linear function of CEC. The CEC increased with the increase of mineral percentages and vice versa. Therefore, multicollinearity in the regression model may occur if all the parameters are incorporated in statistical analysis.

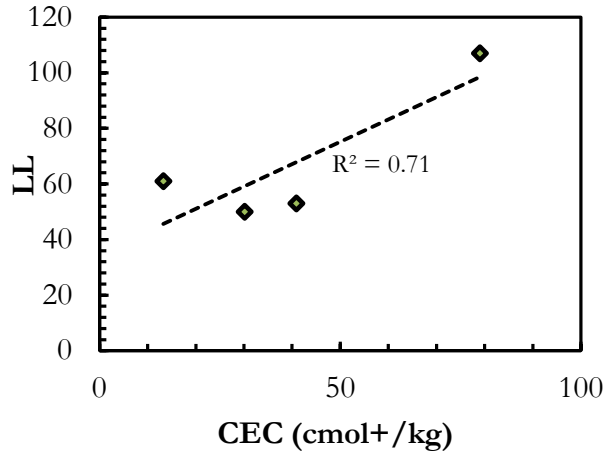

(a)

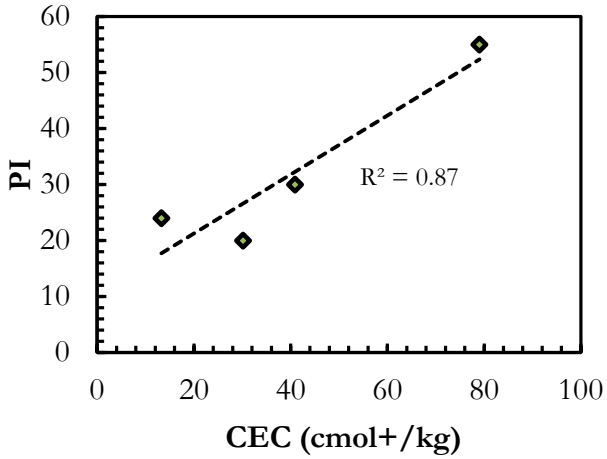

(b)

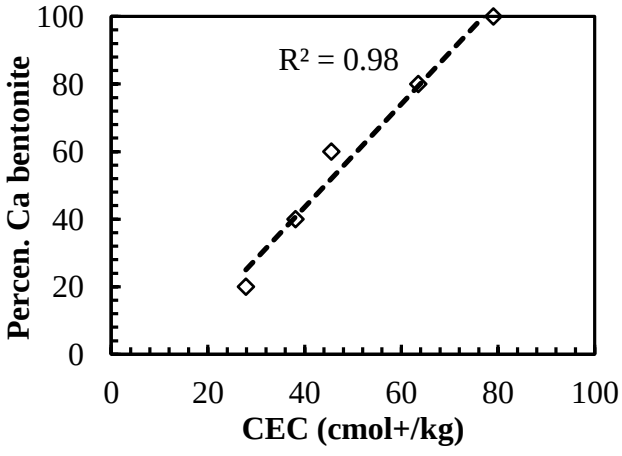

(c)

Figure 6.3 The correlations of CEC with (a) LL (b) PI (c) percentages Ca bentonite in artificial soil samples

The variation of CEC with pore water properties are presented in Figure 6.4. According to the experimental results, CEC can be utilized as an estimator of pore water conductivity and sulphate content. As the specimens with high CEC have high amount of exchangeable ions, the electrical conductivity increases in the presence of ions.

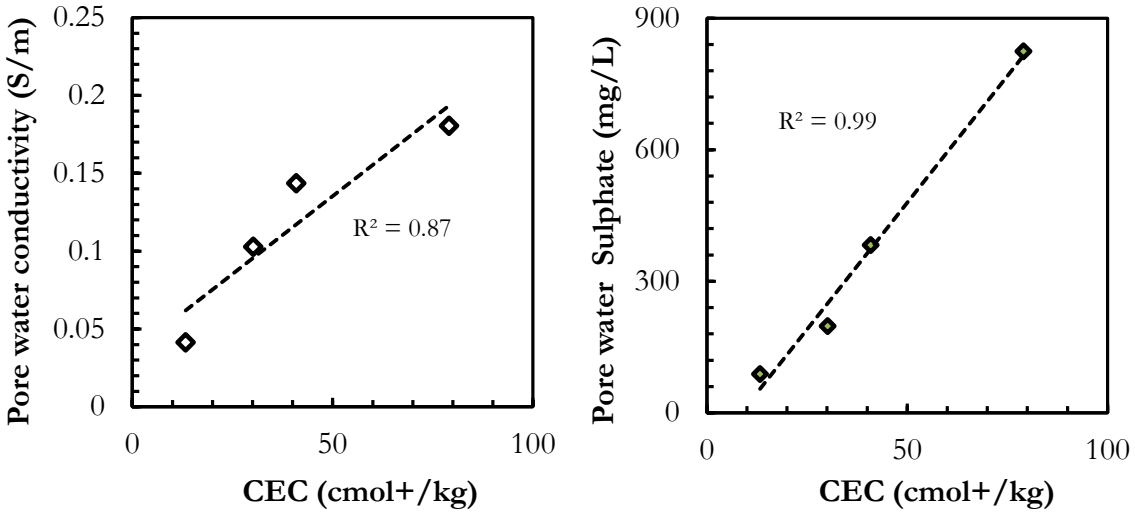

(a) (b)

Figure 6.4 The correlation of CEC with (a) pore water conductivity (b) pore water sulphate in compacted clays specimens

According to the study of Shah and Singh (2005), the clay fraction can be linearly correlated with CEC of the soils. The presence of fine content causes an increase in Atterberg limits in most of the clayey samples; therefore, CEC can be correlated with LL and PI. Shewartz et al. (2008) conducted a study to quantify field-scale moisture content using 2D resistivity imaging. Archie's law was calibrated to quantify the moisture content from observed field resistivity. To avoid potential difficulty of moisture extraction from the soil, exchangeable cations (Ca/Mg) were used as a proxy of pore water properties.

Based on the previous studies and analysis of the current test results, CEC was selected as a predictor variable in the MLR model to represent the clay properties affecting electrical resistivity of clayey soils.

6.3 MLR model for Electrical Resistivity of Compacted Clays

The experimental results of four set of compacted soil samples i.e. high plasticity clay (CH), lean clay (CL), Ca-bentonite, and kaolinite were utilized to develop multiple linear regression (MLR) model for compacted clays. In the current study, Ca-bentonite and kaolinite were used to determine two specific clay conditions. Ca-bentonite can be referred as montmorillonite, and characterized by high surface charge and ion substitution activities. On the other hand, the ion exchange property is not prominent in kaolinite. In addition, kaonite is composed of siloxane and $(OH)^-$ group surface (Meunier, 2005). Typically, these surfaces are electrically neutral and restrict the adsorption of ions or molecules in the interlayer surfaces.

A detail investigation was conducted to identify the influential parameters affecting electrical resistivity of clayey soils. A total of 748 resistivity tests were performed on different soil samples, moisture content, dry unit weight, and temperatures. The experimental results at different temperatures were corrected for a reference of 15.5 deg. C. The number of tests ranged from 11 to 25 in each moisture and unit weight conditions. Thereafter, results were randomized, and mean of the any eleven (11) randomized results was considered as a scatter point in the MLR model. A total of 44 data points were utilized for the model development.

6.3.1 Scatter Plot and Correlation among Variables

The scatter plot of the independent and response variables are presented in Figure 6.5. The scatter plots of resistivity with degree of saturation and CEC showed an overall downward trend; however, the observed relationships were not linear. In addition, the scatter plot of degree of saturation vs. CEC indicated that there was no correlation between the predictor variables.

In addition to graphical point of view, an analysis was conducted on the experimental data to determine the correlations between different predictor variables as presented in Table 6.1. It was observed that resistivity decreased with the increase of degree of saturation and CEC with R^2 value of 0.43 and 0.40, respectively. Moreover, the correlation coefficients between degree of saturation and CEC was 0.078 (<0.7).

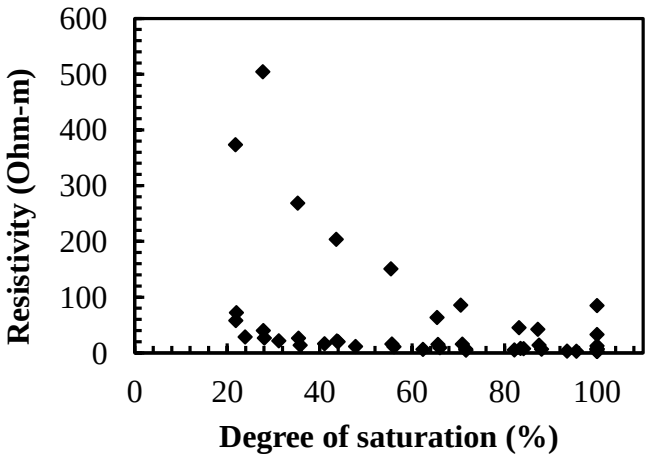

(a)

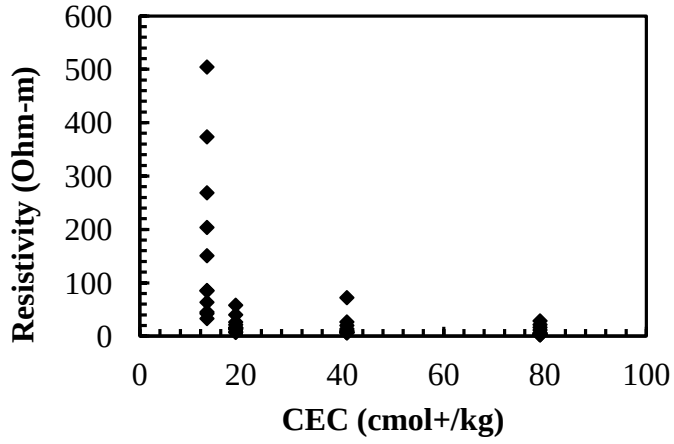

(b)

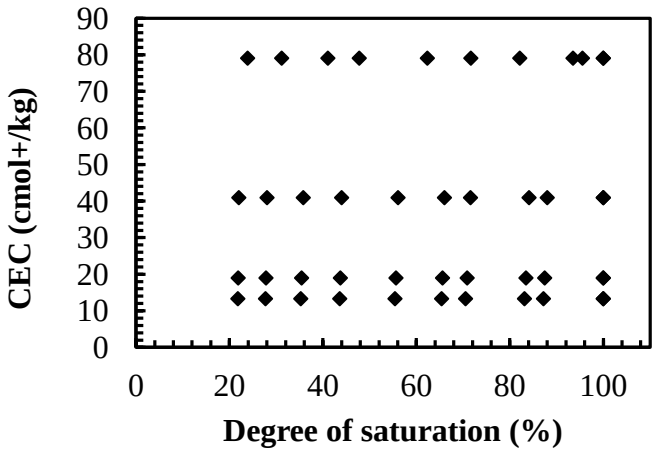

(c)

Figure 6.5 Scatter plot for MLR model of compacted clays (a) resistivity vs. degree of saturation (b) resistivity vs. CEC (c) CEC vs. degree of saturation

Table 6.1 Correlations among the variables

	Resistivity	**Degree of Saturation**	**CEC**
Resistivity	1.00	-0.43	-0.40
Degree of Saturation	-0.43	1.00	0.08
CEC	-0.40	0.08	1.00

6.3.2 Verification of Preliminary Model

A preliminary multiple linear regression model correlating resistivity with degree of saturation and CEC can be presented as:

$$Y_i = \beta_0 + \beta_1 X_{i1} + \beta_2 X_{i2} + \varepsilon_i \quad (6.4)$$

Where, i = 1, 2,..... n observations, X_{i1} = Degree of saturation (%), X_{i2} = Cation exchange capacity (CEC) (cmol+/kg), Y_i = Electrical resistivity (Ohm-m), β_0, β_1, and β_2 are regression parameters and $\boldsymbol{\varepsilon}_i$ is random error.

The physical meaning of regression parameters can be explained as the variation in the mean response E[Y] per unit increase of a predictor variable when all other independent variables in the regression model remain constant, and so on. The predictor variables in the current model were quantitative in nature, and the regression parameters were estimated using the least square method.

Analyses were conducted to observe the relationship among the variables. The summary of the ANOVA obtained from SAS is presented in Table 6.2. The ANOVA table suggested very high error sum of square (SSE), regression sum of squares (SSR), and total sum of squares (SSTO). The coefficient of correlation was 31.8% in the current data set. Therefore, the model explained only 31.8% of the variation in resistivity (Ohm-m).

Table 6.2 ANOVA of preliminary analysis of compacted clay specimens

Source	DF	Sum of Squares	Mean Square	F Value	Pr > F
Model	2	140188	70094	9.57	0.0004
Error	41	300375	7326.22		
Corrected Total	43	440563			

Root MSE	85.59334	R-Square	0.3182
Dependent Mean	54.20619	Adj R-Sq	0.2849
Coeff Var	157.90325		

Parameter Estimates								
Variable	**Label**	**DF**	**Parameter Estimate**	**Standard Error**	**t Value**	**Pr > |t|**	**Type I SS**	**Variance Inflation**
Intercept	Intercept	1	203.37723	37.2009	5.47	<.0001	129286	0
x1	Degree of saturation	1	-1.47431	0.47862	-3.08	0.004	80449	1.00615
x2	CEC	1	-1.43169	0.50137	-2.86	0.007	59740	1.00615

In addition to ANOVA, it is important to verify the appropriateness of the model for the data under consideration. The intended MLR model should be justified in terms of constant error variance, normality of error terms, outliers, and multicollinearity among the predictor variables (Stevens, 1995; Kutner et al. 2005, Huda, 2011). In the current research, the model assumptions were diagnosed using graphical plots and statistical tests.

6.3.2.1 MLR Model form

The residuals can be plotted against predictor variables to identify the applicability of linear regression for a data set. The prototype cases of the residual plots can be presented in Figure 6.6. Figure 6.6 (a) shows that residuals are located within a horizontal band centered on the horizontal axis. The points are scattered, and there is no systematic trends of the points. This is an appropriate situation for the applicability of linear regression model. On the other hand, Figure 6.6 (b) and (c) indicate situations where linear regression model is not appropriate. A specific curvature may indicate the requirement of adding quadratic term in the model.

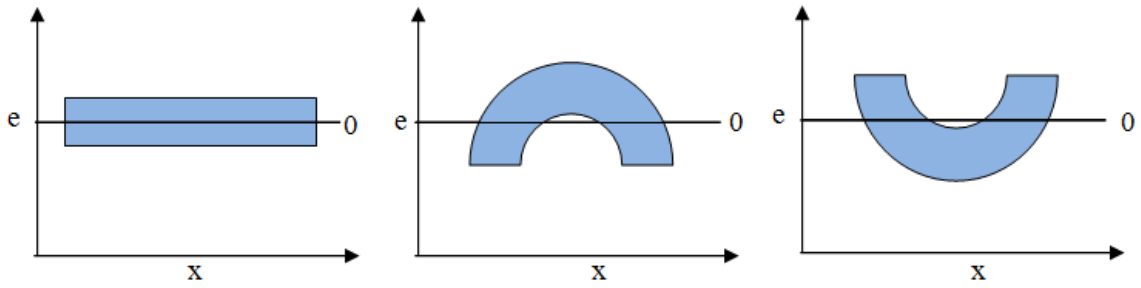

(a) (b) (c)

Figure 6.6 Protype plots for the assesment of linear model form (a) scatter (b) downward curve (c) upward curve

To evaluate model form, residuals are plotted against each predictor variable. Residual vs. predictor variable plots are presented in Figure 6.7. It was observed that the residuals were not scattered around the horizontal axis. Although specific curves were not identified from diagnostic plots, transformation on the predictor variables might be required to increase the scatter in the residuals.

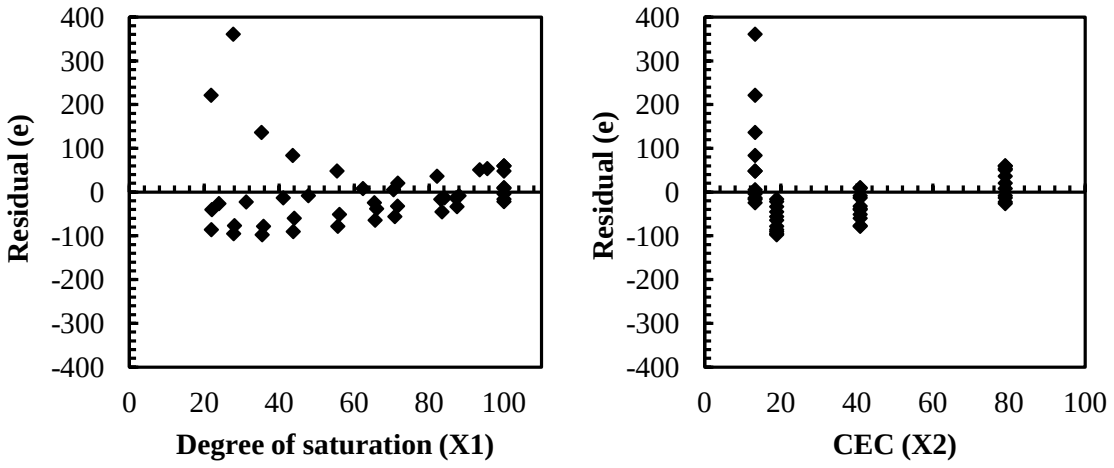

Figure 6.7 Residual vs. predictor variable plots (a) residual vs. degree of saturation (b) residual vs. CEC

6.3.2.2 Constant Variance

The graphical plot between residuals and fitted values can be utilized to determine the constant error variance assumption of the MLR model. In case of constant error variance, the residuals are scattered and do not follow any specific trends. The presence of funnel shape in the residual plots indicates non-constant error variance. The prototype cases of error variance are presented in Figure 6.8.

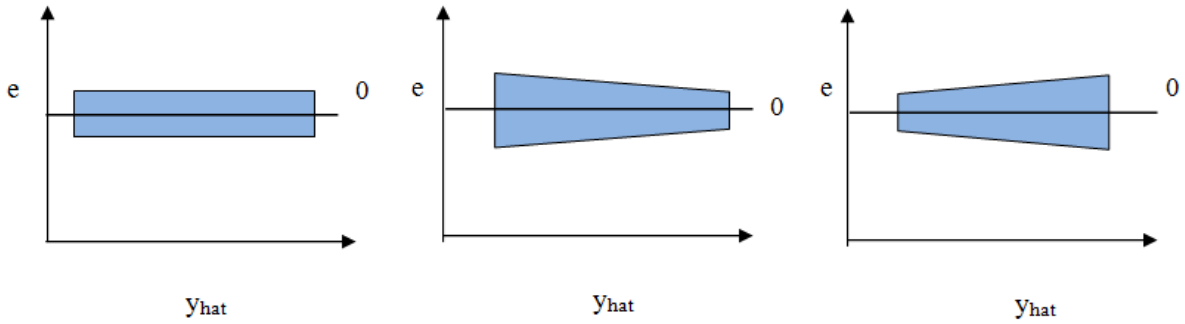

(a) (b) (c)

Figure 6.8 Residual vs. predicted variable plots (a) scatter (b) funnel towards low predicted value (c) funnel towards high predicted value

The residuals are plotted against predicted value ($\hat{Y}$) as presented in Figure 6.9. It was observed that the residuals were not scattered around horizontal axis. Moreover, there was a possible funnel shape in the residual vs. predicted value ($\hat{Y}$) plot. The presence of funnel shape indicated that the error variance of the model was not constant, and requirement of transformation of response variable.

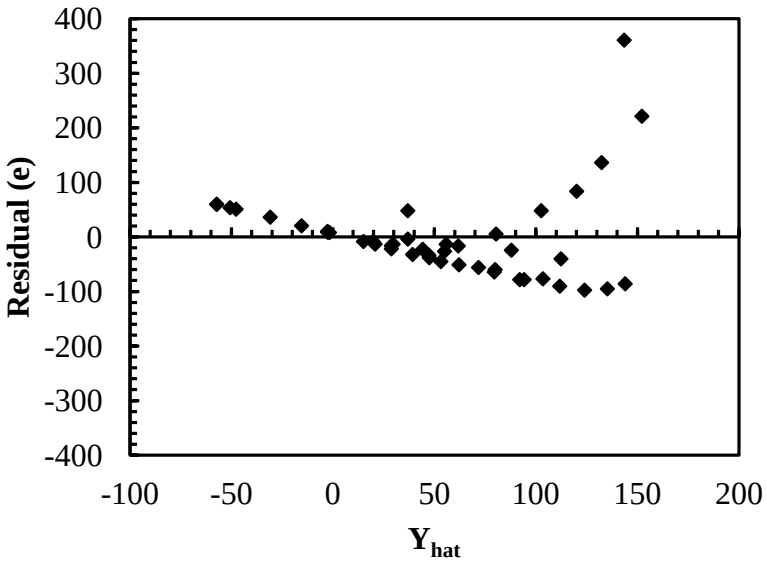

Figure 6.9 Residual vs. predicted value ($\hat{Y}$) plot

6.3.2.3 Normality

A normal probability plot can be utilized to observe the normality of the error terms in MLR models. A moderately linear plot indicates that the error distribution is normal. The normal probability plot in the current analysis is presented in Figure 6.10. The plot indicated that there was a long and short tail at the right and left side, respectively. Therefore, the errors of the model were not normally distributed.

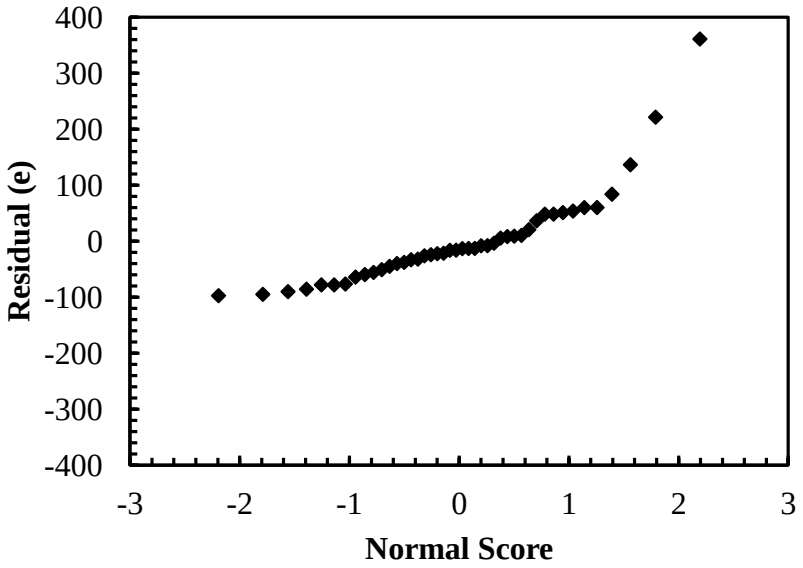

Figure 6.10 Residual vs. normal score plot

6.3.2.4 Outlier and their Influence

Outliers are known as extreme observation in a data set. It can create major problem in least square method by pulling the fitted line disproportionally towards the outlying observation (Kutner et al. 2005). The presence of outliers in an MLR model can be checked using residual plots and statistical tests.

The potential outliers in the current model were diagnosed using Leverage values and Bonferroni outlier test. In addition, the influences of outliers were determined by DEFITS, DFBETAS, and Cook's distance. Leverage values, Studentized deleted residuals, DEFITS, DFBETAS, and Cook's distance were obtained from SAS output. A discussion on the outlier and their influence are presented herein. The SAS output for the diagnostic of outliers are attached in Appendix A.

X outlier

For X outlier, observations with Leverage value greater than 2p/n were flagged. Here p=3, n=44, So, 2p/n=0.1364. The observation 1 was flagged as an X outlier because h_{ii} (0.5523)>0.1364.

Y outlier

Bonferroni outlier test was used for checking Y outlier. The guideline is to flag the Studentized deleted residual value greater than $t\left(1-\frac{\alpha}{2n};n-p-1\right)$.

$t\left(1-\frac{\alpha}{2n};n-p-1\right)= t\left(1-\frac{0.1}{88};44-3-1\right)= t\ (0.999;40)$=3.307

Therefore observation 16 was identified as an Y outlier because $\left|t_i\right|$ = 4.3964> 3.307

Influence

After identifying the outliers, their influence on the regression model was determined. The outliers are influential when their exclusion causes major changes in the regression model. The influences were determined by DEFITS, DFBETAS, and Cook's distance.

DFFITS: DEFITS considers the influence of the observation on the predicted value. The guideline is to flag the absolute values of DEFITS greater than 1.0 as an influential outlier for small to medium data set. It was observed that the absolute DEFITS value of observation 16 is 1.7715 which is greater than 1.0. Therefore, influence of observation 16 was required to be checked by other methods.

Cook's Distance: Cook's distance considers the influence of any observation on all predicted values. The guideline is to flag if Di > F (0.50, p, n-p). Here, F(0.5, p, n-p)= F(0.5, 3, 41)=0.80

For the data set presented here, Cook's distance was always less than 0.80. Therefore, none of the observations was flagged as influential.

DFBETAS: The guideline is to flag absolute DFBETAS are greater than 1.0 in a medium to large data set. It was observed that DFBETAS were greater than 1.0 in observation 16 (for X_1).

6.3.2.5 Multicollinearity

Variance inflation factor (VIF) is a measure of the multicollinearity among the predictor variables. The guideline indicates that serious multicollinearity occurs among the predictor variables when VIF (mean) >>1.0. A model with individual VIF more than 5 is also an indication of the presence of multicollinearity. The VIFs of the current model are presented in Table 6.3. It was observed that VIF of X_1 and X_2 were close to 1.0. As the predictor variables were selected based on the investigation of interrelationship among different influential parameters, the problem of multicollinearity was not observed in the current model.

Table 6.3 Variance inflation factor

Variable	Label	DF	Parameter Estimate	Standard Error	t Value	Pr > |t|	Type I SS	Variance Inflation
Intercept	Intercept	1	203.377	37.201	5.47	<.0001	129286	0
x1	Degree of saturation	1	-1.4743	0.4786	-3.08	0.004	80449	1.006
x2	CEC	1	-1.4317	0.5014	-2.86	0.004	59740	1.006

6.3.3 Transformation of Variables and Check for MLR assumptions

The diagnostic plots indicated that the normality and constant error variance assumptions were not satisfied in the current MLR model. In addition, there was a possible curvature problem in residual vs. predicted variable. Therefore, variance-stabilizing transformation was performed to eliminate these issues. The power of the transformation of dependent variable was -0.25, which was determined using Box-Cox method. The SAS results of Box-Cox method is presented in Figure 6.11. In addition, the predictor variable CEC (X_2) was transformed as $X_2{}' = X_2{}^{-1.5}$ to increase the scatter in the residuals vs.X_2 plot.

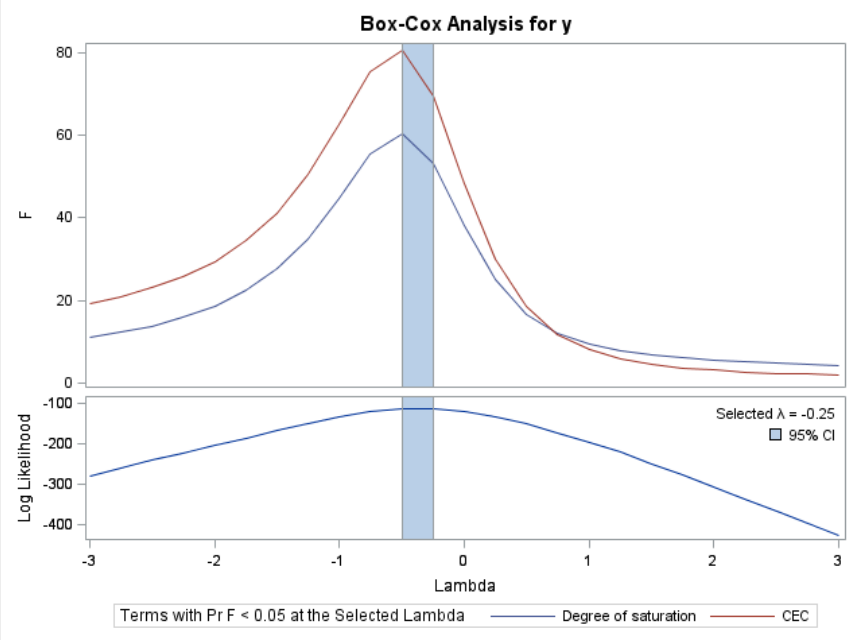

Figure 6.11 Box-Cox plot for transformation of dependent variable

The transformed model was,

$$Y' = \beta_0 + \beta_1 X_{i1} + \beta_2 X'_{i2} + \varepsilon_i \qquad (6.5)$$

Where, $Y' = Y^{-0.25}$ and $X_2{}' = X_2{}^{-1.5}$

The adequacy of the transformed model was verified using diagnostic plots as presented in Figure 6.12. It was observed that the residuals were scattered around horizontal axis and did not follow any specific trend in both cases. Therefore, the assumption of linear model was satisfied after transformation.

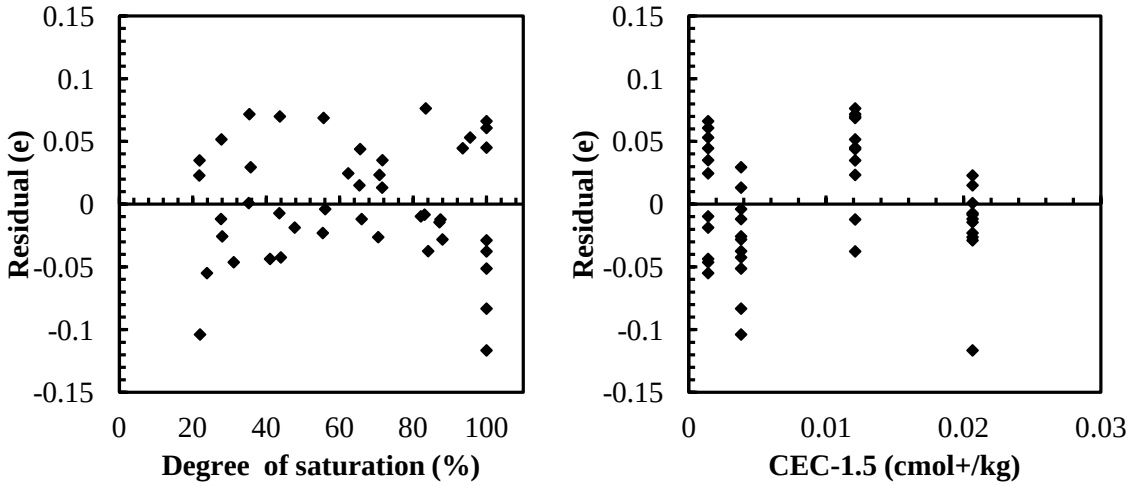

(a) (b)

Figure 6.12 Residual vs. predictor variable plots after transformation (a) residual vs. degree of saturation (b) residual vs. CEC

The assumption of constant error variance in the model after transformation was diagnosed using residual vs. predicted value plot, and Modified Levene tests. The residuals are plotted against predicted value ($\hat{Y}$) as presented in Figure 6.13. The funnel shape of the curve disappeared after transformation; therefore, the problem of non-constant variance was not observed in the transformed model.

To conduct Modified Levene test the data were divided into two groups based on the median (0.499655) of Y_{hat} value. SAS output of Modified Levene test performed on transformed variables is presented in Table 6.4.

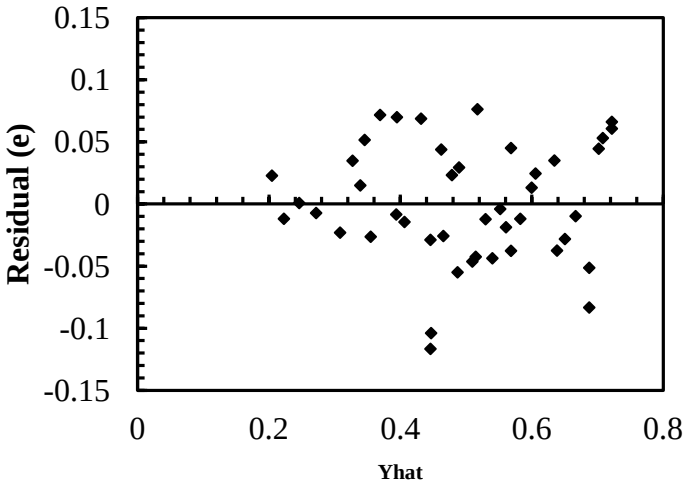

Figure 6.13 Residual vs. Y_{hat} plot after transformation of the model

Table 6.4 SAS output for Modified Levene test for transformed model

Group	N	Mean	Std Dev	Std Err	Minimum	Maximum
1	22	0.0388	0.0312	0.00666	0.00402	0.1134
2	22	0.0372	0.0263	0.0056	0.00107	0.0871
Diff (1-2)		0.0016	0.0289	0.0087		

Group	Method	Mean	95% CL Mean		Std Dev	95% CL Std Dev	
1		0.0388	0.0249	0.0526	0.0312	0.024	0.0446
2		0.0372	0.0255	0.0488	0.0263	0.0202	0.0375
Diff (1-2)	Pooled	0.0016	-0.016	0.0192	0.0289	0.0238	0.0367
Diff (1-2)	Satterthwaite	0.0016	-0.016	0.0192			

Method	Variances	DF	t Value	Pr > |t|
Pooled	Equal	42	0.18	0.8549
Satterthwaite	Unequal	40.801	0.18	0.8549

Equality of Variances				
Method	Num DF	Den DF	F Value	Pr > F
Folded F	21	21	1.41	0.4341

Test Statistics

Hypothesis:

$H_0: \sigma_{d1} = \sigma_{d2}$ $(Variances\ are\ equal)$

Vs. $H_a: \sigma_{d1} \neq \sigma_{d2}$ $(Variances\ are\ not\ equal)$

Decision rule: reject H_0 if $p < \alpha(0.1)$

From SAS output, P = 0.4341

As, $p > \alpha$, Variances are equal.

Hypothesis:

$H_0: Variances\ are\ constant$

Vs. $H_a: Variances\ are\ not\ constant$

Decision rule: reject H_0 if $p < \alpha$ (0.1)

From SAS output with unequal variances: P = 0.8549

As, $p > \alpha$, Variances are constant.

We conclude that the error variance is constant at α = 0.1.

The normal probability plot of transformed model is presented in Figure 6.14. It was observed that the normality changed after transformation. The residual vs. normal score plot was mostly liner; however, a slightly shorter tail existed at the right side of the distribution.

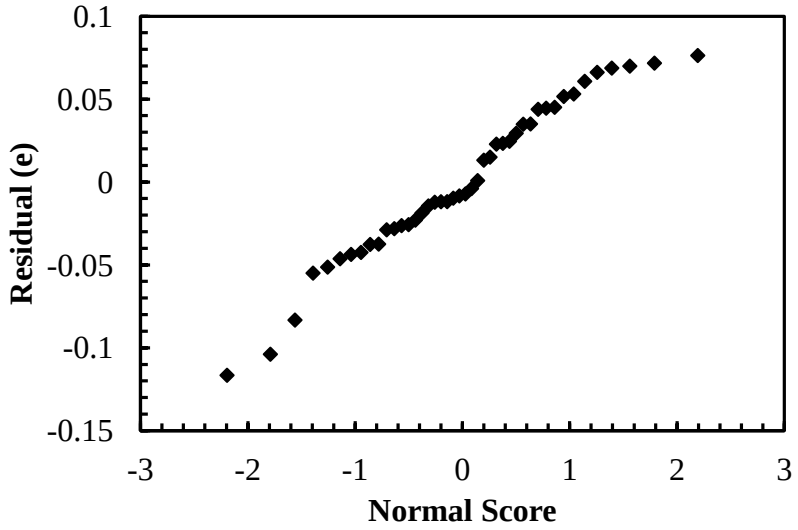

Figure 6.14 Residual vs. normal Score plot after transformation

Normality was further tested at 0.1 level of significance. The SAS output for normality test is given Table 6.5.

Table 6.5 SAS output for normality test in transformed model

	e	**enrm**
e	1	0.98546
Residual		<.0001
enrm	0.98546	1
'Normal Scores'	<.0001	

Test Statistics

Hypothesis:

$H_0: Normality\ is\ Ok$ vs. $H_a: Normality\ is\ violated$

Decision rule: reject H_0 if $\hat{\rho} < C\ (\alpha; n)$

For $\alpha = 0.10$ and n=44, $C\ (0.1; 44) = 0.9798$

And $\rho = 0.98546 > C\ (0.1; 44) = 0.9798$ (FTR H_0)

So, Normality ok at $\alpha = 0.1$.

6.3.3.1 Outlier Test for the Transformed Model

Similar to preliminary model, outliers were checked using Leverage values and Bonferroni outlier test. The observed $(h_{ii})_{max}$ was 0.1225 < 0.1364 (2p/n=0.1364); therefore, no observation was flagged as X-outlier after transformation. Moreover, Bonferroni outlier test indicated that $|t_i|_{max} = 2.7689 < 3.307[t\left(1 - \frac{\alpha}{2n}; n - p - 1\right)]$. Thus, no observation was identified as Y-outlier. The influence of an observation was investigated using DEFITS, DFBETAS and Cook's distance. Based on the SAS output and test statistics, influential outlying observation was not identified in the transformed model. SAS outputs for outlier test on transformed model is presented in appendix A.

6.3.3.2 ANOVA of Transformed Model

The preliminary model incorporating resistivity (Y) with degree of saturation and cation exchange capacity (CEC) after transformation is presented below:

$$Y' = 0.43398 + 0.00309X_1 - 14.35204X'_2 \quad (6.6)$$

Where, $Y' = Y^{-0.25}$ and $X_2' = X_2^{-1.5}$

The DC resistivity of a soil was not possible to be measured at zero degree of saturation. Furthermore, the CEC is a clay property and cannot be zero for soils with high percentages of fine content. Thus, the scope of the model did not include X_1=X_2= 0, and the intercept "0.43398" did not have a particular meaning as a separate term in the model. β_1=$0.00309X_1$ indicates the increase in the mean response of Y' by 0.00309 Ohm-m for per unit increase in the degree of saturation when CEC remains constant. Likewise, β_2=-14.35204 presents the decrease in mean response in Y' by 14.35204 Ohm-m for per unit increase in X_2' when degree of saturation was constant. Parameter estimates and ANOVA of the current model is presented in Table 6.6.

Table 6.6 Parameter estimate of the primary model

Parameter Estimates								
Variable	**Label**	**DF**	**Parameter Estimate**	**Standard Error**	**t Value**	**Pr > |t|**	**Type I SS**	**Variance Inflation**
Intercept	Intercept	1	0.43398	0.02135	20.33	<.0001	10.81455	0
x1	Degree of saturation	1	0.00309	0.00027	11.43	<.0001	0.35278	1.00315
x2	$CEC^{-1.5}$	1	-14.352	0.9647	-14.88	<.0001	0.51714	1.00315

Analysis of Variance					
Source	**DF**	**Sum of Squares**	**Mean Square**	**F Value**	**Pr > F**
Model	2	0.86992	0.435	186.16	<.0001
Error	41	0.0958	0.002		
Corrected Total	43	0.96572			

Root MSE	0.04834	R-Square	0.901
Dependent Mean	0.49577	Adj R-Sq	0.896
Coeff Var	9.75002		

ANOVA indicated that the SSE, SSR, and SSTO of the model were 0.86992, 0.09580, and 0.96572, respectively. The coefficient of regression (R^2) of the model was 90.1%. Therefore, the model explained 90.1 % of the variation in resistivity (Ohm-m) in response to degree of saturation and CEC of compacted clays.

The significance of each predictor in the primary model can be measured by the obtained p value in the SAS output (Table 6.6) indicated that the predictors in the model were significant at 0.1 level of significance.

F test can be conducted to determine whether there is a regression relationship between response variable and the predictor variables. The p value was <0.0001. Therefore, a regression relationship exists between response variable and all the predictor variables at 0.1 level of significance.

6.3.4 Exploration of Interaction Term

The potential interaction terms were explored through a set of residual plots i.e. residual vs. X_1X_2', residual vs. $std\ X_1X_2'$, and partial regression plot of X_1X_2' as presented in Figure 6.15. It was observed that there was a slight downward trend in partial regression plot of X_1X_2'. However, the trend lines were not prominent in residual vs. X_1X_2' and residual vs. $std\ X_1X_2'$ plots. The effect of the interaction term was further justified by conducting regression analysis on Y' over X_1, X_2, and $std\ X_1X_2'$. The effect of addition of X_1X_2' was not substantial because coefficient of regression increased from 90.1% to 91.9% only after incorporating X_1X_2'in the model.

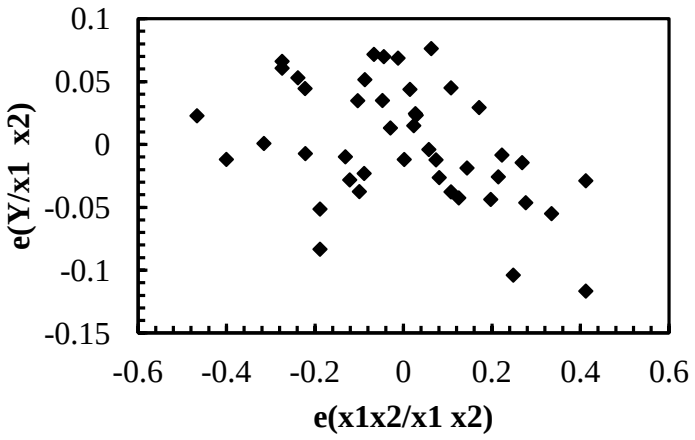

(a)

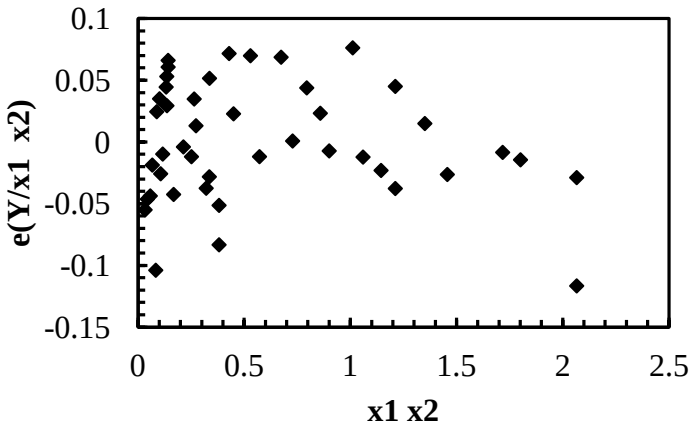

(b)

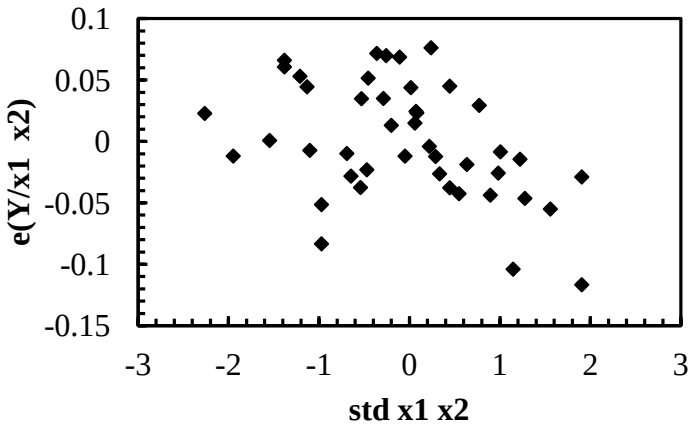

(c)

Figure 6.15 Exploration of interaction term (a) partial regression (b) residual vs. x1x2 (c) residual vs. std x1x2

6.3.5 Selection of Final Model

The potential best model and relative influences of the predictor variables were analyzed using best subset method, stepwise regression, and backward elimination methods.

Best subset selection

Best subset method determines possible best models based on the R^2, R_{adj}^2, Mallow's C_p, and Akaike's Information Criteria (AIC). In the current analysis, the potential best models may contain one/two variables. A potential good model should have high R^2, R_{adj}^2, and low Mallow's Cp and Akaike's Information Criteria (AIC). The summary of results are presented in Table 6.7.

Table 6.7 Summary of best subset selection algorithm

Number in Model	Adjusted R-Square	R-Square	C(p)	AIC	SBC	Variables in Model
2	0.896	0.9008	3	-263.708	-258.35	x1 x2
1	0.5746	0.5845	131.7	-202.679	-199.11	x2

Backward Elimination

During Backward elimination, the analysis started including all the parameters in the model. Thereafter, statistically insignificant variables are removed from the model in the following steps. The analyses continue until insignificant variable remains in the model and no parameters can be removed. Eventually the backward elimination algorithm provides one best model. In the current analysis, all the predictor variables are significant at 0.05 level of significance and no predictor variables were removed.

Stepwise regression

Stepwise regression method can be utilized to obtain potential good models from backward elimination and forward selection algorithm. During analyses, the parameter with highest statistical significance is included first in the model and regression analysis is carried out. After the completion of first analysis, another parameter is added in the previous model and the procedure is repeated. Statistical significance tests (i.e. F statistic) are utilized to select the parameters sequentially (Kutner et al. 2005).

The summary of Stepwise regression results are presented in Table 6.8. It should be mentioned that the tests were conducted at 0.05 level of significance.

Table 6.8 Summary of stepwise regression

Step	**Variable Entered**	**Number Var. In**	**Partial R-Square**	**Model R-Square**	**C(p)**	**F Value**	**Pr > F**
1	x2	1	0.5845	0.5845	131.7	59.07	<.0001
2	x1	2	0.3163	0.9008	3	130.75	<.0001

All three methods showed that both degree of saturation and CEC were required to explain electrical resistivity. Therefore, the best model correlating resistivity with degree of saturation and CEC can be presented as follows:

$$Y^{-0.25} = 0.43398 + 0.00309X_1 - 14.35204X_2^{-1.5} \qquad (5.7)$$

here, Y= Electrical resistivity (Ohm-m) corrected at 15.5 deg temperature according to ASTM G187-05, X_1=Degree of saturation (%), X_2= Cation exchange capacity (CEC) (cmol+/kg)

Range of the model: Y= [2.6, 504.3], X_1= [21.8, 100], X_3= [13.28, 79.03]

6.3.6 Interaction Surface

The combined effect of degree of saturation and CEC on electrical resistivity of compacted clays is illustrated in Figure 6.16. According to the interaction surface, the resistivity was very high below 30% degree of saturation and CEC of 20 cmol+/kg. However, rate of changes reduced after this degree of saturation and CEC. The interaction surface also showed that the resistivity surface became parallel to horizontal plane at relatively high degree of saturation and CEC.

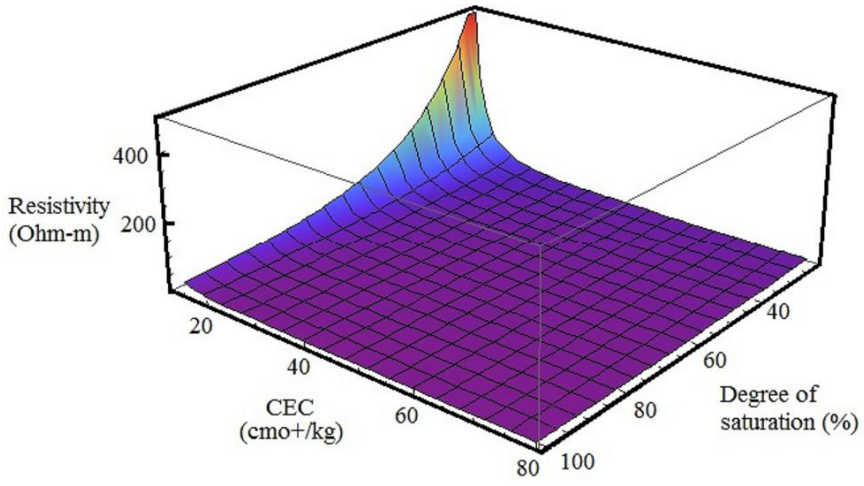

Figure 6.16 Interaction surface correlating resistivity with degree of saturation and CEC

6.3.7 Comparison of Model Predicted Resistivity with Experimental Results

The experimental results of artificial soil samples were utilized to compare the model predicted results. The objective of comparing with new data sets was to evaluate the applicability of the model for different types of clayey soils. A total of four artificial soils were used for the model validation. Electrical resistivity tests were conducted at

varied degree of saturations and the observed results were corrected for 15.5 deg. C temperature. The CEC of five artificial soils are presented in Table 6.9.

Table 6.9 Soil specimens used for the comparison of model predicted resistivity

Mineral by weight (%)	**Sand by weight (%)**	**CEC (cmol+/kg)**
80	20	63.3
60	40	47.6
40	60	31.8
20	80	16.4

The interaction surface indicated that the resistivity sharply increased below CEC of 20 cmol+/kg, and degree of saturation less that 30%. It was identified that the percentages error in the prediction was over 5 Ohm-m, when the CEC and degree of saturation were very low (soils with 40% bentonite or less). However, the error was within ± 5 Ohm-m when CEC was larger than 30 cmol+/kg, and degree of saturation was higher than 30%, approximately. A comparison of model predicted and observed resistivity is presented in Figure 6.17.

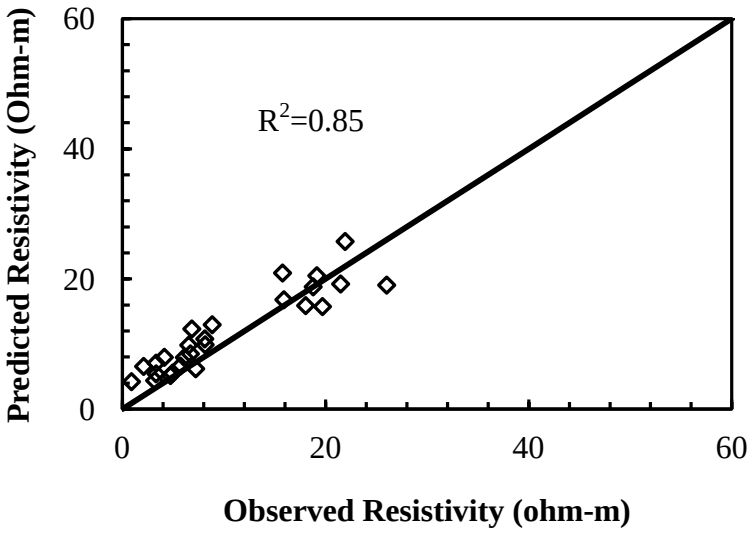

Figure 6.17 Comparison of model predicted and observed resistivity

6.3.8 Resistivity Vs Degree of Saturation for Typical Clay Soils

A number of electrical resistivity vs. degree of saturation charts were developed at different CECs for compacted clay soils. The electrical resistivity (at 15.5 deg. C temperature) was estimated at varied degree of saturations using the proposed MLR model. It can be mentioned that the CEC of clayey soils can be measured in the laboratory according to ASTM D7503 standard. Moreover, CEC of soils can be determined using Atterberg limits according to Farrar and Coleman (1967), Smith et al. (1985), and Yukselen and Kaya (2006) correlations. The correlations between resistivity and degree of saturation at different CEC are presented in Figure 6.18.

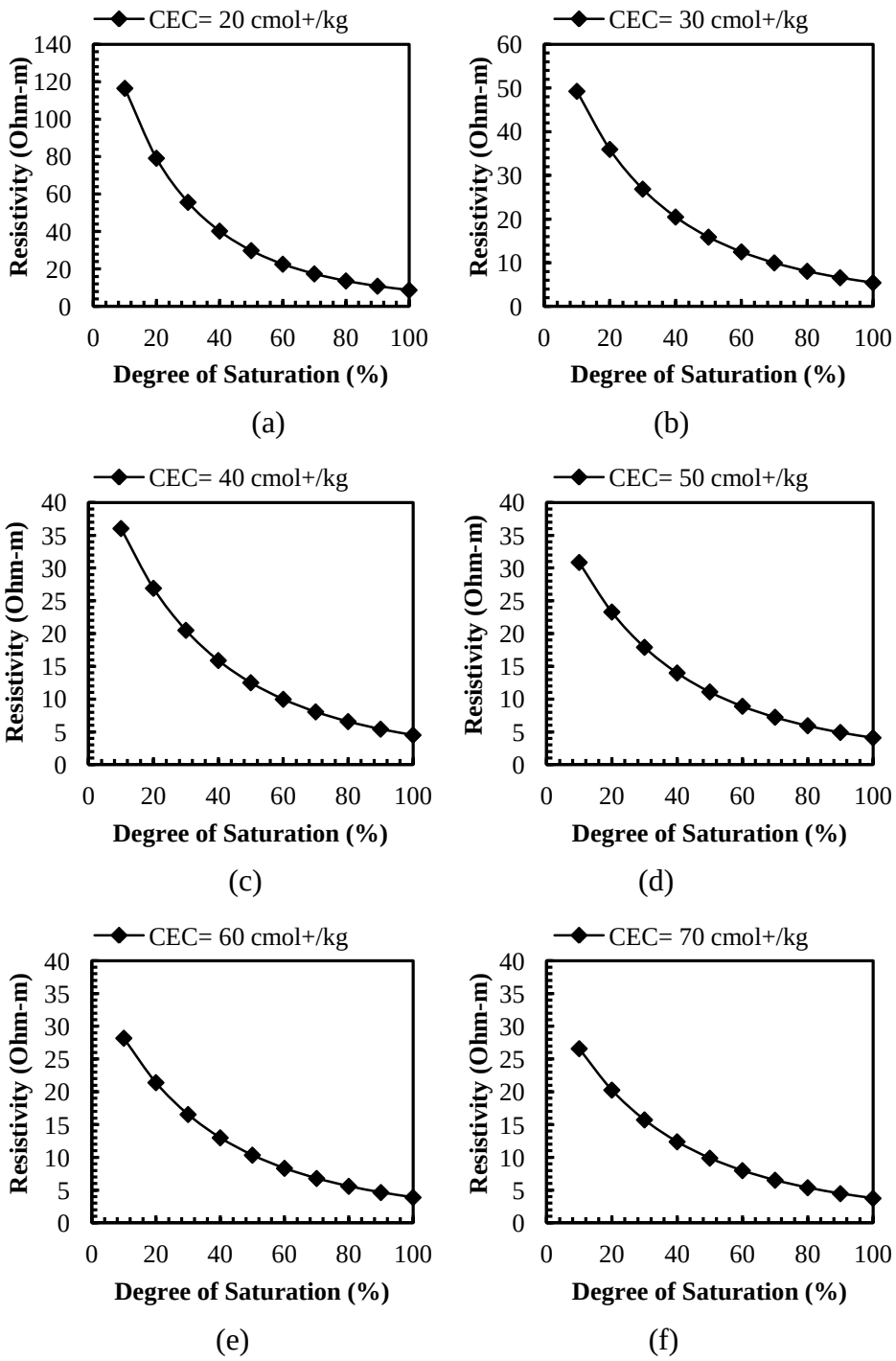

Figure 6.18 Variation of resistivity with degree of saturation at different CEC for compacted clays (a) CEC 20 cmol+/kg (b) CEC 30 cmol+/kg (c) CEC 40 cmol+/kg (d) CEC 50 cmol+/kg (d) CEC 60 cmol+/kg (f) CEC 70 cmol+/kg

6.4 MLR model for Electrical Resistivity of Undisturbed Soils

A separate MLR model was developed using test results of undisturbed soil samples. Similar to the previous model (MLR of compacted clays), degree of saturation and CEC were selected as independent variables. An initial analysis was conducted and model assumptions were examined. Transformation was performed on the response variable to satisfy the model assumptions. Once the model form was finalized, the predictive capability of the model was compared with the observed test results of a different soil sample.

6.4.1 Scatter Plot and Correlation among Variables

The scatter plots of the predicator and response variables are presented in Figure 6.19. It was observed that resistivity decreased with the increase of degree of saturation; however, the correlation was not linear. It should be mentioned that the correlation between resistivity and CEC was not substantial for the current data set. Nonetheless, CEC was incorporated in the model to represent the clay properties. The Pearson coefficients among the variables are presented in Table 6.10. According the SAS results, the predictor variables were not correlated with each other.

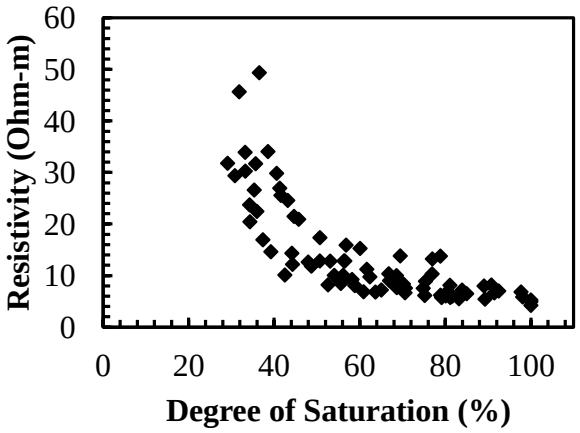

(a)

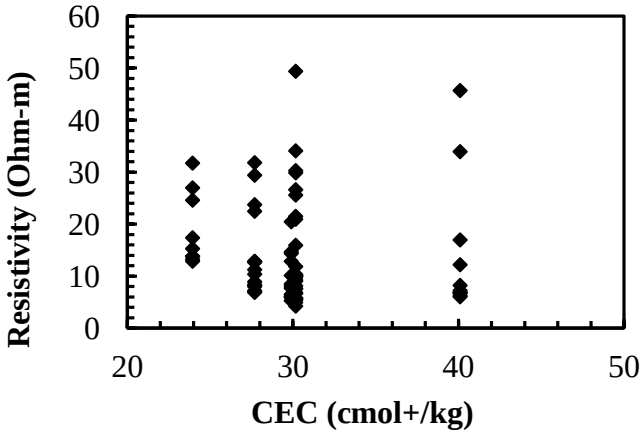

(b)

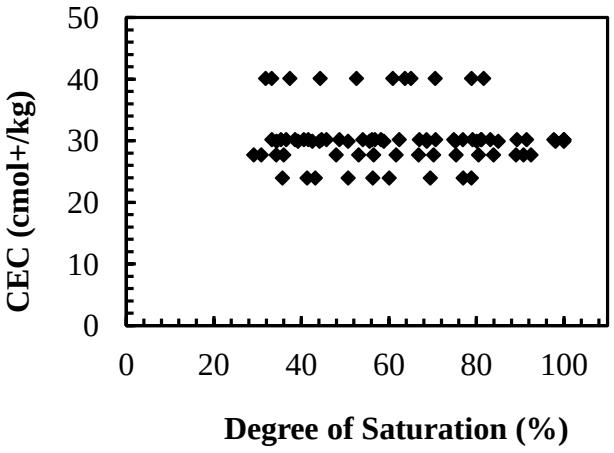

(c)

Figure 6.19 Scatter plots for experimental results of undisturbed soils (a) resistivity vs. degree of saturation (b) resistivity vs. CEC, and (c) CEC vs. degree of saturation

Table 6.10 Pearson's coefficients of the variables

	Resistivity	**Degree of Saturation**	**CEC**
Resistivity	1.00	-0.77	-0.067
Degree of Saturation	-0.77	1.00	0.05
CEC	-0.067	0.05	1.00

6.4.2 Verification of Preliminary Model

The ANOVA chart of the statistical analysis is presented in Table 6.11. It was identified that the SSE, SSR, and SSTO were 4415.5, 2855.5, and 7271.04 in the MLR model. The coefficient of correlation was 60.7% in the current data set. Therefore, the model explained 60.7% of the variation in resistivity (Ohm-m).

Table 6.11 ANOVA of the current model

Source	**DF**	**Sum of Squares**	**Mean Square**	**F Value**	**Pr > F**
Model	2	4415.47	2207.74	57.21	<.0001
Error	74	2855.56	38.5887		
Corrected Total	76	7271.04			

Root MSE	6.212	R-Square	0.6073
Dependent Mean	13.98	Adj R-Sq	0.5967
Coeff Var	44.43		

The adequacy of the model was verified using diagnostic plots as presented in Figure 6.20. A curvature was identified in the residual vs. degree of saturation plot; therefore, the model form was not appropriate. The assumption of constant error variance was investigated using residual vs. predicted value plots. A funnel shape was observed in the diagnostic plot, which indicated that the error variance was not constant in the model.

The normality curve for the current statistical model of undisturbed soil samples showed that there was a long and short tail on the right and left side, respectively (Figure 6.19). Therefore, the residuals were not normally distributed.

6.4.2.1 Outlier

The observation with a Leverage value greater than 2p/n can be consider as X-outlier. It was observed that the Leverage value was more than (2p/n>0.0779) 0.0779 in observation 14, 15, 16, 21, 22, 23, and 24. Moreover, Bonferronni outlier test indicated the observation 24 and 77 as Y-outlier.

The influence of the outlying observation on regression model was analyzed using DEFITS, DFBETAS and Cook's distance. The SAS results showed that the observation 24 might influence the model as the DFFITS and DFBETAS were more than 1.0 in the observation. However, Cook's distance was below the threshold 0.796 in the data set. The SAS output for the outlier test is attached in Appendix A.

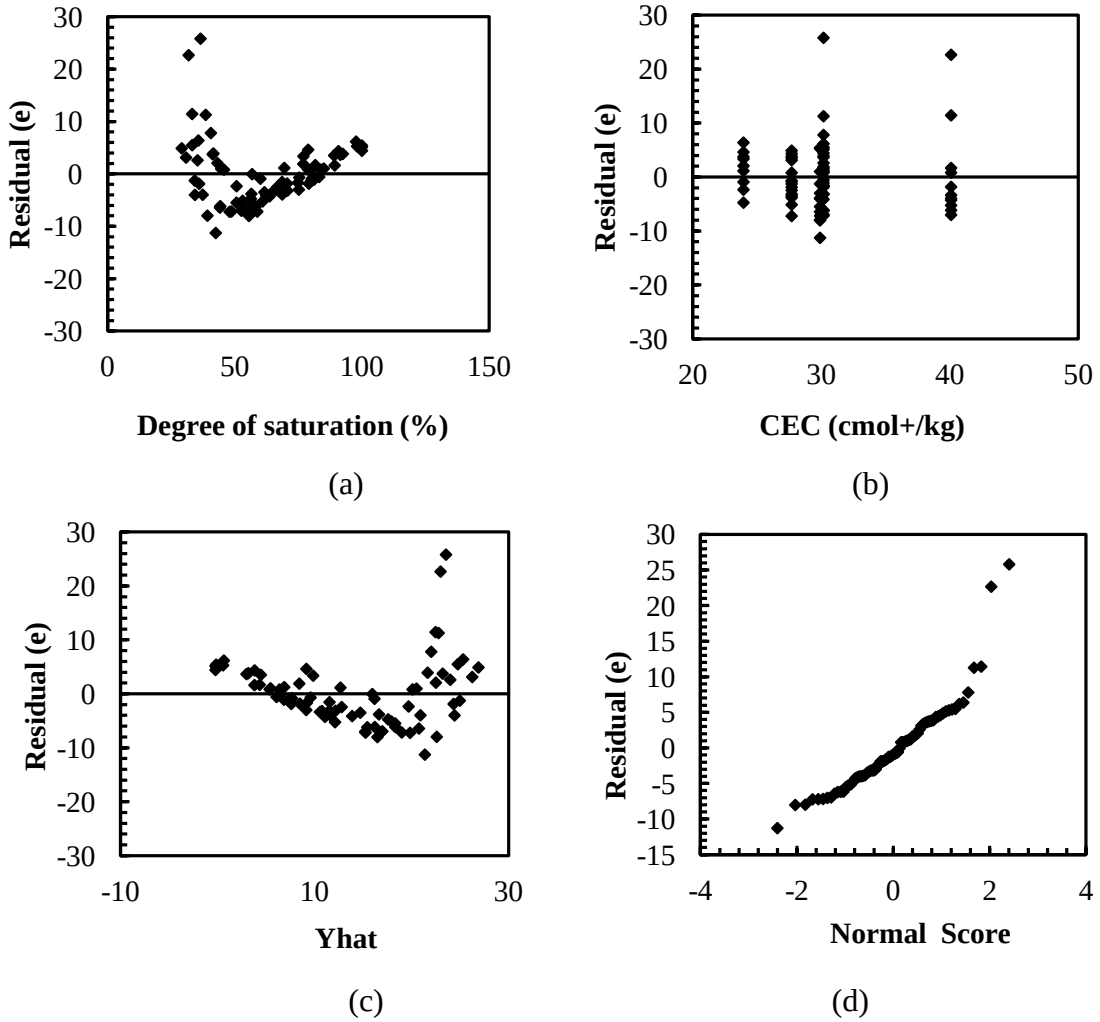

Figure 6.20 Diagnostic plots undisturbed soil model (a) residual vs. degree of saturation (b) residual vs. CEC (c) residual vs. predicted value (d) normality

6.4.2.2 Multicollinearity

The Pearson's coefficients of the data set suggested that the predictor variables were not correlated with each other. Similar results were obtained from SAS output. The VIFs among the predictor variables were close to 1.0; therefore, serious multicollinearity was not identified in the model. The VIFs and the parameter estimates are presented in Table 6.12.

Table 6.12 VIF and parameter estimate of the model

Parameter Estimates								
Variable	**Label**	**DF**	**Parameter Estimate**	**Standard Error**	**t Value**	**Pr > |t|**	**Type I SS**	**Variance Inflation**
Intercept	Intercept	1	44.26395	5.43245	8.15	<.0001	15049	0
x1	Degree of saturation	1	-0.37437	0.03513	-10.66	<.0001	4332.53	1.00264
x2	CEC	1	-0.23299	0.15892	-1.47	0.1469	82.9472	1.00264

6.4.3 Transformation

Diagnostic plots showed that the assumption of linear model form, constant error variance, and normal distribution of the error terms were not satisfied in the model. Moreover, non-constant variance and non-normality occurred together. Therefore, variance stabilization transformation was conducted using Box-Cox method. It was identified that the F statistic was high when power of transformation was -0.75. Therefore, analyses were performed after transforming the response variable ($Y'=Y^{-0.75}$). The graphical illustration of the Box-Cox method is presented in Figure 6.21.

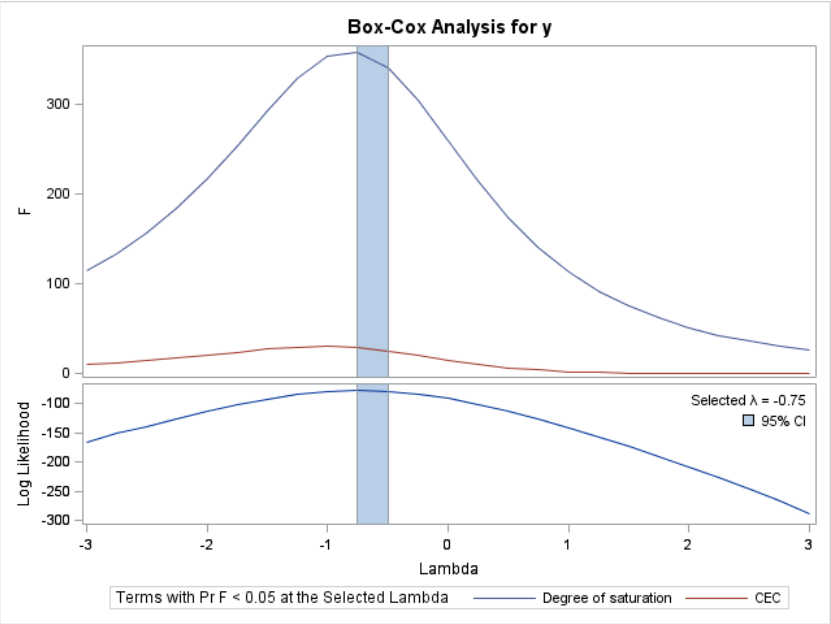

Figure 6.21 Box-Cox transformation of Y variable for undisturbed soil samples

6.4.3.1 ANOVA and Diagnostics of Transformed model

According to the SAS analysis, the SSE, SSR, and SSTO of the model decreased substantially after transformation. Furthermore, the value of F statistics increased from 57.2 to 188.7. The model explained 83.6% variation in resistivity, with responses to degree of saturation and CEC in undisturbed soil samples. The ANOVA and estimated model parameter is summarized in Table 6.13.

Table 6.13 ANOVA and estimated parameters after transformation of the model for undisturbed samples

Analysis of Variance					
Source	**DF**	**Sum of Squares**	**Mean Square**	**F Value**	**Pr > F**
Model	2	0.3039	0.15195	188.7	<.0001
Error	74	0.05959	0.00080526		
Corrected Total	76	0.36349			

Root MSE	0.02838	R-Square	0.8361
Dependent Mean	0.17512	Adj R-Sq	0.8316
Coeff Var	16.2047		

Parameter Estimates								
Variable	**Label**	**DF**	**Parameter Estimate**	**Standard Error**	**t Value**	**Pr > |t|**	**Type I SS**	**Variance Inflation**
Intercept	Intercept	1	-0.13063	0.02482	-5.26	<.0001	2.36125	0
x1	Degree of saturation	1	0.00304	0.00016	18.93	<.0001	0.28099	1.00264
x2	CEC	1	0.00387	0.000726	5.33	<.0001	0.02291	1.00264

The MLR assumptions were further checked using diagnostic plots and statistical tests. The residual plots are presented in Figure 6.22. It was determined that the curvature in the residual vs. degree of saturation plot disappeared after transformation. In addition, the funnel shape was not existed in the residual vs. predicted value plot. The error variance was also examined using Modified Levene test. The test results illustrated that the error variances were constant and equal at 0.1 level of significance. The residuals

were normally disturbed according to the diagnostic plots and statistical tests. The details of Modified Levene and normality test are presented in Appendix A.

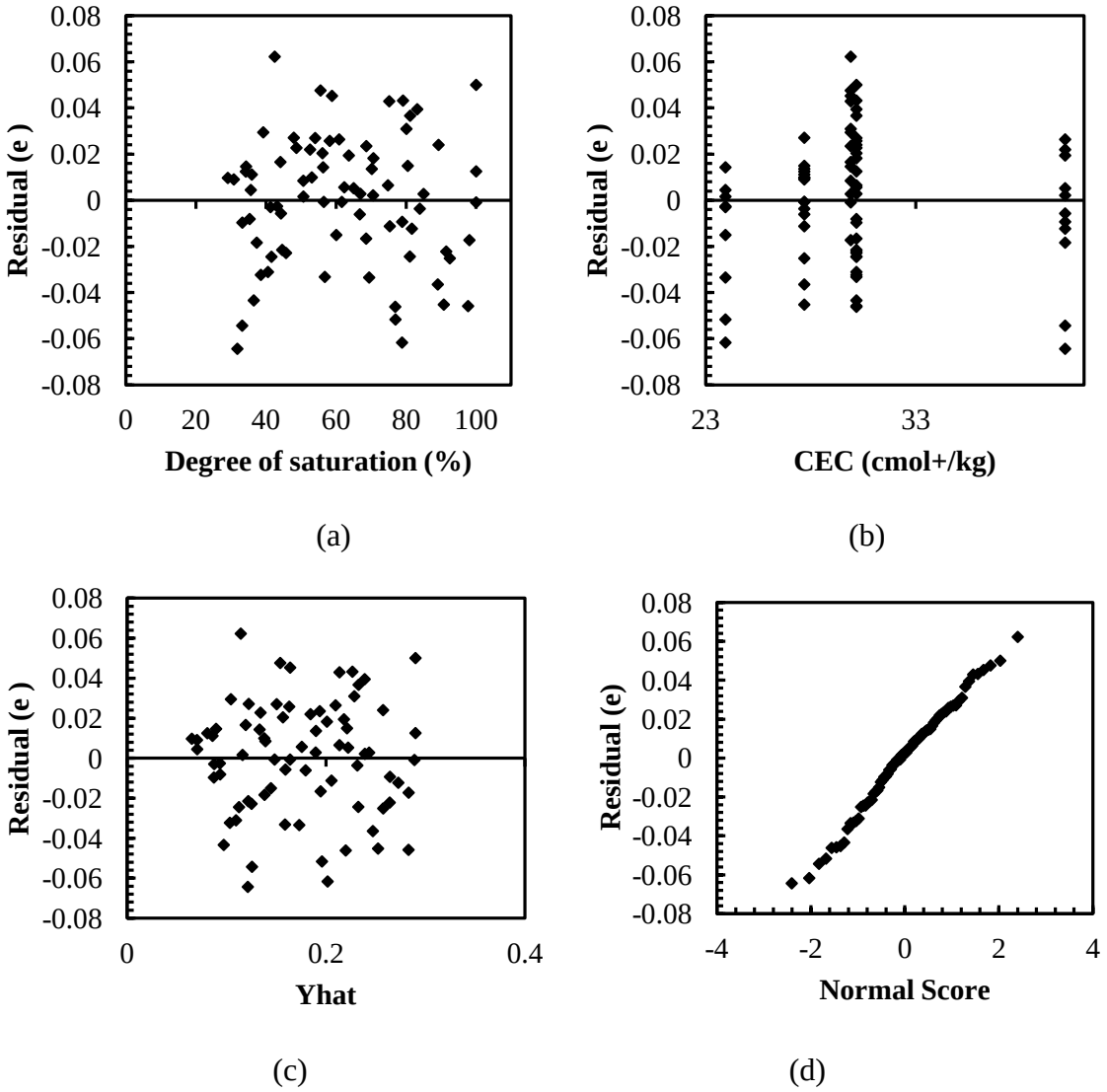

Figure 6.22 Diagnostic plots for the model of undisturbed soil samples after transformation (a) residual vs. degree of saturation (b) residual vs. CEC (c) residual vs. predicted value (d) normality

6.4.3.2 Outlier test

It was observed that the Leverage value was more than (h_{ii}>0.0779) 0.0779 in observation 14, 15, 16, 21, 22, 23 and 24. However, no observation was flagged as Y-

outlier according to Bonferronni outlier test. The influences of the observation on regression model were analyzed using DEFITS, DFBETAS and Cook's distance. The SAS results showed that the DEFITS, DFBETAS, and Cook's distance were below the threshold. Therefore, the outliers were not influential after transformation of dependent variable. The SAS results of the outlier tests is attached in Appendix A.

6.4.4 Exploration of Interactions

The requirement of interaction term was investigated using a set of residual plots i.e. residual vs. X_1X_2, residual vs. std X_1X_2, and partial regression plot of X_1X_2 as presented in Figure 6.23. The scatter plot did not show any specific trend; therefore, interaction term was not considered in the current model.

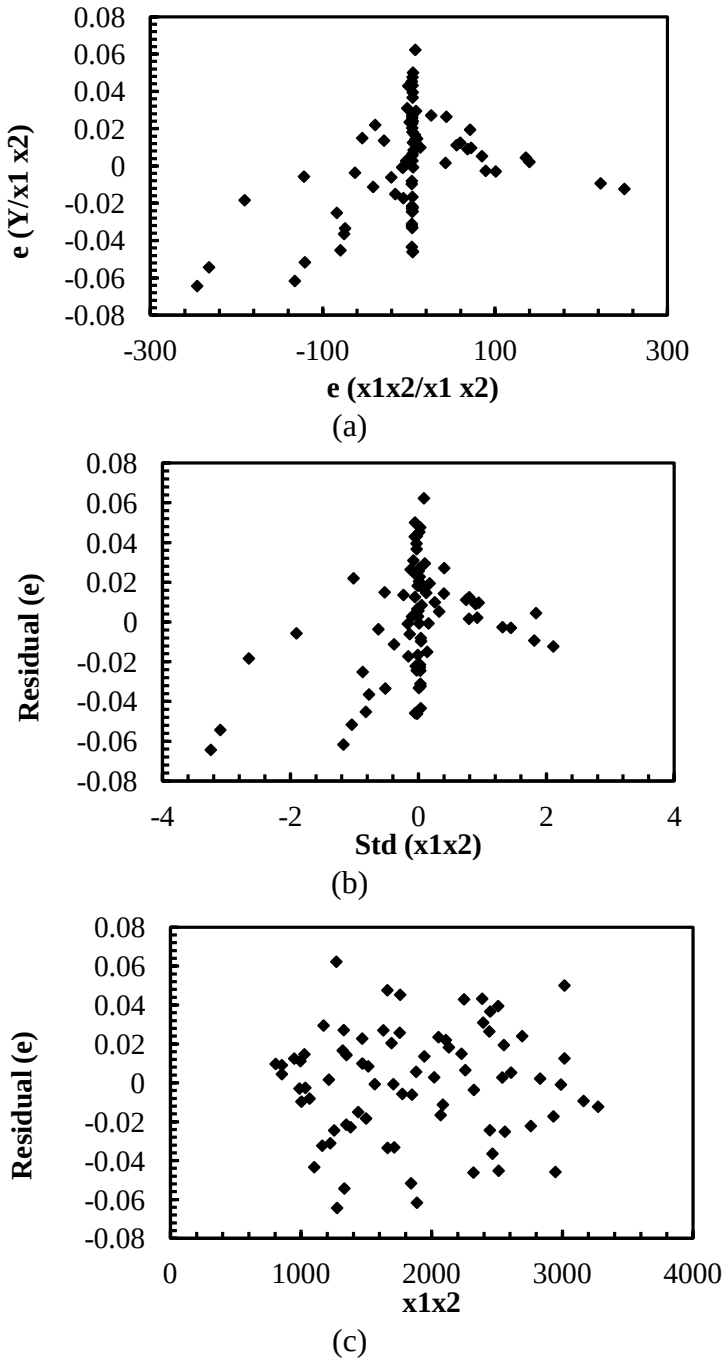

Figure 6.23 Exploration of interaction term (a) partial regression (b) residual vs. x1x2 (c) residual vs. std x1x2

6.4.5 Selection of Best Model

The potential best model and relative influence of the predictor variables were analyzed using best subset method, stepwise regression, and backward elimination methods. It was identified that the model was not highly sensitive with the variation of CEC for the current data set. Based on the SAS analysis, two potential models were determined for undisturbed soil samples: a) the model correlated resistivity with degree of saturation and CEC (two-parameter model) b) the model correlated resistivity as a function of degree of saturation (one-parameter model). The two-parameter model explained 83.6% variation in resistivity with the response of degree of saturation and CEC, whereas the coefficient of regression was 77.3% in the model correlating resistivity with degree of saturation. Therefore, one parameter model can be used for the prediction of degree of saturation from resistivity for the soils with CEC ranged from 23.94 to 40.1 cmol+/kg. The two best models are presented below:

Two-parameter model:

$$Y^{-0.75} = -0.13063 + 0.00304X_1 + 0.00387X_2 \quad (6.8)$$

Here, Y= Electrical resistivity (Ohm-m) of undisturbed soil samples corrected at 15.5 deg temperature according to ASTM G187-05, X_1=Degree of saturation (%), X_2= Cation exchange capacity (CEC) (cmol+/kg).

Range of the model: Y= [4.21, 49.4], X_1= [29.1, 100], X_3= [23.94, 40.1]

One parameter model:

$$Y^{-0.75} = -0.0106 + 0.00299X_1 \quad (6.9)$$

Here, Y= Electrical resistivity (Ohm-m) of undisturbed soil samples corrected at 15.5 deg temperature according to ASTM G187-05, X_1=Degree of saturation.

Range of the model: Y= [4.21, 49.4], X_1= [29.1, 100]

The ANOVA of the one parameter model is given in Table 6.14.

Table 6.14 ANOVA for one-parameter model of undisturbed soil samples

Analysis of Variance					
Source	**DF**	**Sum of Squares**	**Mean Square**	**F Value**	**Pr > F**
Model	1	0.28099	0.28099	255.46	<.0001
Error	75	0.08249	0.0011		
Corrected Total	76	0.36349			

Variable	**Parameter Estimate**	**Standard Error**	**Type II SS**	**F Value**	**Pr > F**
Intercept	-0.0106	0.01222	0.0008274	0.75	0.3885
x1	0.00299	0.0001873	0.28099	255.46	<.0001

Model selection analyses results are attached in Appendix A.

6.4.6 Interaction Surface

The coupled effect of degree of saturation and CEC on electrical resistivity of undisturbed soil specimen is presented in Figure 6.24. According to the interaction surface, the effect of degree of saturation was high compared to CEC. At degree of saturation 100%, the variation of resistivity in response to CEC was not substantial. In addition the surface was fairly parallel with the horizontal plane over 80% degree of saturation.

It can be mentioned that resistivity was highly sensitive to both CEC and degree of saturation in compacted clay samples; however, resistivity was mostly influenced by degree of saturation in undisturbed soil samples. A specific comparison between the models cannot be made because of the following reasons:

- Test methodologies for electrical resistivity measurements were different in cases of undisturbed and compacted soil samples.
- The compacted soil specimens consisted of Ca-bentonite and kaolinite as two specific clay soil conditions. In contrast, high and low plasticity clay samples were utilized in the model development for undisturbed soil specimens. The statistical analysis indicated that resistivity was not highly sensitive to CEC in the 23.94 to 40.1 cmol+/kg range.

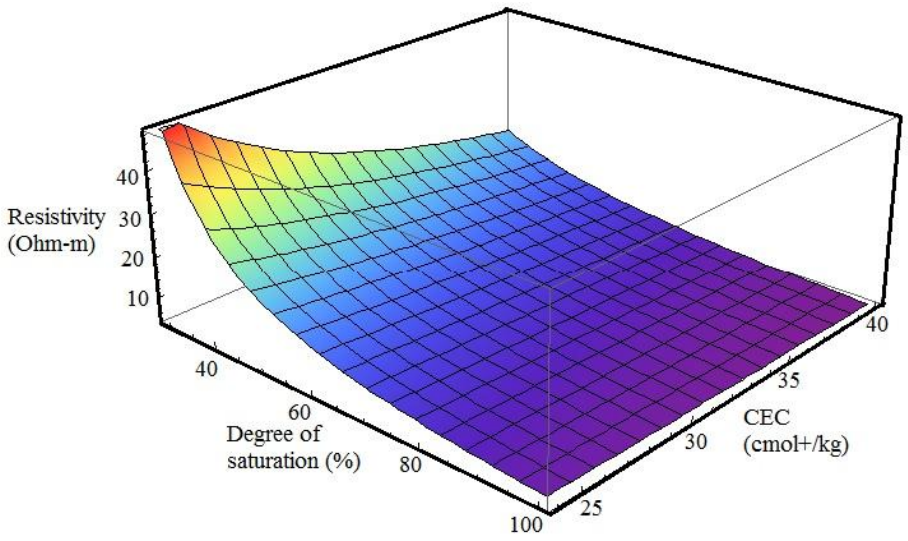

Figure 6.24 Coupled effect of degree of saturation and CEC on electrical resistivity of undisturbed samples

6.4.7 Comparison of Model Prediction with Different Experimental Results

The experimental results of soil sample B1-20 was utilized to evaluate the predictive capacity of the resistivity model for undisturbed soil specimens. Similar to the previous undisturbed soil samples, resistivity tests were determined at subsequent drying stages and corrected at 15.5 deg. C temperature. The CEC of the B1-20 sample was 40.9 cmol+/kg, and degrees of saturation were varied from 51 to 94% during resistivity tests. Both two and one parameter model was used for the estimation of resistivity using degree of saturation and CEC as presented in Figure 6.25. The maximum errors in estimation were 1.7 and 4.4 Ohm-m in two and one parameter model, respectively. However, error in prediction was less than 1 Ohm-m in one parameter model at degree of saturation over 73%.Therefore, one parameter model can be utilized for the prediction of degree of saturation from resistivity measurement when CEC of the specimen was in the range of 23.94 to 40.1 cmol+/kg, and anticipated degree of saturation is over 73%.

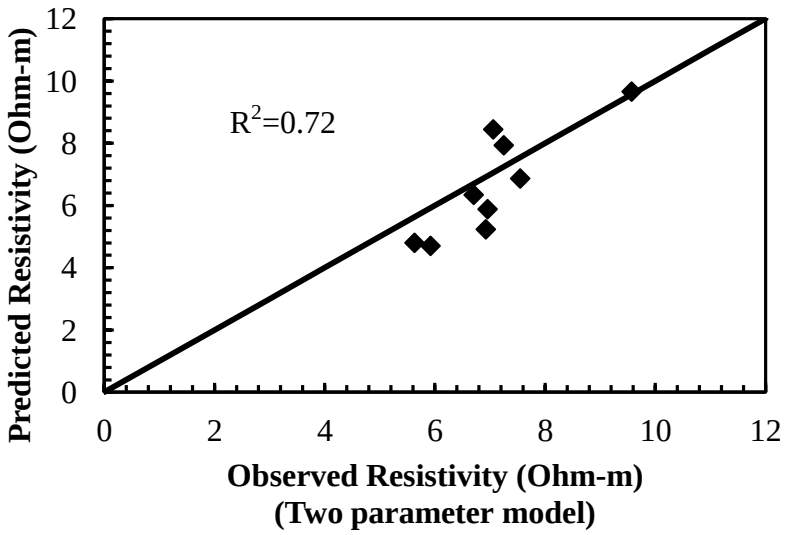

(a)

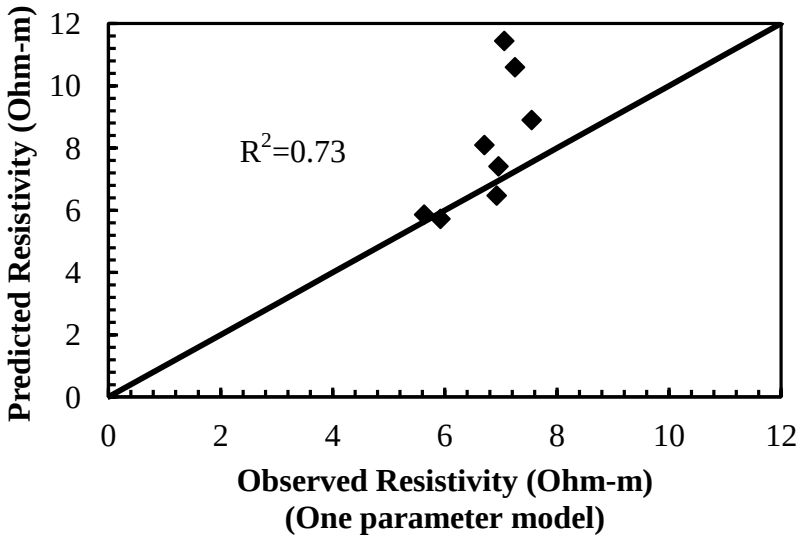

(b)

Figure 6.25 Comparison of estimated resistivity with experimental observations (a) Two-parameter model (b) One-parameter model

6.5 Summary

The objective of statistical analyses was to develop practically applicable models, which can correlate resistivity with influential geotechnical properties of clayey soils. Both compacted and undisturbed soil samples were considered for the model development. Based on the investigation, degree of saturation and CEC were selected as predictor variables in the model. Multiple linear regression (MLR) was performed using statistical analysis software SAS. The summary of the statistical analyses can be presented herein:

1. A total of 748 electrical resistivity tests were conducted for compacted clays at varied temperatures, moisture contents, and dry unit weights on four types of soils. The electrical resistivity results were corrected at 15.5 deg C temperature, and in each case (i.e. for a fixed soil type, moisture content and dry unit weight) the results were randomized to take mean of any eleven numbers. The obtained mean resistivity values were utilized in the statistical modeling.
2. The MLR assumptions were not satisfied in the preliminary model. Thus, Box-Cox analysis was conducted to determine the power of transformation of dependent variable. Moreover, CEC (X_2) was transformed to increase the scatter in the residual plots. The interaction term was not required in the model. The finalized model form for compacted clays can be mentioned as:

$$Y^{-0.25} = 0.43398 + 0.00309X_1 - 14.35204{X_2}^{-1.5}$$

here, Y= Electrical resistivity (Ohm-m) corrected at 15.5 deg temperature according to ASTM G187-05, X_1=Degree of saturation (%), X_2= Cation

exchange capacity (CEC) (cmol+/kg). Range of the model: Y= [2.6, 504.3 Ohm-m], X_1= [21.8, 100%], X_3= [13.28, 79.03 cmol+/kg]. The model explained 90.1% of the variation in resistivity (Ohm-m) in response to degree of saturation and CEC of compacted clays

3. The predictive capability of the model was compared using artificial soil specimens. The estimated resistivity was within $\pm 5\ \mathrm{Ohm-m}$ for soils with CEC and degree of saturation higher than 30 cmol+/kg and 30%, respectively.
4. A separate model was developed for undisturbed soil specimens. MLR analysis was conducted, and model assumptions were diagnosed. The initial model was not able to satisfy the adequacy of linear model form, constant error variance, and normality assumptions. Therefore, Box-Cox method was employed to determine the power of transformation.
5. The potentially good models were selected using backward elimination, stepwise regression, and best subset method. Two potential models were determined for undisturbed soil samples: a) the model correlated resistivity with degree of saturation and CEC (two-parameter model) b) the model correlated resistivity as a function of degree of saturation (one-parameter model). The two-parameter model explained 83.6% variation in resistivity with the response of degree of saturation and CEC, whereas the coefficient of regression was 77.3% in the model correlating resistivity with degree of saturation.

   The two best models are presented below:

Two-parameter model:

$$Y^{-0.75} = -0.13063 + 0.00304X_1 + 0.00387X_2$$

One parameter model:

$$Y^{-0.75} = -0.0106 + 0.00299X_1$$

Here, Y= Electrical resistivity (Ohm-m) of undisturbed soil samples corrected at 15.5 deg temperature according to ASTM G187-05, X_1=Degree of saturation (%), X_2= Cation exchange capacity (CEC) (cmol+/kg). Range of the model: Y= [4.21, 49.4 Ohm-m], X_1= [29.1, 100%], X_3= [23.94, 40.1 cmol+/kg]

6. The experimental results of soil sample B1-20 were utilized to evaluate the predictive capacity of the resistivity model for undisturbed soil specimens. The maximum errors in estimation were 1.7 and 4.4 Ohm-m in two- and one-parameter model, respectively. However, error in prediction was less than 1 Ohm-m in one parameter model at degree of saturation over 73%.
7. A specific comparison between the models of compacted and undisturbed specimens cannot be made because of the following reasons:
    - Test methodologies for electrical resistivity measurements were different in undisturbed and compacted soil samples.
    - Pure minerals (i.e Ca-bentonite and kaolinite) were not used in the electrical resistivity tests of undisturbed soil samples.

CHAPTER 7

FIELD ASSESMENT OF STATISTICAL MODEL

7.1 Introduction

During the site investigation using Resistivity Imaging (RI), a current is injected through the point electrodes and resulting voltage differences are measured. Apparent Resistivity of subsoil is determined employing a geometric factor into the determined potential difference and provided current. The observed resistivity at different locations of subsurface can be further analyzed using finite element algorithm and inversion modeling to get a continuous resistivity profile. Resistivity image can provide useful information about the change in moisture condition, heterogeneity, and presence of voids.

In the current study, the electrical resistivity models were utilized for the prediction of degree of saturation in the field condition using RI results. RI tests were conducted on compacted clay liner of a landfill and two slopes. Then the predictive capability of the model was evaluated using field resistivity results.

7.2 Resistivity Imaging at City of Denton Landfill

The performance of MLR model developed using remolded specimens was evaluated using RI tests on compacted clay liner. A total of three RI tests were performed parallel to each other, and combined to develop a quasi 3D profile. Thereafter, a horizontal resistivity contour was determined at clay liner depth using the 3D resistivity profile. Based on the observed resistivity and CEC of in-situ soils at different locations of the clay liner, degrees of saturation were calculated from the model. Moreover, the model predicted results were compared with the measured in-place degrees of saturation. A flow

diagram for the comparison of model predicted degree of saturation with in-situ tests is presented in Figure 7.1.

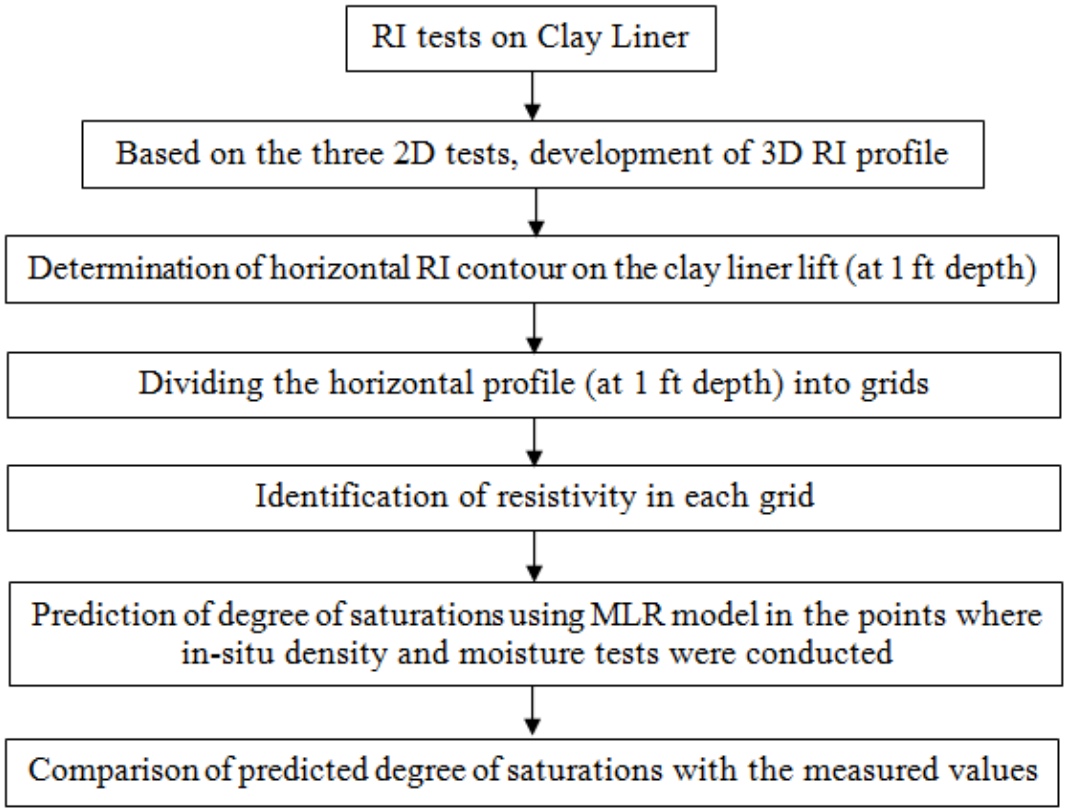

Figure 7.1 Flow chart for field assessment of model developed using compacted clays

7.2.1 Description of the Study Area

The City of Denton municipal solid waste (MSW) Landfill is located 40 miles northwest of Dallas area. The conventional operation of the landfill began in 1984; however, the facility started functioning as an enhanced leachate recirculated (ELR) system in May 2009. The City of Denton Landfill was subjected to expansion during 1984-present (Manzur, 2013).

The geology of Denton county is characterized by Woodbine, Eagle Ford, Pawpaw, Weno limestone, undivided Denton clay, Fort Worth limestone, and undivided Duck creek formation. Woodbine, Fort Worth limestone, and Duck creek formation consisted of 45% of the area (USGS, 2012).

The footprint of the landfill is divided into different cells as presented in Figure 7.2. During the study (September, 2013), cell 4A was under construction.

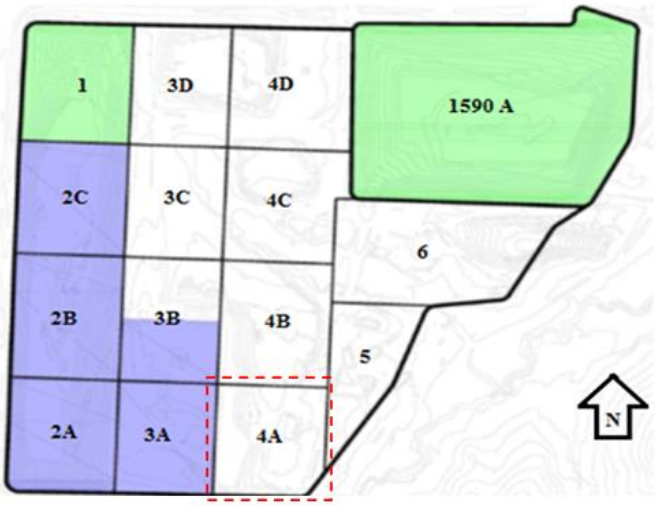

Figure 7.2 Different cells of city of Denton MSW landfill

It should be mentioned that the construction of clay liner was not completed during RI tests on September 16, 2013. At the foundation soil, 45 cm clay liners were constructed in three lifts. In addition to that 20 cm loosely compacted clayey soils were placed on top of the clay liner. The top soil layer provided working platform for the conduction of RI tests. Moreover, this soil layer ensures further resistance to avoid potential leakage in the liner system. Additional layers were proposed to be placed on top of the loosely compacted soils. The cross section of the liner during RI tests is presented in Figure 7.3.

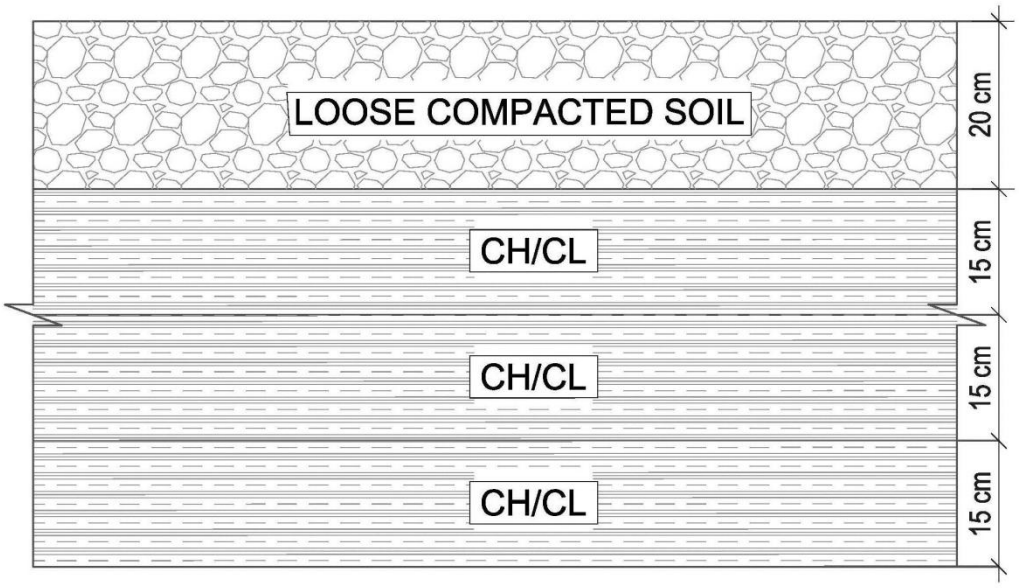

Figure 7.3 Cross section of the clay liner during RI tests (September 16, 2013)

Resistivity Imaging (RI) tests were conducted using Super Sting R8/IP multichannel system manufactured by Advanced Geosciences Inc. (AGI), Austin, TX. The equipment measures apparent resistivity up to 8 points for a single current injection. Four passive cables, each containing 14 takeouts, were attached with the resistivity meter. The power supply of the equipment was provided from a 12V battery. A switch box was utilized to develop a close form circuit with the electrodes, cable, and Super Sting R8/IP equipment.

The spacing between electrodes can be as much as 6 m; however, an increase in spacing may result poor resolution in the image. The investigation depth is 20% of length of the profile approximately. Although the RI tests can be performed utilizing 56 electrodes, the equipment allows using 28 electrodes when site access is limited, and

required area of investigation is less. The RI equipment and switch box are illustrated in Figure 7.4.

Figure 7.4 Super Sting R8/IP multichannel system and switch box

7.2.2 RI tests in the Compacted Clay Liner

2D Resistivity imaging (RI) tests were conducted on the cell 4A after the completion of three lifts, and placement of 20 cm loosely compacted soils. A total of 28 electrodes with a spacing of 1.52 m were used in the RI tests. Therefore, the length of each profile was 41.2 m as presented in Figure 7.5. The distances of profile CL1 from the end of the Cell 3 and the access road were 45.6 and 30.5 m, respectively. The RI profile CL2 and CL3 were located 22.9 and 53.4 m apart from line CL1. According to the literature, dipole-dipole has the advantages of low electromagnetic coupling and high sensitivity in response to the variation in horizontal direction (Loke, 2001). Therefore, dipole-dipole array was utilized to conduct RI tests.

(a) (b)

Figure 7.5 Location of RI tests (a) cell 4A (the photograph was taken from the top of Cell 3) (b) schematic of RI profiles

The electrode penetration depth was less than 20 cm during RI tests. Once the RI tests were completed, the insertion points of electrodes were sealed with the bentonite. The operational setup of the RI tests in the clay liners are presented in Figure 7.6.

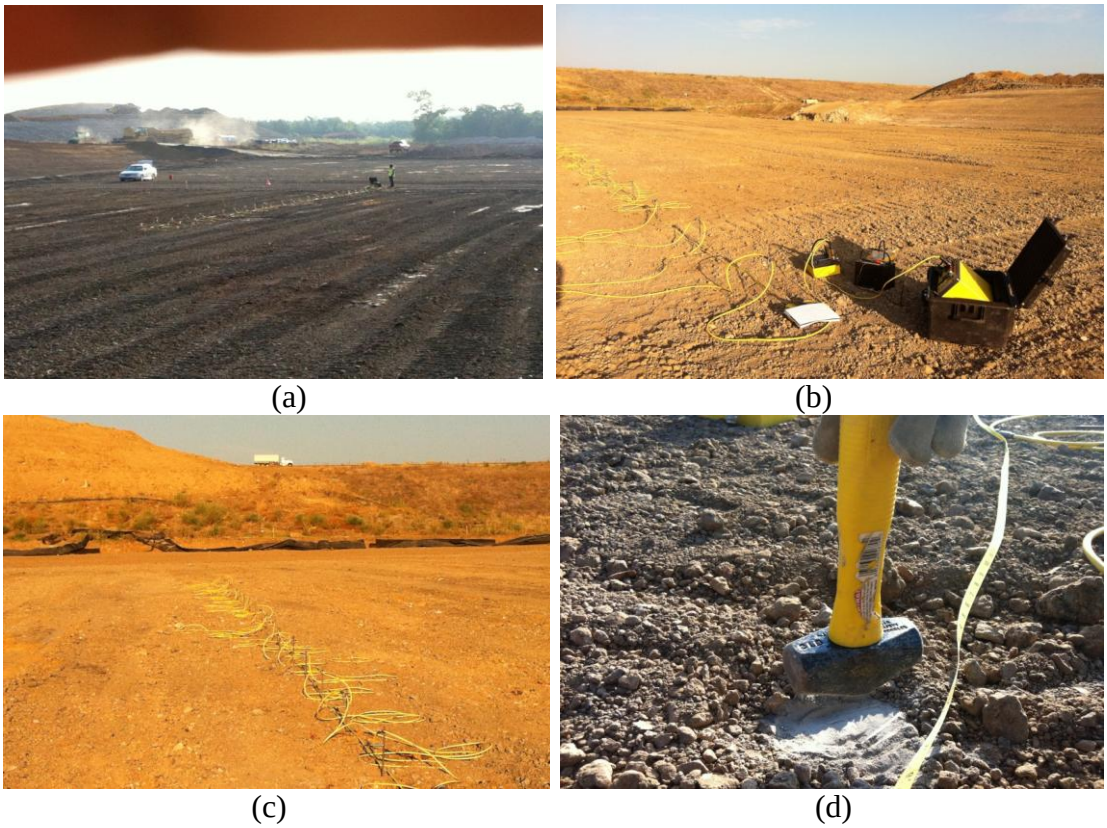

Figure 7.6 Operational setup of RI test in compacted clay liner (a) location of tests (b) RI equipment and switch box (c) layout of electrodes and cables (d) sealing of insertion points

7.2.3 2D Resistivity Imaging Results

In the current study, EarthImager 2D software was utilized for the data analysis and resistivity image construction. At the initial condition, a smooth inversion method was adopted for the analysis of measured apparent resistivity. The finite element method, with Cholesky decomposition equation solver, was employed for forward modeling. In addition, Dirichlet boundary condition was used in the forward model. The RMS error of 3% was considered for the stopping criteria of the iteration.

The RI images along CL1, CL2, and CL3 are shown in Figure 7.7. At surface, the resistivity was as much as 15 Ohm-m. However, resistivity decreased substantially in

between depths of 0.5 to 1.2 m, and the resistivity was below 6.5 Ohm-m up to a depth of 2.5 m. The observed resistivity was over 10 Ohm-m below 2.5 m from the surface.

The observed variation in resistivity can be explained by the existing subsurface conditions. At the surface, resistivity was high because of the presence of loosely compacted soil. The resistivity decreased between depths of 0.5 and 1.2 m because of the presence of compacted clay lifts. According to Qian et al. (2002), clay liners should be constructed at minimum 95% of the maximum dry unit weight at Standard Proctor, and 0-4% wet of optimum moisture content. Therefore, the observed resistivity was low because of the high degree of saturation in this zone. Another important observation was the effect of compaction below clay liners. The voids in the subgrade soil might decrease due to the construction of lifts, which caused a reduction in resistivity. Therefore, the influence of compaction beneath the clay liner was also identified using RI test. According to the investigation, the effect of compaction extended up to 2.5 m.

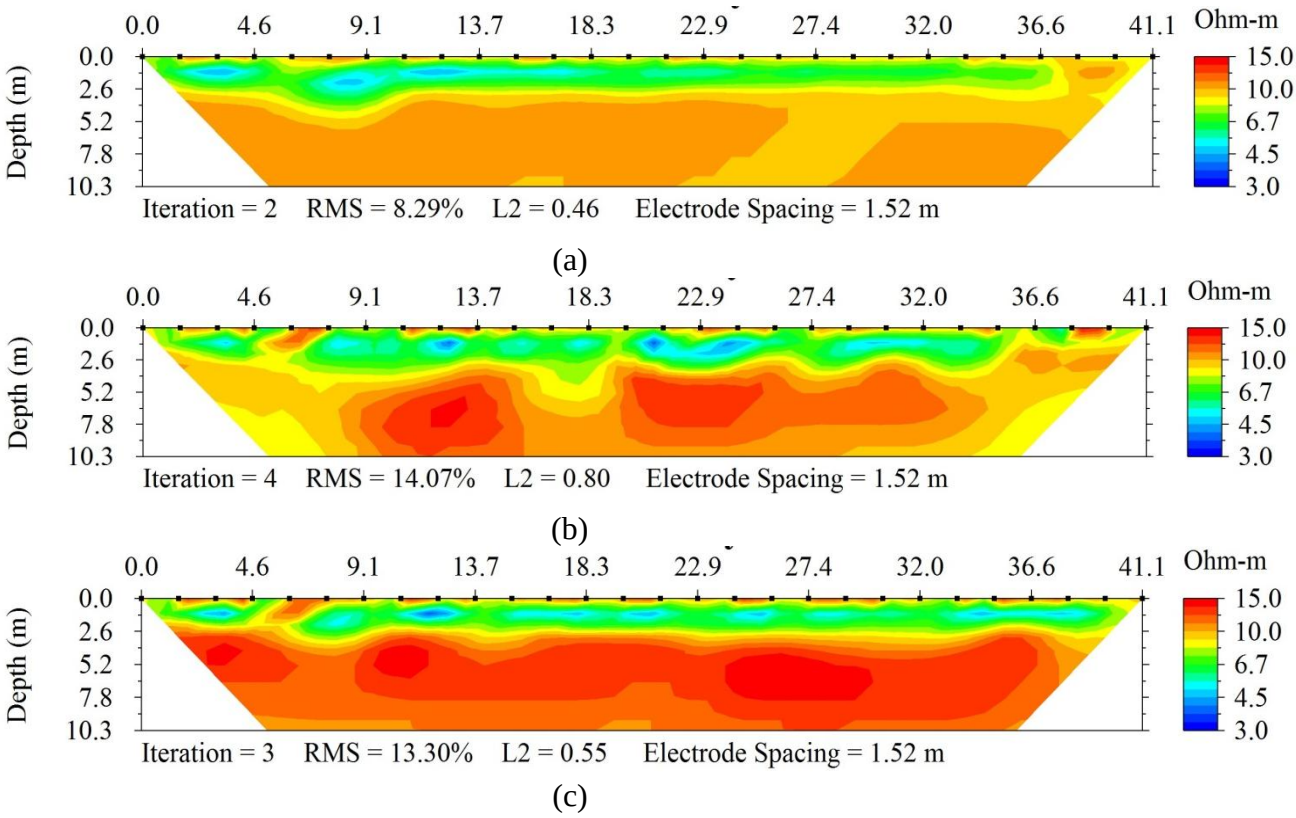

Figure 7.7 2D resistivity image on compacted clay liner along (a) CL1 (b) CL2 (c) CL3 (tests conducted on September 16, 2013)

7.2.4 Determination of Quasi 3D and Horizontal RI Profile at Clay liner

A quasi 3D RI section was developed using the parallel 2D profiles. In a quasi 3D section, the measured 2D resistivity values were merged into a 3D data format. Then the new 3D data file was analyzed using EarthImager 3D software to obtain a quasi 3D image. During the analyses, the forward and inversion modeling parameters were similar to the 2D data analyses; however, the stabilizing and damping factors were set to high values (equal to 1000) to minimize model roughness. The observed 3D resistivity profile is presented in Figure 7.8.

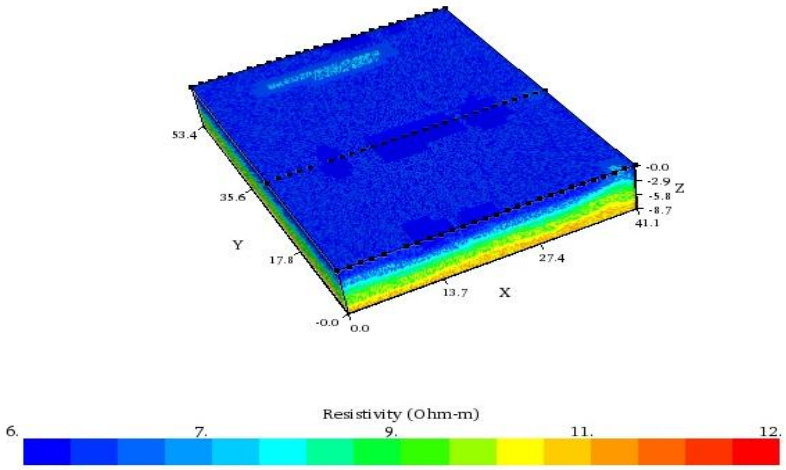

Figure 7.8 Quasi-3D resistivity profile of the investigated area

The 3D resistivity profile was utilized to determine horizontal resistivity contour at the depth of clay liner. The horizontal slice was developed using static slice option of EarthImager 2D software. The horizontal resistivity profile at 0.31 m depth below the surface is presented in Figure 7.9. It was observed that the resistivity was in between 5 to 8.5 Ohm-m in this depth.

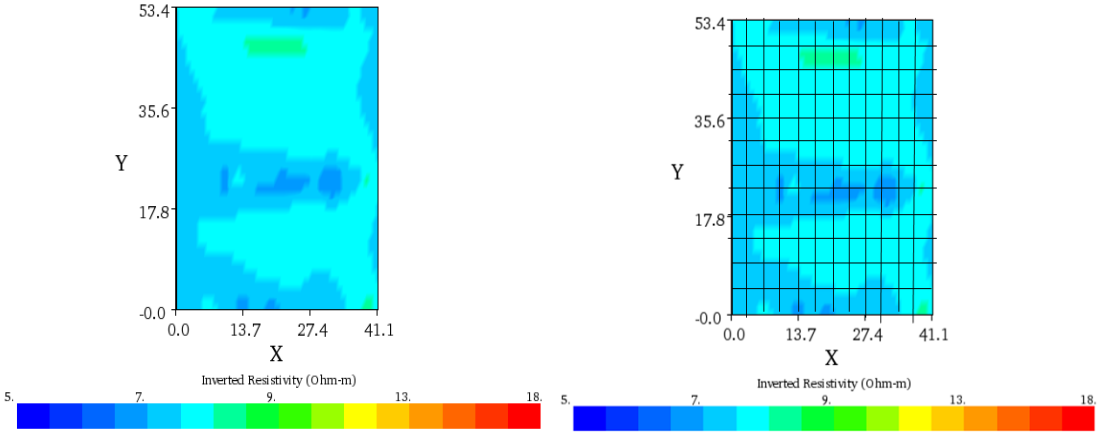

Figure 7.9 Horizontal resistivity profile at depth of clay liner (a) at 0.31 m /1 ft from surface (b) dividing the profile into grids

To quantify electrical resistivity at different locations, the horizontal profile was divided into several grids as presented in Figure 7.9 (b). At each grid point, resistivity was measured from the profile.

7.2.5 Comparison of Model Predicted Degree of Saturation

As a part of the construction quality control, in-situ tests were performed on the compacted clay liners. The co-ordinates of test locations were plotted in the Google map of the cell 4A using Geographic Information System (GIS) as illustrated in Figure 7.10. Figure 7.10 indicated that the in-situ tests were carried out in several locations of the cell. However, the test results under the boundary of 3D RI profile was utilized for the comparison.

Figure 7.10 Location of in-situ tests for compaction quality control (@Google Maps, 2013)

The co-ordinates of the horizontal profile, and in-situ tests were matched to identify the resistivity at the locations of in-place density tests. The Atterberg limits and Standard Proctor compaction tests were also carried out on the collected soil samples

from the test locations. A summary of the soil properties utilized in the comparison are presented in Table 7.1.

Table 7.1 Soil properties at location of in-situ tests (data provided by City of Denton landfill authority, September 16, 2013)

Test	Coordinates		In-situ test		LL	PI	Soil Type	CEC (cmol+/kg)	Relative density
	N	W	Moisture content (%)	Dry Unit wt (kN/m^3)					
33	33.1864	-97.081	15.7	17.8	34	22	CL	23.12	97.10%
125	33.1862	-97.081	17.5	17.4	49	33	CL	26.16	99.90%
135	33.1861	-97.081	18.1	16.8	52	36	CH	26.77	99.90%
42	33.1862	-97.081	18.3	16.9	37	23	CL	23.73	99.30%
36	33.1863	-97.081	15.5	18.3	34	22	CL	23.12	99.70%
66	33.1862	-97.08	17.2	17.7	34	22	CL	23.12	96.50%
127	33.1861	-97.08	19.7	17	49	33	CL	26.16	97.90%
41	33.1861	-97.08	19.4	16	52	36	CH	26.77	95.10%

It can be mentioned that the MLR model correlates resistivity with degree of saturation and CEC of compacted clays. Although CEC of the samples were not determined in the current data set, liquid limits were utilized to calculate CEC (cmol+/kg) of the samples using the correlation of Yukselen and Kaya (2006):

$$CEC = 0.2027LL + 16.231 \quad (7.1)$$

As the horizontal resistivity profile was located at 0.31 m beneath the surface, the temperature at 0.31 m depth was assumed to be similar as ambient temperature (16.2 deg C). Therefore, quantified resistivity values were corrected with respect to 16.2 deg. C. according to ASTM G187-05 method. The calculated CEC and corrected resistivity values were used to predict degrees of saturation according to the following equation:

$$Y^{-0.25} = 0.43398 + 0.00309X_1 - 14.35204\mathrm{X}_2{}^{-1.5} \quad (7.2)$$

here, Y= Electrical resistivity (Ohm-m) corrected at 15.5 deg temperature according to ASTM G187-05, X_1=Degree of saturation (%), X_2= Cation exchange capacity (CEC)

The predicted degrees of saturation were compared with the measured values at the site condition. The in-place density and moisture content were incorporated with specific gravity (2.65 for all cases) to obtain degrees of saturation at test locations. Thereafter, model predicted results were compared with the measured degrees of saturation in the field. The summary of the comparison is presented in Table 7.2, and is illustrated in Figure 7.11.

Table 7.2 Summary of comparison

In-situ Test ID	**Observed Degree of Saturation (%)**	**Predicted Degree of Saturation (%)**	**Variation (%)**
33	90.8	88.7	2.1
125	93.2	90.5	2.7
135	88	78.4	9.6
42	89.4	82.2	7.2
36	98.3	97.5	0.8
66	97.9	97.5	0.4
127	98.9	90.5	8.4
41	82.6	87.4	-4.8

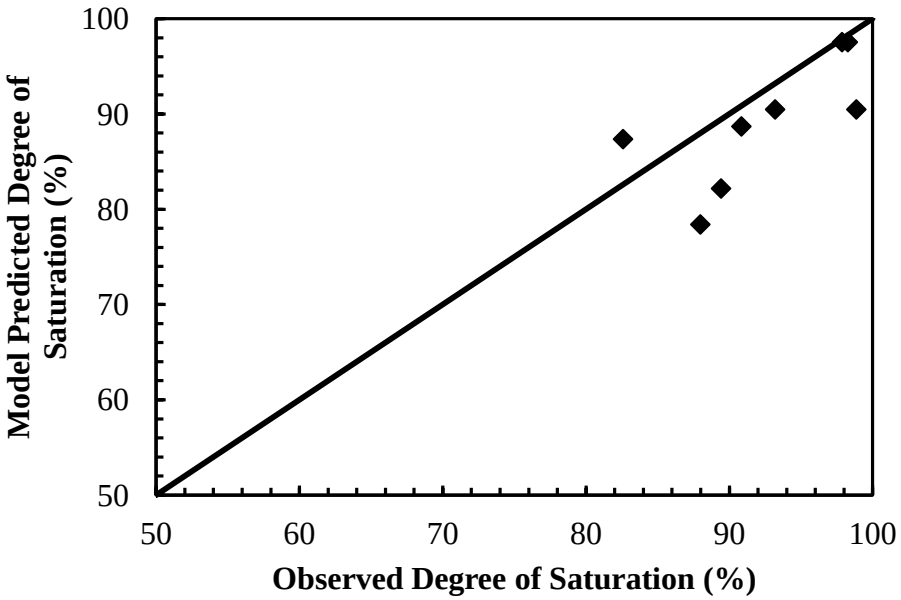

Figure 7.11 Comparison of model predicted results with field degrees of saturation

Table 7.2 indicated that the prediction error ranged from 0.4 to 9.7%; therefore, the performance of the model was quite satisfactory for the current data set. A degree of saturation contour was plotted using Surfer assuming an average CEC of 24.8 cmol+/kg. During the development of degree of saturation profile, resistivity at each grid point (Figure 7.9 b) was corrected at 15.5 deg C temperature, and used as an input parameter in the model (equation 7.2). The developed saturation profile is presented in Figure 7.12.

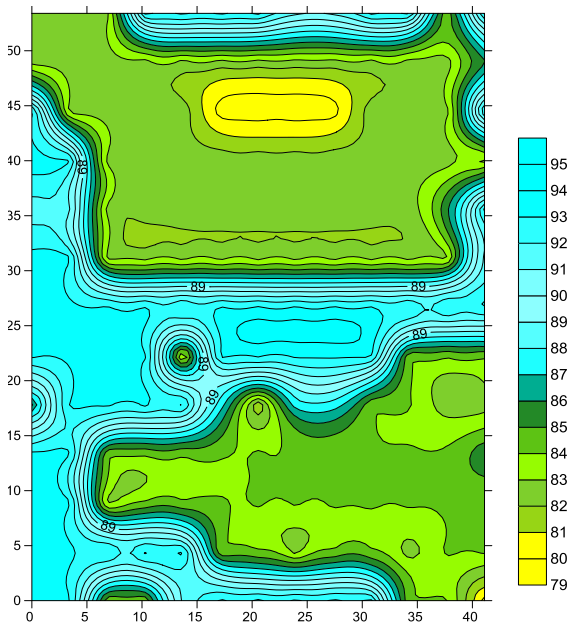

Figure 7.12 Degree of saturation profile for the measured horizontal resistivity at 0.31 m depth

7.3 Resistivity Imaging at Slopes

The performance of MLR models correlating resistivity of undisturbed soil samples with degree of saturation and CEC was evaluated using RI tests at slopes along highway Loop 12 and US 287 south. The RI test was performed on the day before soil test boring in slopes along highway Loop 12. The observed electrical resistivity results along boreholes were utilized to predict the degree of saturation using MLR models. Moreover, moisture sensors were installed for the determination of active zone in highway slope US 287 (Hossain, 2012) to accomplish Texas Department of Transportation (TxDOT) project requirements. The RI tests were conducted along the moisture sensors, and observed data were used for the comparison of predicted degrees of saturation with field results. The research program can be presented using a flowchart (Figure 7.13).

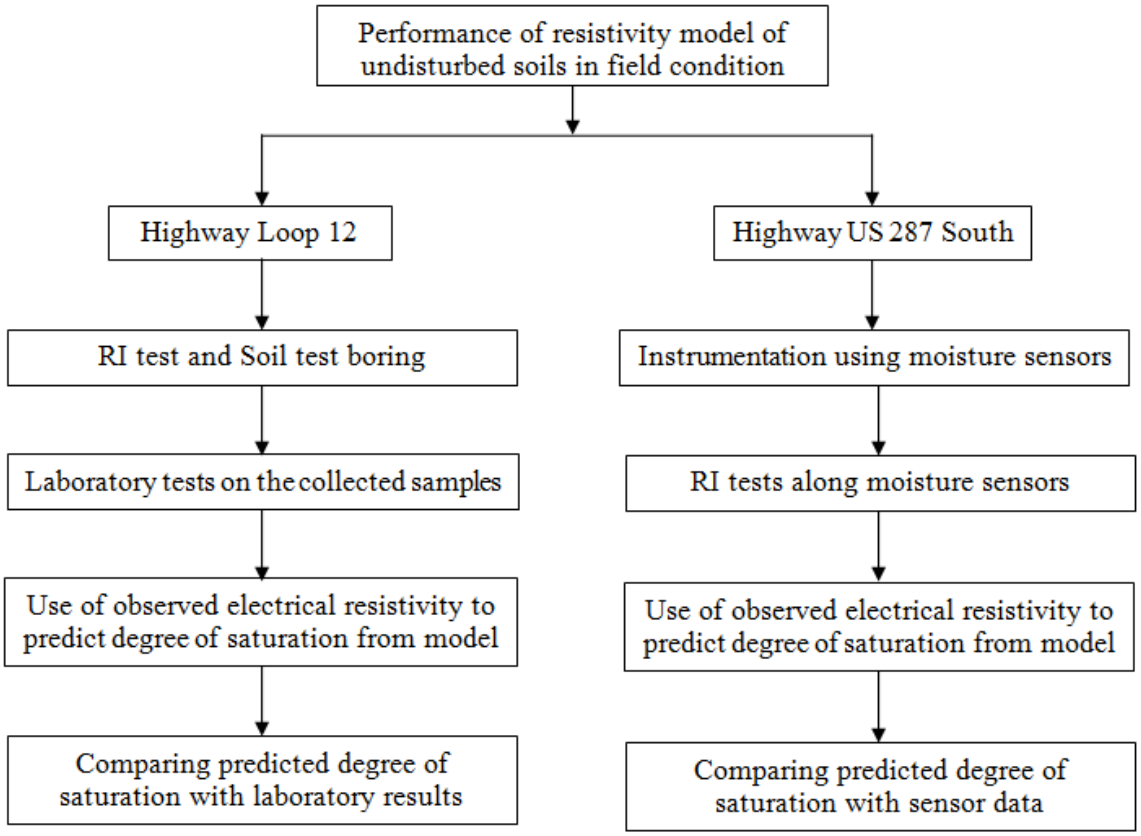

Figure 7.13 Flow chart for the comparison of MLR model predicted degrees of saturation with field results

7.3.1 RI at Loop 12

Resistivity imaging (RI) was conducted on a slope along highway Loop 12 near Union Pacific Rail Road (UPRR), Dallas, TX. As a part of slope stability analysis, two soil test borings were conducted on site. A detail of soil test results can be found in Chapter 3.

The RI tests were carried out on the day before soil test boring. 2D multi-electrode arrays were utilized for RI tests using Super Sting R8/IP equipment. The spacing of the electrodes was selected based on the required resolutions, size of objects

under investigations, and depth of penetration required for the site investigations (Hossain et al. 2011). RI was performed at the crest of the slope along highway Loop 12 using dipole-dipole array. A total of 56 electrodes were placed at a spacing of 1.52 m; therefore, 84 m long profile was considered in the investigation. EarthImager 2D software was utilized for the modeling, and image construction. Based on an initial smooth inversion model, forward and inversion modeling were conducted on the measured apparent resistivity. The finite element model adopted for forward modeling consisted of Cholesky decomposition equation solver and Dirichlet boundary condition. The RMS error of 3% was considered for the stopping criteria of the iteration. RI at the crest of the slope is presented in Figure 7.14.

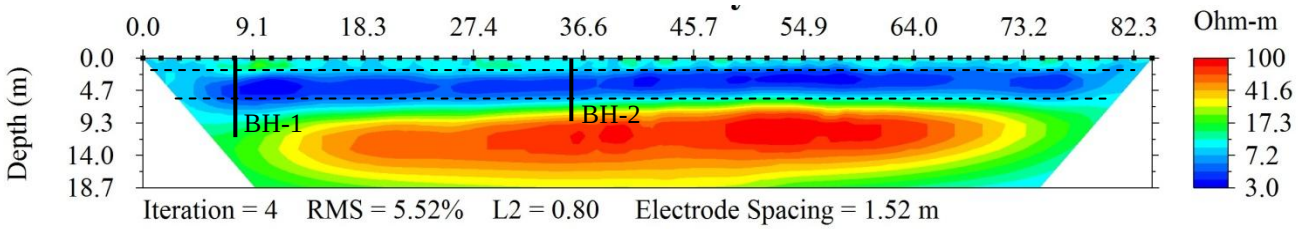

Figure 7.14 RI at the crest of the slope along highway Loop 12

It was observed that there was a low resistivity zone at depths between 2.15 to 7 m as indicated by the parallel dotted lines in Figure 7.14. The resistivity in this zone was less than 10 Ohm-m (approximately). However, substantial increase in resistivity was identified at a depth below 8.5 m from the ground surface. The obtained resistivity was more than 30 Ohm-m below at this depth.

The resistivity values of subsoil along borehole locations were measured from RI profiles using EarthImager 2D software. The objective of 1D resistivity quantification

was to evaluate the predictive capability of the proposed model with soil test results. The extracted resistivity along borehole locations are presented in Figure 7.15.

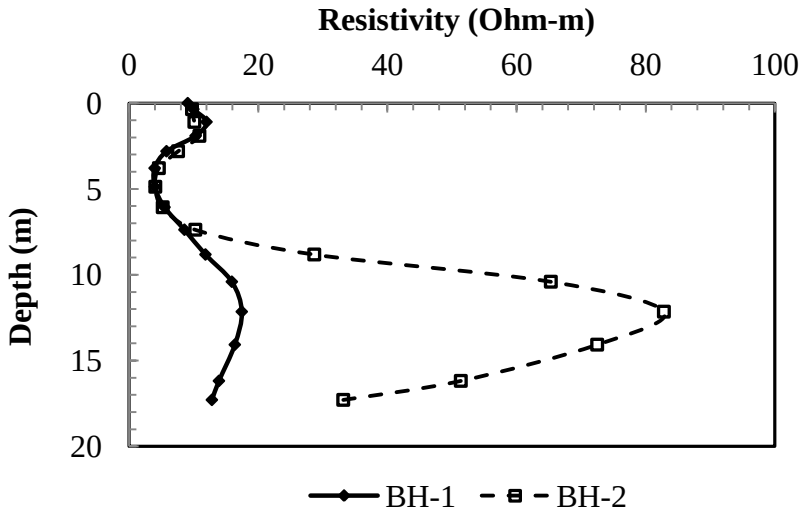

Figure 7.15 Resistivity along boreholes in Loop 12 site

The observed resistivity should be corrected at 15.5 deg. C according to ASTM G187-05 to predict degrees of saturation from the developed MLR model. Therefore, it is important to determine the variation of temperature with depths.

7.3.1.1 Investigation of Temperature Variation with Depths

To predict degrees of saturation from field resistivity measurements, it is important to identify the variation in subsurface temperature with depths. The effect of temperature on resistivity was indicated by the study of Kibria et al. (2014) and Abu-Hassanein et al. (1996). According to Campbell (1948), electrical resistivity decreased as much as 2.02% per degree Celsius increase in temperature. Therefore, the resistivity measurements should be presented with respect to a specific temperature.

Subsurface temperature variation is a complex phenomena which depends on the ambient air temperature, soil types, soil moisture contents, vegetation types, and thickness of layers, snow coverage, ground elevation, slope aspect, wind etc (Simunek et al. 2002). In the current study, the variation of temperature in the subsurface was determined using the following equation:

$$T_z = T_m \pm A_s \exp\left[-\frac{z}{\sqrt{\frac{\alpha p}{\pi}}}\right] + gz \quad (7.3)$$

here, T_z = temperature in degree Fahrenheit at depth z, A_s = surface temperature amplitude in degree Fahrenheit [0.5 (Max. temperature – Min. temperature)], P = period of time under consideration, T_m = mean temperature of air in degree Fahrenheit, α = thermal diffusivity (ft^2/hr), g = thermal gradient, 1.7 deg. F per 100 ft depth.

The thermal diffusivity of a soil is correlated with specific heat, thermal conductivity, and dry unit weight of soil as presented below:

$$\alpha = \frac{k}{\rho c} \quad (7.4)$$

where, k = thermal conductivity (BTU/ft. hr. deg F), c = specific heat (BTU/lb. deg F), ρ = dry density (lb/ft^3).

The thermal conductivity and specific heat are functions of freezing condition, moisture content, and fine fraction. In the current analysis, these thermal parameters were determined using a monograph, which correlates thermal properties with moisture content (Farouki, 1981). The observed moisture contents from laboratory tests were utilized for the determination of thermal conductivity and specific heat. The obtained thermal parameters at different depths are presented in Table 7.3 and 7.4.

Table 7.3 Summary of thermal properties for BH-1 in Loop 12

Borehole	Depth (ft)	Moisture Content (%)	K (BTU/ft. hr. deg F)	C (BTU/lb. deg F)	α (ft^2/hr)
BH-1	5	15.21	1.15	37.5	0.031
BH-1	10	29.69	0.8	43	0.019
BH-1	15	32.36	0.82	43.5	0.019
BH-1	20	22.38	0.95	40.5	0.023
BH-1	25	18.00	1.05	39	0.027
BH-1	30	14.50	1.15	37.5	0.031
BH-1	35	13.94	1.18	37	0.032

Table 7.4 Summary of thermal properties for BH-2 in Loop 12

Borehole	Depth (ft)	Moisture Content (%)	K (BTU/ft. hr. deg F)	C (BTU/lb. deg F)	α (ft^2/hr)
BH-2	5	22.22	0.95	40.5	0.023
BH-2	10	22.18	0.95	40.5	0.023
BH-2	15	40.00	0.74	45.5	0.016
BH-2	20	27.57	0.85	42.5	0.020
BH-2	30	12.73	1.35	36.5	0.037

It should be mentioned that the equation 7.3 assumes a saturated condition for the variation of temperature over depths. Moreover, the thermal properties were determined using the monograph of fine-grained soil. The temperature variations over depths along BH-1 and BH-2 are illustrated in Figure 7.16.

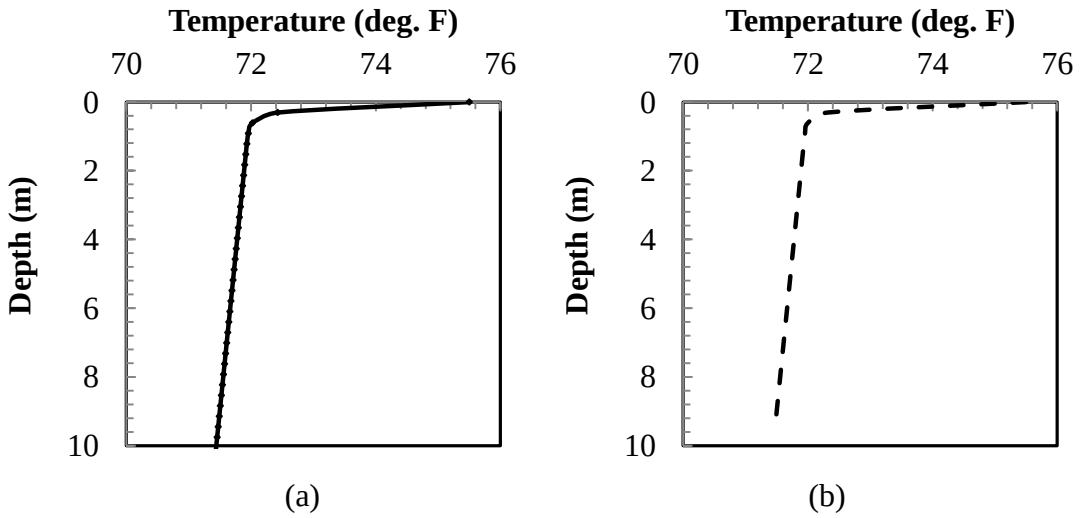

Figure 7.16 Variaiton of temperature over depths (a) BH-1 (b) BH-2

7.3.1.2 Comparison of Model Predicted Degree of Saturation

Once the temperature at different depths were determined, the observed resistivity at a specific depth was corrected at 15.5 deg. C. Then the MLR models were used to predict degrees of saturation using corrected resistivity and CEC at different depths. It can be mentioned that two MLR models were developed using experimental results of undisturbed soil samples as presented in equation 7.5 and 7.6. The degrees of saturation at varied depths were evaluated from field results using the models.

Two-parameter model:

$$Y^{-0.75} = -0.13063 + 0.00304X_1 + 0.00387X_2 \quad (7.5)$$

One parameter model:

$$Y^{-0.75} = -0.0106 + 0.00299X_1 \quad (7.6)$$

here, Y= Electrical resistivity (Ohm-m) of undisturbed soil samples corrected at 15.5 deg temperature according to ASTM G187-05, X_1=Degree of saturation (%), X_2= Cation

exchange capacity (CEC) (cmol+/kg). Range of the model: Y= [4.21, 49.4], X_1= [29.1, 100], X_3= [23.94, 40.1]

The comparison of observed degrees of saturation from laboratory experiments at different depths with model predicted results are presented in Figure 7.17.

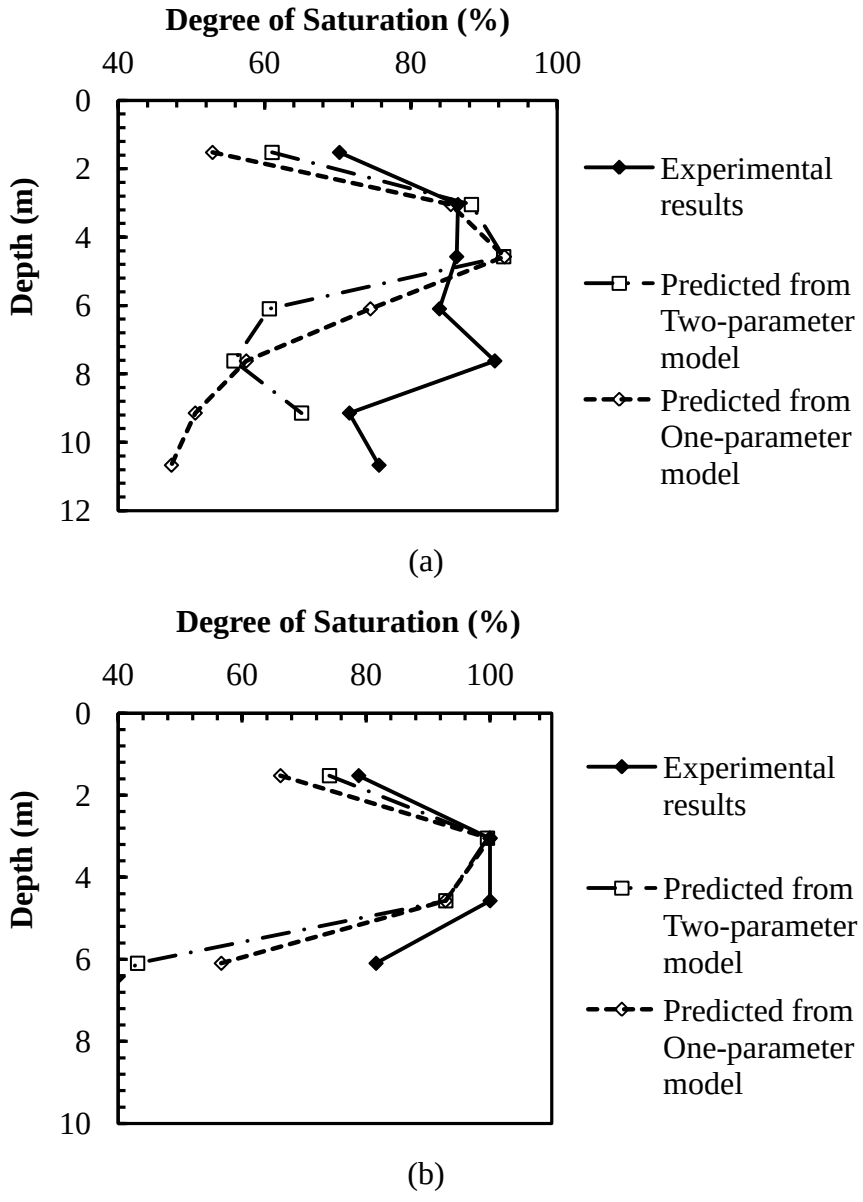

Figure 7.17 Comparison of model predicted results with experimental observations in Loop 12 (a) BH-1 and (b) BH-2

The comparison between model predicted and observed degrees of saturation indicated that the error percentage in estimation was less than 10% in up to a depth of 4.6 m for BH-1 and BH-2, when two–parameter model was utilized. Therefore, the model predictions were in good agreement with the field results at shallow depths. However, a substantial increase in error was identified at depths below 4.6 m.

In addition, the performance of two-parameter model was better compared to the one-parameter model. The error was as much as 17.4% within 4.6 m depths in BH-1; nonetheless, maximum 12.6% variation was observed in BH-2 when one parameter model was used for prediction.

7.3.2 RI at US 287 South

In addition to Loop 12 site, RI tests were conducted along slopes of highway US 287 south near the St. Paul overpass in Midlothian, Texas. Hossain (2012) conducted a study on the determination of active zone in slopes using real time moisture and matric suction data. To accomplish the objective of that study, moisture sensors were installed at the crest and toe of the slope. In the current study, moisture sensors located at depths 1.22 m at the crest of the slope, and 2.44 m at the toe were utilized to compare the predictive capability of the MLR models. Soil samples were collected during test boring to determine CEC. The CECs of the soil samples collected from 1.22 and 2.44 m depths were 27.5 and 30.6 cmol+/kg, respectively.

The geology of the study area is characterized by Austin Chalk, Eagle ford shale, Ozan formation, Wolf city formation, Neylandville and Marlbrook Marls, alluvium, and

terrace deposits. Austin Chalk and Ozan formation are dominant geologic units, and consist around 60% of the geologic formation (USGS, 2012).

RI tests were carried out along sensor locations at crest and toe of the slope during October 2012 to July 2013. During the RI tests, moisture sensor data were collected, and ambient temperatures were recorded. The RI tests were conducted using dipole-dipole array with the spacing ranged from 0.91 to 1.52 m .The apparent resistivity was analyzed using EarthImager 2D software. A finite element method with Cholesky decomposition equation solver and Dirichlet boundary condition was adopted for the forward modeling. Moreover, high stabilizing (1000) and damping factor (1000) were used in the modeling because traffic movement might cause potential noisy data during the measurements. The locations of moisture sensor in slopes and RI tests are presented in Figure 7.18.

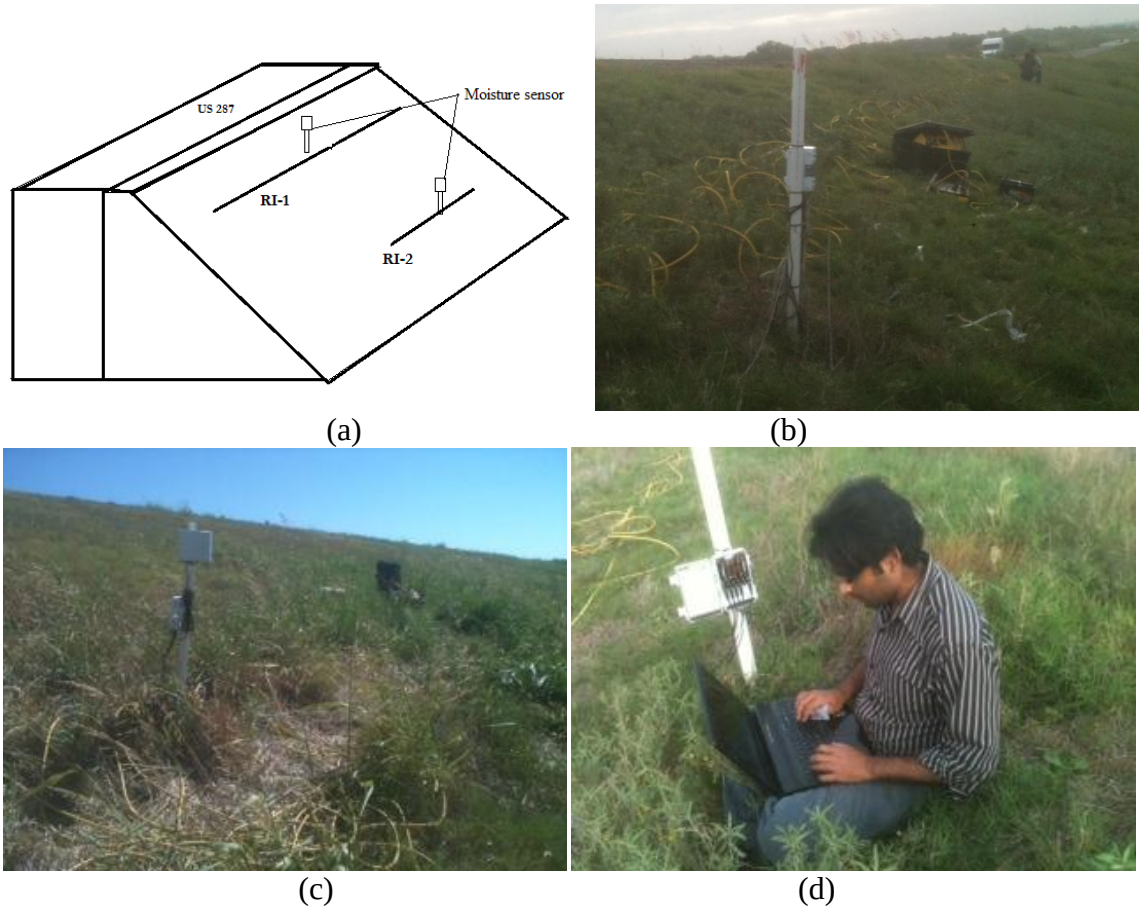

Figure 7.18 (a) Location of moisture sensor and RI layout (b) RI at the crest (c) RI at toe (d) collection of moisture sensor data

7.3.2.1 Prediction of the Degree of Saturation at the Crest of the Slope

The RI results at crest of the slope during October 2012 to July 2013 are presented in Figure 7.19. A low resistivity zone was identified in between depths 1 to 4 m (approximately). Moreover, the resistivity was as low as 3 Ohm-m at 5.5 m depth. The variations of resistivity over depths along the location of moisture sensor are determined using EarthImager 2D and inverted resistivity sections. Based on the profile, resistivity at 1.22 m depth was identified. The resistivity profiles along the sensor locations are

presented in Figure 7.20. The observed resistivity was below 15 Ohm-m; however, an increase in resistivity was observed at 0.8 m depth on October 2012.

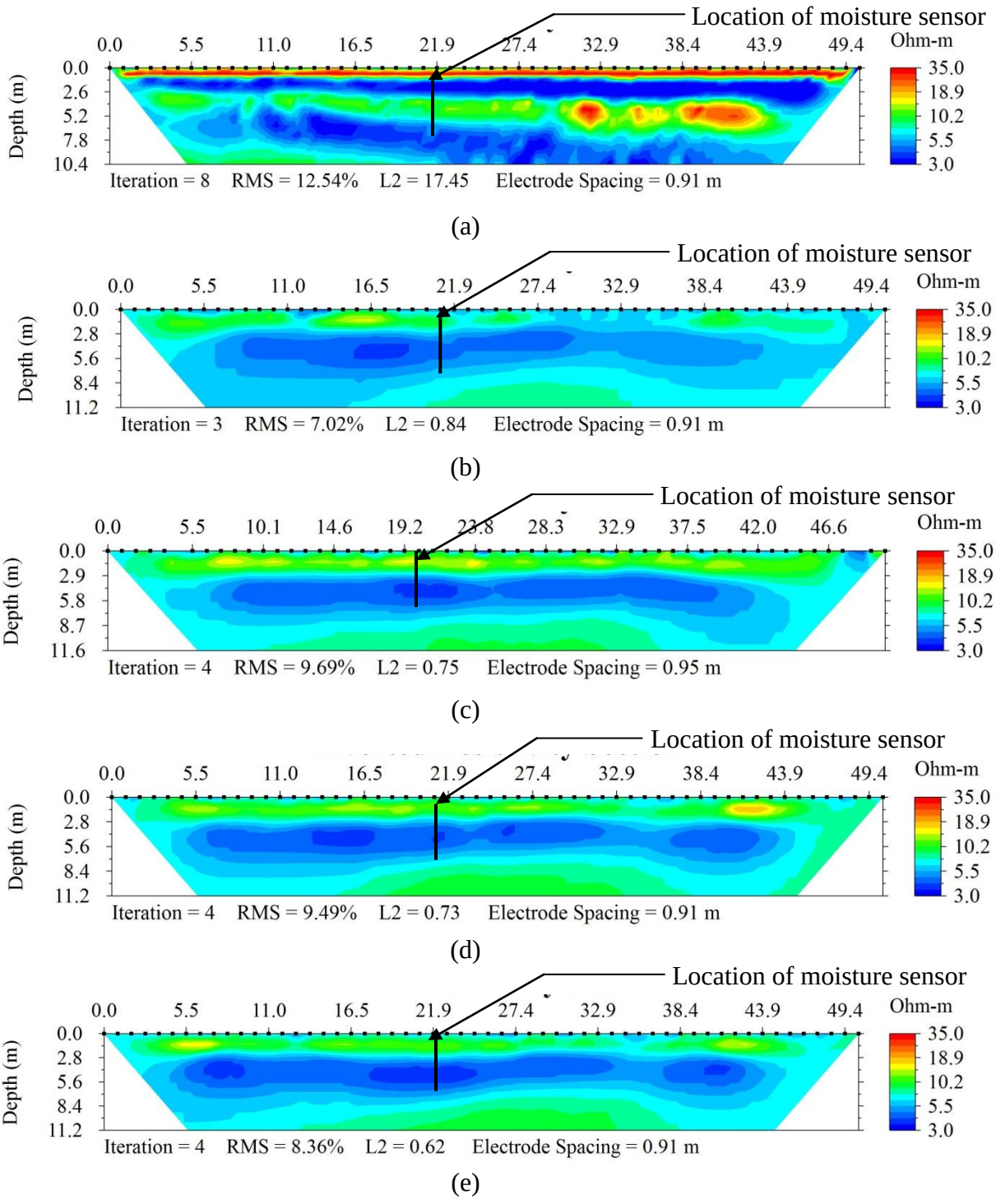

Figure 7.19 RI test results during October 2012 to July 2013 at the crest of slope along US 287 (a) October 2012, (b) November 2012, (c) March 2013, (d) May 2013, and (e) July 2013

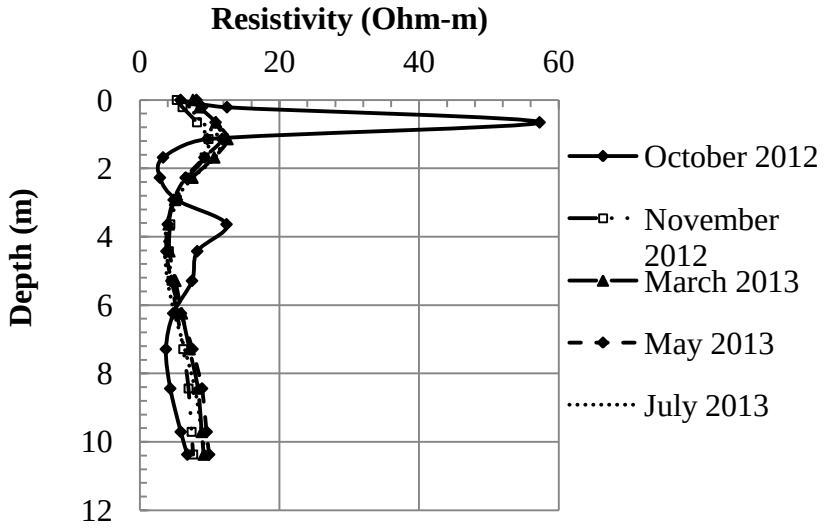

Figure 7.20 Variation of resistivity over depths along sensor location

7.3.2.1.1 Subsurface Variation in Temperature

The observed resistivity at 1.22 m depth was required to be corrected at the 15.5 deg. C. Therefore, subsurface temperature variations were evaluated using equation 7.3. It should be mentioned that the in-situ moisture contents during RI tests were utilized for the determination of thermal coefficients as presented in Table 7.5.

Table 7.5 Summary of thermal properties in slopes along highway US 287

Date of RI test	**Temperature (deg. F)**	**Observed Moisture content (%)**	**K_u (BTU/ft. hr. deg F)**	**C_u (BTU/lb. deg F)**	**A (ft^2/hr)**
12-Oct-12	70	21.14	1	40.7	0.023
20-Nov-12	77	23.08	1	41	0.024
24-Mar-13	52	19.79	1	40	0.025
22-May-13	69	16.69	1.1	38.2	0.029
8-Jul-13	77	18.67	1.1	39	0.027

The variation of temperature with depths during field tests are presented in Figure 7.21.

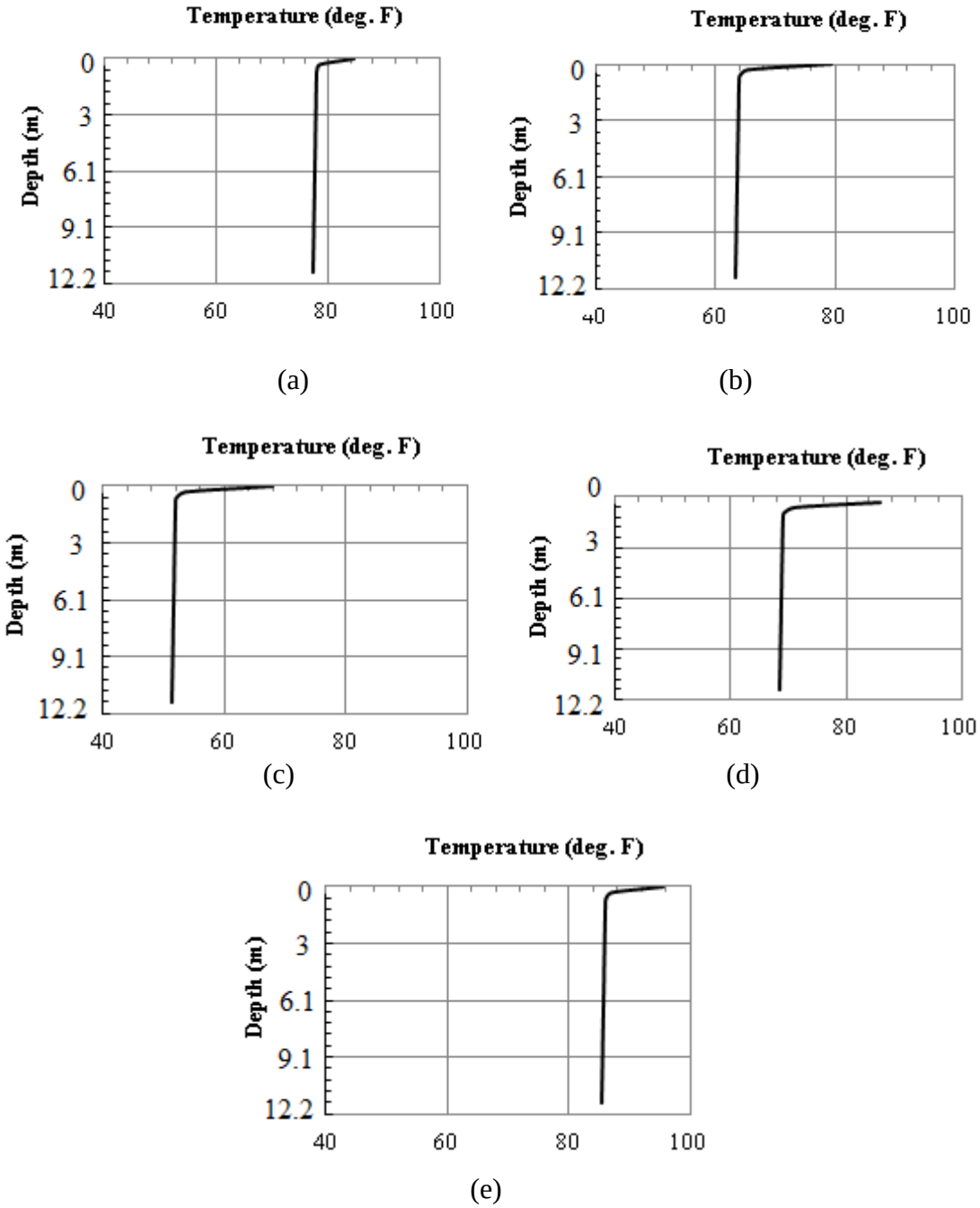

Figure 7.21 Variation of subsurface temperature with depths along slopes of US 287 south (a) October 12, 2012, (b) November 20, 2012, (c) March 24, 2013, (d) May 22, 2013, and (e) July 13, 2013

7.3.2.1.2 Comparison of Observed Degree of Saturation at Crest

The temperature at 1.22 m depth was determined, and the observed resistivity was corrected accordingly. The resistivity and CEC (27.5 cmol+/kg) were utilized in the two- and one-parameter MLR models to determine degrees of saturation. The predicted saturations were compared with the sensor results. It should be mentioned that the volumetric moisture contents were obtained from moisture sensors, and degrees of saturation were calculated from the observed volumetric moisture contents.

It was identified that both two- and one-parameter models predicted degrees of saturation close to the field results. The maximum prediction errors were 7.47 and 11.17% in two- and one-parameter MLR models, respectively. Summary of comparison between model predicted and observed degree of saturation is presented in Table 7.6.

Table 7.6 Summary of comparison between predicted and observed degree of saturation at crest

Date of RI tests	**Corrected Resistivity (Ohm-m)**	**Observed Degree of saturation**	**Predicted Degree of saturation (Two parameter model)**	**Variability (%)**	**Predicted Degree of saturation (One parameter model)**	**Variation (%)**
12-Oct-12	9.38	66.41	69.36	-2.95	65.97	0.44
20-Nov-12	9.92	72.50	66.80	5.70	63.37	9.13
24-Mar-13	9.78	62.17	67.45	-5.29	64.03	-1.86
22-May-13	11.81	52.42	59.60	-7.18	56.04	-3.63
8-Jul-13	14.97	58.65	51.18	7.47	47.49	11.17

7.3.2.2 Prediction of Degree of Saturation at the Toe of the Slope

Similar to the crest of the slope, RI tests were performed at the toe during October 2012 to July 2013 using dipole-dipole array. The depth of investigation should be more than 2.4 m; therefore, a total of 28 electrodes were used in the tests. RI results indicated that the resistivity ranged from 7.5 to 12.7 Ohm-m at 2.4 m during the investigation period. The RI results at the toe of the slope are presented in Figure 7.22.

The resistivity profiles along the sensor location were also identified as illustrated in Figure 7.23. Moreover, the variations of subsurface temperatures were evaluated using equation 7.3. Once, the resistivity at 2.4 m depth was corrected for temperature, both two- and one-parameter models were used for the prediction of degrees of saturation. The obtained volumetric moisture contents were used in the development of subsurface temperature profiles. The thermal properties and temperature variations at the toe of the slope were determined using the similar methods presented in Subsection 7.3.1.1.

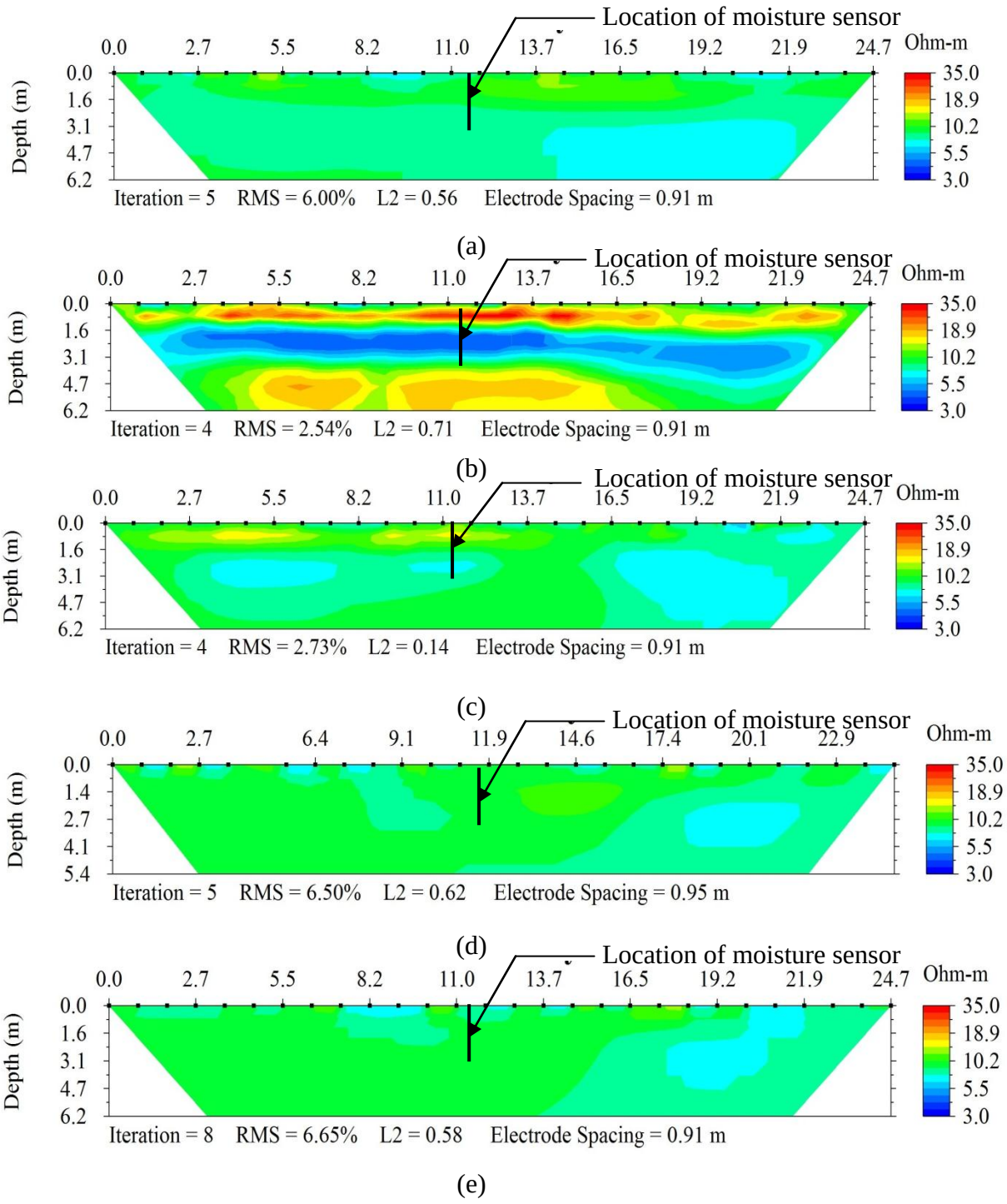

Figure 7.22 RI test results during October 2012 to July 2013 at the toe of slope along US 287 (a) October 2012, (b) November 2012, (c) March 2013, (d) May 2013, and (e) July 2013

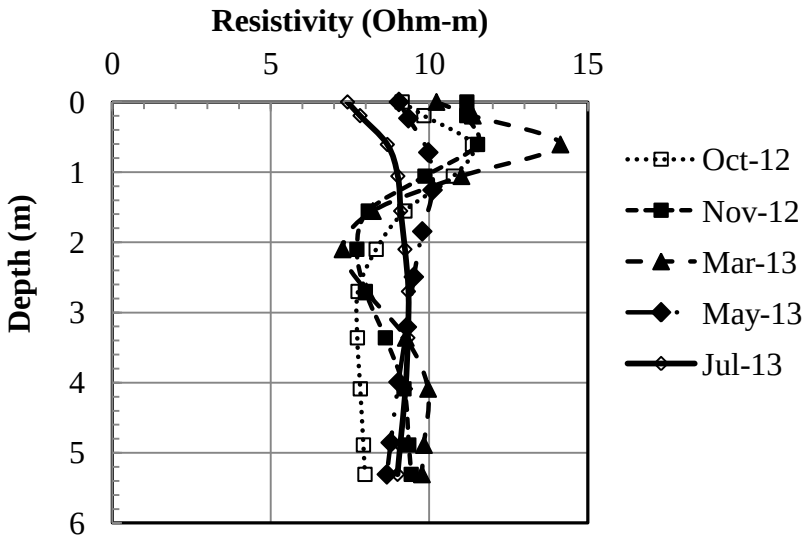

Figure 7.23 Resistivity profile along sensor location at the toe of slope along US 287

7.3.2.2.1 Comparison of Observed Degree of Saturation at Toe

A summary of comparison between model predicted and observed degrees of saturation is presented in Table 7.7. The comparison between model predicted and observed degrees of saturation indicated that the percentages of error was as much as 19.77% in two-parameter model. However, one-parameter model showed maximum 16.28% error in prediction.

Table 7.7 Summary of comparison between predicted and observed degree of saturation at toe

Date of RI tests	Corrected Resistivity (Ohm-m)	Observed Degree of saturation	Predicted Degree of saturation (Two parameter model)	Variation (%)	Predicted Degree of saturation (One parameter model)	Variation (%)
12-Oct-12	9.88	72.87	67.01	5.86	63.58	9.29
20-Nov-12	8.23	72.72	75.64	-2.92	72.35	0.36
24-Mar-13	8.09	60.30	76.54	-16.25	73.27	-12.98
22-May-13	10.83	43.29	63.06	-19.77	59.57	-16.28
8-Jul-13	12.73	43.44	56.77	-13.33	53.17	-9.73

7.3.3 Discussions on the Comparison

The variation in resistivity can be explained by the anisotropy of electrical field in 2D resistivity survey. According to Abu Hassanein et al. (1996), the field measurement of electrical resistivity may vary from laboratory test results because of the following reasons:

- The effect of 3D or 2D electrical field in the RI tests
- Spatial variability of anisotropy and its influence in the results
- Spatial variation in electrical properties in the subsurface condition
- Influence of anomalies in the electrical properties in the subsoils
- Influence of boundary condition

It should be mentioned that the presence of cobbles were encountered at shallow depths during instrumentation. The variation in hydraulic and electrochemical properties

in the subsoil condition might cause the observed variation. In addition, degree of anisotropy in the 2D electrical field might increase with the increase in depths.

7.4 Summary

The objective of this chapter was to evaluate the applicability of developed MLR models in the field condition. Resistivity imaging (RI) tests were conducted in the sites to determine electrical resistivity. Based on the observed resistivity, degrees of saturation were predicted using MLR models. A summary of the results are presented herein:

1. 2D Resistivity imaging (RI) tests were conducted on the cell 4A of City of Denton Landfill after the completion of three lifts, and placement of 20 cm loosely compacted soils. A total of 28 electrodes with a spacing of 1.52 m were used in the RI tests.
2. As a part of the construction quality control, in-situ tests were performed on the compacted clay liners. The co-ordinates of test locations were plotted in the Google map of the cell 4A using Geographic Information System (GIS). The co-ordinates of the horizontal profile, and in-situ tests were matched to identify the resistivity at the locations of in-place density tests.
3. Liquid limits were utilized to calculate CEC (cmol+/kg) of the samples using the correlation of Yukselen and Kaya (2006):

$$CEC = 0.2027LL + 16.231$$

4. A horizontal resistivity profile was evaluated at the depth of clay liner (0.31 m). The temperature at 0.31 m depth was assumed to be similar as ambient temperature (16.2 deg. C). Therefore, quantified resistivity values were corrected

with respect to 16.2 deg. C. The calculated CEC and corrected resistivity values were used to predict degrees of saturation according to the following equation:

$$Y^{-0.25} = 0.43398 + 0.00309X_1 - 14.35204X_2{}^{-1.5}$$

5. The predicted degree of saturation was compared with the measured values at the site condition. The prediction error ranged from 0.4 to 9.7%; therefore, the performance of the model was quite satisfactory for the current data set. Moreover, a degree of saturation contour was plotted using Surfer assuming an average CEC of 24.8 cmol+/kg.
6. The performance of MLR models correlating resistivity of undisturbed soil samples with degree of saturation and CEC was evaluated using RI tests at slopes along highway Loop 12 and US 287 south.
7. In the current study, the variation of temperature in the subsurface was determined using the following equation:

$$T_z = T_m \pm A_s \exp\left[-\frac{z}{\sqrt{\frac{\alpha p}{\pi}}}\right] + gz$$

here, T_z = Temperature in degree Fahrenheit at depth z, A_s = surface temperature amplitude in degree Fahrenheit [0.5 (Max. temperature – Min. temperature)], P = period of time under consideration, T_m = Mean temperature of air in degree Fahrenheit, α = Thermal diffusivity (ft^2/hr), g = Thermal gradient, 1.7 deg. F per 100 ft depth.

8. Once the temperatures at different depths were determined, the observed resistivity at a specific depth was corrected at 15.5 deg. C. Then the MLR models were used to predict degree of saturation using corrected resistivity and CEC at different depths according to following equations:

   Two-parameter model:

$$Y^{-0.75} = -0.13063 + 0.00304X_1 + 0.00387X_2$$

   One parameter model:

$$Y^{-0.75} = -0.0106 + 0.00299X_1$$

9. The comparison between model predicted and observed degrees of saturation at Loop 12 site indicated that the error percentages in estimation was less than 10% in upto a depth of 4.6 m (15 ft) for BH-1 and BH-2, when two–parameter model was utilized. Therefore, the model predictions were in good agreement with the field results at shallow depths. However, a substantial increase in error was identified at depths below 4.6 m.
10. In addition to Loop 12 site, RI tests were conducted along slopes of highway US 287 south near the St. Paul overpass in Midlothian, Texas. Moisture sensors (installed at depths 1.22 m at the crest of the slope, and 2.44 m at the toe) were utilized to compare the predictive capability of the MLR models. The CECs of the soil samples collected from 1.22 and 2.44 m depths were 27.5 and 30.6 cmol+/kg, respectively.
11. RI tests were carried out along sensor locations at crest and toe of the slope during October 2012 to July 2013. During the RI tests, moisture sensor data were

collected, and ambient temperatures were recorded. The RI tests were conducted using dipole-dipole array with the spacing ranged from 0.91 to 1.52 m. The apparent resistivity was analyzed using EarthImager 2D software.

12. It was identified that both two- and one-parameter models predicted degrees of saturation close to the field results at crest. The maximum prediction errors were 7.47% and 11.17% in two- and one- parameter MLR models, respectively.
13. The comparison between model predicted and observed degrees of saturation at toe indicated that the percentages of error was much as 19.77% in two-parameter model. However, one-parameter model showed maximum 16.28% error in prediction.
14. It should be mentioned that the presence of cobbles were encountered at shallow depths during instrumentation. The variation in hydraulic and electrochemical properties in the subsoil condition might cause the observed deviation. In addition, degree of anisotropy in the 2D electrical field might increase with the increase in depths.

CHAPTER 8

CONCLUSIONS AND FUTURE RECOMMENDATIONS

8.1 Introduction

Resistivity imaging (RI) is a promising approach to obtain continuous profile of subsurface. However, the application of RI in geotechnical engineering is limited because electrical resistivity responses of soils under different conditions are not well understood. Moreover, at present, only qualitative information of subsurface can be obtained using RI. A study on the quantification of saturation profile has become important for rigorous use of RI in the evaluation of geohazard potential and construction quality control of landfill liner system. The overall objective of this study is to develop correlation between geotechnical properties and electrical resistivity. To accomplish the objective, an experimental program was developed to determine geotechnical and electrical properties of the specimens. Thereafter, MLR models were developed to correlate resistivity with degree of saturation and CEC.

8.2 Summary of Accomplished Tasks

A summary of conducted research in the current study can be presented below:

1. The properties of clayey soils, mineralogy, characterization methods, and their effects on electrical resistivity were reviewed.
2. Both disturbed and undisturbed soil samples were collected from soil test boring using truck mounted rig from highway slopes near Loop 12, Dallas, TX. In addition, Ca-bentonite and kaolinte were utilized to evaluate resistivity responses of two specific clay minerals.

3. Grain size distribution, Atterberg limits, specific gravity, free swell ratio, and cation exchange capacity (CEC) tests were conducted on the test specimens.
4. Soil composition and fabric study were analyzed using energy dispersive x-ray spectroscopy (EDS) and scanning electron microscope (SEM). Moreover, pore water properties were determined using ion chromatography (IC).
5. Soil resistivity tests were carried out on compacted soil samples using four-electrode configuration. All the measured resistivity values were corrected at 15.5 deg. C temperature, and mean values were considered for the analysis. The soil samples consisted of Ca bentonite, kaolinite, high and low plasticity clay.
6. In case of undisturbed soil samples, resistivity tests were conducted at subsequent drying phases and the observed results were corrected at 15.5 deg. C temperature. A total of six soil samples were considered in the experiments.
7. A modified oedometer was designed to evaluate the effect of compressibility on four undisturbed soil specimens.
8. A detail investigation was performed to identify the influential parameters on electrical resistivity. Based on the analysis, degree of saturation and CEC were selected as potential parameters for development of multiple linear regression (MLR) models.
9. Statistical analysis software SAS (2009) was used to correlate electrical resistivity with degree of saturation and CEC. Two MLR models were developed for compacted clays and undisturbed soil samples. The models were validated using separate set of results.

10. Resistivity Imaging tests were conducted on compacted clay liner and slopes to evaluate the applicability of the developed models in the field condition.

8.3 Conclusions

Based on the experimental results and field tests, following conclusions can be drawn from the current research:

1. The soil samples were classified as highly plastic clay (CH) and low plasticity clay (CL) according to USCS. Based on the physical tests, SEM, and EDS analysis, it was identified that the dominant mineral was kaolinite with some traces of magnesium, calcium, potassium, and iron.
2. Electrical resistivity of soils were substantially influenced by moisture content, dry unit weight, and void ratio. These parameters can be represented by a single parameter i.e. degree of saturation. Electrical resistivity decreased as much as 11 times of initial value (28.6 to 2.6 Ohm-m) for the increase of degree of saturation 23 to 100% in Ca-bentonite. The observed reductions ranged in between 6 and 11.3 times in kaolinite (373 to 33 Ohm-m), CL (58.1 to 7 Ohm-m), and CH (72 to 6 Ohm-m), respectively at this condition. In case of undisturbed soil samples, resistivity decreased as much as sixteen fold (49.4 to 3.2) for an increase of saturation from 31 to 100%.
3. It was observed that the resistivity results were different for the specimens at a specific degree of saturation. The variation might occur due to varied isomorpohous substitution of clay particles. Therefore, resistivity of the compacted and artificial specimens were plotted against CEC. According to the

test results, resistivity was significantly affected by CEC at relatively low degrees of saturation. A total reduction in resistivity was as much as 385 Ohm-m for the increase of CEC from 13.3 to 79 cmol+/kg at 25% degree of saturation. On the other hand, the total reduction in resistivity was 43.3 Ohm-m at 100% degree of saturation in these CEC range. In case of Ca-bentonite-sand specimens, resistivity decreased from 64 to 37 Ohm-m, for the increase of CEC from 27.8 to 63.5 cmol+/kg, respectively at 25% saturation. Therefore, test results emphasized the effect of ion exchange at low degrees of saturation.

4. An overall downward trend was observed in each case when resistivity was plotted against liquid limits, plasticity indices, specific surface area, and mineralogical contents.
5. It was identified that pore water conductivity and sulphate content of pore water influenced electrical resistivity of the soil samples significantly. According to the results, pore-water conductivity of kaolinite mineral was 414 micro-Siemens/cm and associated resistivity values were 435, 140, 75, and 45 Ohm-m at 25, 50, 75, and 100% saturation, respectively. Nonetheless, pore-water conductivity of Ca-bentonite, CL, and CH were 1805, 1028, and 1436 micro-Siemens/cm, and the observed resistivity was below 50 Ohm-m at each saturation level due to the high conductivity of extracted pore water.
6. Sets of correlations were developed between electrical resistivity and moisture content, degree of saturation, volumetric moisture content, cation exchange capacity, liquid limits, and plasticity indices of the disturbed and undisturbed soil

samples (considering Ca-bentonite, CH, and CL). In addition, previous studies were compared with the proposed correlations for compacted clay specimens.

7. In addition to physical properties, compressibility of clays was correlated with electrical conductivity. Based on the investigation, it was determined that the electrical conductivity vs. pressure curves followed similar trends as e vs. logp curves. Moreover, pre-consolidation pressures were closely associated with the point of inflections in electrical conductivity vs. pressure curves. The variation in electrical conductivity was related with the structural change, co-ordination number, and cementation of the soil samples under consideration.
8. The trends of resistivity changes with time were similar to the consolidation vs. time curves. The coefficients of consolidations were determined using Taylor's method from displacement vs. time and resistivity vs. time curves. The comparisons of coefficients of consolidations indicated that the coefficients of consolidations can be evaluated using electrical resistivity.
9. The relationship between 1D vertical strain with electrical conductivity was determined. For the current experimental results, the correlation between void ratio and electrical conductivity can be presented as:

$$\frac{\Delta\sigma}{1+\sigma v} = 3.233\frac{\Delta e}{(1+e)} + 0.023$$

where, Δe= change in void ratio, e= initial void ratio, $\Delta\sigma$ = change in vertical conductivity, σ_v= Initial vertical conductivity,

10. Although permeability was related with the electrical conductivity for individual specimen, a reliable correlation between hydraulic and electrical conductivity was

not identified. The variation in cementation factors and packing arrangement of the particles might be responsible for the observed results. Moreover, the changes in soil fabric were not same in the soil samples under the application of pressure.

11. For the development of multiple linear regression (MLR) model, degree of saturation and CEC were selected as two most important parameters influencing resistivity. It was observed that the other clay properties such as mineral percentages, PI, LL, and pore water conductivity were linearly correlated with CEC. Therefore, only CEC was considered as independent variable representing clay parameters. The compressibility parameters were related to the structural component of soils; therefore, were not considered in the model development.
12. The MLR assumptions were not satisfied in the preliminary model. Thus, Box-Cox analysis was conducted to determine the power of transformation of dependent variable. Moreover, CEC (X_2) was transformed to increase the scatter in the residual plots. The finalized model form for compacted clays can be mentioned as:

$$Y^{-0.25} = 0.43398 + 0.00309X_1 - 14.35204\mathrm{X}_2{}^{-1.5}$$

here, Y= Electrical resistivity (Ohm-m) corrected at 15.5 deg temperature according to ASTM G187-05, X_1=Degree of saturation (%), X_2= Cation exchange capacity (CEC) (cmol+/kg). Range of the model: Y= [2.6, 504.3], X_1= [21.8, 100], X_3= [13.28, 79.03]

13. The predictive capability of the model was compared using artificial soil specimens. The estimated resistivity was within $\pm 5\ \mathrm{Ohm-m}$ for soils with CEC and degree of saturation higher than 30 cmol+/kg and 30%, respectively.
14. Based on the developed model, series of charts were developed to determine degree of saturation from resistivity measurement at varied CECs.
15. Two separate models were developed for undisturbed soil specimens. Similar to compacted clay samples, MLR analysis was conducted, and model assumptions were diagnosed. The initial model was not able to satisfy the adequacy of linear model form, constant error variance, and normality assumptions. Therefore, Box-Cox method was employed to determine the power of transformation. The potentially good models were selected using backward elimination, stepwise regression, and best subset method. The following two potential models were determined for undisturbed soil samples:

    Two-parameter model:

    $$Y^{-0.75} = -0.13063 + 0.00304X_1 + 0.00387X_2$$

    One parameter model:

    $$Y^{-0.75} = -0.0106 + 0.00299X_1$$

    Here, Y= Electrical resistivity (Ohm-m) of undisturbed soil samples corrected at 15.5 deg temperature according to ASTM G187-05, X_1=Degree of saturation (%), X_2= Cation exchange capacity (CEC) (cmol+/kg). Range of the model: Y= [4.21, 49.4], X_1= [29.1, 100], X_3= [23.94, 40.1].

16. The experimental results of soil sample B1-20 were utilized to evaluate the predictive capacity of the resistivity model for undisturbed soil specimens. The maximum errors in estimation were 1.7 and 4.4 Ohm-m in two- and one - parameter model, respectively. However, error in prediction was less than 1 Ohm-m in one parameter model at degree of saturation over 73%.
17. 2D Resistivity imaging (RI) tests were conducted on the cell 4A of City of Denton Landfill to evaluate the predictive capability of MLR models developed from compacted clays.
18. The predicted degree of saturation was compared with the measured values at the site condition. The prediction error ranged from 0.4 to 9.7%; therefore, the performance of the model was quite satisfactory for the current data set. Moreover, a degree of saturation contour was plotted using Surfer assuming an average CEC of 24.8 cmol+/kg.
19. The performance of MLR models correlating resistivity of undisturbed soil samples with degree of saturation and CEC was evaluated using RI tests at slopes along highway Loop 12 and US 287 south.
20. The comparison between model predicted and observed degrees of saturation at Loop 12 site indicated that the error percentages in estimation was less than 10% upto a depth of 4.6 m for BH-1 and BH-2, when two–parameter model was utilized. Therefore, the model predictions were in good agreement with the field results at shallow depths. However, a substantial increase in error was identified at depths below 4.6 m.

21. In addition to Loop 12 site, RI tests were conducted along slopes of highway US 287 south near the St. Paul overpass in Midlothian, Texas. Moisture sensors were utilized to compare the predictive capability of the MLR models.
22. It was identified that both two- and one-parameter models predicted degrees of saturation close to the field results at crest. The maximum prediction errors were 7.47 and 11.17% in two- and one- parameter MLR models, respectively.
23. The comparison between model predicted and observed degrees of saturation at toe indicated that the percentages of error was much as 19.77% in two-parameter model. However, one-parameter model showed maximum 16.28% error in prediction.
24. It should be mentioned that the presence of cobbles were encountered at shallow depths during instrumentation. The variation in hydraulic and electrochemical properties in the subsoil condition might cause the observed deviation. In addition, degree of anisotropy in the 2D electrical field might increase with the increase in depths.

8.4 Recommendations for Future Study

1. The current study assumed isotropic electric field. However, electrical resistivity is different in horizontal and vertical direction. A future study can incorporate anisotropy factor in the model to reduce error percentages of prediction.
2. The range of CEC of undisturbed soil samples were in between 23.3 to 40.9 cmol+/kg. A robust model can be developed using different types of clayey samples with wide range of ion exchange properties.

3. The direct current (DC) was utilized in this research to evaluate electrical resistivity of soils. In future, similar study can be conducted using alternative current (AC) because the effects of surface charges are different under the application of frequency.
4. To correlate resistivity with degree of saturation and CEC, multiple linear regression method was utilized. However, similar analysis can be performed using artificial neural network (ANN) and genetic programming to compare the efficiency of different models.
5. Although stainless steel was used in the current study, non-polarizing electrode i.e. electrodes made of carbon core from exhausted electric cells, can be used to measure electrical resistivity.
6. The sensitivity of different arrays in RI tests can be studied for the further advancement of the proposed models.
7. As the degree of saturation and structure of soil particles significantly influence resistivity, a future study can be conducted to correlate SWCC with electrical resistivity.
8. In future, the variation of shear strength, SPT blow counts, and shear wave velocity with electrical resistivity of soils can be investigated.

APPENDIX A

STATISTICAL MODELING

Table A1: Experimental data set for MLR model of compacted clays

Obs.	Resistivity (Ohm-m)	Degree of Saturation (%)	Cation exchange capacity (cmol+/kg)
1	28.647	23.885	79.03
2	11.568	47.771	79.03
3	4.973	71.656	79.03
4	2.975	95.542	79.03
5	21.686	31.172	79.03
6	6.33	62.345	79.03
7	3.218	93.517	79.03
8	2.59	100	79.03
9	16.45	41.063	79.03
10	5.361	82.125	79.03
11	2.663	100	79.03
12	373.441	21.798	13.28
13	203.735	43.596	13.28
14	63.567	65.395	13.28
15	42.344	87.193	13.28
16	504.284	27.71	13.28
17	150.782	55.419	13.28
18	45.278	83.129	13.28
19	33.032	100	13.28
20	268.647	35.259	13.28
21	85.698	70.517	13.28
22	84.949	100	13.28
23	72.2	22.001	40.9
24	20.085	44.002	40.9
25	9.418	66.002	40.9
26	6.66	88.003	40.9
27	26.713	28.038	40.9
28	11.078	56.076	40.9
29	7.655	84.114	40.9
30	7.495	100	40.9
31	13.792	35.792	40.9
32	7.076	71.583	40.9
33	6.099	100	40.9
34	58.058	21.865	18.95
35	21.427	43.73	18.95
36	15.227	65.594	18.95
37	13.928	87.459	18.95

Table A1-Continued			
38	40.105	27.817	18.95
39	15.956	55.635	18.95
40	8.044	83.452	18.95
41	7.054	100	18.95
42	26.443	35.433	18.95
43	15.753	70.866	18.95
44	12.589	100	18.95

Table A2. SAS output for outlier test before transformation (compacted samples)

Obs.	Residual	RStudent	Hat Diagonal	DFFITS	DFBETAS		Cook Distance
					X1	X2	
1	-26.37	-0.33217	0.13977	-0.13243	0.0866	-0.0913	0.00598
2	-8.233	-0.10097	0.09231	-0.03181	0.0116	-0.0259	0.00035
3	20.386	0.24839	0.08054	0.07267	0.0058	0.0606	0.0018
4	53.602	0.66176	0.10444	0.22442	0.1085	0.1572	0.01702
5	-22.587	-0.28155	0.12151	-0.10353	0.0605	-0.0756	0.00365
6	8.015	0.09768	0.08089	0.02862	-0.003	0.0242	0.00028
7	50.861	0.62672	0.10103	0.20853	0.0951	0.1491	0.01471
8	59.791	0.74165	0.11285	0.26304	0.1419	0.1758	0.02332
9	-13.242	-0.16326	0.10204	-0.05438	0.0253	-0.0426	0.00101
10	36.209	0.44264	0.08662	0.13496	0.0373	0.1065	0.00619
11	59.863	0.74254	0.11285	0.26337	0.142	0.176	0.02338
12	221.214	2.71629	0.0947	0.95826	-0.7037	-0.3938	0.25728
13	83.646	1.005	0.05447	0.24124	-0.1076	-0.1406	0.01939
14	-24.385	-0.29137	0.04395	-0.06177	-0.0052	0.0429	0.0013
15	-13.472	-0.16261	0.06315	-0.04171	-0.0232	0.0257	0.00059
16	360.772	4.39644	0.08086	1.77154	-1.202	-0.8041	0.56677
17	48.123	0.57535	0.04508	0.12397	-0.0222	-0.0824	0.00521
18	-16.529	-0.19889	0.05731	-0.04846	-0.0237	0.031	0.0008
19	-3.902	-0.04774	0.08828	-0.01467	-0.0104	0.0079	0.00007
20	136.265	1.6476	0.06635	0.44894	-0.2627	-0.2307	0.0643
21	5.297	0.06336	0.04579	0.01371	0.003	-0.0095	0.00006
22	48.016	0.58751	0.08828	0.18134	0.129	-0.0981	0.01114
23	-40.185	-0.48932	0.07941	-0.14237	0.12	-0.0178	0.00688
24	-59.864	-0.71239	0.03611	-0.13705	0.0826	-0.0185	0.00634
25	-38.096	-0.4503	0.02308	-0.06853	-0.0039	-0.0072	0.0016
26	-8.417	-0.10038	0.04032	-0.02032	-0.0133	-0.0006	0.00014
27	-76.772	-0.92735	0.06452	-0.24311	0.195	-0.0312	0.01977

Table A2-Continued							
28	-51.07	-0.60433	0.02521	-0.09643	0.0285	-0.0123	0.00315
29	-13.156	-0.15647	0.03507	-0.02947	-0.0173	-0.0013	0.0003
30	10.105	0.12193	0.06247	0.03109	0.0247	0.0001	0.00033
31	-78.261	-0.93746	0.04873	-0.21186	0.1539	-0.028	0.01501
32	-32.209	-0.38102	0.02459	-0.05986	-0.0152	-0.0052	0.00122
33	8.709	0.10509	0.06247	0.0268	0.0213	0.0001	0.00025
34	-85.953	-1.05109	0.08723	-0.32537	0.2514	0.1028	0.0352
35	-90.349	-1.08092	0.04638	-0.23888	0.1175	0.1141	0.01894
36	-64.313	-0.76505	0.03542	-0.14585	-0.0126	0.0871	0.00716
37	-33.377	-0.401	0.05436	-0.09515	-0.0566	0.0498	0.00308
38	-95.13	-1.15445	0.07315	-0.32568	0.2347	0.1155	0.03506
39	-78.268	-0.93167	0.03671	-0.18156	0.0373	0.1024	0.01102
40	-45.168	-0.54103	0.04865	-0.12128	-0.0639	0.0661	0.00499
41	-21.762	-0.26488	0.07871	-0.07654	-0.0569	0.0348	0.002
42	-97.564	-1.17465	0.05836	-0.29383	0.1853	0.1207	0.02851
43	-56.015	-0.66697	0.03725	-0.1303	-0.0309	0.0774	0.00574
44	-16.226	-0.19751	0.07871	-0.05705	-0.0424	0.0259	0.00111

Table A3. SAS output for outlier test after transformation (compacted soils)

Output Statistics							
Obs.	**Residual**	**RStudent**	**Hat Diag. H**	**DFFITS**	**DFBETAS**		**Cook's distance**
					X1	X2	
1	-0.055	-1.2089	0.1036	-0.411	0.2992	0.2221	0.0557
2	-0.0187	-0.3956	0.0589	-0.099	0.0412	0.0679	0.0033
3	0.035	0.7377	0.0497	0.1688	0.0245	-0.1204	0.0096
4	0.053	1.1458	0.0761	0.329	0.1976	-0.1807	0.0358
5	-0.0464	-1.0032	0.0862	-0.3081	0.2032	0.1802	0.0316
6	0.0245	0.5148	0.0491	0.1169	-0.0104	-0.0855	0.0046
7	0.0445	0.9542	0.0725	0.2668	0.153	-0.1508	0.0238
8	0.0661	1.4482	0.085	0.4414	0.2886	-0.2273	0.0633
9	-0.0437	-0.9356	0.0678	-0.2524	0.1342	0.1634	0.0213
10	-0.0098	-0.2068	0.0569	-0.0508	-0.0193	0.0332	0.0009
11	0.0607	1.3239	0.085	0.4036	0.2638	-0.2078	0.0533
12	0.0228	0.4988	0.1225	0.1864	-0.1195	0.1115	0.0118
13	-0.0073	-0.1552	0.0827	-0.0466	0.0167	-0.035	0.0007
14	0.0149	0.3171	0.0725	0.0886	0.0062	0.0734	0.0027
15	-0.0145	-0.311	0.0919	-0.0989	-0.0459	-0.075	0.0033
16	-0.0119	-0.2579	0.1088	-0.0901	0.0523	-0.0577	0.0028
17	-0.0231	-0.4913	0.0735	-0.1384	0.0188	-0.1122	0.0065

Table A3-Continued							
18	-0.0085	-0.1808	0.086	-0.0555	-0.0223	-0.0432	0.0011
19	-0.0289	-0.6316	0.1171	-0.23	-0.1426	-0.1572	0.0179
20	0.00078	0.0167	0.0944	0.0054	-0.0026	0.0038	1.00E-05
21	-0.0264	-0.5623	0.0744	-0.1594	-0.0278	-0.1313	0.0086
22	-0.1166	-2.7689	0.1171	-1.0086	-0.6252	-0.6891	0.2917
23	-0.1039	-2.3853	0.0942	-0.7693	0.607	0.3175	0.177
24	-0.0425	-0.9005	0.0498	-0.2062	0.1103	0.1107	0.0142
25	-0.012	-0.249	0.0356	-0.0478	-0.0009	0.0286	0.0008
26	-0.0282	-0.5944	0.0515	-0.1385	-0.0771	0.0647	0.0065
27	-0.0258	-0.5508	0.079	-0.1613	0.1197	0.0716	0.0088
28	-0.004	-0.0839	0.0383	-0.0167	0.0044	0.0099	0.0001
29	-0.0375	-0.791	0.0465	-0.1747	-0.0847	0.0869	0.0103
30	-0.0833	-1.8422	0.0729	-0.5167	-0.3698	0.1957	0.0841
31	0.0293	0.6224	0.0629	0.1612	-0.1062	-0.0787	0.0088
32	0.0131	0.2733	0.0368	0.0534	0.0096	-0.031	0.001
33	-0.0514	-1.1072	0.0729	-0.3105	-0.2223	0.1176	0.032
34	0.0348	0.7465	0.08	0.2202	-0.1819	0.0303	0.0163
35	0.0698	1.4951	0.0379	0.2967	-0.1701	0.0697	0.0285
36	0.0438	0.9161	0.0256	0.1483	0.0097	0.0488	0.0074
37	-0.0123	-0.2564	0.043	-0.0543	-0.0347	-0.0156	0.001
38	0.0515	1.1058	0.0656	0.293	-0.2293	0.0467	0.0285
39	0.0687	1.46	0.0275	0.2454	-0.0668	0.0733	0.0195
40	0.0762	1.6406	0.0376	0.3242	0.1843	0.0973	0.0337
41	0.045	0.9627	0.0665	0.2569	0.2019	0.0631	0.022
42	0.0716	1.5464	0.0504	0.3562	-0.2506	0.0685	0.0409
43	0.0233	0.4831	0.027	0.0805	0.0196	0.0266	0.0022
44	-0.0377	-0.8042	0.0665	-0.2146	-0.1686	-0.0527	0.0155

Table A4. Experimental data for undisturbed soil specimen

Resistivity (at 15.5 C)	**Degree of Saturation**	**CEC**
Ohm-m	%	cmol+/kg
5.26	100.00	29.9
5.85	98.08	29.9
6.49	85.00	29.9
6.05	80.10	29.9
6.14	75.19	29.9
7.66	68.65	29.9
8.06	58.85	29.9
8.46	55.58	29.9
12.83	50.67	29.9
14.33	44.13	29.9
10.10	42.50	29.9
14.62	39.23	29.9
20.44	34.33	29.9
6.02	81.66	40.1
6.19	78.89	40.1
6.66	70.58	40.1
7.20	65.05	40.1
6.80	63.66	40.1
6.86	60.90	40.1
8.20	52.59	40.1
12.18	44.29	40.1
16.94	37.37	40.1
33.91	33.22	40.1
45.66	31.83	40.1
7.00	92.48	27.69
8.16	90.77	27.69
7.98	89.06	27.69
7.19	83.92	27.69
6.86	80.49	27.69
8.89	75.35	27.69
8.36	70.22	27.69
10.35	66.79	27.69
11.22	61.65	27.69
12.83	56.52	27.69

Table A4-Continued		
12.80	53.09	27.69
12.62	47.95	27.69
22.45	35.96	27.69
23.72	34.25	27.69
29.38	30.83	27.69
31.79	29.11	27.69
6.82	97.70	30.17
6.64	91.47	30.17
8.11	81.07	30.17
10.32	76.91	30.17
7.53	74.84	30.17
7.57	70.68	30.17
9.99	68.60	30.17
9.75	62.36	30.17
9.24	58.21	30.17
10.06	56.13	30.17
10.04	54.05	30.17
20.92	45.73	30.17
25.56	41.58	30.17
26.59	35.34	30.17
30.26	33.26	30.17
13.77	78.85	23.94
13.23	76.97	23.94
13.81	69.46	23.94
15.27	60.08	23.94
12.84	56.32	23.94
17.35	50.69	23.94
24.58	43.18	23.94
26.95	41.30	23.94
31.70	35.67	23.94
4.21	100.00	30.17
4.93	100.00	30.17
5.42	89.27	30.17
5.50	83.19	30.17
5.75	81.16	30.17
5.74	79.13	30.17
9.01	66.95	30.17
15.91	56.81	30.17

Table A4-Continued		
11.83	48.69	30.17
21.48	44.64	30.17
29.83	40.58	30.17
34.06	38.55	30.17
49.36	36.52	30.17

Table A5. SAS output for outlier test before transformation (undisturbed samples)

Output Statistics									
Obs.	**Residual**	**RStudent**	**Hat Diag H**	**Cov Ratio**	**DFFITS**	**DFBETAS**			
						Intercept	**x1**	**x2**	**cookdi2**
1	5.399	0.8947	0.059	1.0713	0.224	-0.0662	0.1975	0.0007	0.01676
2	5.2728	0.8715	0.0544	1.0679	0.2091	-0.06	0.1822	0.0002	0.01462
3	1.0101	0.164	0.0298	1.0725	0.0288	-0.0056	0.0215	-0.0006	0.00028
4	-1.2656	-0.2048	0.0234	1.0648	-0.0317	0.0045	-0.0211	0.001	0.00034
5	-3.0093	-0.4865	0.0185	1.0511	-0.0669	0.0045	-0.0363	0.0031	0.00151
6	-3.933	-0.6352	0.0145	1.0396	-0.0769	-0.0047	-0.0236	0.0053	0.00199
7	-7.2105	-1.1716	0.0134	0.9985	-0.1367	-0.0379	0.0219	0.0131	0.0062
8	-8.027	-1.3079	0.0145	0.986	-0.1584	-0.0533	0.0488	0.0159	0.00829
9	-5.4958	-0.8912	0.0173	1.0261	-0.1182	-0.0475	0.0582	0.0122	0.00467
10	-6.4431	-1.0503	0.0234	1.0197	-0.1627	-0.0737	0.1081	0.0164	0.00882
11	-11.283	-1.8706	0.0254	0.9288	-0.3021	-0.1392	0.2103	0.0301	0.02942
12	-7.9866	-1.3117	0.0299	1.0012	-0.2301	-0.1088	0.1724	0.0224	0.01748
13	-4.0067	-0.655	0.0378	1.0637	-0.1298	-0.0628	0.105	0.0122	0.00566
14	1.6646	0.2793	0.091	1.1423	0.0884	-0.0768	0.0363	0.0751	0.00264
15	0.8	0.1339	0.0874	1.1406	0.0414	-0.0358	0.0152	0.0358	0.00058
16	-1.8346	-0.3059	0.0794	1.1272	-0.0899	0.0746	-0.0195	-0.0807	0.00272
17	-3.3656	-0.5612	0.0766	1.1136	-0.1616	0.1286	-0.0175	-0.1469	0.00879
18	-4.2844	-0.7152	0.0762	1.1042	-0.2054	0.1612	-0.0164	-0.1869	0.01415
19	-5.2654	-0.8803	0.0757	1.0919	-0.252	0.192	-0.0059	-0.2293	0.02123
20	-7.0301	-1.1813	0.0773	1.0666	-0.342	0.232	0.0499	-0.305	0.03878
21	-6.1654	-1.0372	0.0833	1.0876	-0.3127	0.1817	0.0948	-0.266	0.03257
22	-3.9901	-0.6715	0.0917	1.1259	-0.2134	0.1058	0.0892	-0.1716	0.01529
23	11.4252	1.9743	0.0982	0.9882	0.6516	-0.2905	-0.3121	0.5039	0.13618

Table A5-Continued									
24	22.6553	4.27	0.1006	0.5933	1.4283	-0.6135	-0.7111	1.0894	0.55156
25	3.8115	0.6256	0.0459	1.0744	0.1372	-0.001	0.1081	-0.0371	0.00633
26	4.3324	0.7104	0.0427	1.0659	0.1501	0.0021	0.1155	-0.0424	0.00756
27	3.5088	0.5738	0.0397	1.0702	0.1167	0.0042	0.0875	-0.0345	0.00458
28	0.7915	0.1286	0.0319	1.0753	0.0234	0.0026	0.0157	-0.0079	0.00018
29	-0.8212	-0.1332	0.0276	1.0705	-0.0224	-0.0039	-0.0136	0.0083	0.00017
30	-0.7098	-0.1148	0.0226	1.0652	-0.0175	-0.0048	-0.0083	0.0073	0.0001
31	-3.1675	-0.5123	0.0193	1.0508	-0.0718	-0.0283	-0.0222	0.0333	0.00174
32	-2.461	-0.3975	0.018	1.0539	-0.0538	-0.0254	-0.0094	0.0262	0.00098
33	-3.5117	-0.5677	0.0175	1.0463	-0.0757	-0.0437	0.0032	0.0383	0.00193
34	-3.8261	-0.6191	0.0186	1.0449	-0.0853	-0.0558	0.0216	0.0427	0.00245
35	-5.133	-0.8331	0.0203	1.0335	-0.1201	-0.0825	0.0455	0.0584	0.00483
36	-7.2373	-1.1827	0.0243	1.0085	-0.1868	-0.1329	0.0994	0.0848	0.01156
37	-1.8966	-0.3097	0.0402	1.081	-0.0634	-0.0447	0.0477	0.0235	0.00136
38	-1.2721	-0.208	0.0432	1.0868	-0.0442	-0.031	0.0341	0.0159	0.00066
39	3.1078	0.5107	0.0498	1.0846	0.1169	0.0808	-0.0942	-0.0397	0.0046
40	4.8795	0.8054	0.0534	1.0716	0.1913	0.1312	-0.1569	-0.0632	0.01225
41	6.1574	1.0192	0.0536	1.055	0.2426	-0.0757	0.2111	0.0074	0.0196
42	3.6469	0.5968	0.0406	1.0701	0.1228	-0.0344	0.1013	0.0032	0.00507
43	1.2286	0.199	0.0246	1.0661	0.0316	-0.0061	0.0217	0.0004	0.00034
44	1.8838	0.3045	0.02	1.0589	0.0435	-0.0061	0.0258	0.0003	0.00064
45	-1.6874	-0.2724	0.0182	1.0578	-0.0371	0.004	-0.0199	-0.0001	0.00046
46	-3.2025	-0.517	0.0154	1.0464	-0.0646	0.0021	-0.0254	0.0004	0.0014
47	-1.5601	-0.2514	0.0144	1.0541	-0.0303	-0.0003	-0.0094	0.0004	0.00031
48	-4.1372	-0.6679	0.013	1.0363	-0.0767	-0.0114	-0.0011	0.0022	0.00197
49	-6.2051	-1.0058	0.0135	1.0132	-0.1175	-0.0279	0.0221	0.0045	0.0046
50	-6.1635	-0.9993	0.0141	1.0144	-0.1196	-0.033	0.0338	0.0051	0.00477
51	-6.9617	-1.1314	0.0151	1.0038	-0.1399	-0.0434	0.0517	0.0064	0.0065
52	0.8041	0.13	0.0215	1.0638	0.0193	0.0078	-0.0121	-0.0011	0.00013
53	3.894	0.6327	0.0264	1.0525	0.1042	0.0446	-0.0743	-0.0059	0.00365
54	2.5898	0.4222	0.0358	1.0725	0.0814	0.0367	-0.065	-0.0048	0.00223
55	5.4777	0.8986	0.0395	1.0493	0.1823	0.083	-0.1494	-0.0107	0.01111
56	4.6055	0.7572	0.0469	1.0676	0.168	0.093	0.0673	-0.1224	0.00946
57	3.3574	0.5505	0.0452	1.0775	0.1197	0.0702	0.0429	-0.0892	0.00483
58	1.1317	0.1848	0.0405	1.0841	0.038	0.0271	0.0063	-0.0303	0.00049
59	-0.9286	-0.1515	0.0398	1.0838	-0.0308	-0.0259	0.003	0.0252	0.00032

Table A5-Continued									
60	-4.7592	-0.7803	0.041	1.0595	-0.1614	-0.1409	0.0324	0.131	0.00873
61	-2.3566	-0.3859	0.0446	1.0837	-0.0834	-0.0754	0.0286	0.0655	0.00235
62	2.0562	0.338	0.0526	1.0944	0.0797	0.0729	-0.0399	-0.0584	0.00214
63	3.7288	0.6149	0.0552	1.0855	0.1486	0.1359	-0.0795	-0.1067	0.00742
64	6.3711	1.0611	0.0642	1.0631	0.2779	0.2512	-0.1727	-0.1868	0.02569
65	4.4177	0.7308	0.059	1.083	0.183	-0.0588	0.1616	0.0058	0.01124
66	5.1284	0.8495	0.059	1.0748	0.2127	-0.0683	0.1879	0.0067	0.01514
67	1.6113	0.2626	0.0367	1.0783	0.0512	-0.0136	0.0412	0.0012	0.00089
68	-0.5888	-0.0955	0.0273	1.0705	-0.016	0.0034	-0.0116	-0.0003	0.00009
69	-1.1023	-0.1785	0.0247	1.0666	-0.0284	0.0055	-0.0195	-0.0004	0.00027
70	-1.8732	-0.3031	0.0223	1.0614	-0.0458	0.0078	-0.0296	-0.0005	0.00071
71	-3.1622	-0.51	0.0138	1.045	-0.0602	-0.0028	-0.0142	0.001	0.00122
72	-0.0547	-0.0088	0.0139	1.0563	-0.001	-0.0003	0.0003	0	0
73	-7.1783	-1.1694	0.0187	1.004	-0.1615	-0.0609	0.0893	0.0085	0.00865
74	0.9537	0.1543	0.0227	1.0648	0.0235	0.0096	-0.0154	-0.0013	0.00019
75	7.7909	1.2774	0.0278	1.0027	0.2159	0.0933	-0.1574	-0.0124	0.0154
76	11.2613	1.8722	0.0307	0.9336	0.3331	0.1467	-0.2529	-0.0193	0.03577
77	25.7986	4.8177	0.0339	0.471	0.902	0.4034	-0.708	-0.0525	0.20859

A6. Outlier tests

For X outlier, observations with Leverage value greater than 2p/n were flagged. Here P=3, n=77, So, 2p/n=0.0779.

The observation 14, 15, 16, 21, 22, 23 and 24 were flagged as an X outlier because h_{ii}>0.0779 in these observations.

Bonferroni outlier test was used for checking Y outlier. The guideline is to flag the Studentized deleted residual value greater than $t\left(1-\frac{\alpha}{2n};n-p-1\right)$.

$t\left(1-\frac{\alpha}{2n};n-p-1\right)= t\left(1-\frac{0.1}{154};77-3-1\right)= t\,(0.999;73)$=3.206

Therefore observation 24 and 77 were identified as an Y outlier because $|t_i| > 3.206$ in these observations.

After identifying the outliers, their influence on the regression model was determined. The outliers are influential when their exclusion causes major changes in the regression model. The influences were determined by DEFITS, DFBETAS and Cook's distance.

DFFITS: DEFITS considers the influence of the observation on the predicted value. The guideline is to flag the absolute values of DEFITS greater than 1 as an influential outlier for small to medium data set. As we had 24 observations, we considered our data set was in the large to medium category. It was observed that the absolute DEFITS value of observation 24 is 1.43 which is greater than 1. The influence of observation 24 was required to be checked by other methods.

Cook's Distance: Cook's distance considers the influence of any observation on all predicted values. The guideline is to flag if Di > F (0.50, p, n-p)

F(0.5, p, n-p)= F(0.5, 3, 74)=0.796

For the data set presented here, Cook's distance was always less than 0.80. Therefore, none of the observations was flagged.

DFBETAS: The DFBETAS indicates the way that the inclusion of a case causes change in the estimated regression coefficient. The guideline for a small to medium range data set is to flag when absolute DFBETAS are greater than 1. It was observed that DFBETAS were greater than 1 in observation 24 for X_2.

Based on the analysis, it was determined that the observation 24 was an influential outlier.

Table A7. SAS output for outlier test after transformation (undisturbed samples)

Output Statistics									
Obs.	Residual	RStudent	Hat Diag H	Cov Ratio	DFFITS	DFBETAS			
						Intercept	x1	x2	cookdi2
1	-0.0009	-0.0341	0.059	1.1069	-0.0085	0.0025	-0.0075	0	0.00002
2	-0.0173	-0.6242	0.0544	1.0842	-0.1497	0.0429	-0.1305	-0.0002	0.00754
3	0.00273	0.0969	0.0298	1.0733	0.017	-0.0033	0.0127	-0.0003	0.0001
4	0.0309	1.1046	0.0234	1.0149	0.171	-0.024	0.1136	-0.0056	0.00972
5	0.0429	1.54	0.0185	0.9643	0.2117	-0.0142	0.1149	-0.01	0.01467
6	0.0235	0.8311	0.0145	1.0275	0.1006	0.0062	0.0309	-0.0069	0.00339
7	0.0452	1.6225	0.0134	0.9494	0.1893	0.0526	-0.0303	-0.0182	0.01169
8	0.0476	1.7104	0.0145	0.9394	0.2072	0.0697	-0.0638	-0.0208	0.01395
9	0.00845	0.2984	0.0173	1.0561	0.0396	0.0159	-0.0195	-0.0041	0.00053
10	0.0166	0.5882	0.0234	1.0516	0.0911	0.0413	-0.0606	-0.0092	0.00279
11	0.0622	2.2835	0.0254	0.869	0.3687	0.1699	-0.2567	-0.0367	0.04288
12	0.0294	1.0535	0.0299	1.0262	0.1848	0.0874	-0.1385	-0.018	0.01137
13	0.0146	0.5228	0.0378	1.0705	0.1036	0.0501	-0.0838	-0.0097	0.00361
14	-0.0123	-0.4534	0.091	1.1363	-0.1435	0.1246	-0.0589	-0.1219	0.00693
15	-0.0094	-0.3431	0.0874	1.1359	-0.1062	0.0916	-0.0388	-0.0918	0.0038
16	0.00213	0.0778	0.0794	1.1313	0.0228	-0.019	0.005	0.0205	0.00018
17	0.00522	0.1902	0.0766	1.1264	0.0548	-0.0436	0.0059	0.0498	0.00101
18	0.0194	0.7089	0.0762	1.1046	0.2035	-0.1598	0.0163	0.1853	0.0139
19	0.0264	0.9661	0.0757	1.0849	0.2765	-0.2107	0.0064	0.2516	0.02551
20	0.022	0.8034	0.0773	1.0995	0.2326	-0.1578	-0.0339	0.2074	0.01812
21	-0.0057	-0.2096	0.0833	1.1343	-0.0632	0.0367	0.0192	-0.0537	0.00135
22	-0.0184	-0.6771	0.0917	1.1255	-0.2152	0.1067	0.09	-0.173	0.01554
23	-0.0544	-2.061	0.0982	0.9748	-0.6802	0.3033	0.3258	-0.526	0.14773
24	-0.0644	-2.4739	0.1006	0.9097	-0.8275	0.3554	0.412	-0.6312	0.21347
25	-0.0252	-0.9069	0.0459	1.0557	-0.1989	0.0014	-0.1567	0.0538	0.01322
26	-0.0452	-1.6481	0.0427	0.9752	-0.3482	-0.0048	-0.2679	0.0984	0.0395
27	-0.0365	-1.319	0.0397	1.0108	-0.2683	-0.0096	-0.2011	0.0793	0.02376
28	-0.0037	-0.1307	0.0319	1.0752	-0.0237	-0.0027	-0.016	0.008	0.00019
29	0.0149	0.5303	0.0276	1.059	0.0894	0.0155	0.0543	-0.033	0.00269
30	-0.0113	-0.3994	0.0226	1.0588	-0.0607	-0.0169	-0.029	0.0254	0.00124
31	0.0136	0.4805	0.0193	1.0521	0.0673	0.0266	0.0208	-0.0312	0.00153

Table A7-Continued									
32	-0.0061	-0.2161	0.018	1.0587	-0.0292	-0.0138	-0.0051	0.0143	0.00029
33	-0.0007	-0.0256	0.0175	1.0601	-0.0034	-0.002	0.0001	0.0017	0
34	-0.0007	-0.0254	0.0186	1.0614	-0.0035	-0.0023	0.0009	0.0018	0
35	0.0099	0.3503	0.0203	1.058	0.0505	0.0347	-0.0191	-0.0245	0.00086
36	0.0271	0.966	0.0243	1.0277	0.1525	0.1085	-0.0812	-0.0693	0.00776
37	0.0111	0.3981	0.0402	1.0782	0.0815	0.0574	-0.0613	-0.0302	0.00224
38	0.0124	0.4453	0.0432	1.0799	0.0946	0.0663	-0.0731	-0.0341	0.00302
39	0.00903	0.3244	0.0498	1.0915	0.0743	0.0513	-0.0599	-0.0252	0.00186
40	0.00968	0.3484	0.0534	1.0949	0.0827	0.0568	-0.0679	-0.0273	0.00231
41	-0.0459	-1.6822	0.0536	0.982	-0.4004	0.1249	-0.3485	-0.0122	0.05214
42	-0.0222	-0.7981	0.0406	1.0579	-0.1643	0.046	-0.1355	-0.0043	0.00904
43	-0.0244	-0.8691	0.0246	1.0354	-0.1379	0.0266	-0.0946	-0.0019	0.00636
44	-0.0462	-1.6635	0.02	0.9507	-0.2379	0.0331	-0.1411	-0.0017	0.01843
45	0.00648	0.2289	0.0182	1.0587	0.0312	-0.0033	0.0167	0.0001	0.00033
46	0.0182	0.6439	0.0154	1.0401	0.0804	-0.0026	0.0316	-0.0005	0.00217
47	-0.0166	-0.5876	0.0144	1.042	-0.0709	-0.0008	-0.0219	0.0008	0.00169
48	0.00562	0.1981	0.013	1.0537	0.0227	0.0034	0.0003	-0.0006	0.00017
49	0.0257	0.9116	0.0135	1.0206	0.1065	0.0253	-0.02	-0.0041	0.00379
50	0.0204	0.721	0.0141	1.0343	0.0863	0.0238	-0.0244	-0.0036	0.0025
51	0.027	0.9567	0.0151	1.0188	0.1183	0.0367	-0.0437	-0.0054	0.00467
52	-0.0229	-0.8124	0.0215	1.0362	-0.1205	-0.0485	0.0759	0.0066	0.00486
53	-0.0245	-0.8739	0.0264	1.037	-0.144	-0.0616	0.1026	0.0082	0.00693
54	-0.0081	-0.2901	0.0358	1.0767	-0.0559	-0.0252	0.0446	0.0033	0.00106
55	-0.0097	-0.3467	0.0395	1.0792	-0.0703	-0.032	0.0576	0.0041	0.00167
56	-0.0617	-2.2899	0.0469	0.8876	-0.508	-0.2813	-0.2035	0.3702	0.08136
57	-0.0517	-1.8965	0.0452	0.9444	-0.4125	-0.242	-0.1477	0.3073	0.05481
58	-0.0335	-1.2085	0.0405	1.023	-0.2483	-0.1772	-0.0415	0.1981	0.02043
59	-0.0151	-0.5392	0.0398	1.0719	-0.1097	-0.0921	0.0107	0.0898	0.00405
60	0.0143	0.5111	0.041	1.0747	0.1057	0.0923	-0.0212	-0.0858	0.00376
61	0.00159	0.0569	0.0446	1.0902	0.0123	0.0111	-0.0042	-0.0097	0.00005
62	-0.0026	-0.0944	0.0526	1.0991	-0.0222	-0.0204	0.0111	0.0163	0.00017
63	-0.003	-0.1072	0.0552	1.102	-0.0259	-0.0237	0.0139	0.0186	0.00023
64	0.00444	0.1606	0.0642	1.1119	0.0421	0.038	-0.0261	-0.0283	0.0006
65	0.05	1.8459	0.059	0.9654	0.4623	-0.1485	0.4082	0.0147	0.06899
66	0.0125	0.4521	0.059	1.0977	0.1132	-0.0364	0.1	0.0036	0.00432
67	0.024	0.8595	0.0367	1.0491	0.1677	-0.0446	0.1347	0.004	0.00941

Table A7-Continued									
68	0.0394	1.4192	0.0273	0.9869	0.2376	-0.0512	0.1719	0.0041	0.01856
69	0.0366	1.3134	0.0247	0.9957	0.2088	-0.0405	0.1436	0.003	0.01439
70	0.0432	1.5541	0.0223	0.9663	0.2347	-0.0398	0.1517	0.0026	0.01802
71	0.00279	0.0983	0.0138	1.0558	0.0116	0.0005	0.0027	-0.0002	0.00005
72	-0.0332	-1.1821	0.0139	0.9979	-0.1403	-0.037	0.0354	0.0057	0.00652
73	0.0227	0.8061	0.0187	1.0337	0.1113	0.0419	-0.0615	-0.0058	0.00415
74	-0.0215	-0.7654	0.0227	1.0406	-0.1167	-0.0478	0.0763	0.0065	0.00456
75	-0.0311	-1.1133	0.0278	1.0186	-0.1881	-0.0813	0.1372	0.0108	0.01176
76	-0.0324	-1.1607	0.0307	1.0173	-0.2065	-0.091	0.1568	0.0119	0.01415
77	-0.0434	-1.5718	0.0339	0.9757	-0.2943	-0.1316	0.231	0.0171	0.02831

A8. Modified Levene Test after transformation (Undisturbed specimens)

group	N	Mean	Std Dev	Std Err	Minimum	Maximum
1	39	0.0216	0.0169	0.00271	0	0.066
2	38	0.0229	0.0172	0.00279	0.000031	0.0645
Diff (1-2)		-0.00126	0.0171	0.00389		

group	Method	Mean	95% CL Mean		Std Dev	95% CL Std Dev	
1		0.0216	0.0161	0.0271	0.0169	0.0138	0.0218
2		0.0229	0.0172	0.0285	0.0172	0.014	0.0222
Diff (1-2)	Pooled	-0.00126	-0.00901	0.00649	0.0171	0.0147	0.0203
Diff (1-2)	Satterthwaite	-0.00126	-0.00901	0.00649			

Method	Variances	DF	t Value	Pr > |t|
Pooled	Equal	75	-0.32	0.7472
Satterthwaite	Unequal	74.876	-0.32	0.7472

Equality of Variances				
Method	Num DF	Den DF	F Value	Pr > F
Folded F	37	38	1.03	0.9293

Hypothesis:

H_0: $\sigma_{d1} = \sigma_{d2}$ $(Variances\ are\ equal)$

Vs. H_a: $\sigma_{d1} \neq \sigma_{d2}$ $(Variances\ are\ not\ equal)$

Decision rule: reject H_0 if $p < \alpha(0.1)$

From SAS output, P = 0.9293

As, P $> \alpha$, Variances are equal.

Hypothesis:

H_0: $Variances\ are\ constant$

Vs. H_a: $Variances\ are\ not\ constant$

Decision rule: reject H_0 if $p < \alpha$ (*0.1*)

From SAS output with unequal variances: P = 0.7472

As, $p > \alpha$, Variances are constant.

We conclude that the error variance is constant at α = 0.1.

A9. Normality test after transformation (undisturbed sample)

	e	**enrm**
e	1	0.99525
Residual		<.0001
enrm	0.99525	1
'Normal Scores'	<.0001	

Hypothesis:

H_0: $Normality\ is\ ok$ vs. H_a: $Normality\ is\ violated$

Decision rule: reject H_0 if $\widehat{\rho} < C\ (\alpha; n)$

For α = 0.10 and n=77, $C\ (0.1; 77)$ = 0.9867

And ρ = 0.99525 > $C\ (0.1; 77)$ = 0.9867 (FTR H_0)

So, Normality ok at α =0.1.

A10.Model Selection (Undisturbed soil samples)

Best subset selection

Number in Model	Adjusted R-Square	R-Square	C(p)	AIC	SBC	Variables in Model
2	0.8316	0.8361	3	-545.635	-538.60362	x1 x2
1	0.77	0.773	29.4455	-522.5896	-517.90197	x1

Backward Elimination

Backward Elimination: Step 0

All Variables Entered: R-Square = 0.8361 and C(p) = 3.0000

Analysis of Variance					
Source	**DF**	**Sum of Squares**	**Mean Square**	**F Value**	**Pr > F**
Model	2	0.3039	0.15195	188.7	<.0001
Error	74	0.05959	0.0008053		
Corrected Total	76	0.36349			

Variable	Parameter Estimate	Standard Error	Type II SS	F Value	Pr > F
Intercept	-0.13063	0.02482	0.02231	27.71	<.0001
x1	0.00304	0.0001605	0.28853	358.31	<.0001
x2	0.00387	0.000726	0.02291	28.45	<.0001

Stepwise regression

Summary of Stepwise Selection								
Step	**Variable Entered**	**Variable Removed**	**Number Vars In**	**Partial R-Square**	**Model R-Square**	**C(p)**	**F Value**	**Pr > F**
1	x1		1	0.773	0.773	29.4455	255.46	<.0001
2	x2		2	0.063	0.8361	3	28.45	<.0001

REFERENCES

1. Abu-Hassanein, Z. S., Benson, C. H., and Blotz, L. R. (1996). “Electrical resistivity of compacted clays.” *Journal of Geotechnical Engineering*, 122(5), 397-406.
2. Aizebeokhai, A. P. (2010). "2D and 3D geoelectrical resistivity imaging: Theory and field design." *Scientific Research and Essays*, 5(23), 3592-3605.
3. Archie, G. E. (1942). "The electrical resistivity log as an aid in determining some reservoir characteristics." *Petroleum Technology, T.P. 1422*, Shell Oil Co. Houston, TX.
4. Arulanandan, K. (1969). Hydraulic and electrical flows in clays. *Clays Clay Minerals*, *17*, 63-76.
5. Arjwech, R. (2011). “Electrical resistivity imaging for unknown bridge foundation depth determination.” *Ph.D. Dissertation*, Texas A & M University, College Station, TX.
6. ASTM. “Annual book of standards, volume 04.08, soil and rock.” West Conshohocken, PA.
7. Bardet, J. P. (1997). “Experimental soil mechanics.” *Prentice Hall, Inc.*, NJ.
8. Benson, C.H., Daniel, D.E., and Boutwell, G.P. “Field performance of compacted clay liners.” *Journal of Geotechnical and Geoenvironmental Engineering*, 125(5), 390-403.
9. Bergaya, F. and Lagaly, G. (2006). General introduction: clays, clay minerals, and clay science. *Developments in Clay Science*, *1*, 1-18.

10. Besson, A., Cousin, I., Dorigny, A., Dabas, M., and King, D. (2008). “The temperature correction for the electrical resistivity measurements in undisturbed soil samples: Analysis of the existing conversion models and proposal of a new model.” *Soil Science*, *173*(10), 707-720.
11. Brunet, P., Clément, R., and Bouvier, C. (2010). "Monitoring soil water content and deficit using electrical resistivity tomography (ERT)-A case study in the Cevennes area, France." *Journal of Hydrology*, 380(1-2), 146-153.
12. Bryson, L. S. (2005). "Evaluation of geotechnical parameters using electrical resistivity measurements." *Proc., Earthquake Engineering and Soil Dynamics, GSP 133, Geo-Frontiers 2005,* ASCE, Reston, VA.
13. Campbell, R. B., Bower, C. A. and Richards, L. A. (1948). “Change of electrical conductivity with temperature and the relation of osmotic pressure to electrical conductivity and ion concentration for soil extracts.” *Soil Science Society of America Journal*, Vol. 13, 1948, pp. 66-69.
14. Comina, C., Foti, S., Musso, G., & Romero, E. (2008). “EIT Oedometer: an advanced cell to monitor spatial and time variability in soil with electrical and seismic measurements.” *Geotechnical Testing Journal*, *31*(5), 564.
15. Croney, D., Coleman, J., and Currer, E. (1951). "The electrical resistance method of measuring soil moisture." *British Journal of Applied Physics,* 2 (4), 85-91.
16. Chittoori, B. and Puppala, A. J. (2011). “Quantitative estimation of clay mineralogy in fine grained soils.” *Journal of Geotechnical and Geoenvironmental Engineering*, 137(11), 997-1007.

17. Deng, Y., White, G. N. and Dixon, J. B. (2009). “Soil mineralogy.” *Texas A&M University Electron Microscopy Center*, College Station, TX
18. Delleur, J. W. (Ed.). (2010). “The handbook of groundwater engineering”. CRC press.
19. Ekwue, E., and Bartholomew, J. (2010). "Electrical conductivity of some soils in Trinidad as affected by density, water and peat content." *Biosystems Engineering.*, 108 (2), 95-103.
20. Farouki, O.M. (1981). “Thermal properties of soils.” *U.S. Army Cold Regions Research and Engineering Laboratory, Report No: CRREL Monograph 81-1*, Hanover, New Hampshire.
21. Fukue, M., Minato, T., Horibe, H., and Taya., N. (1999). “The micro-structures of clay given by resistivity measurements.” *Engineering Geology,* 54 (1-2), 43-53.
22. Friedman, S. P. (2005). “Soil properties influencing apparent electrical conductivity: a review.” *Computers and electronics in agriculture*, *46*(1), 45-70.
23. Farrar, D. and Coleman, J. (1967). “The Correlation of surface area with other properties of nineteen British Clay soils.” *Journal of Soil Science,* Vol. 18, 118-124.
24. Giao, P., Chung, S., Kim, D., and Tanaka, H. (2003). "Electric imaging and laboratory resistivity testing for geotechnical investigation of Pusan clay deposits." *Journal of Applied Geophysics*, 52(4), 157-175.

25. Goyal, V.C., P.K. Gupta, S.M. Seth and V.N. Singh. (1996) "Estimation of temporal changes in soil moisture using resistivity method." *Journal of Hydrological Processes*, Vol. 10, 1147-1 154.
26. Harris, W. G. and White, G. N. (2008). "X-ray diffraction techniques for soil mineral identification." *Methods of soil analysis, part*, 81-116.
27. Hamamoto, S., Moldrup, P., Kawamoto, K., Wickramarachchi, P.N., Nagamori, M., and Komatsu, M. (2011). "Extreme compaction effect on gas transport parameters and estimated climate gas exchange for a landfill final cover soil." *Journal of Geotechnical and Geoenvironmental Engineering*, 137(7), 653-662.
28. Hakonson, T.E. (1997). "Capping as an alternative for landfill closures-perspectives and approaches." *Environmental Science and Research Foundation, Proceedings, Landfill Capping in the Semi Arid West: problems, perspectives, and Solutions*. Grand Teton National Park, Wyoming, May 21-22, ESRF,1-18.
29. Holtz, R. D., and Kovacs, W. D. (1981). "An introduction to geotechnical engineering." *Prentice-Hall, Inc*., Englewood Cliffs, NJ.
30. Hossain, M. S., Dharmateja, M. and Hossain, J. (2010). "Assessment of geo-hazard potential and site investigations using Resistivity Imaging." *International Journal of Environmental Technology and Management*, *13*(2), 116-129.
31. Hossain, J. (2012). "Geohazard potential of rainfall induced slope failure on expansive clay." *Ph.D. Dissertation,* University of Texas at Arlington, TX.
32. Kalinski, R., and Kelly, W. (1993). "Estimating water content of soils from electrical resistivity." *Geotechnical Testing Journal. ASTM*, 16(3), 323-329.

33. Kibria, G., and M. S. Hossain., 2012. “Investigation of geotechnical parameters affecting electrical resistivity of compacted clays.” *Journal of Geotechnical and Geoenvironmental Engineering*, 138 (12), 1520-1529.
34. Kutner, M.H., Nachtscheim, C. J., Neter, J. and Li, W. (2005). “Applied linear statistical model.” *5th ed., McGraw Hill Inc.,* NY.
35. Loke, M. H. (2000). Electrical imaging surveys for environmental and engineering studies. *A practical guide to 2-D and 3-D surveys.*
36. Manzur, S.R. (2013). “Hydraulic performance evaluation of different recirculation systems for ELR/Bioreactor landfills.” *Ph.D. Dissertation,* University of Texas at Arlington, TX.
37. Matsui, T., Park, S. G., Park, M. K., & Matsuura, S. (2000, November). “Relationship between electrical resistivity and physical properties of rocks.” In*Proceedings of An International Conference on Geotechnical & Geological Engineering,“GeoEng2000”, Melbourne, Australia G* (Vol. 987).
38. Meunier, A. (2005). “Clays.” Springer. ISBN 3-540-21667-7
39. Mitchell, J., and Soga, K. (2005). "Fundamentals of soil behavior.” *John Wiley and Sons, Inc.,* Hoboken, NJ.
40. Mojid, M. A and Cho, H. (2006). “Estimating the fully developed diffuse double layer thickness from the bulk electrical conductivity in clay.*” Applied clay science,* 33(3), 278-286.
41. McCarter, W. (1984). "The electrical resistivity characteristics of compacted clays." *Geotechnique,* 34(2), 263.

42. McCarter, W. J., and Desmazes, P. "Soil characterization using electrical measurements." *Geotechnique*, 47 (1), 179-183.
43. McCarter, W. J., Blewett, J., Chrisp, T. M. and Starrs, G. (2005). "Electrical property measurements using a modified hydraulic oedometer." *Canadian geotechnical journal*, *42*(2), 655-662.
44. Ozcep, F., Tezel, O., and Asci, M. (2009). "Correlation between electrical resistivity and soil-water content: Istanbul and Golcuk." *International Journal of Physical Sciences, 4*(6), 362-365.
45. Prakash, K. and Sridharan, A. (2004). "Free swell ratio and clay mineralogy of fine-grained soils." *Geotechnical Testing Journal*, 27(2), 220-225.
46. Pozdnyakov, A., Pozdnyakova, L., and Karpachevskii, L. (2006). "Relationship between water tension and electrical resistivity in soils." *Eurasian Soil Science*, 39(S1), 78-83.
47. Qian, X., Koerner, R.M., and Gray, D.H. (2002). "Geotechnical aspects of landfill design and construction." *Princeton Hall,* NJ.
48. Revil, A., Darot, M. and Pezard, P. A., (1996). "From surface electrical properties to spontaneous potentials in porous media." *Surveys in geophysics*, 17(3), 331-346.
49. Revil, A., Cathles, L. M., Losh, S. and Nunn, J. A. (1998). "Electrical conductivity in shaly sands with geophysical applications." *Journal of Geophysical Research: Solid Earth*, 103(B10), 23925-23936.

50. Rinaldi, V. A., and Cuestas, G. A. (2002). "Ohmic conductivity of a compacted silty clay." *J. Geotechnical and Geoenvironmental Engineering,* 128 (10), 824-835.

51. Shah, P., and Singh, D. (2005). "Generalized Archie's law for estimation of soil electrical conductivity." *Journal of ASTM International*, 2(5), 1-19.

52. Sadek, M.S. (1993). "A comparative study of the electrical and hydraulic conductivities of compacted clay." *Ph.D. Dissertation*, University of California, Berkeley, CA.

53. Samouëlian, A., Cousin, I., Tabbagh, A., Bruand, A. and Richard, G. (2005). "Electrical resistivity survey in soil science: a review." *Soil Tillage Research*, 83(2), 173-193.

54. Santamarina, J. C., Klein, K.A. and Fam, M.A. (2001). "Soil and Waves: Particulate material behavior, characterization and monitoring." *John Wiley and Sons*, NY.

55. Sauer, M. C., Southwick, P. F., Spiegler, K. S. and Wyllie, M. R. J. (1955). "Electrical conductance of porous plugs-ion exchange resin-solution systems." *Industrial and Engineering Chemistry*, 47(10), 2187-2193.

56. Schwartz, B. F., Schreiber, M. E., and Yan, T. (2008). "Quantifying field-scale soil moisture using electrical resistivity imaging." *Journal of Hydrology.*, 362(3-4), 234-246.

57. Shang, J. Q., Lo, K. Y., & Inculet, I. I. (1995). Polarization and conduction of clay-water-electrolyte systems. Journal of geotechnical engineering, 121(3), 243-248.

58. Shevnin, V., Mousatov, A., Ryjov, A., and Delgado-Rodriquez, O. (2007). "Estimation of clay content in soil based on resistivity modelling and laboratory measurements." *Geophysical Prospecting*, *55*(2), 265-275.

59. SAS Institute Inc. (2009). "SAS® 9.2 macro language: reference." SAS Institute Inc., Cary, NC.

60. Shihada, H. (2011). "A non-invasive assessment of moisture content of municipal solid waste in a landfill using resistivity imaging." *Ph.D. Dissertation,* University of Texas at Arlington.

61. Stevens, J. (1996). "Applied multivariate statistics for the social sciences." *Lawrence Erlbaum Associates, Inc*., New Jersey.

62. Skempton, A. W. (1953). "The colloidal activity" of clays." *Proceeding of the 3rd International Conference of Soil Mechanics and Foundation Engineering*. Switzerland, Vol. 1, pp. 57-60.

63. Smith, C.W., Hadas, A., Dan, J., and Koyumdjisky, H. (1985). "Shrinkage and Atterberg limits relation to other properties of principle soil types in Israel." *Geoderma*, Vol. 35, 47-65.

64. Simunek, J., Sejna, M., Saito, H., Sakai, M., and van Genuchten, M.T. (2002). "The Hydrus 1D software package for simulating the one-dimensional movement

of water, heat, and multiple solutes in variably saturated media." *Department of Environmental Sciences, University of California Riverside*, CA.

65. Sposito, G. (2008). "The chemistry of soils." *Oxford University Press*, USA.
66. Tabbagh, A., and Cosenza, P. (2007). Effect of microstructure on the electrical conductivity of clay-rich systems. *Physics and Chemistry of the Earth, Parts A/B/C*, *32*(1), 154-160.
67. Voutou, B. and Stefanaki, E. C. (2008). Electron Microscopy: The Basics. *Physics of Advanced Materials Winter School*, *1*.
68. Waxman, M.H. and Smits, L.J. M. Electrical conductivity in oil bearing shaly sands. *Society of Petroleum Engineering Journal*, June , 1968, pp. 107-122.
69. www.usgs.gov
70. Yang, J. S. (2002). " Three dimensional complex resistivity analysis for clay characterization in hydrogeologic study." *Ph.D. thesis*, University of California, Berkeley.
71. Yukselen, Y., and Kaya, A. (2006). Prediction of cation exchange capacity from soil index properties. *Clay Minerals*, 41(4), 827-837.
72. Zha, F., Liu, S., & Du, Y. (2007). Evaluation of Change in Structure of Expansive Soils upon Swelling Using Electrical Resistivity Measurements. InAdvances in Measurement and Modeling of Soil Behavior (pp. 1-10). ASCE.
73. Zornberg, J.G., Kuhn, J., and Wright, S. (2007). "Determination of Field Suction Values, Hydraulic Properties and Shear Strength in High PI Clays" *Research*

Report 0-5202-1, Center for Transportation Research, University of Texas at Austin.

BIOGRAPHICAL INFORMATION

Golam Kibria was born in Khulna, Bangladesh on December 26, 1986. He graduated with a Bachelor of Science in Civil Engineering from Bangladesh University of Engineering and Technology in March 2009. He started his career as a Junior Engineer in the Institute of Water Modeling, Dhaka in the month of May 2009. He served in the Coast, Port, and Estuary Management Division of the institute till December 2009. The author joined the University of Texas at Arlington in spring 2010 for graduate studies, and completed his Master's in Civil Engineering in August, 2011. After that, he enrolled for Ph.D. in the same school. He had the opportunity to work as graduate research assistant under Dr. Sahadat Hossain. The author's research interest include electrical properties of soil, geophysical testing, application of numerical modeling in geotechnical engineering, Mechanically Stabilized Earth (MSE) wall, slope stability analysis and remediation, application of geosynthetics, non-destructive testing, and geotechnical aspects of municipal solid waste (MSW).